MINERALOGY, GEOCHEMISTRY AND PETROGENESIS OF THE LAVAS OF MOUNT EREBUS, ANTARCTICA

JAMES ALLAN MOORE

Submitted in Partial Fulfillment
of the Requirements for the Degree of
Masters of Science in Geology

New Mexico Institute of Mining and Technology

Socorro, New Mexico

June, 1986

This thesis is accepted on behalf of the faculty of the Institute by the following committee:

Philip R. Kyle

Advisor

Kenneth L. Cousins

Edward A. Olson

July, 1986

Date

For my parents, William and Haroldine,
in thanks for their encouragement and guidance,
and for Mike, for leading me to Jesus Christ.

TABLE OF CONTENTS

LIST OF TABLES

LIST OF FIGURES

ABSTRACT

Mt. Erebus is an active, intraplate anorthoclase phonolite volcano approximately 1 m.y. in age located on Ross Island, Antarctica. The lavas comprising Mt. Erebus define a strongly undersaturated sodic differentiation lineage consisting of basanite, Ne-hawaiite, Ne-mugearite, Ne-benmoreite and anorthoclase phonolite termed the Erebus lineage (EL). Most of the lavas are strongly porphyritic, with phenocrysts of olivine (Mg_{88-51}), clinopyroxene (Mg_{51-39}), titanomagnetite (Usp_{51-76}), feldspar (An_{72-11}) and apatite. The limited compositional range of mafic phenocrysts suggests relatively constant temperature, pressure and oxygen fugacity during evolution of the EL. Fe-Ti oxide pairs in a Ne-hawaiite give a temperature of 1081^{o}C and log f_{O_2} of -9.99.

The EL forms smooth continuous curvilinear trends from basanite to anorthoclase phonolite on all major and trace element variation diagrams. The lavas are light rare earth element (REE) enriched (La_N/Yb_N=13.5-20.2). REE concentrations increase only slightly from basanite to anorthoclase phonolite (La_N 200-400) and there are no significant Eu anomalies.

The geochemistry of the EL suggests it evolved by fractional crystallization of a basanite parental magma. Published Pb and Sr isotopic data (Sun and Hanson, 1975;

Stuckless and Ericksen, 1976) suggest the parental magma came from a depleted ($^{87}Sr/^{86}Sr=0.703$) heterogeneous mantle source typical of oceanic island basalts, and that crustal contamination was negligible during evolution of the EL. Evolution by fractional crystallization of the observed phenocryst phases is supported by mass balance models, which indicate that anorthoclase phonolite is a 24% residual liquid of basanite.

The DVDP lineage of the neighboring Hut Point Peninsula of Ross Island (Kyle, 1981b) consists of similar rock types as the Erebus lineage but contains kaersutite. The DVDP lineage evolved by fractionation in which kaersutite was a major phase. This indicates the DVDP lineage evolved at relatively high water contents and low temperature compared to the EL.

Minor volumes of microporphyritic benmoreite, phonolite and trachyte occur on Mt. Erebus. These lavas are enriched in silica and Fe^{2+} but have lower Zr, Nb and Th relative to the EL, and are termed the enriched iron series (EFS). The geochemistry of the EFS suggests it evolved independently of the EL from an alkali basalt parent. Pb and Sr isotopes (Sun and Hanson, 1975; Stuckless and Ericksen, 1976) suggest crustal contamination in the trachytes.

ACKNOWLEDGMENTS

This work would not have been possible without field mapping and samples collected by Dr. Philip Kyle, Anne Wright and Bill McIntosh. I would particularly like to acknowledge Anne Wright's and Bill McIntosh's excellent mapping of Turks Head and Tryggve Point. Dr. Phil Kyle and Anne Wright also contributed crushed samples for analysis, and Dr. Phil Kyle contributed feldspar and groundmass separates. I would like to thank Dr. Dave Reid of the University of Capetown for donating and loading the fine geochemical data manipulation and plotting programs used in this work. They saved me much time and work and helped greatly in interpreting the data. I wish to thank Dr. Klaus Keil for allowing me to use the electron microprobe facilities at the University of New Mexico, and George Conrad for instructions on using the equipment. I thank Dr. Dave Johnson for his useful instruction on making photomicrographs and letting me use darkroom equipment and supplies. This work has benefited greatly from discussions with Anne Wright, Ted Eggleston, Dr. Dave Reid and Bill McIntosh.

I would like to thank the Naval Support Force Antarctica and ITT Antarctic Services personnel for their support of field work and transport of samples to New

Mexico. I sincerely thank the Geoscience secretary Pat Mills for instruction on using the work processor, for typing abstracts, and for willingly letting me use her office equipment and supplies.

Support for this research came from National Science Foundation Grant DPP 82-18493, to Dr. Philip R. Kyle.

CHAPTER ONE

INTRODUCTION

Purpose

The McMurdo Volcanic Group (MVG) (Kyle and Cole, 1974), occurs on the western margin of the Ross Sea in Victoria Land, Antarctica (Fig 1.1). It consists of late Cenozoic, intraplate, predominantly sodic, alkaline volcanics. The Erebus volcanic province (Kyle and Cole, 1974) of the MVG is located in the McMurdo Sound area (Fig. 1.2). Lavas in the Erebus volcanic province are the most undersaturated in the MVG, comprising a broad basanite to phonolite sequence. Ross Island is a major volcanic center within the Erebus volcanic province. On Ross Island basanite vents at Mt. Terror, Mt. Bird and the Hut Point Peninsula radially surround Mt. Erebus, an active, 3974 m-high volcano. Two distinct volcanic lineages occur on Ross Island. The lavas at the centers surrounding Mt. Erebus consist mainly of basanite with minor intermediate differentiates and phonolite. They are predominantly microporphyritic and contain kaersutite. These lavas were examined in detail in Dry Valley Drilling Project (DVDP) core by Kyle (1981b) and are termed the DVDP lineage.

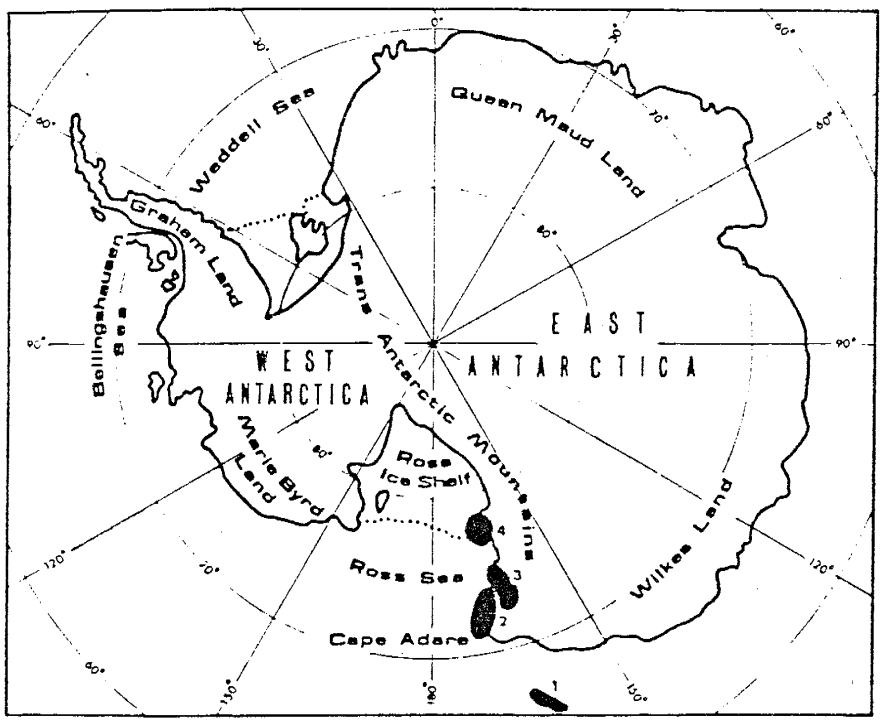

Figure 1.1. Map of Antarctica showing location of McMurdo Volcanic Group and distribution of volcanic provinces. 1 - Balleny province; 2 - Hallett province; 3 - Melbourne province; 4 - Erebus province. From Kyle and Cole (1974).

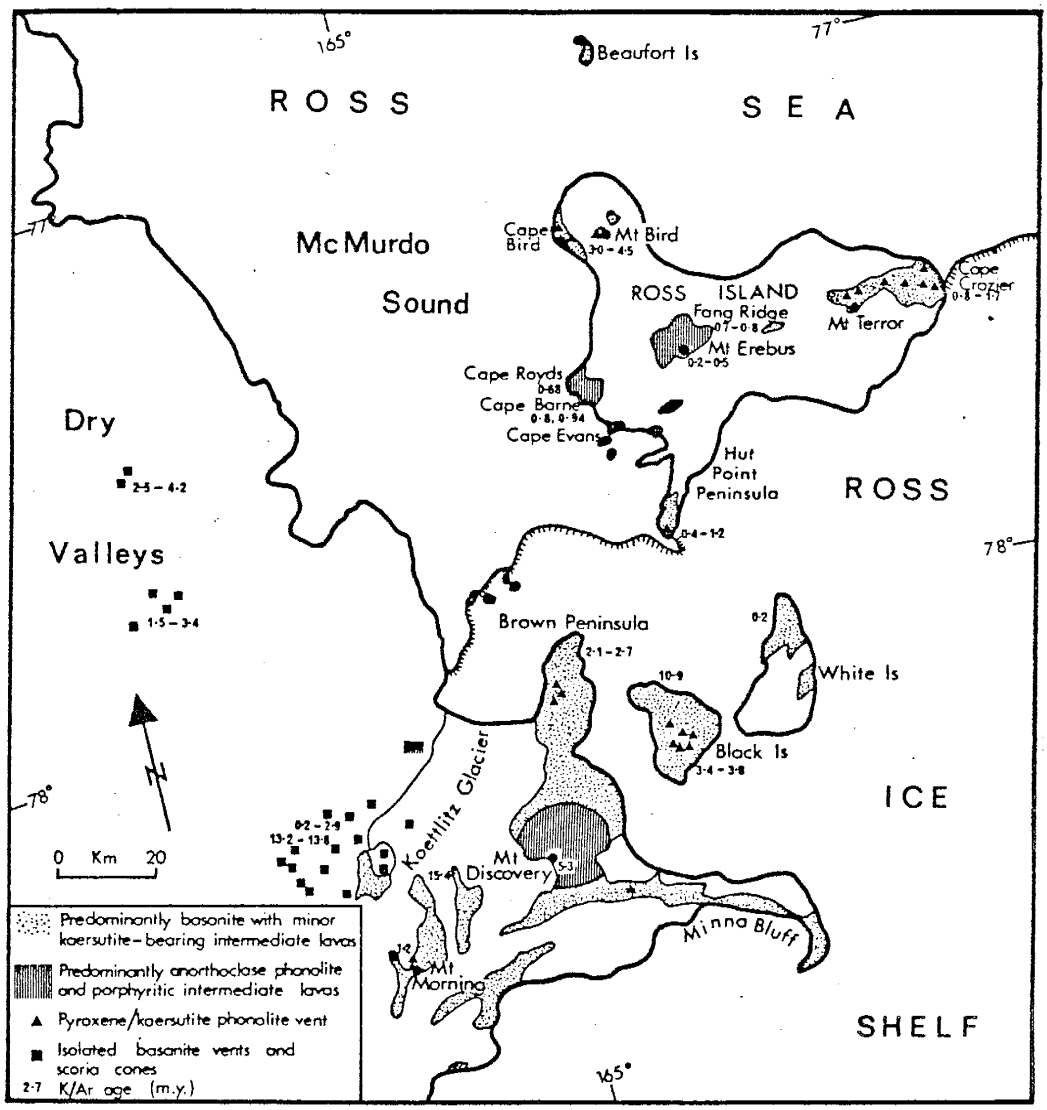

Figure 1.2. Generalized geologic map of Erebus volcanic province. K/Ar age determinations: Armstrong (1978); Forbes et al. (1974); Kyle and Treves (1974c). From Kyle (1976).

In contrast, the lavas of Mt. Erebus are predominantly coarsely porphyritic and lack kaersutite. They are mainly phonolite with minor basanite and lavas of intermediate compositions. These lavas are termed the Erebus lineage (Kyle, 1976). The purpose of this thesis is to investigate the petrogenesis of the Erebus lineage and to compare it to the evolution proposed for the DVDP lineage.

Scope

Research made in this study was predominantly on the geochemistry and mineralogy of rock samples from the Erebus lineage. Standard geochemical, petrographic and microprobe analytical techniques were used. Investigations of volcanic geology and stratigraphy were limited to the local geologic occurrence and stratigraphic positions of samples. Recent volcanic products of Mt. Erebus were not investigated because they are described elsewhere (Kyle, 1977) and are generally similar to older lavas. From the geochemical and mineralogical data, a petrogenetic model is proposed and quantified for the Erebus lineage.

Previous Work

The geology and geochemistry of Mt. Erebus were studied primarily by British scientists during the period from 1840 to the early 1900's, the "heroic era" of Antarctic

exploration (Ross, 1847; Prior, 1898, 1902, 1907; Jensen, 1916; Mawson, 1916; Thomson, 1916; Debenham, 1923; Mountain, 1925). Smith (1954) and Stewart (1956) summarize the geologic, petrographic, and geochemical research of this period. The International Geophysical Year (IGY) (1957-8) marked the beginning of new investigations of Mt. Erebus. Treves (1962; 1968) reported on the geology of Cape Evans and Cape Royds. The geochemistry and mineral chemistry of the anorthoclase phonolite of Mt. Erebus was investigated by Carmichael (1962; 1963; 1964; 1967), Carmichael and MacKenzie (1964), Boudette and Ford (1966), and Berlin and Henderson (1969).

Drilling on the Hut Point Peninsula in 1973 was done as part of the Dry Valley Drilling Project to increase understanding of the geology and petrology of Ross Island. A few samples from Mt. Erebus were included in geochemical investigations of DVDP core by Goldich et al. (1975; 1981), Stuckless and Ericksen (1976), Sun and Hanson (1975; 1976), Stuckless et al. (1981), and Weiblen et al. (1981).

Samples from Mt. Erebus are included in recent comprehensive studies of the MVG, including the geology and geochemistry (Kyle, 1976), K/Ar ages (Armstrong, 1978), rare earth elements (Kyle and Rankin, 1976), Sr isotopes (Jones and Walker, 1972), and structural setting (Kyle and Cole, 1974). Luckman (1974) and Wright et al. (1983) reported on

the geology of older volcanics of Mt. Erebus at Turk's Head and Tryggve Point. Recent studies of the geochemistry of anorthoclase phenocrysts in anorthoclase phonolite have been made by Mason et al. (1982) and Irving and Frey (1984). Jones et al. (1983) reported new Sr isotopic data from the anorthoclase phonolite.

Field Work

General and detailed mapping and sampling of selected areas of Mt. Erebus were made by the author from December, 1983-January, 1984. In addition, this study incorporates samples and mapping made by field parties organized by Dr. Philip Kyle between 1977-1983.

CHAPTER TWO

GEOLOGIC SETTING

Regional Tectonics

The MVG lies at the western margin of the Ross Sea in the proposed margin zone between East and West Antarctica, the two major tectonic provinces comprising Antarctica (McGinnis et al., 1985) (Fig. 1.1). East Antarctica forms the bulk of the continent and is a stable cratonic shield (Craddock, 1983), whereas West Antarctica is thought to have changed from a convergent plate margin in the Mesozoic to an extensional province in the Cenozoic (Le Masurier and Wade, 1976). The tectonics of the region between East and West Antarctica is poorly understood. A topographic depression occurs on the West Antarctica side, part of which forms the Ross and Weddell Seas, while a structural high on the East Antarctica side forms the Transantarctic Mountains.

The margin zone is believed to be a major crustal fault zone or downwarping (Kyle and Cole, 1974) with extensional and possibly transcurrent motion along it (Hayes and Davey, 1975). The Hillary and Rennick faults in Victoria Land trend roughly parallel to the Transantarctic Mountains, and the pronounced topographic break on the east side of the mountains may be a fault escarpment (Kyle and Cole, 1974) (Fig. 2.1). These faults are thought to be continental

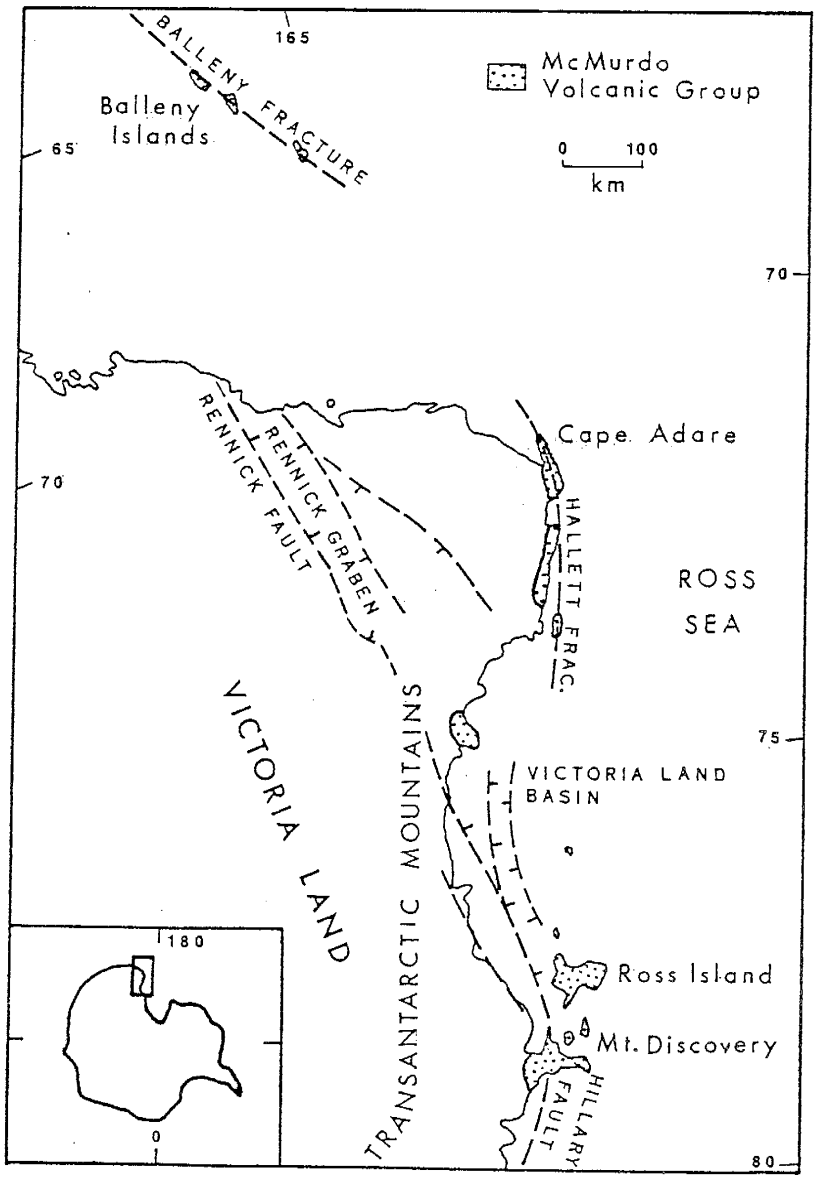

Figure 2.1. Simplified geologic map of Victoria Land and Balleny Islands showing relationship of volcanism to structure. Modified after Kyle and Cole (1974) and Cooper and Davey (1985).

expressions of major fracture zones developed during the breakup of Antarctica and Australia in the Mesozoic (Kyle and Cole, 1974). In southern Victoria Land, rocks have been downdropped at least 2 km to the east along a fault subparallel to the mountain front (Barrett, 1965). The basement of the Ross Sea consists of metamorphic and sedimentary rocks similar to those exposed in the Transantarctic Mountains, as evidenced from drill core (Ford and Barrett, 1975) and xenoliths in volcanic rocks (Thomson, 1916). This again indicates downdropped crust east of the Transantarctic Mountains. Deep seismic profiling in McMurdo Sound in southern Victoria Land (Fig. 1.2) (McGinnis et al., 1983) suggest the basement occurs 4-5 km below sea level. Approximately 30 km away the Transantarctic Mountains rise to almost 4000 m, suggesting 8 km of displacement has occurred along major crustal faults.

A strong gravity gradient across McMurdo sound (Smithson, 1972) is thought to result from a pronounced change in crustal thickness, from 40 to 27 km. The thin crust is believed to have formed by east-west extension in the Ross Sea possibly due to rifting (Kyle and Cole, 1974). Evidence for rifting includes seismic reflections from the basement of McMurdo Sound, which indicate a series of east-dipping listric faults (McGinnis et al., 1983). In addition, the Victoria Land basin in the western Ross Sea and the Rennick graben in northern Victoria Land (Fig. 2.1)

are possible fault block and graben structures (Cooper and Davey, 1985). Thus, the crust of the Ross Sea is strongly extended, possibly in an intracontinental extensional province similar to the East African Rift, Kenya and Basin and Range province, western U.S.A.

Regional Geology

Introduction

The MVG forms a discontinuous zone c.1400 km long and <150 km wide generally lying parallel to the eastern flank of the Transantarctic Mountains in Victoria Land (Fig. 2.1). On the coast of Victoria Land the MVG was erupted onto the stable continental crust of East Antarctica which consists of a basement of Precambrian and lower Paleozoic metasediments intruded by lower Paleozoic granitic plutons. This basement is unconformably overlain by horizontally-bedded Devonian to Triassic sediments (Beacon Supergroup) which were intruded by Jurassic-age dolerite dikes and sills (Ferrar Dolerite Group) (Warren, 1969). The Beacon Supergroup is unconformably capped in the Ross Sea by a thick pile of Oligocene to Recent marine glacial sediments onto which the offshore island of the MVG were erupted (Wong and Christoffel, 1981; Cooper and Davey, 1985).

The MVG is developed along crustal faults and fractures in Victoria Land and the Ross Sea (Kyle and Cole, 1974) (Fig. 2.1). The group is divided, from north to south, into the Balleny, Hallett, Melbourne, and Erebus volcanic provinces (Kyle and Cole, 1974) (Fig. 1.1). Volcanism commenced at least 18 m.y. ago (Muncy, 1979) and has been continuous up to the present. Two volcanoes, Mt. Erebus and Mt. Melbourne, are active (Kyle et al., 1982).

Erebus Volcanic Province

The Erebus volcanic province (Fig. 1.2) includes the Ross Island center (Mt. Bird, Mt. Terror, Mt. Erebus, and Hut Point Peninsula), the Mt. Discovery center (Mt. Discovery, Mt. Morning, Brown Peninsula, and Minna Bluff), Black, White, Beaufort, and Franklin Islands, and small basaltic cones and flows scattered throughout the foothills and valleys of the Transantarctic Mountains in southern Victoria Land. The Erebus volcanic province is situated at the proposed intersection of the southern extension of the north-south trending Rennick fault and the northern extension of the northeast-trending Hillary fault (Fig. 2.1) (Kyle and Cole, 1974). This intersection coincides with a change in trend of the Transantarctic Mountains from north-south to northeast-southwest and one of the areas of greatest uplift in the range (Kyle, 1976). Volcanic activity in the Erebus volcanic province may be the result of its

location at this intersection, which created a zone of weakness facilitating the rise of mantle melts.

The main volcanic centers of Ross Island and Mt. Discovery each consist of a large stratovolcano radially surrounded by subsidiary volcanic centers (Fig. 1.2). The three-fold radial configuration around a central volcano may be controlled by radial fractures in the crust above a rising mantle diapir (Kyle and Cole, 1974).

The Erebus volcanic province comprises a broad basanite to phonolite association (Goldich et al., 1975) with a peralkaline tendency at the Discovery center (Wright et al., 1984). An older group of trachytes occurs at Mt. Morning (Kyle and Muncy, 1978; Muncy, 1979; Wright et al., 1984). K/Ar age determinations on a number of samples from throughout the province (Treves, 1968; Forbes et al., 1974; Kyle and Treves, 1974c; Armstrong, 1978; Muncy, 1979) range from 18.7 to 0.08 m.y. The dates suggest the volcanism is the oldest in the MVG, has been almost continuous up to the present activity of Mt. Erebus on Ross Island, and has not migrated or followed a pattern with time. Each center was active for a period of c.1 m.y., and no two centers were active at the same time (Armstrong, 1978).

Geology of Mt. Erebus

Introduction

Mt. Erebus (3794 m) dominates the three smaller volcanic centers (Mt. Terror (3230 m), Mt. Bird (1766 m) and Hut Point Peninsula) which make up Ross Island. The lavas of Mt. Erebus and the Dellbridge Islands (Fig. 2.2) are characteristically coarsely porphyritic, in contrast to the predominantly aphyric intermediate and felsic lavas of other volcanic centers of the MVG. The major rock type exposed on the surface, and that currently being erupted by Mt. Erebus, is anorthoclase-phyric phonolite (henceforth called anorthoclase phonolite; the volcanic rock classification used in this study is explained in Chapter 3). Mt. Erebus is the most active volcano on the Antarctic continent. It has daily strombolian eruptions and contains a persistent convecting anorthoclase phonolite lava lake (Kyle, 1985). K/Ar age determinations on lavas from Mt. Erebus are given in Table 2.1. An age determination of 0.94 m.y. from an anorthoclase phonolite flow at Cape Barnes (Armstrong, 1978), is the oldest date from Mt. Erebus, suggesting the center is approximately 1 m.y. old.

This study is concerned with the volcanic rocks comprising Mt. Erebus and includes older volcanics of Mt. Erebus which form the Dellbridge Islands (Fig. 2.2). The following sections are descriptions of the volcanic geology,

Table 2.1. K/Ar age determinations on Mt. Erebus lavas.

Locality and description	Date (m.y.) Error (1 sigma)	Source
Anorthoclase phenocryst from anorthoclase phonolite, Cape Barne	0.94±0.05	1
Ne-hawaiite, middle cone, Cape Barne	0.8±0.2	1
Anorthoclase phenocryst from anorthoclase phonolite, summit, Mt. Erebus	0.55±0.15	1
Glass from sample above	0.45±0.2	1
Anorthoclase phenocryst, summit, Mt. Erebus	0.44±0.09	1
Anorthoclase phonolite, caldera rim, Mt. Erebus	0.15±0.05	1
Anorthoclase phenocryst from sample above	0.20±0.07	1
Lowermost flow, Fang Ridge	0.81±0.02	1
Uppermost flow, Fang Ridge	0.73±0.07	1
Youngest anorthoclase phonolite flow, Cape Royds	0.68±0.14	2
Youngest Ne-hawaiite flow, Turks Head	0.86±0.20	3

Sources
1 - Armstrong (1978)
2 - Treves (1968)
3 - Kyle (pers. comm.)

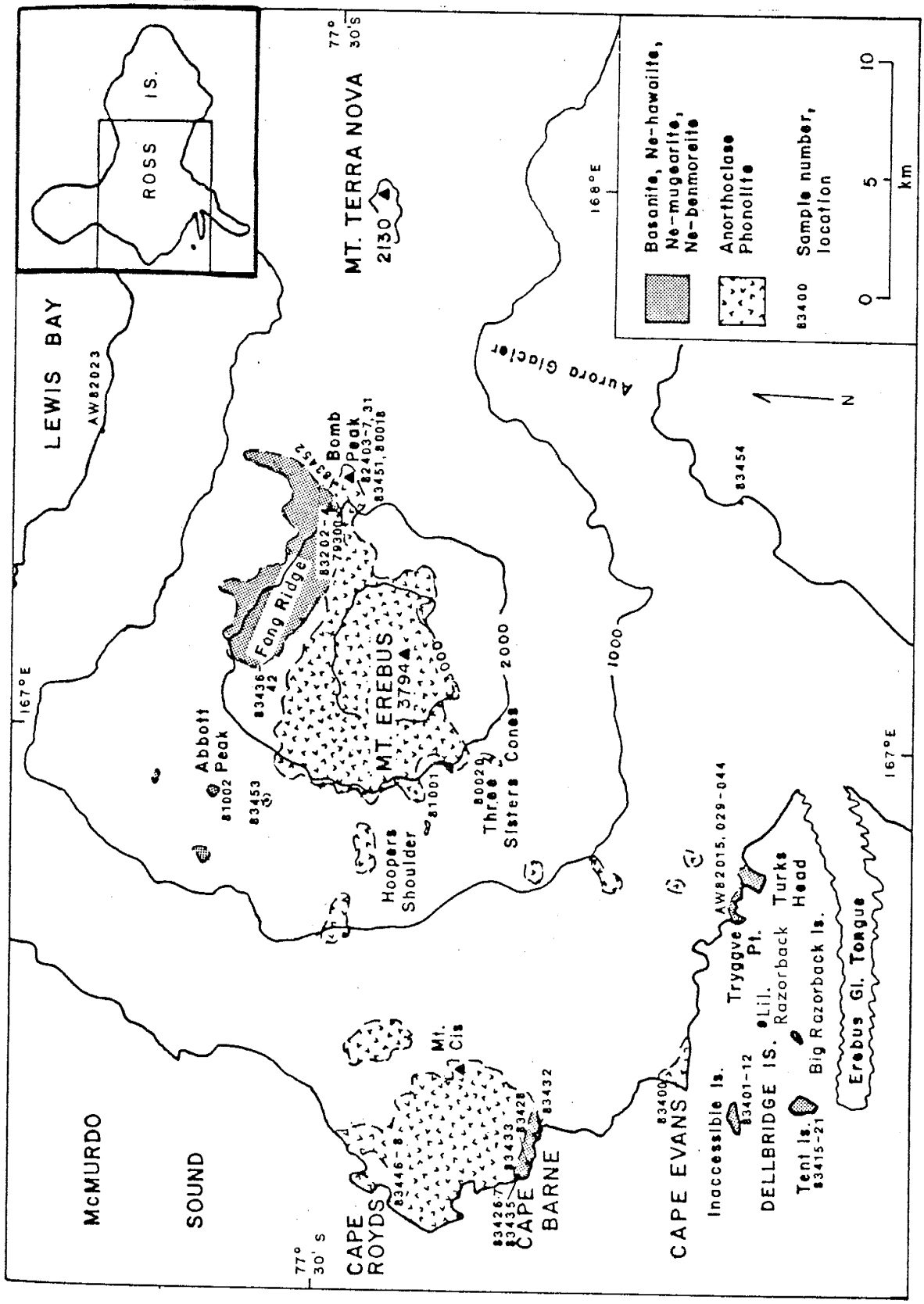

Figure 2.2. Simplified geologic map of Mt. Erebus showing sample locations.

followed by a model of the volcanic evolution.

Dellbridge Islands

This archipelago of four tiny heavily eroded volcanic islands lies approximately 3 km off the southwest coast of Ross Island (Fig. 2.2).

Inaccessible Island is composed of a sequence of Ne-hawaiite and Ne-benmoreite lava flows which dip from 10 to 40^{o} north (Fig. 2.3). At the base of the sequence numerous flows of feldspar-clinopyroxene-phyric Ne-hawaiite 1 to 4 m thick occur (83404-06; numbers are samples described and analyzed in this study). These are overlain by palagonitized pillow lavas, pillow breccias, and hyaloclastites which grade upward into a >60 m thick sequence of numerous 1-10 m thick porphyritic feldspar-rich Ne-hawaiite flows (83401, 83403, 83409), with associated dikes (83411). Thin porphyritic Ne-benmoreite flows (83410) cap Inaccessible Island. Infrequent pebble-sized gabbroic and peridotitic xenoliths, probably cumulates, occur in the porphyritic Ne-hawaiite and Ne-benmoreite flows.

On the eastern end of Inaccessible Island a c.15 m thick weakly porphyritic benmoreite flow (83402) overlain by a series of aphanitic benmoreite flows 1-2 m thick (83412) is interbedded in the sequence of feldspar-rich Ne-hawaiite flows. This flow has a possible feeder dike of aphanitic

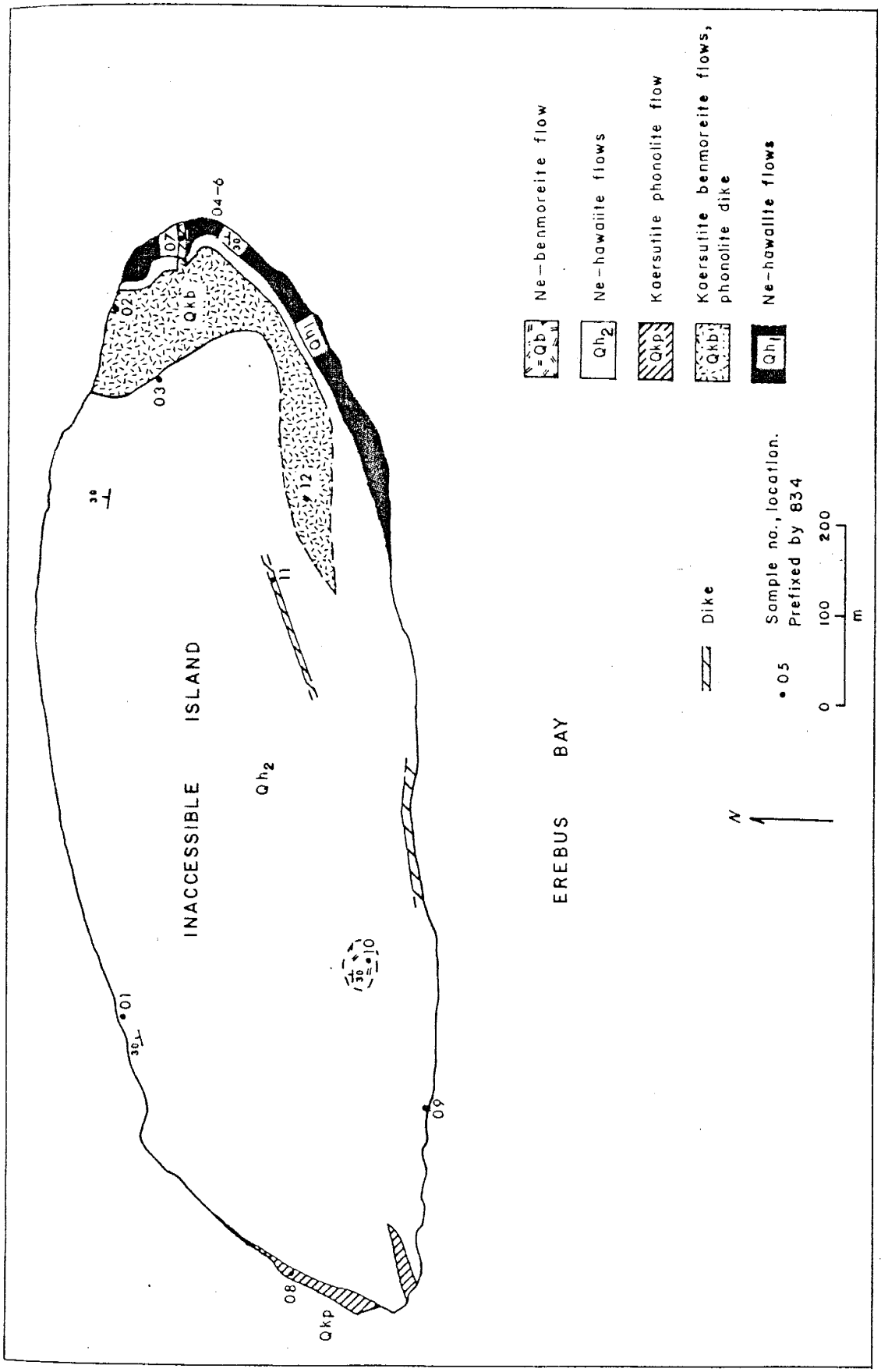

Figure 2.3. Geologic sketch map of Inaccessible Island, showing sample locations.

phonolite (83407). An approximately 10 m thick flow of microporphyritic kaersutite phonolite (83408) is interbedded in the feldspar rich Ne-hawaiite flows at the west end of Inaccessible Island.

Tent Island is approximately 1 km south of Inaccessible Island (Fig. 2.4). At the base of the sequence are pillow lavas and flows of andesine-phyric Ne-hawaiite (83418). Overlying them above a smooth, possibly glacially-formed unconformity are c.20 m of massive blocky lapilli tuff containing heterolithic volcanic blocks ranging from 1 cm to 0.4 m. Clast size decreases upward and sedimentary structures indicate the upper part of the unit has been reworked by fluvial processes. The tuffs are probably lahar deposits.

Dikes of porphyritic Ne-mugearite (83417) intrude the tuff at the southern end of Tent Island and appear to be feeders to porphyritic feldspar-rich Ne-hawaiite flows overlying the tuff (Fig. 2.5). Further to the north the tuff is overlain by a 10 m-thick series of flows of glassy feldspar-olivine-phyric Ne-hawaiite (83415). Thin flows of porphyritic Ne-benmoreite (83421, 25748) cap Tent Island. The upper flows have dips of 10-20^{o} to the southeast and contain infrequent pebble-sized gabbroic inclusions probably of cumulate origin.

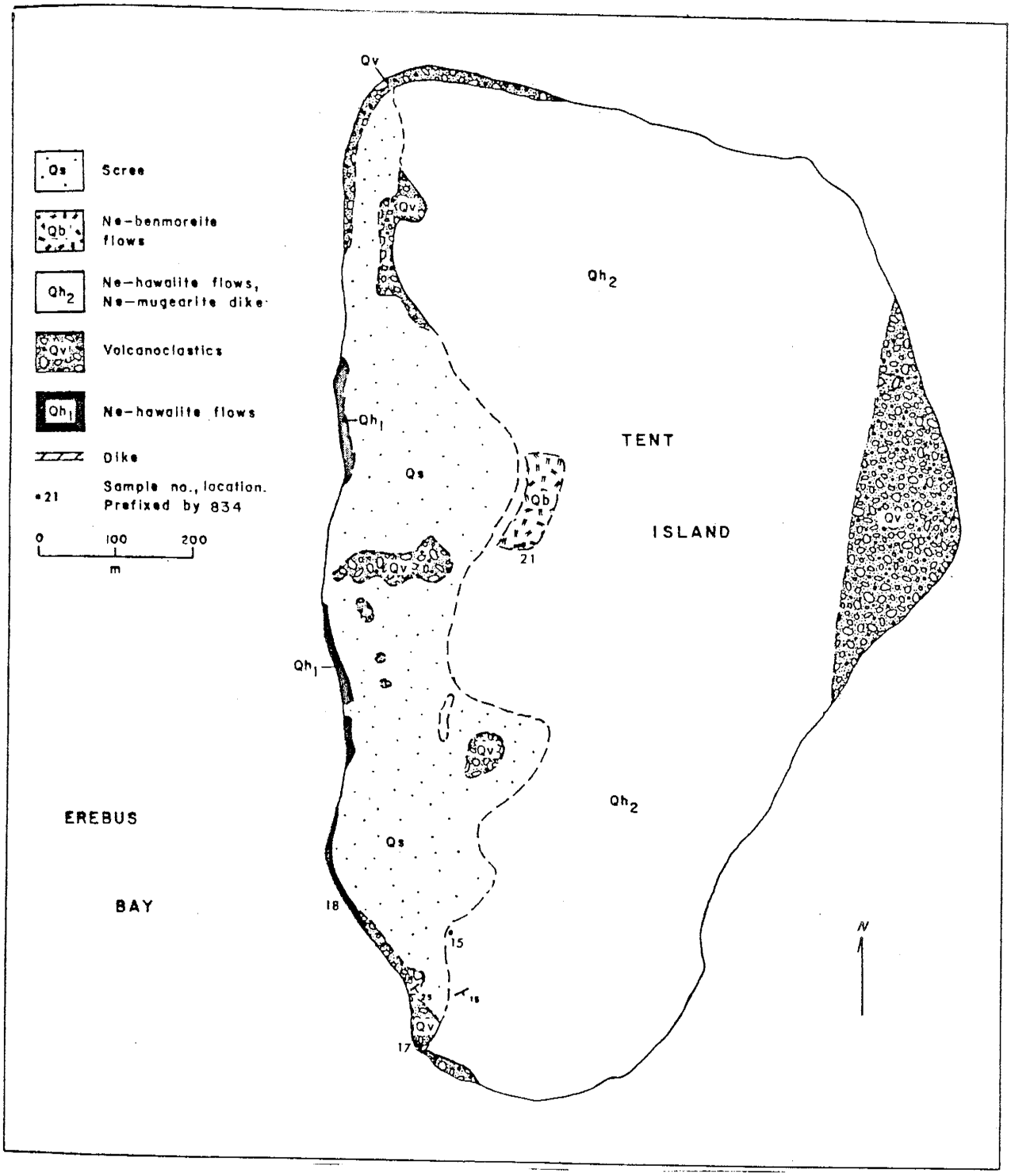

Figure 2.4. Geologic sketch map of Tent Island, showing sample locations.

Figure 2.5. Ne-mugearite dike (sample 83417) crosscutting tuff, southwest end of Tent Island. Ne-hawaiite flows capping cliff. Cliff in foreground c.60 m high. Photo by A.C. Wright.

Debenham (1923) suggested Inaccessible and Tent Islands were part of the same cone. However, differences in the composition, mineralogy, and geology suggests that the islands are more likely remnants of different cones of a volcanic center located west of the islands.

The volcanic geology of Big and Little Razorback Islands (Fig. 2.2) has been summarized by Kyle (1976) and Smith (1954). Little Razorback is composed of 15-20 subaerial Ne-hawaiite flows from 1 to 5 m thick, and dipping 2 to 3^{o} to the northwest. The lower flows are weakly feldspar-clinopyroxene-phyric and the upper flows are strongly feldspar-phyric. Big Razorback is composed of many thin flows of fine grained Ne-mugearite and Ne-benmoreite similar to the weakly porphyritic rocks of Little Razorback. A tower-shaped intrusion at the southwest end of Big Razorback may mark the location of a vent. The Razorback Islands appear to be parts of a cone centered to the east of the islands.

The Dellbridge Islands may be remnants of cones formed by the earliest activity of Mt. Erebus. The age of the lavas is unknown but suggested to be <2 m.y. because of the erosive power of the sea (Kyle, 1976).

Debenham (1923) suggested Inaccessible and Tent Islands were part of the same cone. However, differences in the composition, mineralogy, and geology suggests that the islands are more likely remnants of different cones of a volcanic center located west of the islands.

The volcanic geology of Big and Little Razorback Islands (Fig. 2.2) has been summarized by Kyle (1976) and Smith (1954). Little Razorback is composed of 15-20 subaerial Ne-hawaiite flows from 1 to 5 m thick, and dipping 2 to 3^{o} to the northwest. The lower flows are weakly feldspar-clinopyroxene-phyric and the upper flows are strongly feldspar-phyric. Big Razorback is composed of many thin flows of fine grained Ne-mugearite and Ne-benmoreite similar to the weakly porphyritic rocks of Little Razorback. A tower-shaped intrusion at the southwest end of Big Razorback may mark the location of a vent. The Razorback Islands appear to be parts of a cone centered to the east of the islands.

The Dellbridge Islands may be remnants of cones formed by the earliest activity of Mt. Erebus. The age of the lavas is unknown but suggested to be <2 m.y. because of the erosive power of the sea (Kyle, 1976).

Turks Head and Tryggve Point

Turks Head and Tryggve Point are headlands of Ross Island extending into Erebus Bay (Fig. 2.2). Luckman (1974) and Wright et al. (1984) investigated the volcanic geology (Fig. 2.6). Both promotories consists of similar but probably independent subaqueous to subaerial volcanic sequences with a regional dip of 30° north. At the base of the sequences at both locations are pillow lavas of feldspar-clinopyroxene-phyric Ne-hawaiite (AW82041). These are overlain by a thick sequence of massive Ne-hawaiite pillow and hyaloclastite breccias, which grade upward into subaerial porphyritic feldspar-rich Ne-hawaiite flows at Turks Head. The sequence at Turks Head is capped by a flow of weakly porphyritic Ne-hawaiite (AW82038). At Tryggve Point, the breccias are unconformably overlain by feldspar-phyric Ne-hawaiite flows (AW82029, -032, -044). The western end of Tryggve Point is cut by a dike of feldspar-clinopyroxene-phyric Ne-benmoreite (AW82030). A similar dike occurs at the western end of Turks Head. Flows of anorthoclase-phyric Ne-benmoreite (AW82015), which came from the direction of Mt. Erebus, unconformably overlie the Ne-hawaiite sequences of Turks Head and Tryggve Point.

The volcanics of Turks Head and Tryggve Point were probably erupted from a center located to the south and are believed to be about the same age as the Dellbridge Islands

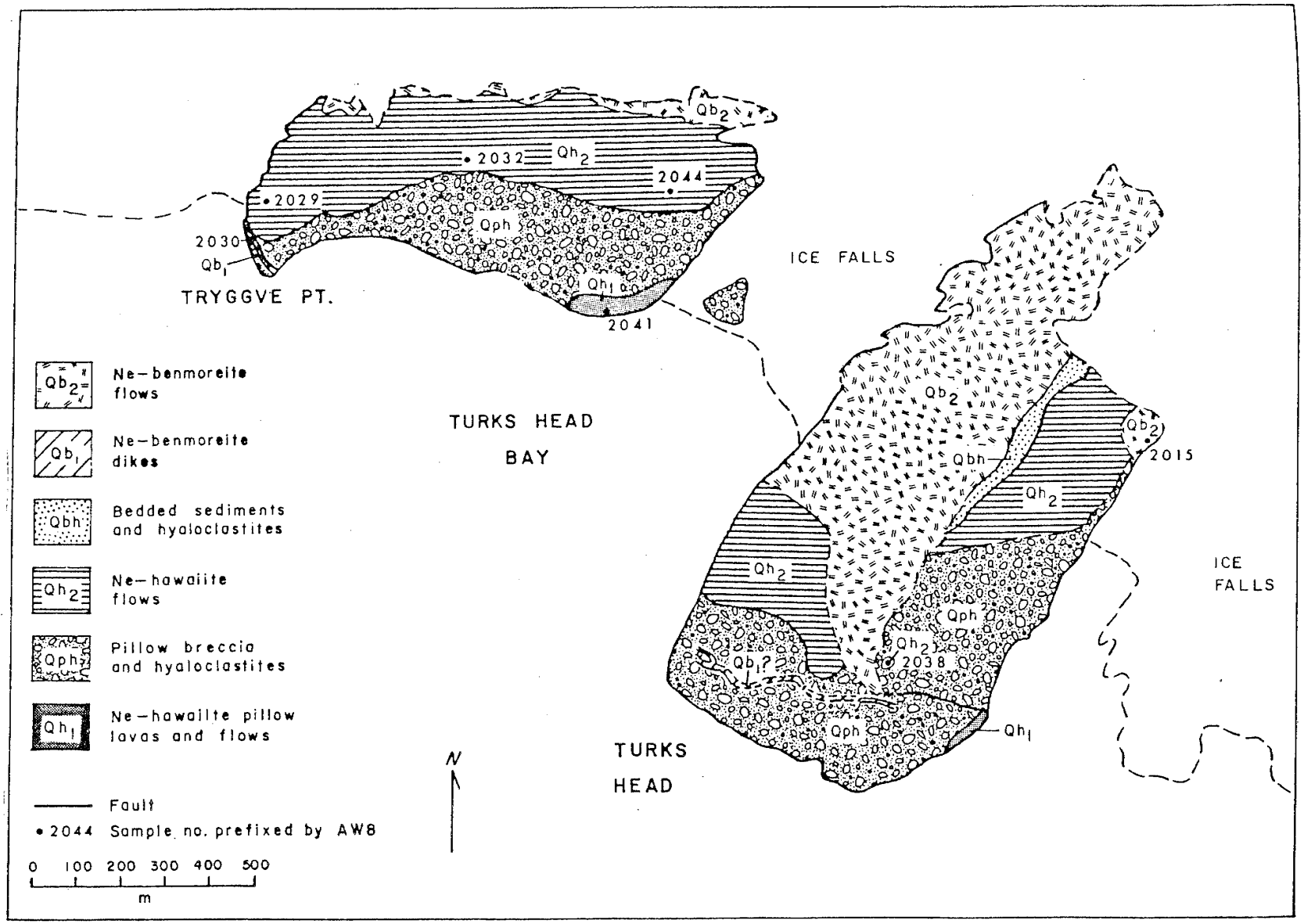

Figure 2.6. Geologic sketch map of Turks Head and Tryggve Point, showing sample location. Modified after Wright (unpubl.).

(Kyle, 1976). A K/Ar date of 0.86±0.20 m.y. was obtained on the uppermost Ne-hawaiite flow at Turks Head (AW82038; Kyle, pers. comm.).

Lower Slopes

Most of the west coast of Ross Island consists of anorthoclase phonolite flows from Mt. Erebus (Fig. 2.2). Cape Evans is composed of two flows up to 15 m thick each in places (Treves, 1962). Sample 83400 is from the center of the lower flow. At Cape Barne (Fig. 2.7), two anorthoclase phonolite flows occur which thicken locally to over 20 m (Kyle, 1976). The surface, though of low relief, is irregular due to numerous pressure ridges and flow lobes which appear to have followed valleys or depressions in the topography (Kyle, 1976). The younger flow (83433) has a K/Ar age of 0.94±0.05 m.y. (Armstrong, 1978).

On the south side of Cape Barne are three small cones of microporphyritic Ne-hawaiite which form a line trending roughly northwest, suggesting they were erupted from a northwest-trending fissure. The three cones are of similar composition and appear to be of the same age. The youngest anorthoclase phonolite flow at Cape Barne appears to lap up against the Ne-hawaiite cones, indicating the cones are older than the flow. A K/Ar age of 0.8±0.2 m.y. (Armstrong, 1978) obtained from the middle cone is analytically indistinguishable from the age of the anorthoclase phonolite

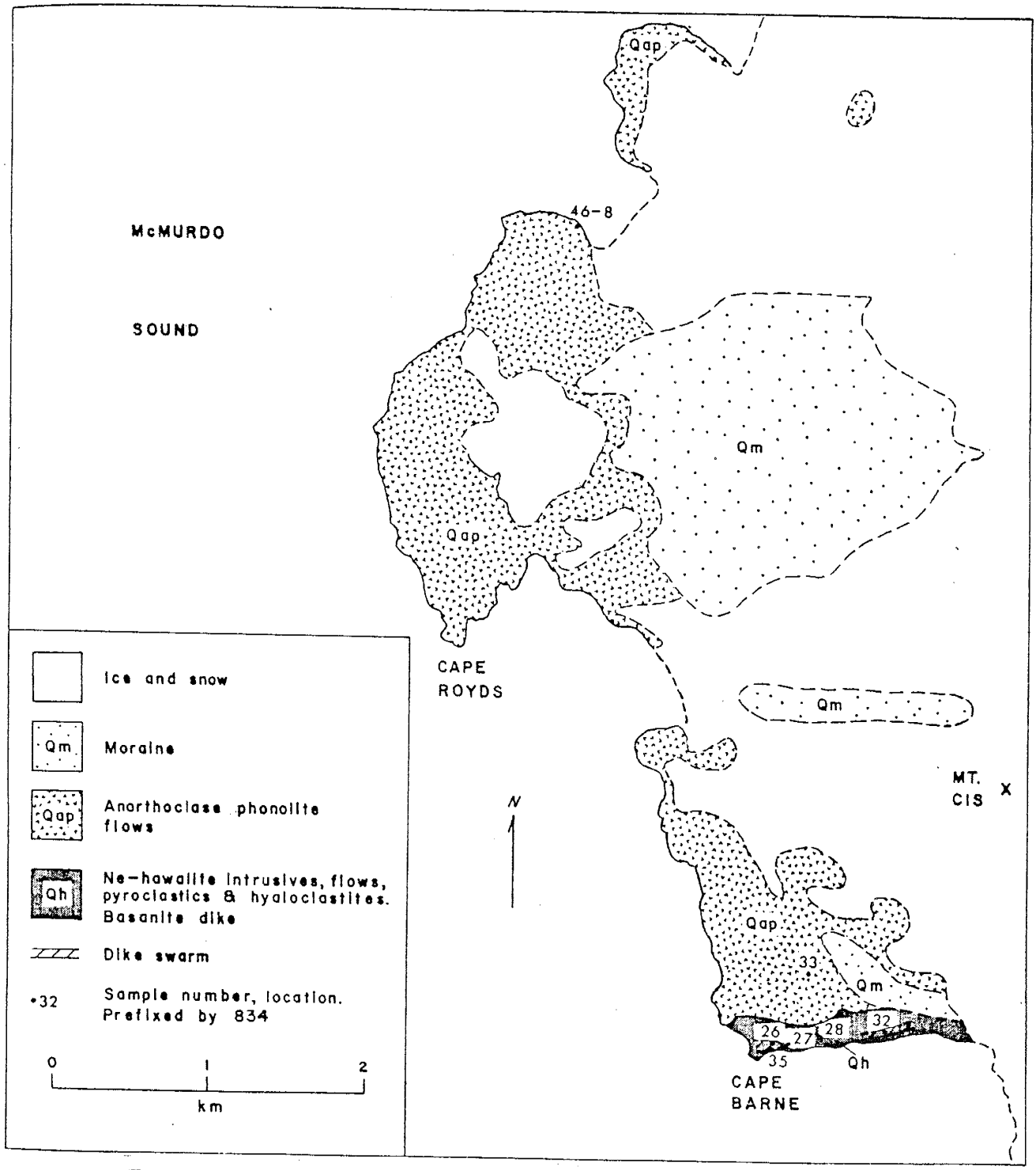

Figure 2.7. Geologic sketch map of Cape Barne and Cape Royds showing sample locations. Modified after Smith (1954).

flow.

The westernmost cone at Cape Barne is composed of palagonitized hyaloclastites, surge deposits, and pillow lavas grading upward into bomb lapilli tuffs interbedded with thin flows (83427) (Fig. 2.8). A number of dikes occur trending northwest and dipping vertical to 40^{o} north (83426). A basanite dike (83435) occurs in the lower part of the cone. The middle cone consists of a thick sequence of palagonitized surge deposits and tuffs intruded by thin dikes and sills and capped by a c.10 m thick flow (83428). The easternmost cone consists dominantly of flows and is crosscut by numerous thin near-vertical dikes mostly trending northwest (83432).

Mt. Cis (Fig. 2.7) is a small outcrop of weakly undersaturated to oversaturated high-K trachyte about 1 km east of Cape Barne (Smith, 1954). The trachyte contains abundant xenoliths of sanidinite and weakly metamorphosed sandstone and dolerite (Thomson, 1916). These xenoliths are similar to rocks exposed in the Transantarctic Mountains, suggesting that downfaulted continental crust underlies Ross Island.

Cape Royds (Fig. 2.7) is composed of at least four flows of anorthoclase phonolite (83446-8). The flows locally reach 10-15 m in thickness and have numerous pressure ridges and pushup domes, similar to the anorthoclase phonolite

Figure 2.8. Westernmost Ne-hawaiite cone, Cape Barne. Anorthoclase phonolite flows on lower slopes of Mt. Erebus in background.

Figure 2.9. Northwest side of Mt. Erebus from west side of Mt. Bird. Sharp ridge in left background is Fang Ridge. Summit cone of Mt. Erebus on skyline in middle background. Peak isolated in snow below and to right of summit cone is Abbott Peak. Photo by A.C. Wright.

flows at Cape Barne. Geochemistry and petrography are also similar to the flows at Cape Barne. The flows are separated by glassy ropey upper surfaces indicating pahoehoe-type flows. The preservation of these glassy flow breaks suggests little erosion occurred between successive flows at Cape Royds, thus the flows must be of similar age. A K/Ar age of 0.68 ± 0.14 was obtained from the uppermost flow (Treves, 1968) suggesting the flows are younger than those at Cape Barne.

The eruptive center of the flows at Cape Barne and Cape Royds is unknown. Kyle (1976) suggested that it may have been near the present coast because the high viscosity of phonolite lava (10^4-10^5 poise) makes it unlikely for flows to travel far. Alternatively, the source may have been near the present center of Mt. Erebus, c.20 km inland, and the volume of lava was sufficiently large to allow the viscous material to travel long distances over low slopes (Kyle, 1976).

Outcrop is very limited over most of the lower slopes of Mt. Erebus (Fig. 2.9). Anorthoclase phonolite flows are exposed at a few places above Cape Royds (Kyle, 1976), and a small plateau south of Abbotts Peak at c.1700 m in elevation is a finely porphyritic Ne-hawaiite flow (83453) (Fig. 2.2). Ice-capped cliffs bordering Lewis Bay on the north side of Mt. Erebus (Fig. 2.2) consist of palagonitized volcanic

breccias unconformably overlain by aphanitic benmoreite flows (AW82023) (A. Wright, pers. comm.). Cliffs west of the Aurora Glacier on the southeast flank of Mt. Erebus (Fig. 2.2) expose a possible subglacial to subaerial trachyte sequence (W. McIntosh, pers. comm.). At the base are bedded tuffs which grade upward into trachyte hyaloclastites and flow lobes. Subaerial trachyte flows (83454) unconformably overlie this unit.

Upper Slopes

The upper slopes of Mt. Erebus, between 1800 m and the caldera rim (c.3000 m; Fig. 2.2), are composed of numerous flows of anorthoclase phonolite (83452) usually with only their flow levees exposed above the snow. The flows vary from 20-70 m in width and generally consist of highly vesicular or scoriaceous lava with thick glassy crusts (Kyle, 1976). The freshness of the glass and the lack of erosion indicates the youthful age of most of the flows. A K/Ar age of 0.15±0.05 m.y. was obtained from a flow on the north side of Mt. Erebus (Armstrong, 1978).

Six small parasitic cones occur at about 1800 m in elevation on the flanks of Mt. Erebus. Hoopers Shoulder, on the west side, is more recent than the flows in the area and built of short flows of relatively nonvesicular glassy anorthoclase phonolite (81001) (Kyle, 1976). About 3 km to the south are the Three Sisters, three small recent

anorthoclase phonolite cones (80020) which form a southwest-trending line. Abbott Peak on the northwest flank of Mt. Erebus is a pyramid-shaped endogenous dome of kaersutite-phyric benmoreite (81002).

Bomb Peak, on the western side of the saddle between Mt. Erebus and Mt. Terra Nova (Fig. 2.2), is about 100 m high and named for the numerous small to large anorthoclase phonolite bombs scattered over its surface (82407). The bombs probably came from a nearby, unexposed parasitic vent (W. McIntosh, pers. comm.). Some bombs consist of xenoliths of anorthoclase-clinopyroxene cumulate (82403) and altered anorthoclase phonolite probably of hypabyssal origin (82431). Bomb Peak itself is an older endogenous dome of aphanitic comenditic trachyte (82405, 83451) and feldspar-kaersutite-phyric phonolite (80018, 82404). The comenditic trachyte contains small anorthoclase phonolite xenoliths and is the only quartz-normative lava known on Mt. Erebus apart from Mt. Cis (Fig. 2.2).

Fang Ridge

Fang Ridge is located at approximately 2400 m on the northeast flank of Mt. Erebus (Figs. 2.2, 2.9). It is approximately 4 km long, trending northwest to southeast (Fig. 2.10). The northeast side is a $>45^{o}$ dip slope of scree and ribs of rubbly flows and flow breccia. Steep cliffs over 150 m high occur on the southwest side, exposing the

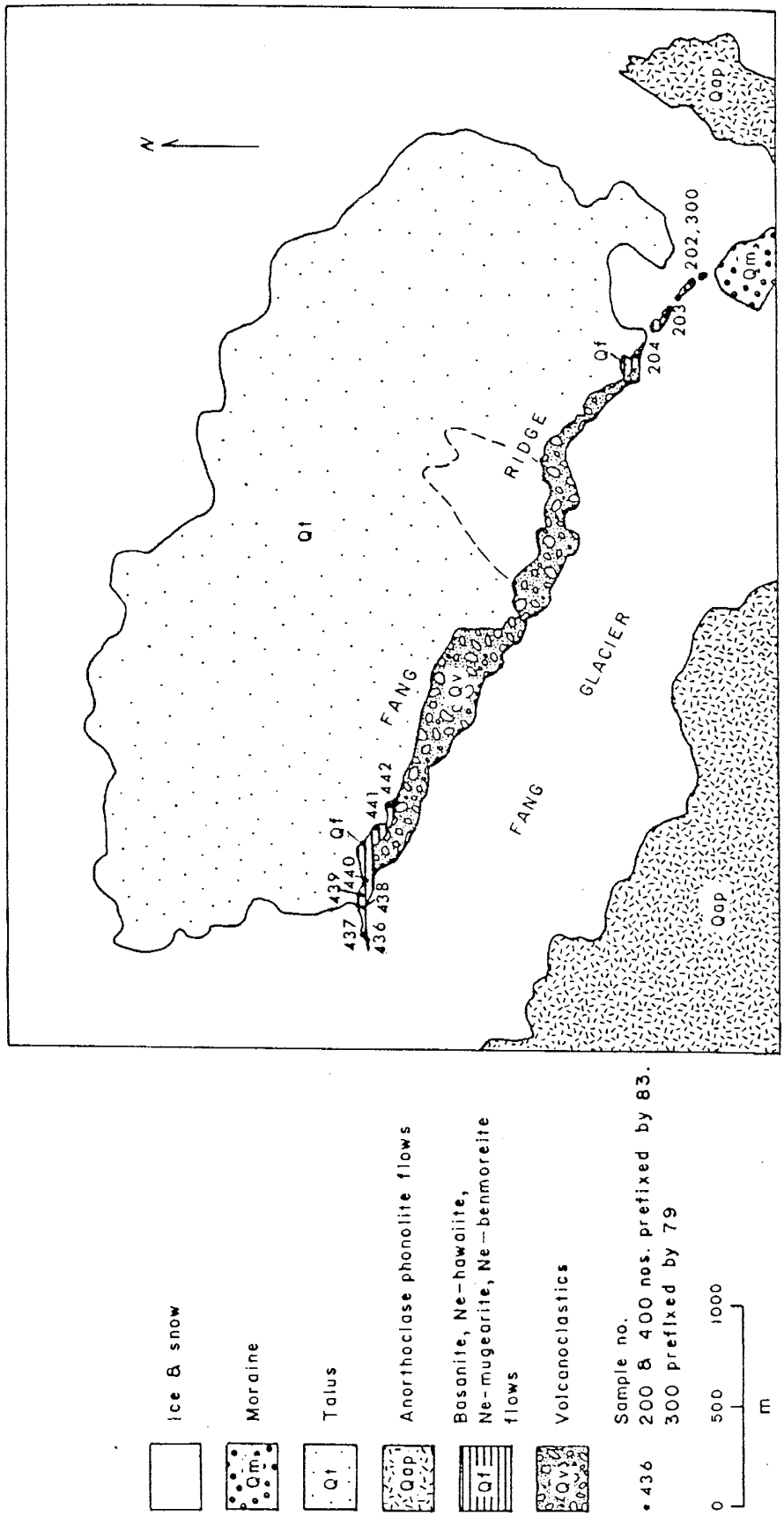

Figure 2.10. Geologic sketch map of Fang Ridge, showing sample locations.

volcanic geology. The lower part of the ridge consists mainly of poorly bedded blocky lapilli tuff. The tuff is probably a lahar deposit, and is intruded by thin dikes and sills.

Scoriaceous lava flows cap the tuff deposit at the northwest and southeast ends of the ridge. The southeastern tip consists of a series of thin flows dipping approximately 30° north and ranging from basanite to Ne-hawaiite to Ne-benmoreite (79300, 83202-04). The flows contain numerous pebble to small boulder-sized volcanic and feldspar-clinopyroxene cumulate inclusions. The northwest end of the ridge is capped by a series of 1/2 to 3 m thick flows dipping 30° to the northwest and interbedded with lahar deposits. The flows have an upward stratigraphic progression from basanite to Ne-mugearite (83436-42).

Fang Ridge is most likely a remnant of an old caldera (Kyle, 1976). K/Ar ages of 0.73 and 0.81 m.y. were obtained from two flows there (Armstrong, 1978), consistent with their stratigraphic positions.

Geologic Evolution of Mt. Erebus

The geologic history of Mt. Erebus is difficult to formulate because of the lack of outcrop, overlapping relationships and age dates. In addition young anorthoclase phonolites from the present summit have K/Ar ages which are

too old (0.55-0.44 m.y.), suggesting excess Ar occurs (Armstrong, 1978). Therefore the timing of events in the summit area is uncertain. The following model of the geologic history of Mt. Erebus is based on known and inferred stratigraphy, geomorphology, and available K/Ar age determinations and paleomagnetic results.

The volcanic activity of Mt. Erebus probably commenced with the deposition of basanite hyaloclastites and pillow lavas on the floor of McMurdo Sound slightly greater than 1 million years ago. Early subaerial activity in the vicinity of Erebus Bay built Ne-hawaiite to Ne-benmoreite cones between 1 m.y. and 0.8 m.y. ago. Minor amounts of microporphyritic benmoreite and phonolite were also erupted. The present volcanic center of Mt. Erebus was active at about the same time. Early activity of this center consisted of basanite and Ne-hawaiite eruptions along a northwest-trending rift at Cape Barne. Between 0.94-0.68 m.y., anorthoclase-phyric Ne-benmoreite and large volumes of anorthoclase phonolite were erupted, building a shield volcano which forms the lower slopes of Mt. Erebus today. Intermediate lavas erupted from a parasitic vent built a cone on top of this shield volcano. This cone collapsed, forming Fang Ridge, c.0.7 m.y. ago. Small parasitic cones at Mt. Cis, Abbott Peak, Bomb Peak, Aurora Glacier and Lewis Bay erupted small volumes of kaersutite-phyric benmoreite and phonolite, and trachyte.

The large volume anorthoclase phonolite eruptions were followed by smaller eruptions after 0.69 m.y., during the Bruhnes normal polarity epoch (McGinnis et al., 1974). These short anorthoclase phonolite flows built a steep summit cone, which collapsed, forming the caldera of the present summit. The caldera was filled by anorthoclase phonolite by 0.15 m.y. Flank eruptions formed Hoopers Shoulder and the Three Sisters Cones. The present summit cone was built during the past 100,000 years. Since its discovery in 1841, the activity of Mt. Erebus has consisted mainly of strombolian eruptions of varying intensity and a permanent convecting anorthoclase phonolite lava lake occupying the Inner Crater of the summit cone (Kyle et al., 1982). This lava lake was buried by a series of large strombolian eruptions beginning in September, 1984, but by December, 1985 a new cycle of activity, marked by the development of a new lava lake, had commenced (Kyle, 1986).

CHAPTER THREE

NOMENCLATURE AND PETROGRAPHY

Nomenclature

Fifty-eight samples representative of the range of lavas on Mt. Erebus were chosen for analysis in this study. Chemical composition and CIPW normative mineralogy were used to classify the samples because the glassy or microcrystalline groundmasses of most made modal classification impossible.

Although the lavas of Mt. Erebus straddle the dividing line between sodic and potassic series in the plot of Na_2O vs. K_2O (Fig. 3.1), the most basic lavas fall in the sodic region, indicating the lavas are sodic in nature. The nomenclature is shown in Figs. 3.2 and 3.3 and is similar to that discussed by Kyle et al. (1979) and Coombs and Wilkinson (1969). The dominant rock types comprising Mt. Erebus form a continuous strongly undersaturated series consisting of basanite, Ne-hawaiite, Ne-mugearite, Ne-benmoreite, and anorthoclase phonolite (Fig. 3.3). The basanite to anorthoclase phonolite series has previously been called the Erebus lineage by Kyle (1976) and will be referred to as such here.

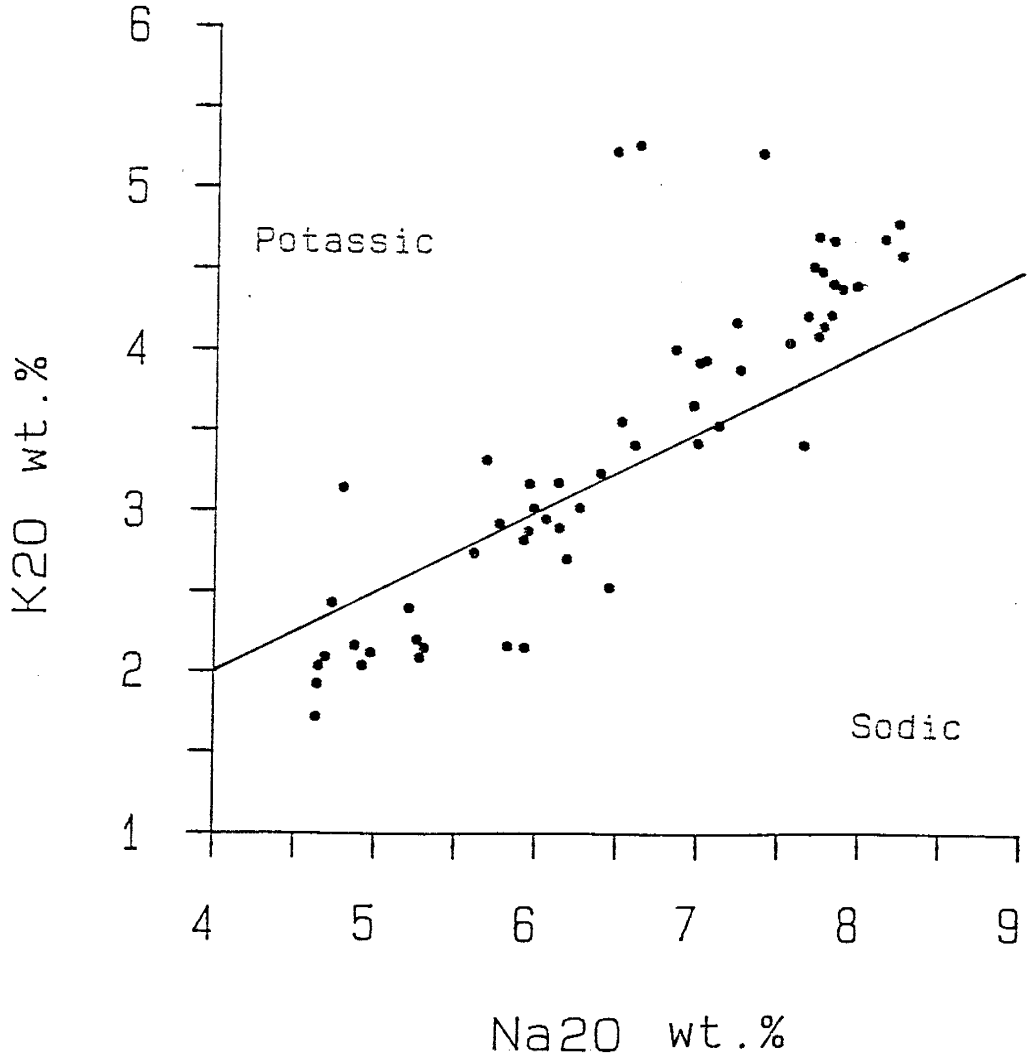

Figure 3.1. Plot of Na_2O against K_2O for Mt. Erebus lavas. The line is drawn through K_2O/Na_2O ratios of 2.0 and is the dividing line between potassic and sodic lineages of MacDonald and Katsura (1964).

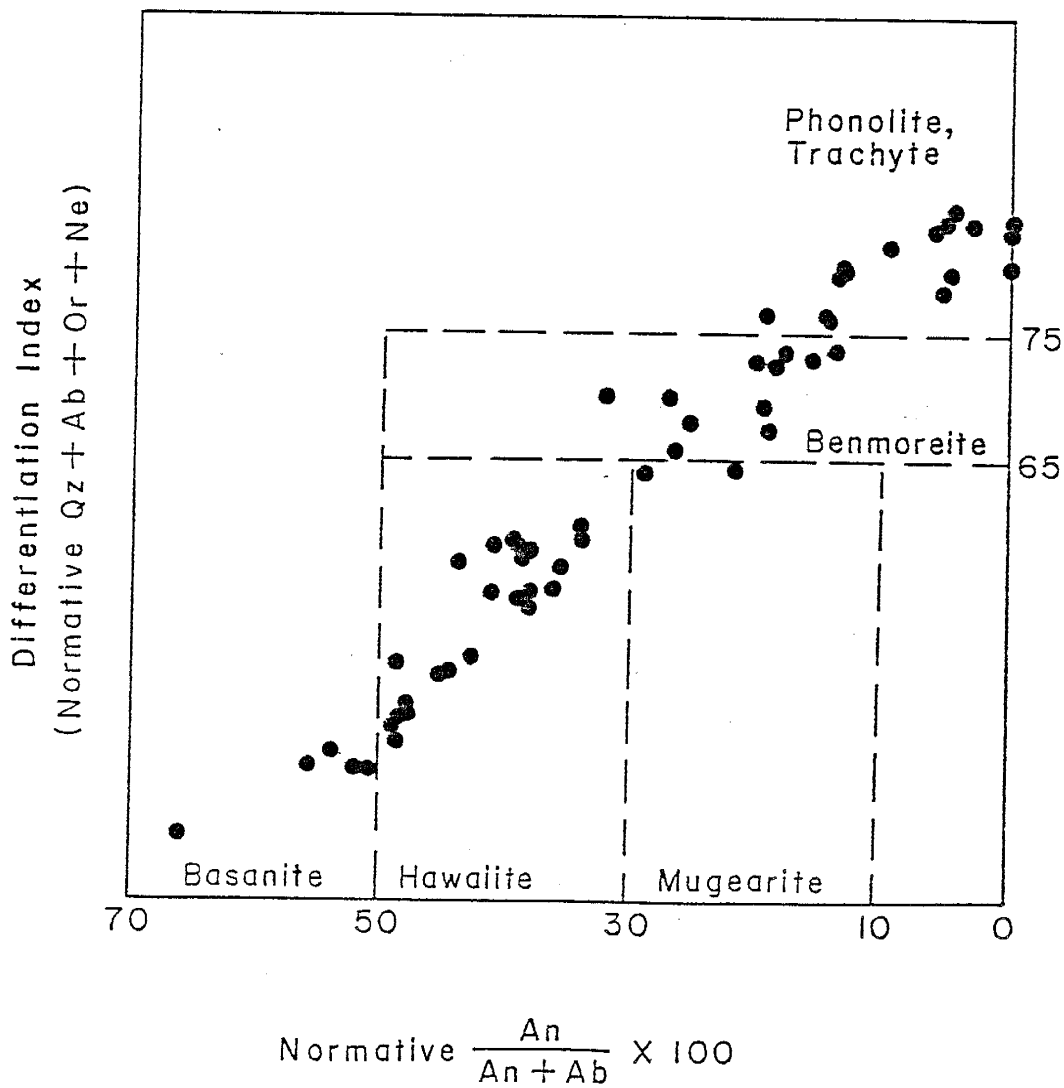

Figure 3.2. Plot of differentiation index against normative plagioclase for samples from Mt. Erebus showing nomenclature. After Coombs and Wilkinson (1969).

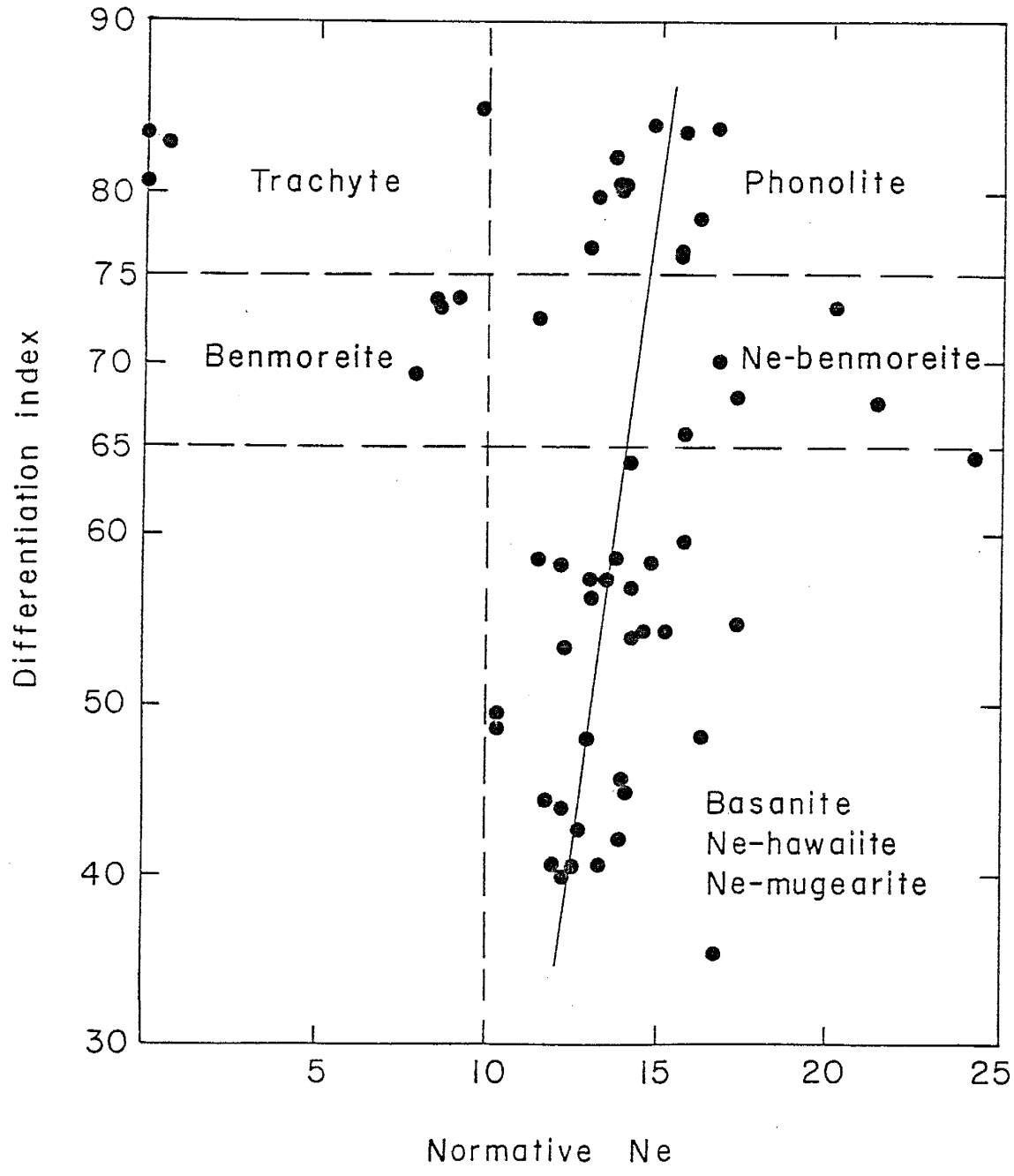

Figure 3.3. Plot of differentiation index against normative Ne for Mt. Erebus lavas showing nomenclature. Line is visually estimated trend of Erebus lineage. After Kyle *et al.* (1979).

Volumetrically insignificant amounts of benmoreite, kaersutite-phyric phonolite (henceforth called kaersutite phonolite) and trachyte also occur on Mt. Erebus. Two trachyte samples are mildly quartz-normative and peralkaline and are classified as comenditic trachyte after the system of MacDonald (1974). One sample (82403) is an anorthoclase-clinopyroxene cumulate inclusion from an anorthoclase phonolite bomb.

A chemical classification recently proposed by the I.U.G.S. Subcommission on the Systematics of Igneous Rocks (Le Maitre, 1984) was not adopted because it is still under discussion. However, the equivalent I.U.G.S. names are given in Appendix A.

Petrography

Generalized summary descriptions of thin section observations made in this study are given here. Detailed petrographic descriptions of the various rock types and individual thin sections are given in Appendix B. Smith (1954) also presents detailed petrographic descriptions of lavas from Mt. Erebus and vicinity.

Basanites

The basanites are finely porphyritic, containing 10-25% seriate glomeroporphyritic phenocrysts of feldspar (bytownite-labradorite), olivine, opaque oxides,

clinopyroxene, and apatite. Feldspar phenocrysts (up to 4 mm) are euhedral and unzoned and may have resorbed cores or embayed, rounded rims. Olivine phenocrysts (up to 1 mm) are euhedral, although a few strongly embayed phenocrysts occur. Clinopyroxene phenocrysts (up to 1.5 mm) are euhedral, discontinuously or oscillatory zoned, and purplish brown in color. Rare colorless cores occur. The groundmass is pilotaxitic and intersertal, containing up to 5% glass and possible interstitial nepheline.

Ne-hawaiites and Ne-mugearites

Some Ne-hawaiites are finely porphyritic, containing 1-20% seriate euhedral phenocrysts $\leq$2 mm of feldspar (labradorite), olivine, opaque oxides, clinopyroxene and apatite. Rare strongly oxidized kaersutite phenocrysts (1 mm) occur in the flow south of Abbott Peak (83453). The groundmass of finely porphyritic Ne-hawaiites is pilotaxitic and intersertal to hyalophitic.

Most of the Ne-hawaiites and Ne-mugearites are coarsely porphyritic. They occur either as feldspar-olivine- or feldspar-clinopyroxene-olivine-phyric types and contain 20-50% seriate, often glomeroporphyritic phenocrysts and microphenocrysts of feldspar (labradorite-andesine), clinopyroxene, olivine, opaque oxides, apatite and rare nepheline (Fig. 3.4). Feldspar phenocrysts (up to 2 cm) are subhedral, oscillatory-zoned and commonly have resorbed

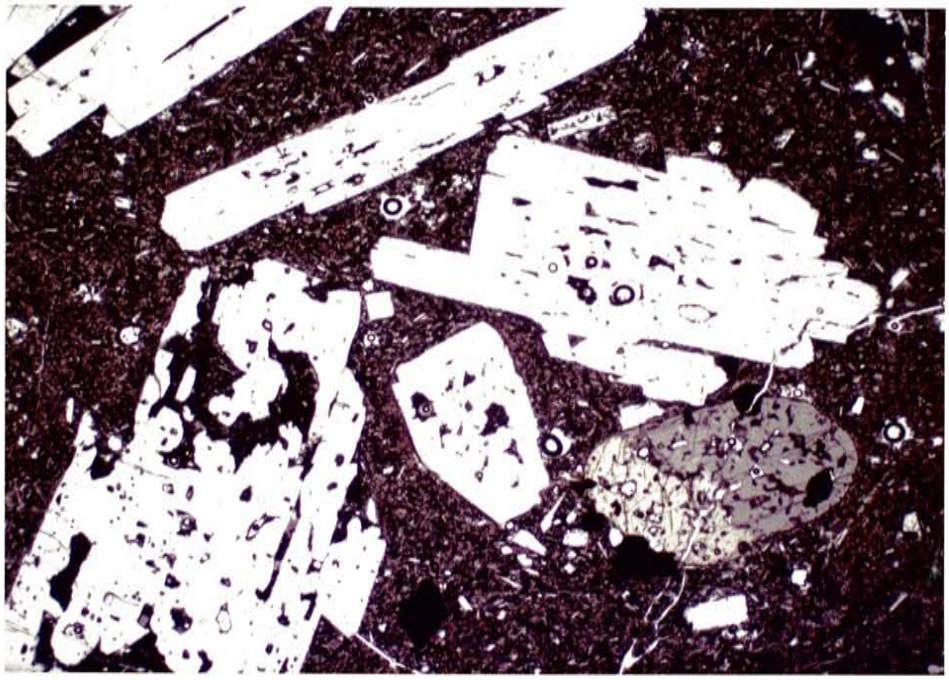

Figure 3.4. Photomicrograph of Ne-hawaiite 83415 showing embayed andesine-labradorite phenocrysts, twinned clinopyroxene phenocryst, and opaque oxides phenocryst. Field of view 7 mm wide.

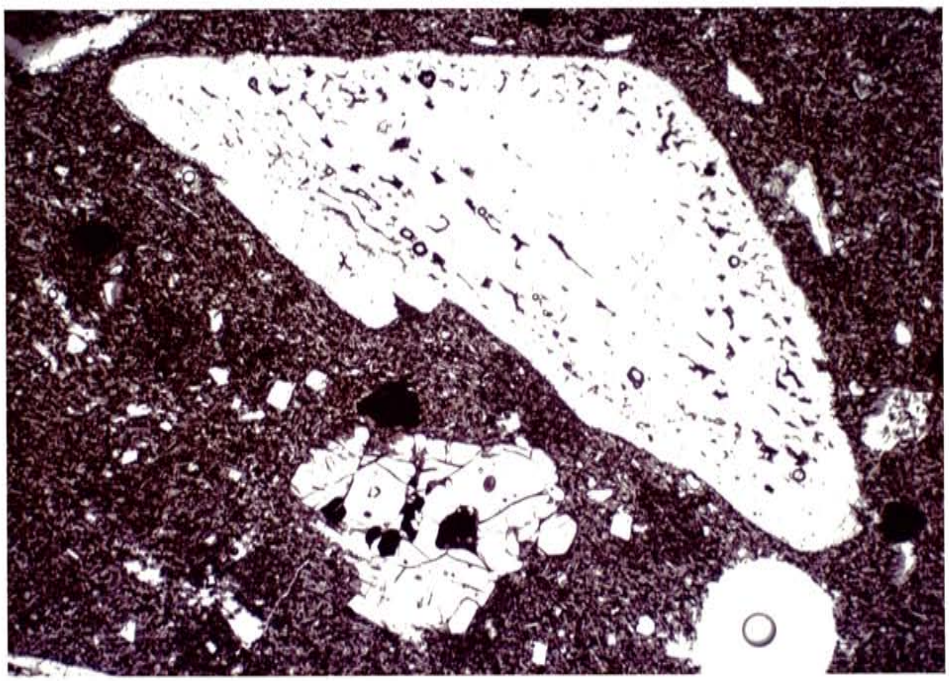

Figure 3.5. Photomicrograph of anorthoclase phonolite 83446. Anorthoclase phenocryst is upper part of photo shows zonal arrangement of glass inclusions. Olivine phenocryst in lower part of photo with opaque oxide and apatite inclusions. Field of view 7 mm wide.

cores and embayed rims. Clinopyroxene phenocrysts (up to 5 mm) are euhedral, purplish brown, oscillatory or discontinuously zoned and slightly embayed. Olivine phenocrysts (up to 4 mm) are subhedral and commonly embayed. Opaque oxides (up to 2 mm) consist of magnetite and rare ilmenite grains and are anhedral and embayed. Blebs of ilmenite (0.02-0.2 mm) and pyrrhotite (0.01 mm) sometimes occur in magnetite phenocrysts. Euhedral apatite phenocrysts occur up to 1 mm. Rare glomeroporphyritic nepheline microphenocrysts <0.5 mm occur moderately altered to feldspar. The groundmass is pilotaxitic and intersertal to hyalophitic. Interstitial alkali feldspar and possibly nepheline occur in some samples. The groundmass of a Ne-mugearite dike (83417) is holocrystalline, consisting of equigranular alkali feldspar and clinopyroxene.

Ne-benmoreites

The Ne-benmoreites are strongly porphyritic, containing 20-50% seriate or hiatal glomeroporphyritic phenocrysts of feldspar (labradorite-andesine), olivine, opaque oxides, clinopyroxene and apatite. Feldspar phenocrysts (up to 2 cm) are subhedral to anhedral and commonly embayed and sieved-textured, with thin discontinuous alkali feldspar rims. Ne-benmoreite AW82015 contains euhedral anorthoclase phenocrysts up to 2 cm. Clinopyroxene phenocrysts (up to 2.5 mm) are pale brown, oscillatory or discontinuously zoned,

subhedral to anhedral and embayed. Olivine occurs up to 2 mm and is usually subhedral and embayed. Rare olivine-augite and olivine-apatite sutured intergrowths occur. Opaque oxides (up to 1 mm) consist of anhedral embayed magnetite, rare ilmenite and rare pyrrhotite blebs (<0.1 mm). The groundmass ranges from intersertal and pilotaxitic to hyalophitic, containing up to 85% glass. Some samples contain interstitial alkali feldspar and possibly nepheline.

Anorthoclase phonolites

The anorthoclase phonolites contain 30-60% seriate phenocrysts of anorthoclase, olivine, opaque oxides, clinopyroxene, apatite, and rare nepheline (Fig. 3.5). Anorthoclase phenocrysts (up to 3 cm) are euhedral and unzoned except for thin discontinuous sanidine overgrowths. Olivine (up to 1.5 mm), clinopyroxene (up to 2.5 mm), and opaque oxide (1 mm) phenocrysts are anhedral to subhedral and sometimes embayed. Pyrrhotite microphenocrysts (0.2-0.5 mm) occur, and pyrrhotite blebs (<0.1 mm) are common in the groundmass and phenocrysts.

Samples from the young flows on the upper slopes of Mt. Erebus are extremely vesicular. Glass inclusions are common in phenocrysts. The groundmass is glassy and may be flow-banded or pilotaxitic and contain minor amounts of sodalite. Samples from older flows along the coast have hypocrystalline, intersertal, felty-textured groundmasses

consisting of alkali feldspar, opaque oxides and clinopyroxene. Olivine, kaersutite, sodalite, aenigmatite, biotite, sodic amphibole, apatite and possibly nepheline are minor to accessory groundmass phases in some samples. In a fine grained anorthoclase phonolite sample from Cape Evans (83400), phenocrysts and groundmass clinopyroxene are zoned from pale brown or purplish brown cores to green aegirine-augite rims, sometimes overgrown by bluish green pyroxene.

Benmoreites

The benmoreites usually are microporphyritic, holocrystalline, and trachytic-textured. A hypocrystalline porphyritic type occurs on Abbott Peak (81002). Benmoreites with trachytic textures contain 10-20% subhedral to euhedral glomeroporphyritic microphenocrysts (<1mm) of feldspar (andesine-oligoclase), opaque oxides and olivine. Rare microphenocrysts of apatite, clinopyroxene and kaersutite also occur. Occasional xenocrysts (?) (~1 mm) of corroded, resorbed olivine, pale green pyroxene partly altered to kaersutite, and corroded, sieved-textured feldspar (labradorite-andesine) occur. The trachytic-textured groundmass is composed of alkali feldspar, opaque oxides and olivine.

The porphyritic benmoreite (81002) contains 60% seriate phenocrysts of feldspar andesine, opaque oxides, clinopyroxene, kaersutite, olivine, and apatite. Feldspar phenocrysts (up to 4 mm) are subhedral, heavily sieved and embayed, and have alkali feldspar rims. Clinopyroxene phenocrysts (up to 1 mm) are euhedral and pale green to brown. Kaersutite phenocrysts (up to 1.5 mm) are subhedral and partly oxidized. The groundmass is hyalophitic and pilotaxitic.

Kaersutite phonolites

The kaersutite phonolites occur as a weakly porphyritic, trachytic type at Inaccessible Island and a moderately porphyritic type at Bomb Peak. The trachytic-textured type contains 3-10% seriate phenocrysts of alkali feldspar, opaque oxides, kaersutite and accessory olivine and clinopyroxene. Feldspar ($\leq$3 mm) is euhedral and sometimes has corroded resorbed andesine cores. Opaque oxides ($\leq$1 mm) are generaly subhedral and embayed. Kaersutite ($\leq$2.5 mm) is subhedral and extensively oxidized. Olivine and clinopyroxene phenocrysts ($\leq$2 mm) are usually anhedral, embayed and resorbed. The groundmass is holocrystalline and trachytic-textured, consisting predominantly of alkali feldspar.

The porphyritic kaersutite phonolites contain 10-15% phenocrysts and microphenocrysts of feldspar, kaersutite, opaque oxides, and accessory clinopyroxene, olivine and apatite. Feldspar ($\leq$1 cm) is subhedral to euhedral, and zoned discontinuously from embayed resorbed labradorite cores to andesine or oligoclase rims. Kaersutite ($\leq$2 mm) is subhedral to euhedral, embayed, and weakly to extensively oxidized. Opaque oxide microphenocrysts ($\leq$0.5 mm) are anhedral, embayed, and contain pyrrhotite inclusions. Clinopyroxene ($\leq$1 mm) is greenish brown, and euhedral. Olivine ($\leq$1 mm) is subhedral and embayed. The groundmass is hyalophitic and pilotaxitic, consisting predominantly of oligoclase and 15-30% leucite.

Trachytes

The trachytes and comenditic trachytes contain rare phenocrysts (<3mm) of alkali feldspar, bright green pyroxene, and opaque oxides (Fig. 3.6). Occasional corroded microxenocrysts (?) of olivine occur. The groundmass is trachytic-textured, sometimes flow-banded and consists of alkali feldspar, pale green clinopyroxene, opaque oxides, and up to 40% glass.

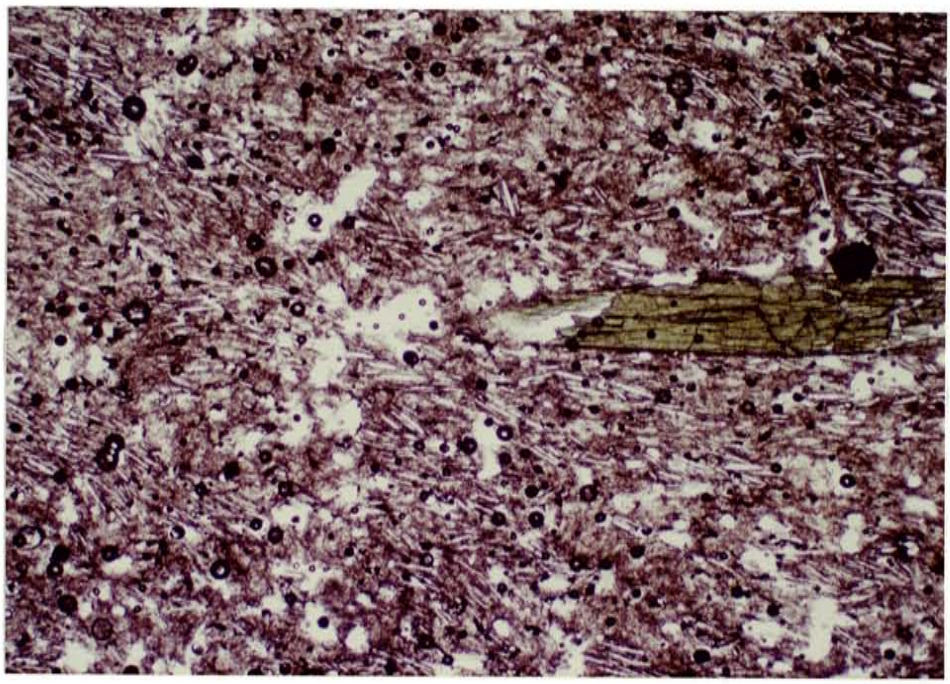

Figure 3.6. Photomicrograph of comenditic trachyte 83451. Aegirine augite phenocryst in center. Groundmass is mostly glass and trachytic-textured feldspar microlites. Field of view 7 mm.

Xenoliths

Inclusions ranging from <1 cm to 30 cm in size were found in the samples from Bomb Peak, the Dellbridge Islands and Turk's Head Bay. 82431 is an anorthoclase phonolite xenolith in an anorthoclase phonolite bomb from Bomb Peak. It contains 17% seriate phenocrysts of anorthoclase ($\leq$1 cm) with andesine cores partly altered to leucite, 2% opaque oxides ($\leq$2 mm) altered to magnetite and ilmenite and 1% clinopyroxene-opaque oxide aggregates (up to 1mm), which possibly are altered olivine phenocrysts. The groundmass consists of alkali feldspar, yellowish-green clinopyroxene, opaque oxides and patches of yellowish-green glass up to 6 mm in diameter which form c.10% of the sample. This xenolith has a texture suggesting it is hypabyssal in origin, a fine grained equivalent of syenite. It may be from a dike or the center of a thick flow, and has been metasomatically altered by an alkali-rich fluid.

82403 is an anorthoclase-clinopyroxene cumulate xenolith in an anorthoclase phonolite bomb from Bomb Peak. It is seriate porphyritic, weakly layered, and consists of anorthoclase (70%), clinopyroxene (15%), opaque oxides (7%), olivine (2%), apatite (1%) and interstitial kaersutite (5%). Anorthoclase (up to 2cm) exhibits undulatory extinction and annealed contacts. Clinopyroxene phenocrysts (up to 2.5 mm) are partly altered to kaersutite. Magnetite phenocrysts (up

to 1mm) are partly altered to biotite. Partially altered pyrrhotite phenocrysts (up to 1mm) occur. This cumulate may have formed at the bottom of an anorthoclase phonolite magma chamber.

Microxenoliths <1 cm in size with allotriomorphic granular fine grained textures were found in thin section in a few Ne-benmoreite and Ne-hawaiite samples, and may be cumulate in origin. These microxenoliths have the following mineralogies:

feldspar-diopsidic augite-opaque oxide-apatite-nepheline(?)

feldspar-opaque oxide-olivine

opaque oxide-sodalite-diopside

Summary

A generalized summary of the petrography of Mt. Erebus lavas is presented in Table 3.1. The lavas of Mt. Erebus are dominantly strongly undersaturated and coarsely porphyritic with a similar phenocryst assemblage consisting mainly of olivine, clinopyroxene, opaque oxides, feldspar and apatite. The groundmass is pilotaxitic. These lavas range in composition from basanite to anorthoclase phonolite and are termed the Erebus lineage. Minor volumes of microporphyritic, trachytic-textured, sometimes kaersutite-phyric benmoreites, phonolites and trachytes also occur on Mt. Erebus, distinctly different in petrography

from the Erebus lineage lavas.

Table 3.1. Generalized petrographic summary of Mt. Erebus lavas

Rock type	Texture	Mineralogy							Groundmass
		Ol	Cpx	Kaer	Op	Fsp	Ap	Fspth	
Basanite	fp(10-25)	p,x	p		p	p	p	g	p,i
Ne-hawaiite	fp(1-20) or cp(20-50)	p,po	r-p,po	r,po,x?	p	p	p	r-g	i,p or gl-h 2c,2o
Ne-mugearite	cp(20-30)	p,po	p,po		p	p	p	g	i,p,2o
Ne-benmoreite	cp(20-50)	p,po,x	r-p		p	p	p	g	i,p or gl
Anorthoclase phonolite	cp(30-60)	p	p	g	p	p	p	r-g	i,p or gl-h,c
Benmoreite	mp(10-20) or p(60)	p,po,x	r-p	r-p,po	p	p-x	r		t or gl,c
Kaersutite phonolite	mp(3-10) or p(10-15)	r-p,x	r-g	r-p, po-co	r-p	p,x	r	g	t or h-i,p
Trachytes	mp(< 5)	g-x	p		p	p			t

Abbreviations

Texture: p-porphyritic; mp-microporphyritic; fp-finely porphyritic; cp-coarsely porphyritic. % phenocrysts to nearest 5% in parentheses.

Mineralogy: Ol-olivine; Cpx-clinopyroxene; Kaer-kaersutite; Op-opaque oxides; Fsp-feldspar; Ap-apatite; Fspth-feldspathoids; p-present (>1%); r-rare (<1%); x-xenocrystic; po-partially oxidized; co-completely oxidized; g-groundmass only.

Groundmass: i-intersertal; p-pilotaxitic; gl-glassy; h-hyalophitic; c-cryptocrystalline; t-trachytic; 2c-secondary carbonate; 2o-secondary oxidation.

CHAPTER FOUR

MINERAL CHEMISTRY

Introduction

Analyses of mineral phases in the lavas of Mt. Erebus were made by electron microprobe at the University of New Mexico. The analytical procedures are described in Appendix C. Thirteen representative samples from Mt. Erebus were examined:

83435: basanite

79300: evolved basanite

83415: Ne-hawaiite

AW82038: Ne-hawaiite

83417: Ne-mugearite

25748: Ne-benmoreite

82403: anorthoclase-pyroxene cumulate xenolith

83448: anorthoclase phonolite flow

83400: evolved anorthoclase phonolite flow

80020: evolved anorthoclase phonolite flow

82431: anorthoclase phonolite xenolith

AW82023: benmoreite

82404: kaersutite phonolite

A complete listing of the analyses appears in Appendix C. Additional microprobe analyses of 25748 made by Dr. Philip Kyle at Victoria University of Wellington are included in

this section.

Olivine

Olivine is an important phase in every rock type from Mt. Erebus except kaersutite phonolite. Olivines exhibit continuous variation in atomic % Mg from 88 in basanite 83435 to 43 in benmoreite AW82032 (Fig. 4.1B). The only significant zoning is seen in a phenocryst in 83435, which is discontinuously zoned from a corroded core of Mg_{88} to a rim of Mg_{81}. An olivine phenocrysts in Ne-benmoreite 25748 has a composition similar to phenocrysts in basanite 79300 and is probably a xenocryst. Olivine ranges from Mg_{58-51} in the anorthoclase phonolite samples, similar to the composition of olivines in recent anorthoclase phonolite ejecta from Mt. Erebus (Kyle, 1977). Olivines in the benmoreite range from Mg_{49-43}.

CaO and MnO variations are shown in plots against FeOT (total Fe analyzed as FeO), an indicator of the degree of olivine evolution (Fig. 4.2). CaO is low in the high Mg phenocryst core in 83435, suggesting the phenocryst core crystallized at higher pressure than the olivines in the other lavas from Mt. Erebus (Stormer, 1973). The corroded nature of this core is probably due to disequilibrium at lower pressure. The relatively constant CaO content in olivines from the rest of the samples may reflect stable pressure conditions.

Figure 4.1. A. Variation of Ca, Mg and (Fe^{2+} + Mn) (all atomic % after charge-balancing) in pyroxenes from Mt. Erebus lavas. Field of Erebus lineage circled, expanded in Fig. 4.4.

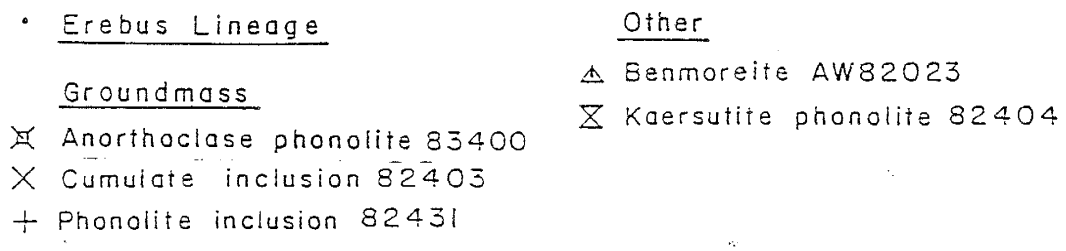

Fig. 4.1. B. Variation of atomic % Mg and Fe in olivines in Mt. Erebus lavas.

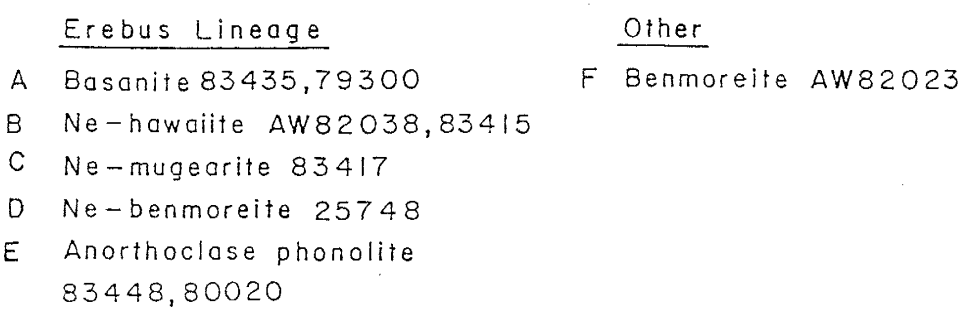

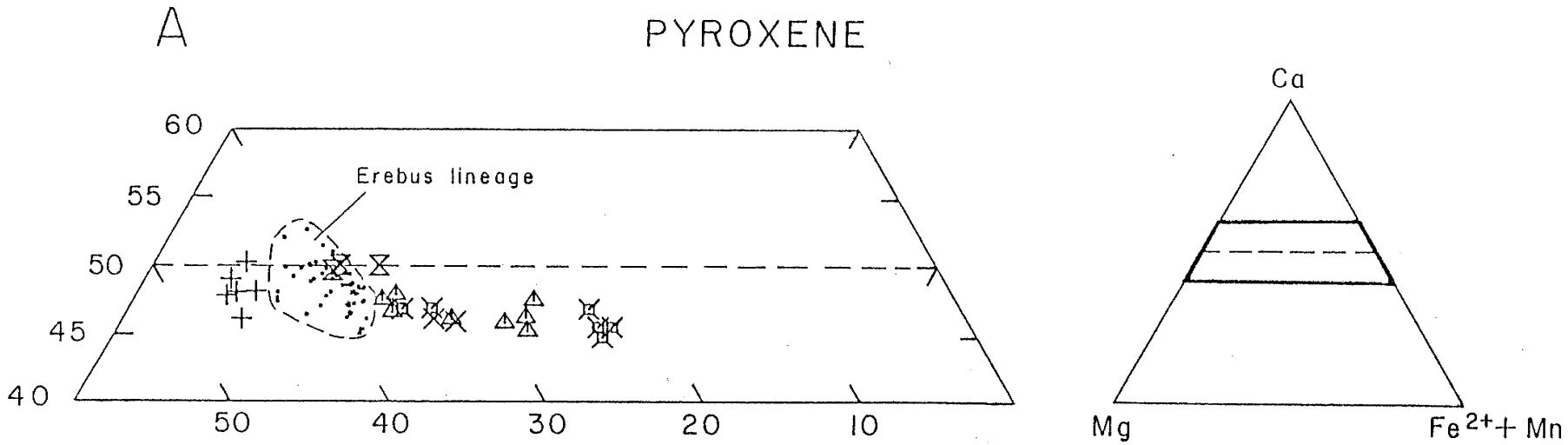
A
PYROXENE
60
55
50
45
40
Erebus lineage
50
40
30
20
10
Ca
Mg
Fe2+ + Mn

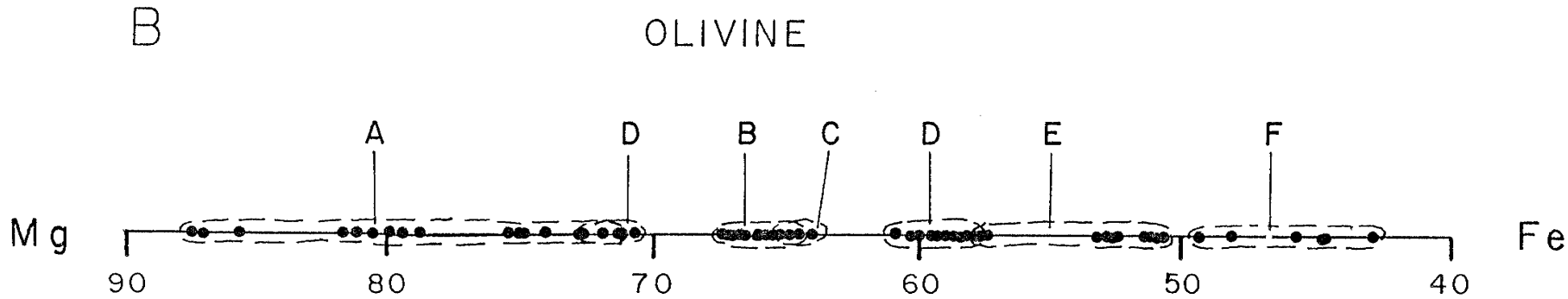
B
OLIVINE
A
D
B
C
D
E
F
Mg
Fe
90
80
70
60
50
40

Fig 4.2. Variation of CaO and MnO against FeOT in olivines from Mt. Erebus lavas. Values in wt.%.

Erebus Lineage

- Basanite 83435,79300
- Ne-hawaiite AW82038,83415
- Ne-mugearite 83417
- Ne-benmoreite 25748
- Anorthoclase phonolite 83448,80020

Other

- Benmoreite AW82023
- Kaersutite phonolite 82404
- Cumulate inclusion 82403
- Phonolite inclusion 82431

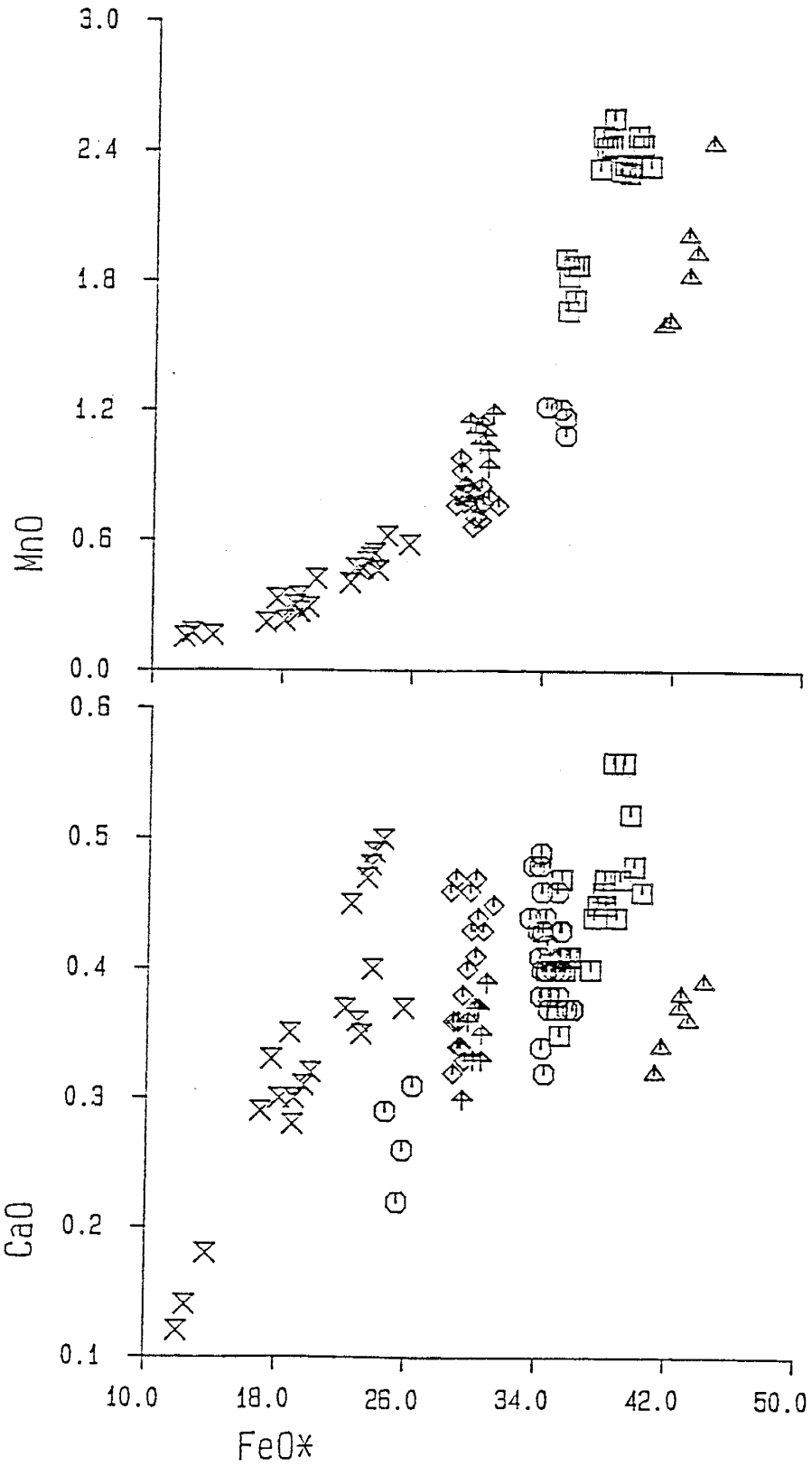
3.0
2.4
1.8
1.2
0.6
0.0
MnO
0.6
0.5
0.4
0.3
0.2
0.1
CaO
10.0
18.0
26.0
34.0
42.0
50.0
FeO*

MnO increases hyperbolically with increasing olivine evolution. The increase is most likely due to increasing silica activity in the melt, and, less importantly, to decreasing temperature (Watson, 1977; Takahashi, 1978; Mysen, 1983).

The occurrence of olivine in each rock type of the Erebus lineage (basanite through anorthoclase phonolite) suggests continuous crystallization, and the lack of zoning indicates that each type of magma crystallized its own unique olivine. This feature was also observed in olivines from the Trans Pecos alkaline magmatic province (Barker and Hodges, 1977). MnO exhibits a smooth, continuous trend in olivines from the Erebus lineage, suggesting a single line of descent for these lavas. Although olivines in benmoreite AW82023 have similar MnO and CaO ranges as those in anorthoclase phonolite, the former have a distinctly higher FeO content and are similar to olivines in alkali basalt-trachyte series lavas (Coombs and Wilkinson, 1969). This suggests that the benmoreite belongs to a different evolutionary trend. It may have crystallized from a relatively reduced, anhydrous melt, enriched in Fe. This is because high oxygen fugacity favors the crystallization of magnetite, impoverishing the magma in Fe relative to Mg (Coombs and Wilkinson, 1969).

Pyroxene

Pyroxenes occur as phenocryst, microphenocryst or groundmass phases in all the rock types from Mt. Erebus. Microprobe analyses of FeOT in pyroxenes was partitioned between Fe_2O_3 and FeO using the iterative charge balancing procedure of Papike et al. (1974). The number of cations in each analysis were calculated based on 6 oxygens per formula unit.

Ca, Mg, Fe

The trends of the three major pyroxene endmembers Ca, Mg and (Fe^{2+}+Mn) (all atomic %) of charge-balanced analyses are shown in Fig. 4.1A. Some pyroxenes plot over the CaMg-CaFe boundary because of their high Al and consequently high Ca Tschermaks molecule content. Theoretical endmembers were calculated in representative analyses using the scheme of Kyle (in press) to give a more realistic approximation of the pyroxene compositions (Table 4.1; Fig. 4.3).

The pyroxenes are all clinopyroxenes which trend in composition from diopside to ferrosalite and ferroaugite, typical of pyroxene in alkaline igneous rocks (Wilkinson, 1956; Gibb, 1973). The clinopyroxenes from the Erebus lineage (basanites, Ne-hawaiites, Ne-mugearites, Ne-benmoreites and anorthoclase phonolites), apart from evolved phenocryst edges and groundmass clinopyroxenes in

Table 4.1. Representative clinopyroxene analyses in Mt. Erebus lavas recalculated according to the scheme of Kyle (in press).

Sample/ grain	83435-6	83435-15	83415-5	83417-7	25748-9
SiO2	43.34	44.89	47.70	49.99	49.40
TiO2	5.15	4.36	3.39	2.54	2.29
Al2O3	11.16	8.72	5.85	4.80	4.44
Fe2O3	2.82	3.70	1.26	1.34	2.23
FeO	4.58	5.11	6.54	7.85	6.54
MnO	--	0.16	0.21	0.39	0.49
MgO	11.77	12.62	12.41	12.61	12.10
CaO	22.17	21.51	21.65	20.79	21.80
Na2O	0.54	0.49	0.75	1.01	0.99
Total	101.54	101.56	99.76	101.32	100.28
Recalculated pyroxene endmembers					
CTTs	14.3	12.1	9.5	7.1	6.4
Ac	3.9	3.5	5.4	7.3	7.2
CFTs	2.0	3.4	0.0	0.0	0.0
CTs	9.9	6.9	3.4	3.5	3.4
Wo	30.6	31.3	37.1	36.1	38.7
En	32.3	34.7	34.7	35.0	33.7
Fs	7.1	8.2	9.7	11.1	10.6

Sample/ grain	83448-22	83400-48	82431-18	83400-44	82403-5
SiO2	50.00	50.72	50.05	50.52	52.06
TiO2	1.84	1.52	1.64	1.21	0.38
Al2O3	3.69	2.96	4.68	1.10	1.14
Fe2O3	2.13	0.76	4.19	0.69	0.81
FeO	7.37	9.42	3.31	15.85	12.04
MnO	0.54	0.76	0.73	0.96	0.83
MgO	12.44	11.69	13.49	7.35	11.12
CaO	20.89	21.39	20.38	19.52	21.70
Na2O	0.99	0.77	1.53	1.41	0.45
K2O	--	0.02	0.03	0.03	--
Total	99.88	100.01	100.03	98.65	100.53
Recalculated pyroxene endmembers					
CTTs	5.2	4.3	4.6	2.6	1.1
NT	--	--	--	2.0	--
Ac	7.2	5.7	11.1	9.0	3.3
CFTs	--	--	0.3	--	--
CTs	3.0	2.3	5.6	--	1.5
Wo	37.9	39.9	35.1	40.4	42.7
En	34.9	32.9	37.2	21.6	31.4
Fs	11.8	14.8	6.3	24.3	19.9

Table 4.1 (cont.)

Sample/ grain	AW82023-3	82404-11
SiO2	51.07	50.58
TiO2	0.86	1.56
Al2O3	2.03	3.18
Fe2O3	1.04	1.68
FeO	14.29	8.05
MnO	0.89	0.40
MgO	9.34	11.75
CaO	21.35	22.99
Na2O	0.57	0.65
K2O	--	0.02
Total	101.44	100.86
Recalculated pyroxene endmembers		
CTTs	2.5	4.4
Ac	4.2	4.7
CTs	2.1	2.6
Wo	41.2	42.5
En	26.5	32.7
Fs	23.5	13.2

Explantion
CTTs: Ca-Ti Tschermak ($CaTiAl_2O_6$)
NT: Na-Ti pyroxene ($NaTi_{.5}(Fe^{2+}, Mg)_{.5}Si_2O_6$)
Ac: Acmite ($NaFe^{3+}Si_2O_6$)
CFTs: Ca-Fe Tschermak ($CaFe^{3+}{}_2SiO_6$)
CTs: Ca Tschermak ($CaAl_2SiO_6$)
Wo: Wollastonite ($CaSiO_3$)
En: Enstatite ($MgSiO_3$)
Fs: Ferrosillite ($(Fe, Mn)^{2+}SiO_3$)

83435: basanite
83415: Ne-hawaiite
83417: Ne-mugearite
25748: Ne-benmoreite
83448, 83400: anorthoclase phonolite
82431: phonolite xenolith
82403: anorthoclase-clinopyroxene cumulate xenolith
AW82023: benmoreite
82404: kaersutite phonolite

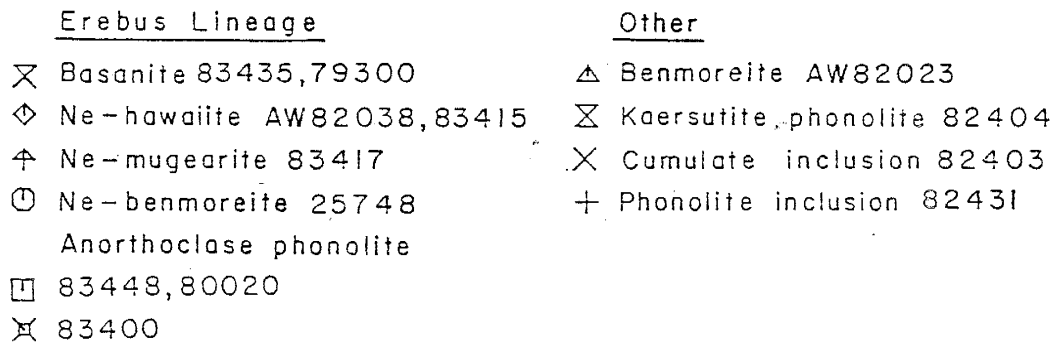
Erebus Lineage
Basanite 83435,79300
Ne-hawaiite AW82038,83415
Ne-mugearite 83417
Ne-benmoreite 25748
Anorthoclase phonolite
83448,80020
83400
Other
Benmoreite AW82023
Kaersutite phonolite 82404
Cumulate inclusion 82403
Phonolite inclusion 82431

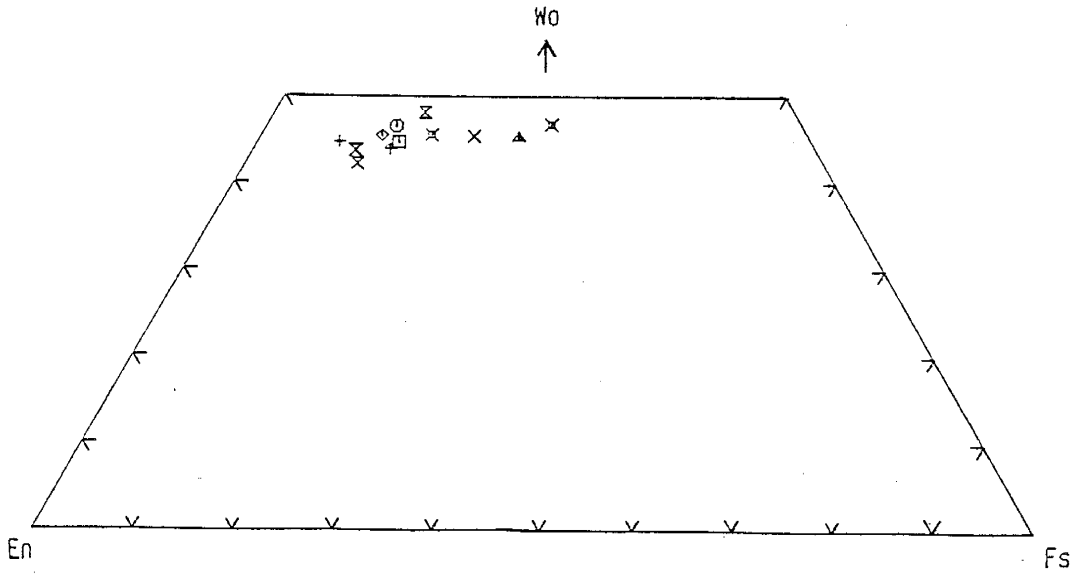

Figure 4.3. Recalculated Wo, En and Fs variation in selected pyroxenes from Mt. Erebus lavas (Table 4.1).

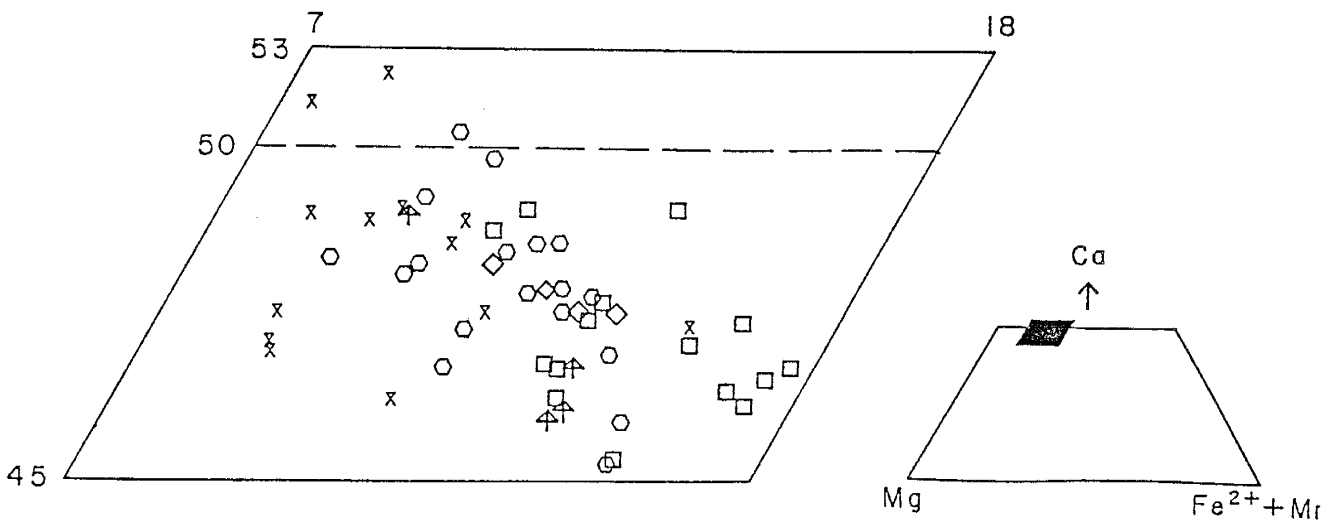

Figure 4.4. Variation of Ca, Mg, and (Fe^{2+}+Mn) (atomic % after charge-balancing) in clinopyroxenes of Erebus lineage lavas. Enlargement of Figure 4.1.

some anorthoclase phonolite samples, show little variation (En_{44-51}) (Fig. 4.4). They plot in the vicinity of the diopside-salite join, have overlapping compositional ranges in the different rock types and show a slight increase in (Fe^{2+}+Mn) with increasing sample differentiation.

Zoning is greatest in phenocrysts from basanite 83435 and Ne-benmoreite 25748. Phenocrysts in 83435 are oscillatory zoned and increase in Mg from core to rim. One phenocrysts has a colorless, corroded core with anomalously high Fe^{2+}, Mn, Na, and K, and low Mg. Groundmass clinopyroxenes and one phenocryst in 83435 are enriched in Ca. Clinopyroxenes from the Ne-hawaiite, Ne-mugearite and Ne-benmoreite show increasing (Fe^{2+}+Mn) and decreasing Ca from core to rim. Phenocrysts in 25748 are normal or oscillatory zoned, and the edges are sometimes enriched in Ca. The composition of clinopyroxenes in the anorthoclase phonolites are similar to clinopyroxenes in recently erupted anorthoclase phonolite lava bombs from Mt. Erebus (Kyle, 1977). Phenocrysts in the kaersutite phonolite are generally higher in Ca than phenocrysts in anorthoclase phonolites. Groundmass clinopyroxenes are generally higher in (Fe^{2+}+Mn) and Ca than phenocrysts in all the samples.

Evolved rims on clinopyroxene phenocrysts in the anorthoclase-pyroxene cumulate are enriched in (Fe^{2+}+Mn) and slightly depleted in Ca (Fig. 4.1). The groundmass

clinopyroxene in anorthoclase phonolite 83400 is continuously zoned from $(Fe^{2+}+Mn)_{19-31}$. Clinopyroxenes in the benmoreite range from $(Fe^{2+}+Mn)_{21-26}$. Groundmass clinopyroxenes in anorthoclase phonolite xenolith 82431 are high in Mg (46-44).

The high Ca content of the clinopyroxenes is most likely due to the early crystallization of olivine, enriching the melt in Ca (Wilkinson, 1956). The lack of significant $(Fe^{2+}+Mn)$ variation indicates relatively constant Fe^{2+}, Fe^{3+} and oxygen fugacity during differentiation of the magma, probably buffered by concomittant olivine and magnetite crystallization according to the reaction

$$3Fe_2SiO_4+O_2 \iff 2Fe_3O_4+3SiO_2$$

(Nash and Wilkinson, 1970; Veiten, 1980; Gibb, 1973). $(Fe^{2+}+Mn)$ enrichment in evolved rims and groundmass clinopyroxenes is most likely the result of $(Fe^{2+}+Mn)$ enrichment in the late stages of crystallization of the lava due to olivine crystallization. The $(Fe^{2+}+Mn)$-rich clinopyroxenes in the benmoreite suggests they crystallized from a relatively Fe-enriched, reduced magma.

The relatively Fe^{2+} and Na-rich core in basanite 83435 is similar in composition to clinopyroxene phenocrysts in anorthoclase phonolites, suggesting it is a xenocryst from an evolved magma. Similar greenish fassaitic augite cores

are observed in clinopyroxene phenocrysts in basanites at other locations (Brooks and Printzlau, 1978; Kyle, 1981b; Duda and Schmincke, 1985). Duda and Schmincke (1985) suggest these Fe and Na-rich cores crystallize from evolved magmas, formed by differentiation of primitive basanite magma in small magma chambers at the mantle/crust boundary. Pulses of fresh basanite magma mix with the evolved magma, entraining the phenocrysts.

The enrichment of Ca in phenocryst edges and groundmass clinopyroxenes may be the result of higher Ca in the late stage liquid because of the crystallization of sodic groundmass feldspar (Gibb, 1973). It also may be due to increased solubility of Ca-Ti Tschermaks ($CaTiAl_2O_6$) in clinopyroxenes at lower pressures (Yagi and Onuma, 1967).

Ti, Al

Ti and Al are plotted against Mg index, an indicator of clinopyroxene differentiation, in Fig. 4.5. Ti is high and decreases slightly with increasing sample differentiation in clinopyroxenes in Erebus lineage lavas. Most of the variation occurs in the basanite and Ne-hawaiite samples, in which Ti is enriched in phenocryst edges and groundmass clinopyroxenes. Clinopyroxenes from the kaersutite phonolite and benmoreite and evolved phenocryst edges and groundmass clinopyroxenes from the anorthoclase phonolites have low Ti concentrations.

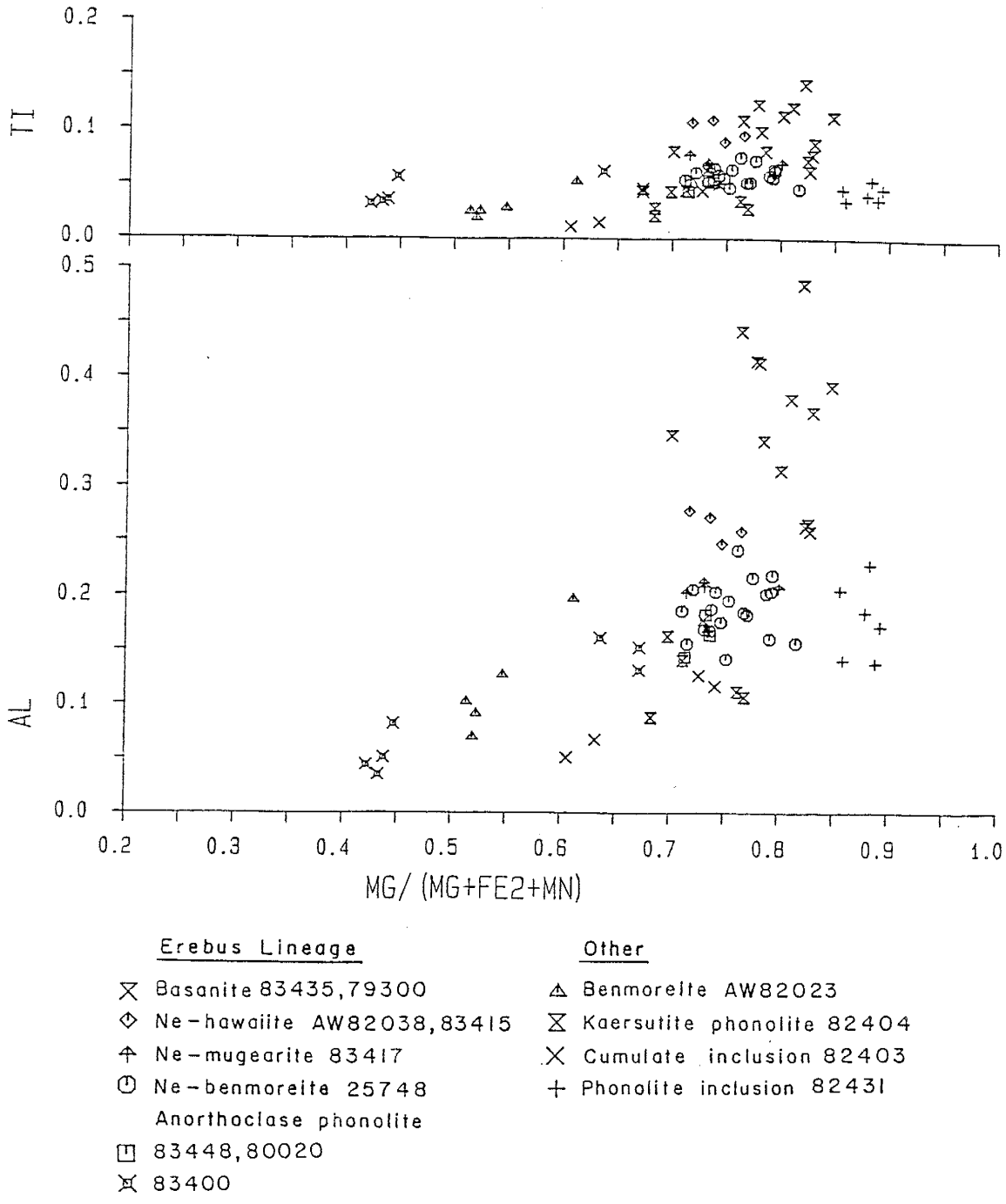

Figure 4.5. Variation of Ti and Al against Mg index (all atomic proportions after charge-balancing) for pyroxenes from Mt. Erebus lavas.

Al shows a larger range than Ti and also decreases in the clinopyroxenes with increasing Fe enrichment. Most of the variation occurs in basanite 83435, in which Al is oscillatory-zoned but generally decreases from cores to rims. Groundmass clinopyroxenes in 83435 have intermediate Al contents. Al oscillates and sometimes increases from cores to rims in clinopyroxenes from Ne-hawaiite, Ne-mugearite and Ne-benmoreite samples. In the anorthoclase phonolites, Al increases from phenocryst cores to rims and is depleted in evolved phenocryst edges and groundmass clinopyroxenes. Clinopyroxenes from the kaersutite phonolite and benmoreite generally have lower Al concentrations than the phenocrysts in the Erebus lineage.

Ti and Al concentrations have a strong correlation in the clinopyroxenes. This fits with Yagi and Onuma's (1967) conclusion that Ti and Al occur primarily as components of Ca-Ti Tschermaks ($CaTiAl_2O_6$) and Ca Tschermaks ($CaAl_2SiO_6$) in clinopyroxenes from alkaline rocks. The decreasing Al and Ti concentrations with differentiation probably reflects rising Si and declining Ti and Al activities in the melt due to the concommittant crystallization of clinopyroxene, Fe-Ti oxides and plagioclase (Gibb, 1973; Kyle, 1981b).

Some of the decline in Al, particularly in the basanite clinopyroxenes, is probably due to declining pressure and, consequently, decreasing solubility of Ca Tschermaks in

clinopyroxenes (Aoki, 1968). Higher Ti and Al in rims and groundmass clinopyroxenes in some samples may be due to enhanced solubility of Ca-Ti Tschermaks at lower pressures (Aoki, 1968). The lower Ti and Al in clinopyroxenes from benmoreite and kaersutite phonolite suggests that they crystallized at a lower pressure than the clinopyroxenes in the anorthoclase phonolite magmas.

Na

Na variation in clinopyroxenes is primarily the result of substitution of $NaFe^{3+}$ for $Ca(Mg, Fe, Mn)^{2+}$ (Kyle, in press). Na variation in the clinopyroxenes of Mt. Erebus is shown in the atomic Na-Mg-Fe^{2+}+Mn plot (Fig. 4.6). Na shows a slight enrichment in clinopyroxenes from basanite to anorthoclase phonolite in the Erebus lineage. Clinopyroxenes from the benmoreite and kaersutite phonolite have low Na contents. The groundmass clinopyroxene in anorthoclase phonolite xenolith 82431 is enriched in Na and depleted in Fe^{2+}. Evolved phenocryst rims in 82403 are depleted in Na, while in 83400 Fe^{2+} and Na are enriched in groundmass clinopyroxene.

In Erebus lineage samples the Na enrichment trend is similar to that of clinopyroxenes in other strongly undersaturated differentiation sequences (e.g. South Qoroq nepheline syenites: Stephenson, 1972; DVDP lineage: Kyle, in press). In contrast, clinopyroxenes in mildly undersaturated

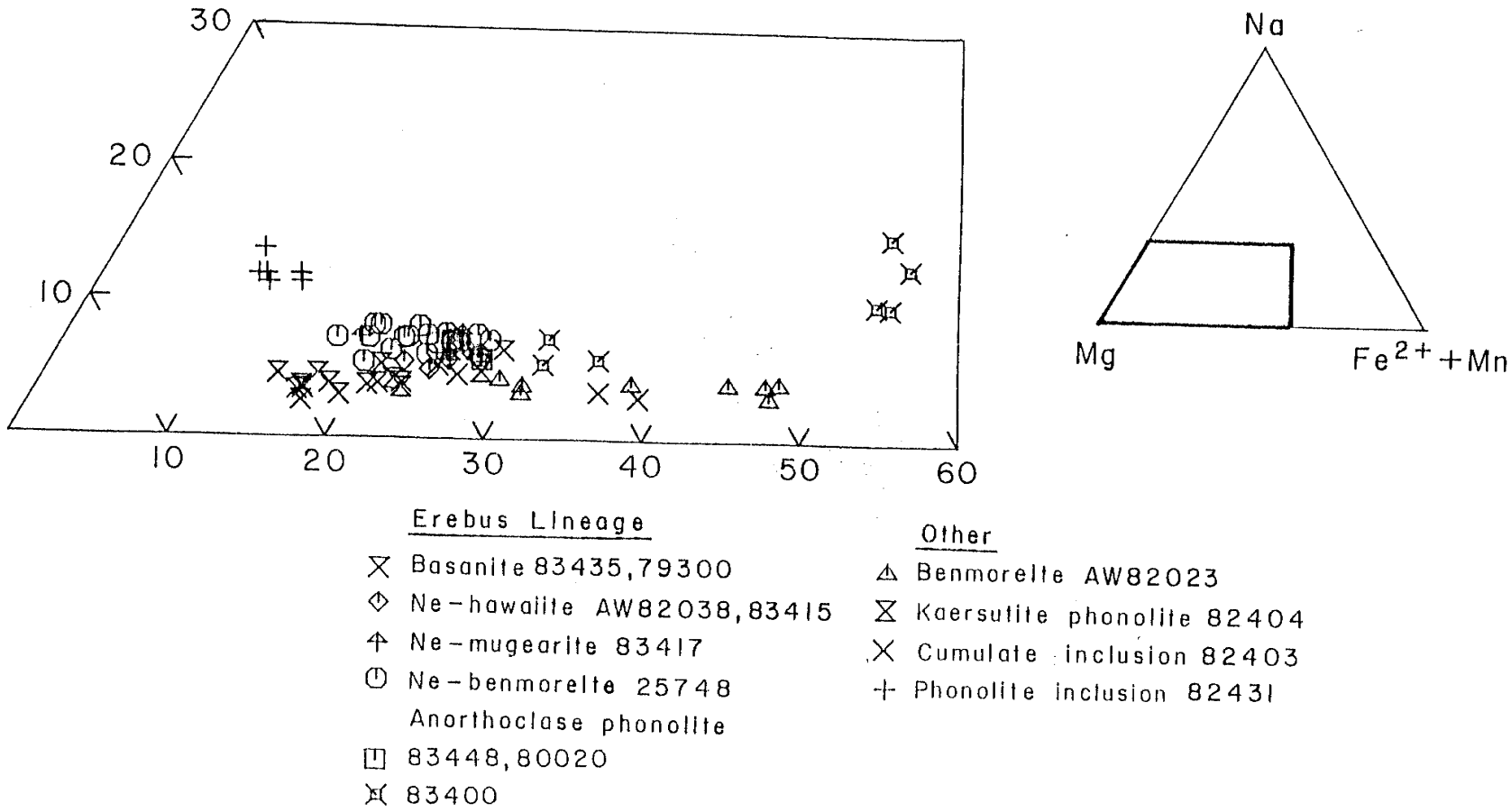

Figure 4.6. Variation of Na, Mg and (Fe^{2+}+Mn) (atomic % after charge balancing) in pyroxenes of Mt. Erebus lavas.

sequences such as The Pleiades (Kyle, in press) and the generalized alkali basalt-trachyte series from Japan (Aoki, 1964) are strongly enriched in Fe^{2+}+Mn with no enrichment in Na until the most evolved lavas. The benmoreite clinopyroxenes may be following this trend. Thus the different Na trends in clinopyroxenes from the Erebus lineage and benmoreite samples may be due to different parental magmas.

The limited Na enrichment in clinopyroxenes from the Erebus lineage suggests limited oxygen fugacity and Fe_2O_3 enrichment during the evolution of these rocks, probably buffered by olivine and magnetite crystallization. The enrichment of Na in groundmass clinopyroxenes from 83400 probably reflects increasing Fe^{3+a} and oxygen fugacity in the melt due to the disappearance of olivine as a crystallizing phase. This fits with the absence of olivine in the groundmass of this sample. Olivine does occur in the groundmass of the benmoreite, and probably limited oxidation of this magma and consequently the $NaFe^{3+}$ content of the clinopyroxenes. The high Fe^{3+} and Na content of groundmass clinopyroxene in 82431 may be due to alteration of this xenolith by an oxidizing fluid.

Kaersutite

Kaersutite phenocrysts occur only in some benmoreites and phonolites and as rare oxidized xenocrysts (?) in Ne-hawaiite 83453. Kaersutite also occurs interstitially and as alteration rims on clinopyroxenes in cumulate xenolith 82403. Kaersutite analyses from 82403 and 82404 are given in Table 4.2. FeOT was partitioned between FeO and Fe_2O_3 using the method of Aoki (1970).

Kaersutite has a near-constant composition similar to kaersutite in DVDP samples (Kyle, 1981b). The kaersutite in 82403 is slightly lower in Ca and FeT+Mn and higher in Mg than the kaersutite in 82404.

Kaersutite is stable up to 23 kb pressure at temperatures $\geq$700°C (Yagi et al., 1975). Merrill and Wyllie (1975) indicated an upper temperature stability of about 1100°C. The crystallization of kaersutite is enhanced by lower SiO_2, lower $Na_2O/(Na_2O+K_2O)$, and higher TiO_2, F, and water pressure (Holloway and Ford, 1973; Merrill and Wyllie, 1975).

Magmatic temperatures greater than 1100°C and low water pressures are possibly the main reasons why kaersutite did not crystallize in Erebus lineage lavas. The kaersutite-bearing benmoreites and phonolites may have formed from magmas with lower temperatures and possibly

Table 4.2. Microprobe analyses of kaersutite in Mt. Erebus lavas.

Sample/		82404		
grain	82403	2	3	4
SiO2	42.12	40.15	40.48	40.49
TiO2	6.72	7.18	7.44	7.66
Al2O3	10.58	12.21	12.50	12.33
Fe2O3	1.88	0.99	0.64	0.72
FeO	10.43	12.41	12.19	11.65
MnO	0.33	0.26	0.30	0.25
MgO	12.34	11.30	11.39	11.74
CaO	11.42	11.60	11.61	11.77
Na2O	2.58	2.44	2.56	2.39
K2O	1.38	1.06	1.01	1.01
Total	99.60	99.23	100.07	99.94
No. of cations on the basis of 23 oxygen				
Si	6.151	5.902	5.903	5.899
Ti	0.738	0.794	0.816	0.839
Al IV	1.821	2.098	2.097	2.101
Al VI	--	0.017	0.051	0.016
Fe3+	0.207	0.110	0.070	0.079
Fe2+	1.273	1.492	1.487	1.419
Mn	0.041	0.032	0.037	0.031
Mg	2.686	2.476	2.476	2.550
Ca	1.790	1.827	1.814	1.837
Na	0.731	0.695	0.724	0.675
K	0.258	0.302	0.188	0.188
Total	15.696	15.746	15.663	15.635
Z	7.972	8.000	8.000	8.000
Y	4.945	4.921	4.937	4.935
X	2.779	2.825	2.726	2.700

Explanation
82403: anorthoclase-clinopyroxene cumulate xenolith
82404: kaersutite phonolite

higher water contents than the magmas which formed the basanite-anorthoclase phonolite suite. The intercumulus and adcumulus kaersutite in 82403 may have crystallized from a hydrous intercumulus liquid.

Opaque Oxides

Opaque oxides are common as phenocryst and groundmass constituents in all samples. FeOT was partitioned between Fe^{3+} and Fe^{2+}, and the molecular proportions of ulvospinel (Usp) and ilmenite (Ilm) were calculated by the charge-balancing procedure of Stormer (1983).

The magnetites range from chromian magnetites to titanomagnetites. No spinels or chromites were found. Rare ilmenite phenocrysts and magnetite-ilmenite pairs occur in the Ne-hawaiites and Ne-benmoreite.

Magnetite in Ne-mugearite 83417 is oxidized and contains fine ilmenite exsolution lamellae. Magnetite in cumulate 82403 also is oxidized but the ilmenite exsolution lamellae are too small to affect analysis with a 1 micron electron beam. In anorthoclase phonolite xenolith 82431 the magnetite has been completely oxidized to fine-grained aggregates of maghemite and ilmenite. The oxides in these aggregates and in the groundmass of this sample have analytical totals after calculation of Fe_2O_3 of <98% due to oxidation.

Figure 4.7. Variation of Al_2O_3, Cr_2O_3, MgO and FeO against TiO_2 in opaque oxides from Mt. Erebus lavas. Values in wt.% after charge-balancing.

Erebus Lineage

- Basanite 83435,79300
- Ne-hawaiite AW82038,83415
- Ne-mugearite 83417
- Ne-benmoreite 25748
- Anorthoclase phonolite 83448,80020

Other

- Benmoreite AW82023
- Kaersutite phonolite 82404
- Cumulate inclusion 82403
- Phonolite inclusion 82431

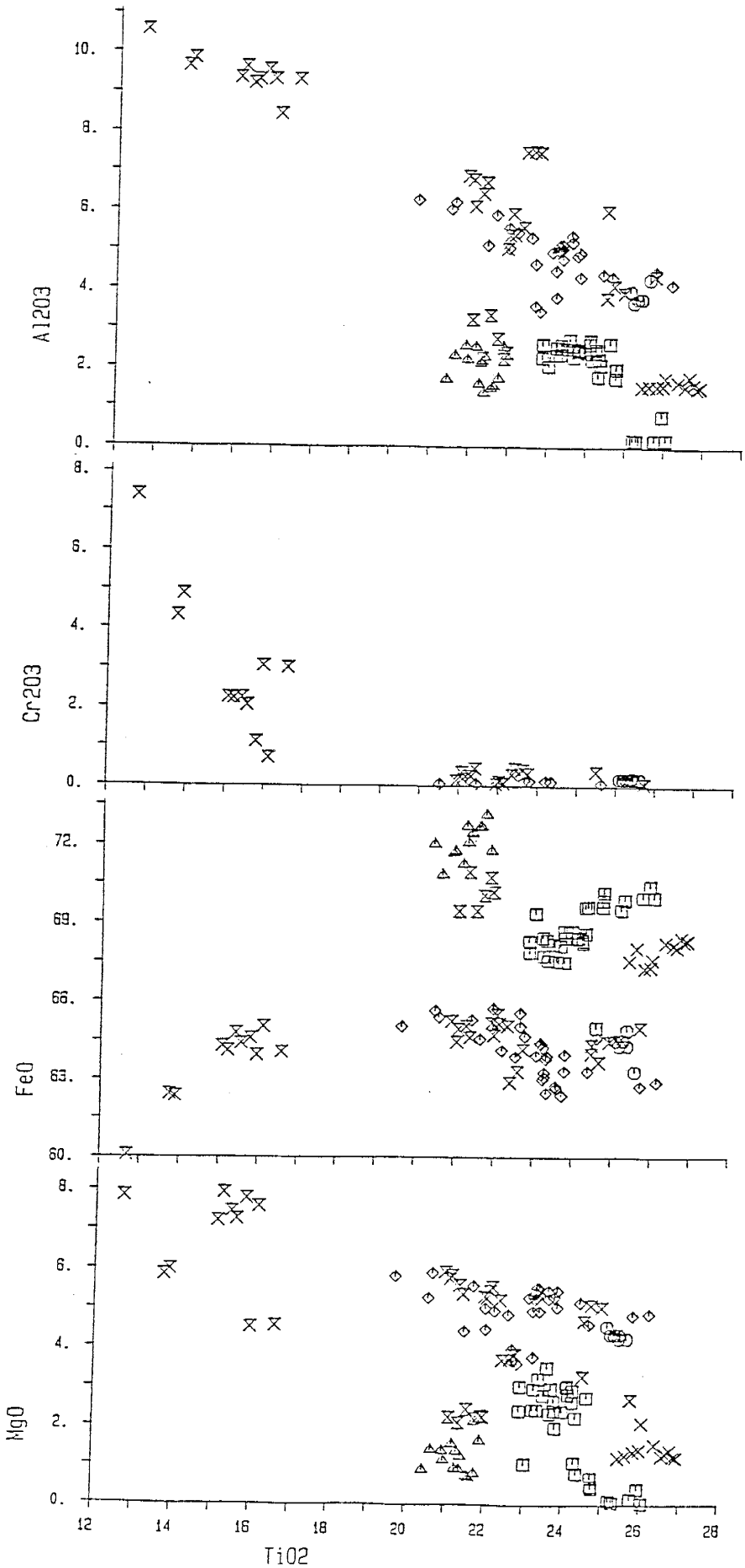
Al2O3
10.
8.
6.
4.
2.
0.
Cr2O3
8.
6.
4.
2.
0.
FeO
72.
69.
66.
63.
60.
MgO
8.
6.
4.
2.
0.
12
14
16
18
20
22
24
26
28
TiO2

The composition of magnetites varies little for all elements except TiO_2 (Fig. 4.7). Al_2O_3, Cr_2O_3 and MgO decrease and TiO_2, FeOT, Fe_2O_3 and MnO increase with increasing sample differentiation, typical of magnetite trends in subaerially extruded volcanic rocks (Haggerty, 1976). The greatest variation is seen in magnetites in the basanites and Ne-hawaiites, in which TiO_2 ranges widely and Al_2O_3 decreases with increasing TiO_2. Chromian magnetite phenocrysts occur in basanite 83435. They are relatively high in Al_2O_3 and MgO, and low in TiO_2. FeOT increases with increasing TiO_2 in the chromian magnetite phenocrysts but is approximately constant in the rest of the basanite magnetites. A compositional gap of c.3% TiO_2 occurs between the chromian magnetite phenocrysts in 83435 and magnetites from the groundmass of 83435 and the rest of the samples.

Magnetites in anorthoclase phonolites are enriched in MnO and depleted in Al_2O_3 and MgO compared with magnetites from the rest of the Erebus lineage. They are similar in composition to magnetites in recent anorthoclase phonolite ejecta from Mt. Erebus (Kyle, 1977). Magnetites from the kaersutite phonolite and benmoreite have similar concentrations of TiO_2, Al_2O_3 and MnO, and are depleted in TiO_2 relative to magnetites from anorthoclase phonolites. Magnetites in the benmoreite have the highest FeO contents.

The lack of spinel in the basanites from Mt. Erebus suggests the basanites are moderately fractionated and formed at temperatures less than 1200°C (Hill and Roeder, 1974). In experiments in which magnetites were crystallized from basaltic melts at various temperatures and oxygen fugacities, Hill and Roeder (1974) found that high oxygen fugacity favored high MgO and Fe_2O_3 and low Cr_2O_3, Al_2O_3 and FeO concentrations. Decreasing temperature favored lower Al_2O_3, Cr_2O_3 and MgO and higher Fe_2O_3, FeO and TiO_2. Sigurdsson and Schilling (1976) suggested that higher pressure favors increased Al in magnetites. These results explain the trends of titanomagnetites in lavas from Mt. Erebus. The chromian magnetite phenocrysts in 83435 probably crystallized at higher temperature and pressure and lower f_{O_2} than magnetites in the rest of the samples. Transport of the basanite magma to higher crustal level and lower pressure may have been accompanied by increased oxygen fugacity and lower temperature. Activities of Al, Cr and Mg in the melt declined due to the crystallization of olivine, clinopyroxene, opaque oxides and plagioclase. These probably caused decreasing Al, Cr, and Mg concentrations in the chromian magnetites (Haggerty, 1976). Conditions probably did not change much during evolution of the rest of the Erebus lineage because the magnetites show only limited variation.

The discontinuity in TiO_2 between the chromian magnetite cores in basanite 83435 and the titanomagnetite in its groundmass suggests a break in magnetite crystallization. Irvine (1965) demonstrated that early Cr-rich magnetite and olivine crystallization is terminated by a peritectic reaction leading to clinopyroxene crystallization. A compositionally distinct magnetite crystallizes later at lower temperature and pressure. The embayed and corroded condition of the chromian magnetites suggests they are out of equilibrium due to decreased pressure.

The titaniferous nature of the magnetites from Mt. Erebus, typical of magnetites in alkaline igneous suites, is most likely due to the generally high Ti content of alkaline magmas (Haggerty, 1976). The higher FeO concentrations in the magnetites from the benmoreite may be due to a different, relatively Fe^{2+}-enriched parental magma.

Temperature and oxygen fugacity

Temperatures and oxygen fugacities in Ne-hawaiites AW82038 and 83415 were calculated using the magnetite-ilmenite geothermometer (Stormer, 1983). A range of temperatures of 1065-1102^{o}C and log f_{O2} of -10.20 to -9.76 were determined for AW82038. Oxide pairs in 83415 gave temperatures from 1061-1090^{o}C and log f_{O_2} from -10.13 to -9.78. The average temperature is 1081$\pm$12^{o}C and log f_{O_2} is

-9.99 ± 0.15 in the Ne-hawaiites.

These temperatures and oxygen fugacities are within the experimental ranges for alkali basalts determined by Duke (1974). They are slightly different than the temperatures and oxygen fugacities of hawaiites and mugearites in Iceland (1030-1050°C; log f_{O_2}: -10.5; Jakobssen et al., 1973).

The average temperature and oxygen fugacity of the Ne-hawaiites from Mt. Erebus falls on the quartz-fayalite-magnetite (QFM) oxygen buffer curve, typical of extrusive basaltic rocks (Haggerty, 1976). Kyle (1977) determined a log f_{O_2} of -12.2 at 1000°C for recent anorthoclase phonolite ejecta from Mt. Erebus, which plots below the QFM buffer, typical of felsic undersaturated extrusive rocks (Nash et al., 1969; Haggerty, 1976).

Pyrrhotite

Pyrrhotite occurs in all samples except the benmoreites, trachytes, most of the kaersutite phonolites, and phonolite xenolith 82431. It increases in modal abundance with increasing sample differentiation and usually occurs as small blebs within or contacting magnetite grains. Microprobe analyses of pyrrhotite are given in Table 4.3.

Pyrrhotites in the Ne-hawaiite and anorthoclase phonolite samples have extremely high molecular % FeS, similar to pyrrhotites in recent volcanic ejecta from Mt.

Table 4.3. Microprobe analyses of pyrrhotite in Mt. Erebus lavas.

Sample/ grain	Wt. % Fe	S	Total	Mol.% FeS
83415-1	61.86	36.68	98.54	0.984
83415-3	62.13	36.71	98.84	0.986
80020-13	61.64	36.76	98.40	0.981
80020-23	61.30	37.12	98.42	0.973
80020-25	61.38	36.86	98.24	0.977
83400-1	62.27	36.26	98.53	0.993
83400-6	62.32	36.39	98.71	0.991
83400-7	61.47	36.94	98.41	0.977
83448-1	60.98	37.53	98.51	0.965
83448-3	60.90	37.85	98.75	0.960
83448-12	61.76	36.56	98.32	0.985
82403-8	58.96	39.26	98.22	0.926
82403-9	60.19	38.57	98.76	0.945
82403-13	61.22	37.80	99.02	0.964
82403-14	59.74	38.74	98.48	0.939
82404-5	59.70	38.79	98.49	0.938
82404-9	59.44	38.98	98.42	0.934
82404-10	59.15	39.07	98.22	0.930
82404-11	60.27	38.83	99.10	0.942
82404-12	60.29	38.07	98.36	0.952

Explanation
83415: Ne-hawaiite
80020: anorthoclase phonolite
83400: anorthoclase phonolite
83448: anorthoclase phonolite
82403: anorthoclase-clinopyroxene cumulate xenolith
82404: kaersutite phonolite

Erebus (Kyle, 1977). Pyrrhotites from cumulate xenolith 82403 and kaersutite phonolite 82404 have lower FeS than pyrrhotites in the Erebus lineage.

The mole fraction of FeS in pyrrhotite decreases with decreasing temperature and increasing sulfur fugacity (Toulmin and Barton, 1964). Thus the formation of the kaersutite phonolite and cumulate xenolith may have occurred at lower temperature or higher sulfur fugacity than existed during evolution of the Erebus lineage.

Sulfur Fugacity

Toulmin and Barton (1964) derived an equation for calculating the sulfur fugacity of magmas from the molecular % FeS in pyrrhotite and the temperature of equilibration. Using an average temperature for the Ne-hawaiites from this study of 1081°C, the log f_{S_2} of the magma is -3.011. This is identical to the S_2 fugacity of gas from Kilauea volcano, Hawaii (Heming and Carmichael, 1973), and slightly lower than the sulfur fugacity calculated for recent anorthoclase phonolite ejecta from Mt. Erebus (log f_{S_2}=-2.75; Kyle, 1977).

Feldspar

Feldspar occurs in all samples, and is the most common groundmass and phenocryst mineral. The modal abundance generally increases with increasing sample differentiation. Feldspars range widely in composition, from An_{72} (bytownite) in basanites to Or_{54} (sanidine) in evolved groundmasses of some samples (Fig. 4.8.). Feldspar phenocrysts are more calcic than groundmass feldspar, and the range in composition follows the classic Bowen crystallization sequence with increasing sample differentiation. Groundmass feldspars in Ne-mugearite 83417 range from anorthoclase to sodic sanidine, probably due to the slow cooling and long period of differentiation of this dike.

Rare earth elements (REE) and some trace elements were measured in Ne-hawaiite and Ne-benmoreite samples and andesine phenocrysts from these samples collected and analyzed for major elements by Kyle (1976) (Appendix D, Part 2). In chrondrite-normalized plots, the andesine shows REE concentrations typical of feldspars (Fig. 5.10). Concentrations are low and light REE and Eu are strongly enriched over heavy REE. Feldspar/whole rock and feldspar/groundmass partition coefficients in the Ne-hawaiite and Ne-benmoreite samples are given in Table 4.4.

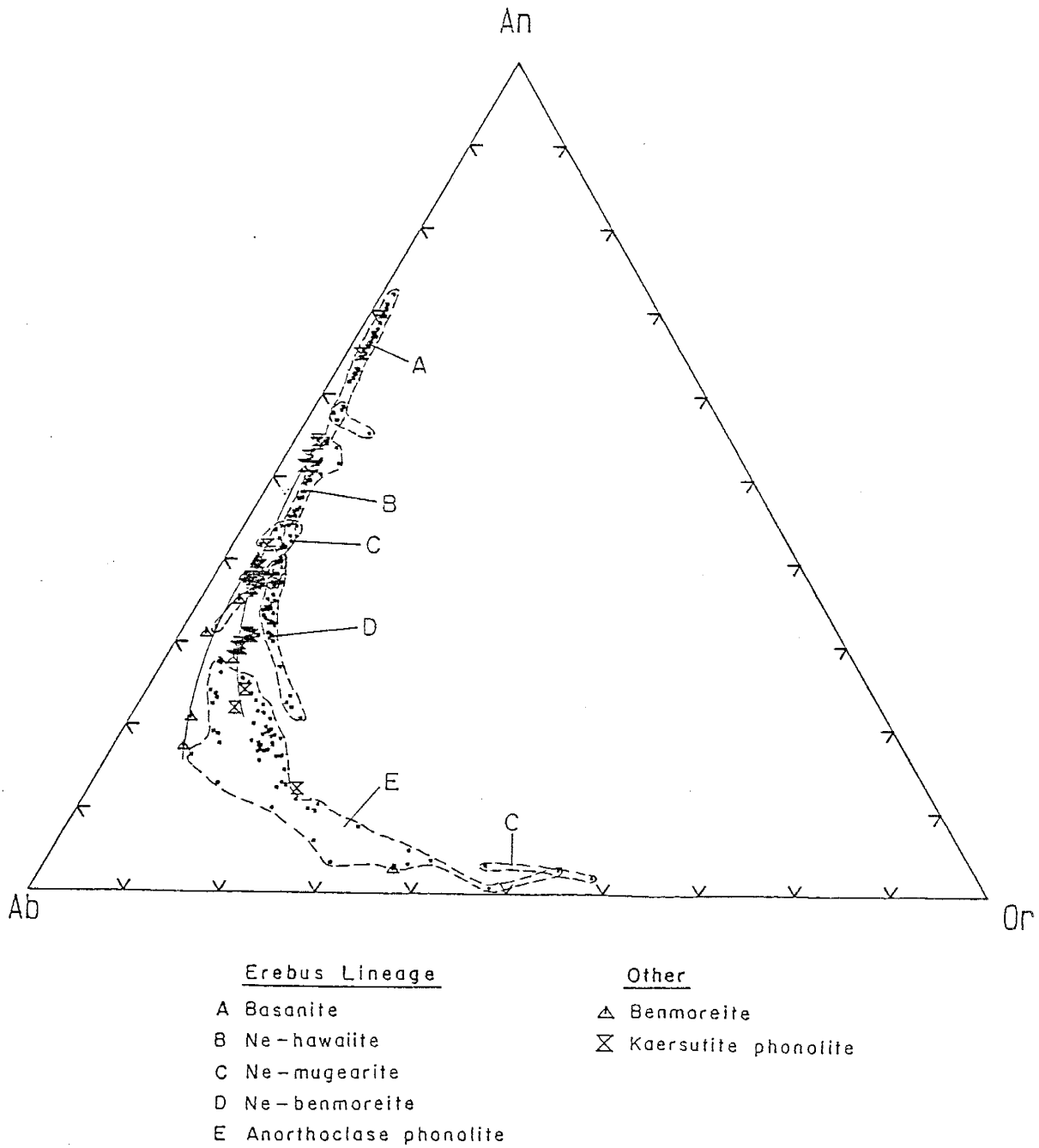

Figure 4.8. Variation of An, Ab and Or in feldspars from Mt. Erebus lavas. Fields of Erebus lineage lavas circled. Lines pass through benmoreite and kaersutite phonolite trends.

Table 4.4. Ne-hawaiite and Ne-benmoreite feldspar/whole rock and feldspar/groundmass partition coefficients.

Sample	25754		25758	
	1	2	1	2
Sc	0.043	0.039	0.049	0.039
Rb	0.055	0.045	0.075	0.059
Sb	0.133	0.077	--	--
Cs	0.074	0.068	0.117	0.108
Ba	0.648	0.726	0.728	0.621
La	0.146	0.131	0.180	0.146
Ce	0.106	0.096	0.143	0.115
Sm	0.064	0.057	0.093	0.074
Eu	0.569	0.544	0.600	0.529
Tb	0.052	0.045	0.059	0.052
Yb	--	--	0.061	0.046
Lu	0.045	0.036	--	--
Hf	0.034	0.030	0.049	0.039
Ta	0.040	0.037	0.047	0.036
Th	0.025	0.023	0.047	0.036

Sample	25778		25748	
	1	2	1	2
Sc	0.020	0.019	0.019	0.017
Cr	--	--	0.5	0.5
Cu	--	--	0.909	0.667
Zn	--	--	0.081	0.066
Rb	--	--	0.059	0.044
Sr	--	--	2.440	5.129
Sb	--	--	0.409	--
Ba	0.652	0.655	1.446	1.553
La	0.168	0.143	--	0.207
Ce	0.119	0.103	0.163	0.138
Sm	0.063	0.056	--	0.079
Eu	0.745	0.765	1.068	1.087
Tb	0.037	0.040	0.067	0.061
Lu	--	--	--	0.026
Hf	0.011	0.009	0.021	0.017
Ta	0.010	0.008	0.015	0.013
Th	0.009	0.007	0.024	0.019

Explanation
1 - feldspar/whole rock
2 - feldspar/groundmass
25754: Ne-hawaiite, Turks Head
25758: Ne-hawaiite, Tryggve Point
25778: Ne-hawaiite, Fang Ridge
25748: Ne-benmoreite, Tent Island

The anorthoclase phonolites take their name from their abundant rhomb-shaped anorthoclase phenocrysts which actually range in composition from $An_{28}Or_6$ (orthoclase) in the less evolved anorthoclase phonolite samples (e.g. 83446) to $An_{10}Or_{25}$ (anorthoclase) in the more evolved anorthoclase phonolite samples (e.g. 80020). Ab shows little variation in all the anorthoclase phonolites (65-71). Zoning is limited to slight increases or decreases in An and Or from cores to rims in the phenocrysts. The phenocrysts sometimes have thin discontinuous sanidine rims (Or_{37-38}). Microphenocrysts are similar in composition to the phenocrysts and groundmass feldspars range from anorthoclase to sanidine.

The cores of feldspar phenocrysts in anorthoclase phonolite xenolith 82431 are andesine and are being replaced by leucite. Phenocryst rims and groundmass feldspars in this sample are anorthoclase. The feldspar phenocrysts in kaersutite phonolite 82404 are discontinuously zoned from corroded, possibly xenocrystic labradorite cores to andesine intermediate zones to oligoclase edges. Rare extensively resorbed labradorite crystals occur and probably are xenocrysts. The microphenocrysts and groundmass feldspars are oligoclase. In the benmoreite, microphenocrysts are andesine and groundmass feldspars generally are andesine and oligoclase.

The range in composition of feldspars in Mt. Erebus lavas is similar to that of feldspars in other alkaline differentiation sequences (e.g. Hawaii: Keil et al., 1972; DVDP: Kyle, 1981b; Gough Island: Le Roex, 1985). Except for kaersutite phonolite 82404, zoning within individual phenocrysts is minor and feldspar xenocrysts are absent. The resorbed and embayed phenocrysts in Ne-hawaiite, Ne-mugearite and Ne-benmoreite samples are similar in composition to groundmass and microphenocryst feldspars, indicating the phenocrysts are not xenocrystic. The complex oscillatory zoning in these phenocrysts suggests rapid growth. Lofgren (1974) showed that feldspars can grow from 1-5 mm/day during magma ascent. Thus these feldspars probably crystallized late in the cooling history of Erebus lineage magmas. The corroded labradorite cores and xenocrysts in the kaersutite phonolite may be the result of mixing with a more basic magma.

Feldspar in the Erebus lineage lavas (basanites, Ne-hawaiites, Ne-mugearites, Ne-benmoreites and anorthoclase phonolites) form a continuous trend, with feldspar from the intermediate rocks overlapping in composition in the oligoclase field. This suggests a single line of descent. On the other hand, feldspar in the kaersutite phonolite and benmoreite samples forms trends slightly more albitic and less potassic than the Erebus lineage trend, suggesting different evolutionary paths for these lavas. Similar

divergent feldspar trends have been observed at other volcaic centers (e.g. Gough Island: Le Roex, 1985; Mt. Kenya: Price et al., 1985). The higher albite content of feldspar from the kaersutite phonolite may be due to increased stability of albite at higher water contents (Tuttle and Bowen, 1958). This fits with the kaersutite phenocrysts in this rock.

Anorthoclase

A number of studies have been made on the anorthoclase phenocrysts from Mt. Erebus (Jensen, 1916; Mountain, 1925; Carmichael and MacKenzie, 1964; Boudette and Ford, 1966; Berlin and Henderson, 1969; Sun and Hanson, 1976; Kyle, 1977; Mason et al., 1982). Anorthoclase compositions determined in this study are similar to the results obtained by these previous workers.

Anorthoclase in recent anorthoclase phonolite ejecta from Mt. Erebus (Kyle, 1977) has an average composition of $An_{16}Ab_{65}Or_{19}$, only slightly different from anorthoclase in the 0.68 m.y. old flows at Cape Royds.

Boudette and Ford (1966) and Mason et al. (1982) showed that anorthoclase from Mt. Erebus has significantly higher An than anorthoclase phenocrysts and megacrysts from other localities. Ba, Sr and Rb concentrations are approximately the same. The high An content could be due to partitioning

of Na into feldspathoids. Boudette and Ford (1966) proposed that Na is partitioned into sodalite in the anorthoclase phonolites. Calculation of the one atm. liquidus mineralogy of anorthoclase phonolites, using the method of Nathan and Van Kirk (1978), suggests nepheline crystallizes before anorthoclase. The partitioning of Na into nepheline may deplete Na in the melt, leading to high An in the anorthoclase. Neither of these theories, however, fit with the lack of sodalite or nepheline phenocrysts in the anorthoclase phonolites.

Rare earth element concentrations in anorthoclase phenocrysts from Mt. Erebus and their host phonolites have been determined by Kyle and Rankin (1976) and Sun and Hanson (1976). Typical anorthoclase/whole rock distribution coefficients are La: 0.31, Eu: 1.32, Lu: 0.13 (Sun and Hanson, 1976). REE in anorthoclase from Mt. Erebus are 2-40 times higher than REE in anorthoclase megacrysts from other locations (Irving and Frey, 1984). Glass and mineral inclusions in Mt. Erebus anorthoclase may account for some of the difference. Alternatively, the megacrysts may have crystallized at high pressures from host magmas with higher dissolved volatile contents than Mt. Erebus anorthoclase phonolite. Consequently, this high pressure magma would have been less polymerized and had lower crystal/liquid partition coefficients for REE (Irving and Frey, 1984).

The compositions of anorthoclase phenocrysts from Mt. Erebus fall in the alkali feldspar (anorthoclase) field of Deer et al. (1963) and in the albite and oligoclase (plagioclase) fields of Smith (1974). Lattice parameters, symmetry, and cross-hatched twinning (Boudette and Ford, 1966) suggests the phenocrysts are alkali feldspars. On the other hand, the anorthoclase responds poorly to staining tests for alkali feldspar but strongly to staining tests for plagioclase (Ford and Boudette, 1968). This may be due to its relatively high An content.

Feldspathoid

With the exception of two trachytes, the samples from Erebus center are strongly undersaturated, containing up to 24% normative nepheline. Rare nepheline phenocrysts occur in some Ne-hawaiite samples. Minor to significant amounts of groundmass feldspathoids were observed in every rock type except benmoreite and trachyte.

Table 4.3 contains microprobe analyses of groundmass feldspathoids in anorthoclase phonolite samples 83400 and 83448 and kaersutite phonolite sample 82404, and leucite analyses in anorthoclase phonolite xenolith 82431 The analytical totals of nepheline in 83400 and 83448 are high because of high SiO_2 and Al_2O_3 determinations. The analyses of leucite in 82404 and 82431 have slightly high SiO_2, but are comparable with leucite analyses reported by Deer et al.

Table 4.5. Microprobe analyses of feldspathoids in anorthoclase phonolites 83400 and 83448, phonolite xenolith 82431 and kaersutite phonolite 82404.

A. Nepheline

Sample	83400	83448
SiO2	49.83	56.76
Al2O3	30.88	26.41
FeOT	1.50	2.07
CaO	--	0.27
Na2O	16.22	11.49
K2O	3.07	4.04
Total	101.51	101.03

B. Leucite

Sample 82431				
SiO2	58.86	59.57	59.79	58.79
Al2O3	22.91	23.13	23.00	23.35
FeOT	0.69	0.90	0.83	0.75
Na2O	1.83	1.94	1.99	1.94
K2O	16.28	16.14	16.12	16.22
Total	100.57	101.67	101.74	101.05
No. of cations on the basis of 6 oxygens				
Si	2.07	2.07	2.07	2.05
Al	0.95	0.95	0.94	0.96
Fe	0.02	0.03	0.02	0.02
Na	0.12	0.13	0.13	0.13
K	0.73	0.71	0.71	0.72
Total	3.89	3.89	3.87	3.88

Sample 82404					
SiO2	59.19	58.93	58.77	58.09	59.40
Al2O3	23.44	23.18	23.63	23.34	22.34
FeOT	0.47	0.32	0.34	0.31	0.33
CaO	--	--	--	--	0.26
Na2O	0.16	0.51	0.22	0.26	0.39
K2O	18.67	17.98	19.67	19.93	19.65
Total	101.96	100.91	102.65	101.95	100.24
No. of cations on the basis of 6 oxygens					
Si	2.06	2.07	2.05	2.04	2.07
Al	0.96	0.96	0.97	0.97	0.92
Fe	0.01	0.01	0.01	0.01	0.01
Ca	--	--	--	--	0.01
Na	0.01	0.03	0.01	0.02	0.03
K	0.83	0.81	0.87	0.89	0.88
Total	3.88	3.87	3.91	3.93	3.92

(1966). Leucite in the anorthoclase phonolite xenolith is higher in Na_2O and lower in K_2O than leucite in 82404.

At water pressures between 1 atm and 1 kbar nepheline crystallizes at a higher temperatures than leucite (Gittins, 1979). Thus the crystallization of nepheline and sodalite in anorthoclase phonolites and leucite in kaersutite phonolites suggests that the anorthoclase phonolite magma may have been at a higher temperature than the kaersutite phonolite magma.

In 82431 leucite is replacing andesine in phenocrysts cores and outward from the cores along fractures. The degree of replacement varies from slight to extensive. The sharp contact of this xenolith with its host anorthoclase phonolite suggests that this inclusion of wall-rock material was altered before being entrained. Leucite may have been stabilized in this inclusion at the expense of andesine by alteration by a K-rich fluid, possibly evolved off of an anorthoclase phonolite magma such as that which hosts the xenolith. This fluid must also have been oxidizing, as clinopyroxenes and opaque oxides in this sample have high Fe_2O_3 contents.

Summary

The continuous compositional trends of olivine, clinopyroxene, opaque oxide and feldspar from basanite to anorthoclase phonolite suggests a single line of descent for

the Erebus lineage lavas. Compositional discontinuities in olivine, clinopyroxene and magnetite phenocrysts in basanite 83435 suggests a decrease in pressure and temperature during the crystallization of this lava. However, the lack of significant variation in composition of clinopyroxenes and titanomagnetites in the rest of the samples suggests stable temperature, pressure and volatile fugacity during evolution of the Erebus lineage. This is supported by the temperature of c.1100^{o}C, log f_{O_2} of -9.99, and log f_{S_2} of -3.0 calculated in the Ne-hawaiite, only slightly different from that of recent anorthoclase phonolite ejecta. The mineral compositions in 0.68 m.y. anorthoclase phonolite at Cape Royds is essentially the same as that in recent anorthoclase phonolite bombs. This suggests remarkably stable evolutionary controls for the Erebus lineage.

The mineral chemistry of the benmoreite and kaersutite phonolite samples indicates they evolved differently from the Erebus lineage. The Fe^{2+}-rich mafic minerals in the benmoreite are similar to those of alkali basalt-trachyte series lavas at other volcanic provinces. This suggests it evolved from a relatively siliceous, reduced magma compared to the Erebus lineage. The enrichment of Ab in feldspars and the presence of kaersutite suggests kaersutite phonolite 82404 evolved from a relatively hydrous, lower temperature magma.

CHAPTER FIVE

GEOCHEMISTRY

Introduction

Major and trace element analyses were made by XRF. Rare earth elements and some trace elements in 40 representative samples were determined by INAA. Sample preparation and analytical procedures are given in Appendix C. Analyses are listed in Appendix E with previous analyses of samples from Mt. Erebus by Kyle (1976).

Major Elements

Ferrous iron was determined by wet chemistry in representative samples of Erebus lineage lavas (Table 5.1). $Fe_2O_3/(Fe_2O_3+FeO)$ ranges from 0.353 to 0.117 and does not correlate well with increasing sample differentiation. The CIPW normative mineralogies of the samples were calculated using standardized Fe_2O_3 values after the convention of Thompson et al. (1972), and are given in Appendix F. The convention is as follows:

1. If $Na_2O+K_2O<4.0$ wt.% then $Fe_2O_3=1.50$ wt.%.
2. If $Na_2O+K_2O=4.0$ to 7.0 wt.% then $Fe_2O_3=2.00$ wt.%.
3. If $Na_2O+K_2O<7.0$ wt.% then $Fe_2O_3=2.5$ wt.%.

With the exception of the trachytes, all of the samples are undersaturated, having 5-24% normative Ne. The trachytes range from slightly undersaturated to slightly oversaturated

Table 5.1. Ferrous iron determinations in representative Erebus lineage samples.

XRF major element analyses

	83435	83426	83415	83204	83452	83446	81001
SiO_2	43.32	45.37	49.53	50.13	55.00	55.63	56.25
TiO_2	3.78	3.10	2.12	2.23	1.36	1.18	1.00
Al_2O_3	15.37	17.27	19.87	18.35	18.29	19.46	18.99
Fe_2O_3*	13.43	12.20	8.24	10.14	7.32	5.63	6.17
MnO	0.22	0.24	0.17	0.24	0.27	0.20	0.25
MgO	6.77	4.13	3.00	2.49	1.64	1.30	0.96
CaO	10.66	9.05	6.93	5.13	3.34	3.16	2.57
Na_2O	4.63	5.26	6.22	7.25	7.77	7.60	8.15
K_2O	1.72	2.13	3.00	4.19	4.39	4.47	4.75
P_2O_5	1.21	1.53	0.85	1.03	0.57	0.46	0.43
LOI	0.03	-0.27	-0.21	-0.40	-0.28	0.03	-0.28
Total	101.16	100.00	99.71	100.77	99.66	99.11	99.23
Ferrous and ferric iron							
Fe_2O_3	4.42	3.18	1.70	1.47	1.43	1.38	0.66
FeO	8.11	8.11	5.88	7.80	5.30	3.82	4.96
New total	100.08	99.07	99.05	99.90	98.55	98.73	98.64
$Fe_2O_3/(Fe_2O_3+FeO)$	0.353	0.282	0.225	0.159	0.213	0.266	0.117

(c.2% Qz).

Total Fe was converted to FeO* and the analyses were recalculated to 100% volatile-free for plotting. Major elements show a broad range in the samples as exhibited in the FMA [(FeO* + MnO)-MgO-alkalies (Na_2O+K_2O)] diagram (Fig. 5.1). The strongly undersaturated Erebus lineage forms a well-defined continuous trend toward the alkali apex. Kaersutite phonolites from Bomb Peak also fall on this trend. Benmoreites, trachytic-textured kaersutite phonolites from Inaccesible Island and trachytes are well removed from the Erebus lineage trend at higher (FeO* + MnO). These lavas are volumetrically insignificant and are here referred to as the enriched iron series (EFS). They are independent of the Erebus lineage (EL).

EL lavas form smooth continuous trends for every major element on silica variation diagrams (Fig. 5.2). Some scatter in the plots is seen, especially for Al_2O_3. This may be due to the porphyritic nature of the samples as well as natural variation in the chemistry. TiO_2, MgO, CaO and P_2O_5 decrease with increasing SiO_2 and level out in the most evolved rocks. Al_2O_3, Na_2O and K_2O increase up to about 52% SiO_2 in EL lavas. Al_2O_3 then decreases and the enrichment trends of Na_2O and K_2O level out. The anorthoclase phonolites show only slight variation in major element goechemistry. EFS lavas form a distinct trend on the FeO*

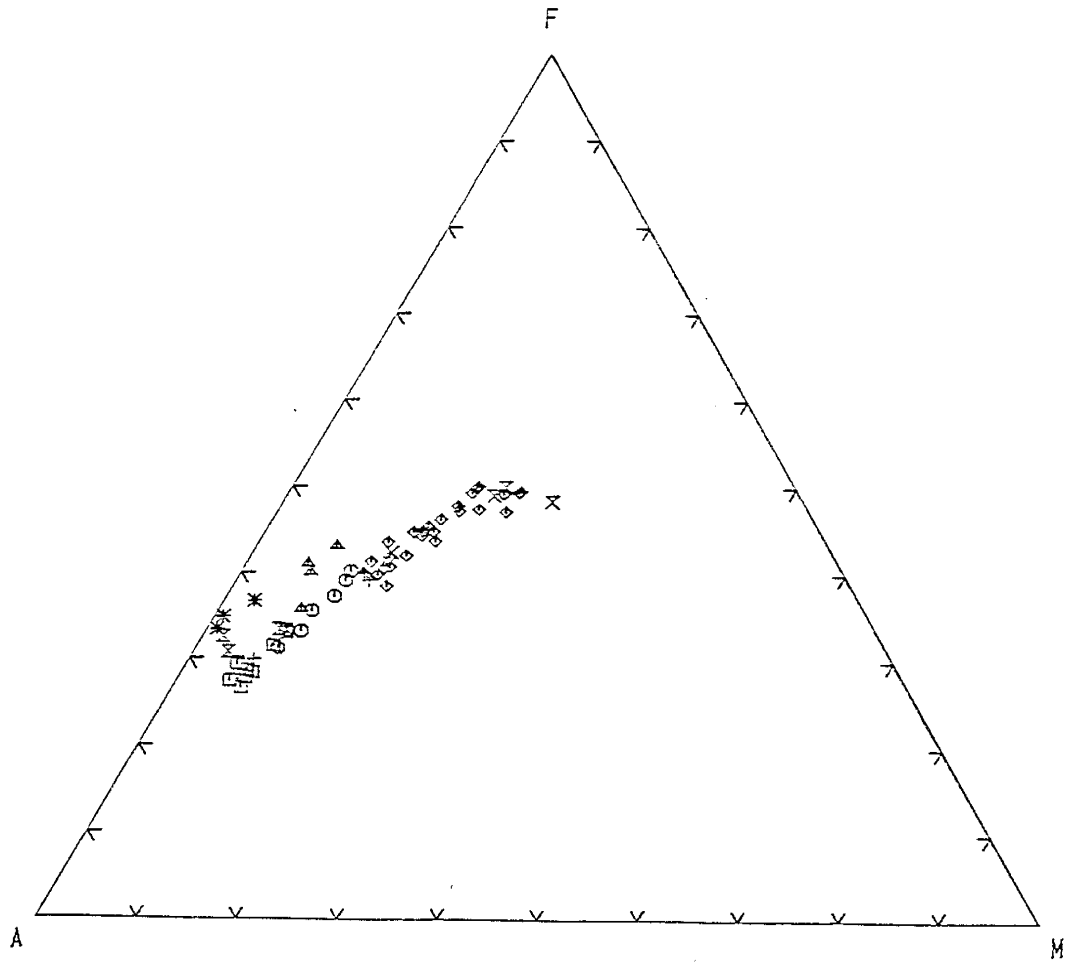

Erebus Lineage

- Basanite
- Ne-hawaiite
- Ne-mugearite
- Ne-benmoreite
- Anorthoclase phonolite

Other

- Benmoreite
- Kaersutite phonolite
- Trachyte
- Cumulate inclusion
- Phonolite inclusion

Figure 5.1. F (FeO*+MnO)-M (MgO)-A (Na_2O+K_2O) variation in Mt. Erebus lavas. Values in wt.%.

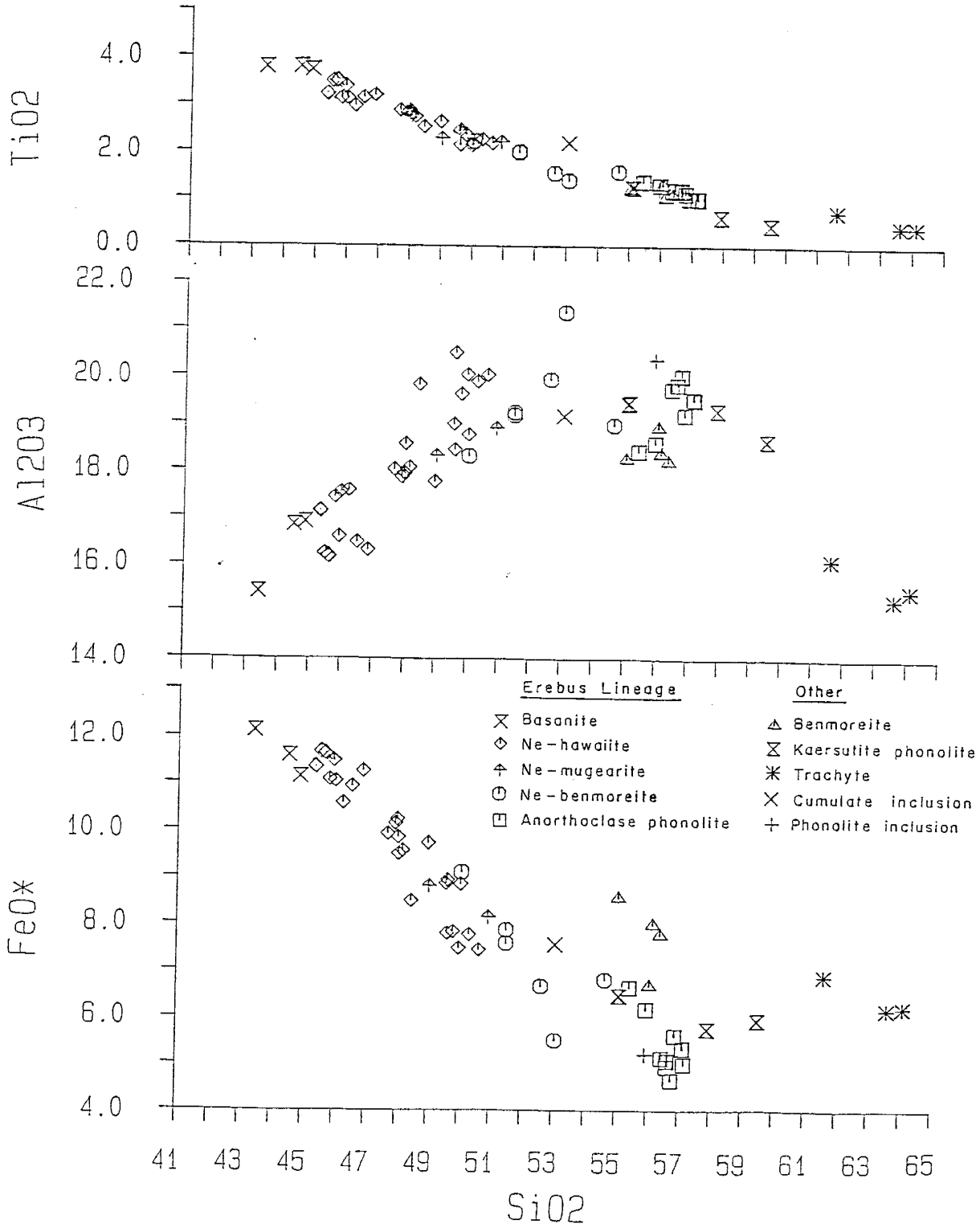

Figure 5.2. Variation of major element oxides against silica in analyses of Mt. Erebus lavas. Values in wt.%.

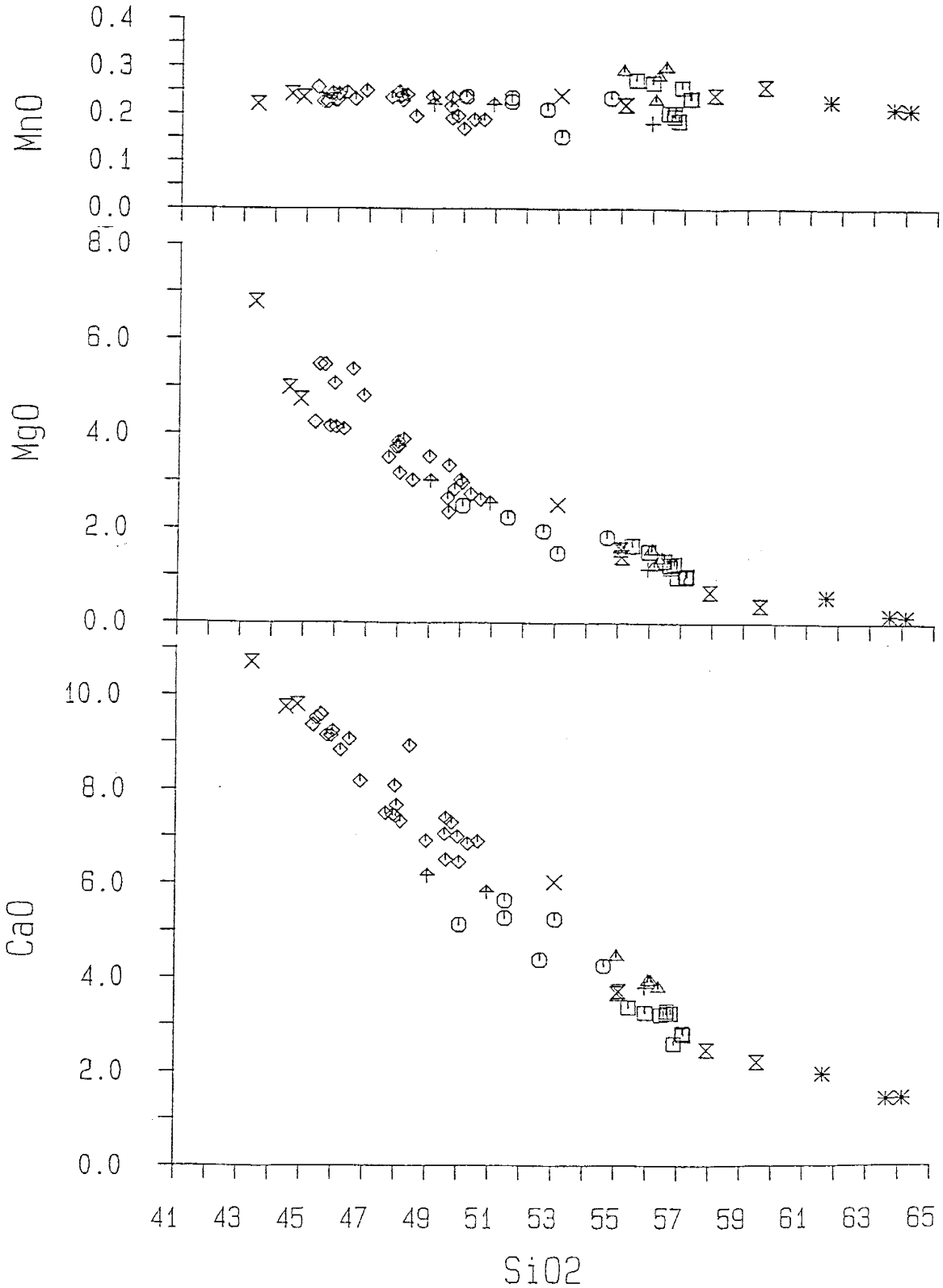

Figure 5.2 continued.

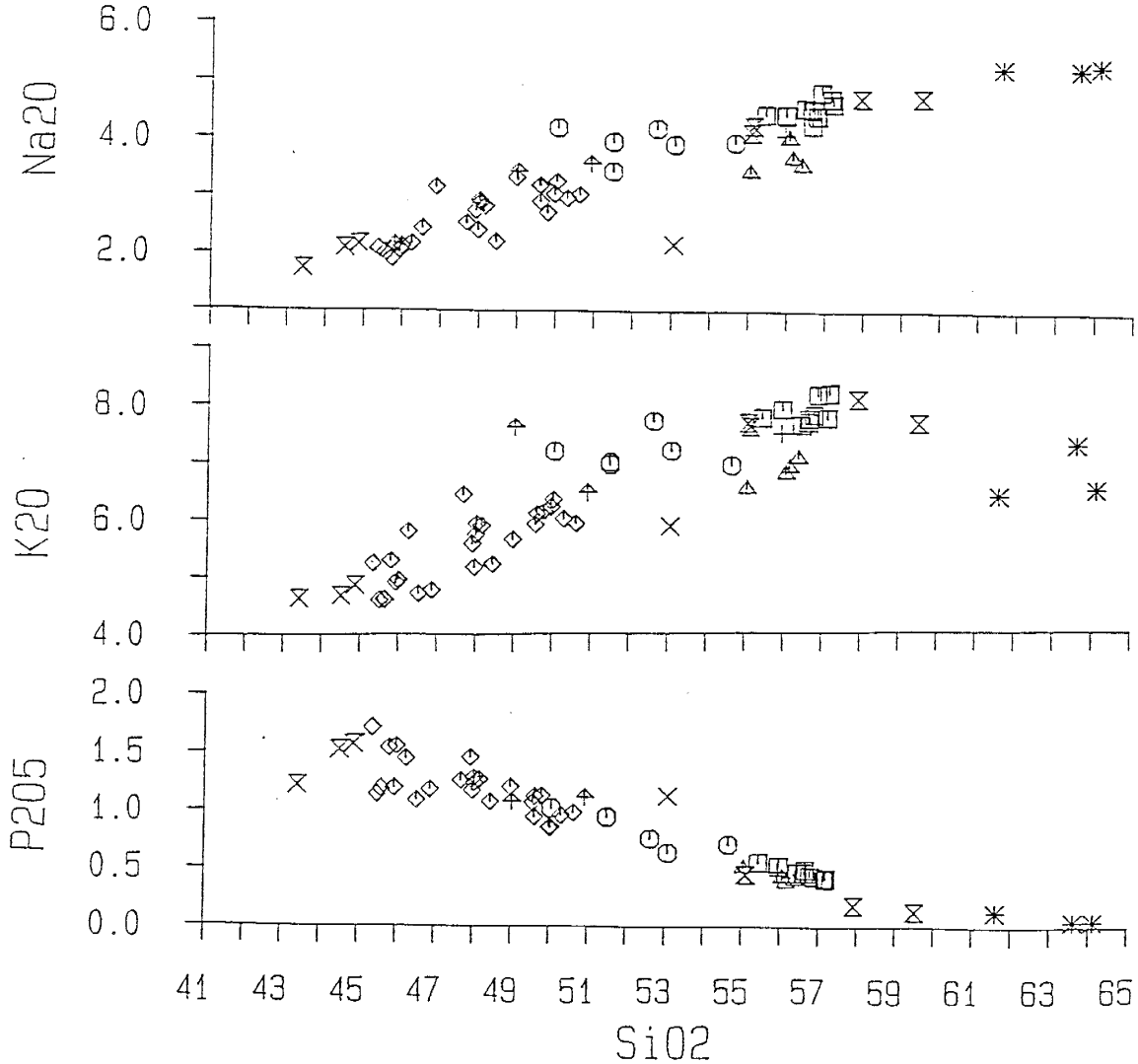

Figure 5.2 continued.

plot and are relatively depleted in Al_2O_3, Na_2O and K_2O compared to EL lavas.

Major element analyses by previous workers exhibit the same trends as the analyses made in this study (Fig. 5.3). Quartz trachyte from Mt. Cis has over 59% SiO_2 and is similar in composition to EFS trachytes. The three published analyses plot separately from the remaining analyses of strongly undersaturated rocks which are considered to be part of the EL. Kyle (1976) analyzed the whole rock and groundmass of Ne-hawaiite, Ne-mugearite and Ne-benmoreite samples. He noted that the whole rock-groundmass trends do not follow the major element trends of whole rock analyses. SiO_2 and Al_2O_3 generally decrease while TiO_2, FeO*, and MgO increase from whole rock to groundmass, opposite to the whole rock trends. Kyle concluded that the glassy groundmasses therefore do not represent liquids in the differentiation sequence. The samples either contain cumulate feldspar or, more likely, the whole rock analyses represent a liquid in which feldspar crystallized late, at low pressures.

Trace Elements

Trace elements in the samples are plotted against Zr as an index of differentiation because mineral/melt partition coefficients for Zr are generally quite small in the samples. Therefore Zr shows one of the strongest enrichments

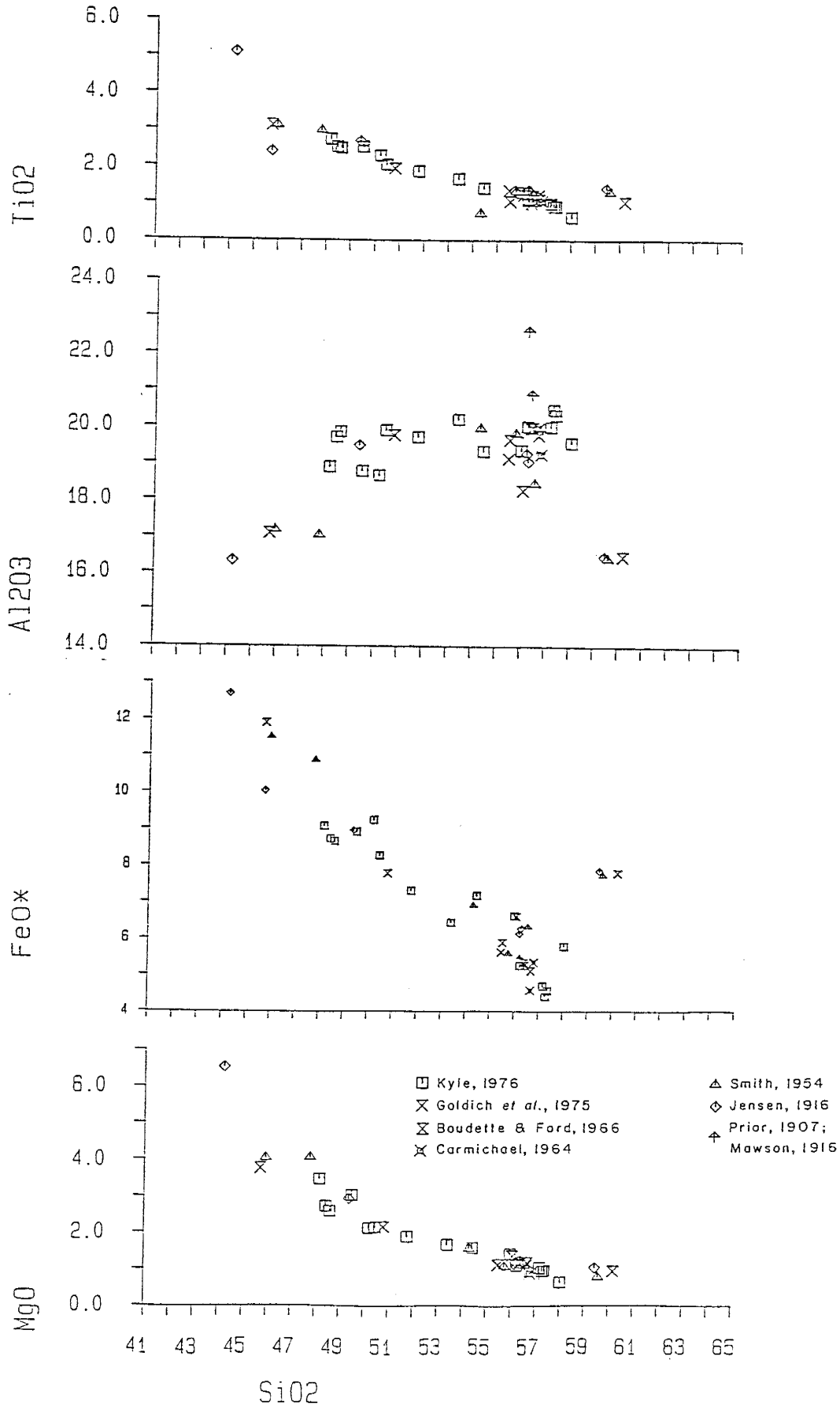

Figure 5.3. Variation of major element oxides against silica in previous analyses of Mt. Erebus lavas. Values in wt.%.

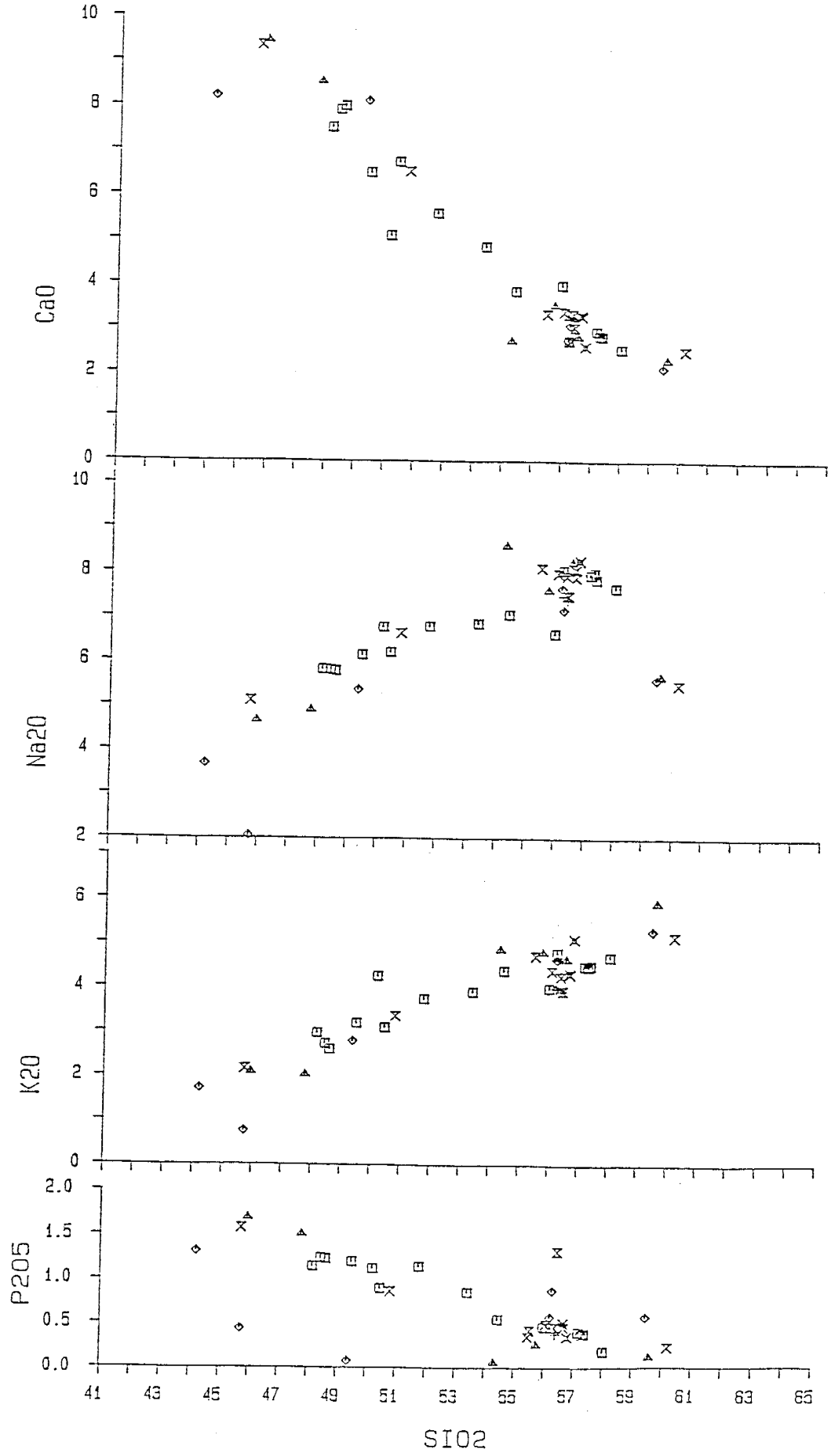

Figure 5.3 continued.

(300 to 1100 ppm).

Like the major elements, analyses of EL samples exhibit smooth continuous trace element trends, as shown in plots for selected elements (Fig. 5.4). The anorthoclase phonolites show a moderate variation in trace elements contents.

Sc, V, Cr, Ni and Cu decrease sharply with increasing Zr to detection limits in the evolved rocks. The most primitive basanite, 83435, is still relatively low in these elements compared to primitive basanites from the DVDP lineage (e.g. Cr: 140 ppm vs. 370-470 ppm in DVDP basanites; Kyle, 1981b).

Sr decreases in EL lavas from a high of ~1500 ppm in the Ne-hawaiites to ~800 ppm in anorthoclase phonolites. Benmoreite, kaersutite phonolite and trachyte samples define a trend with a sharper decline in Sr than the Erebus lineage.

The samples from Mt. Erebus have high concentration of incompatible elements, typical of alkaline igneous rocks. Zn, Cs and Pb remain essentially constant with increasing differentiation in EL lavas and are strongly enriched in the trachytes. Y increases slightly from basanite to anorthoclase phonolite, is strongly enriched in the trachytes, but is depleted in benmoreites and kaersutite

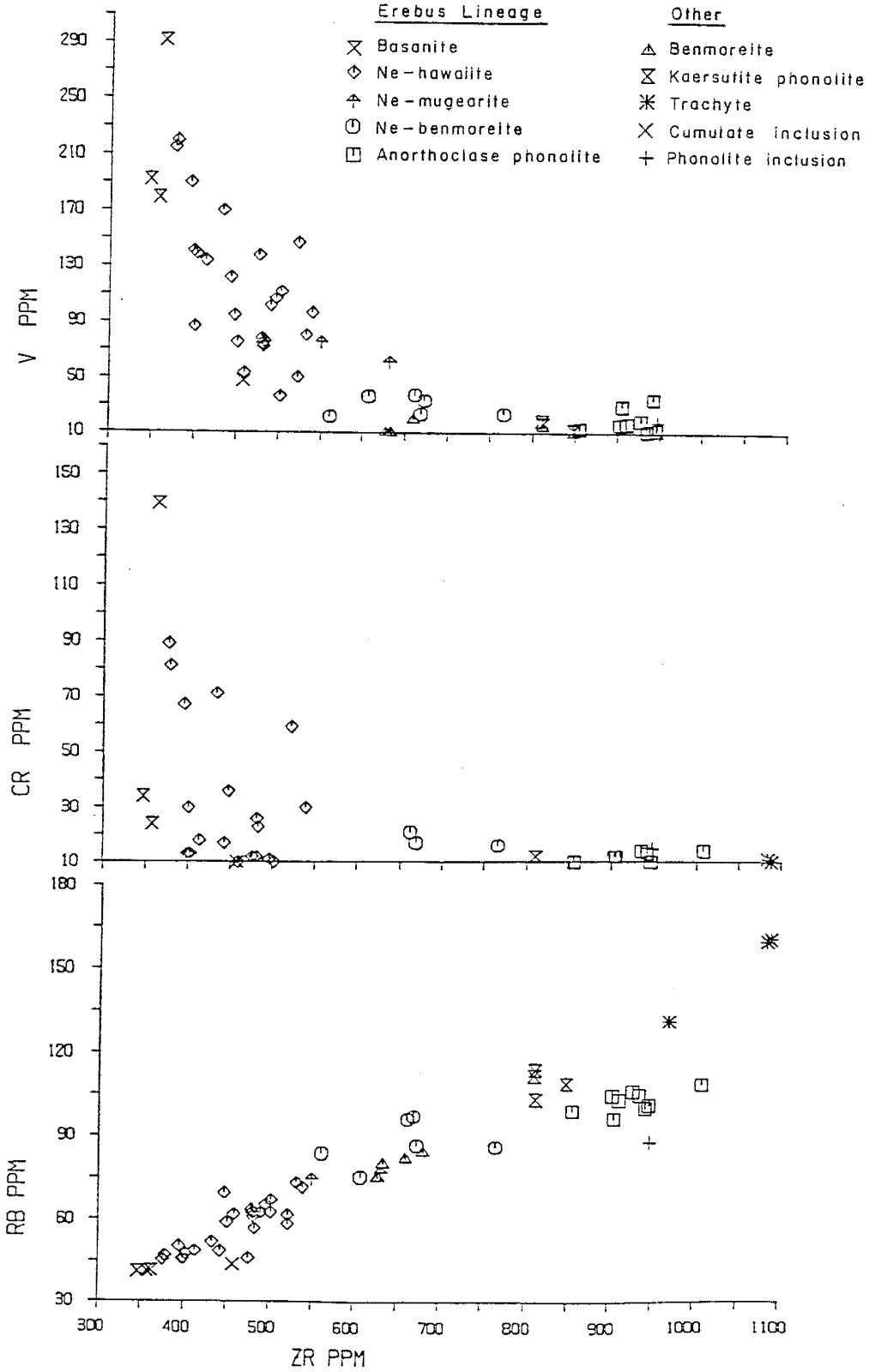

Figure 5.4. Variation of trace elements against Zr in Mt. Erebus lavas. Values in ppm.

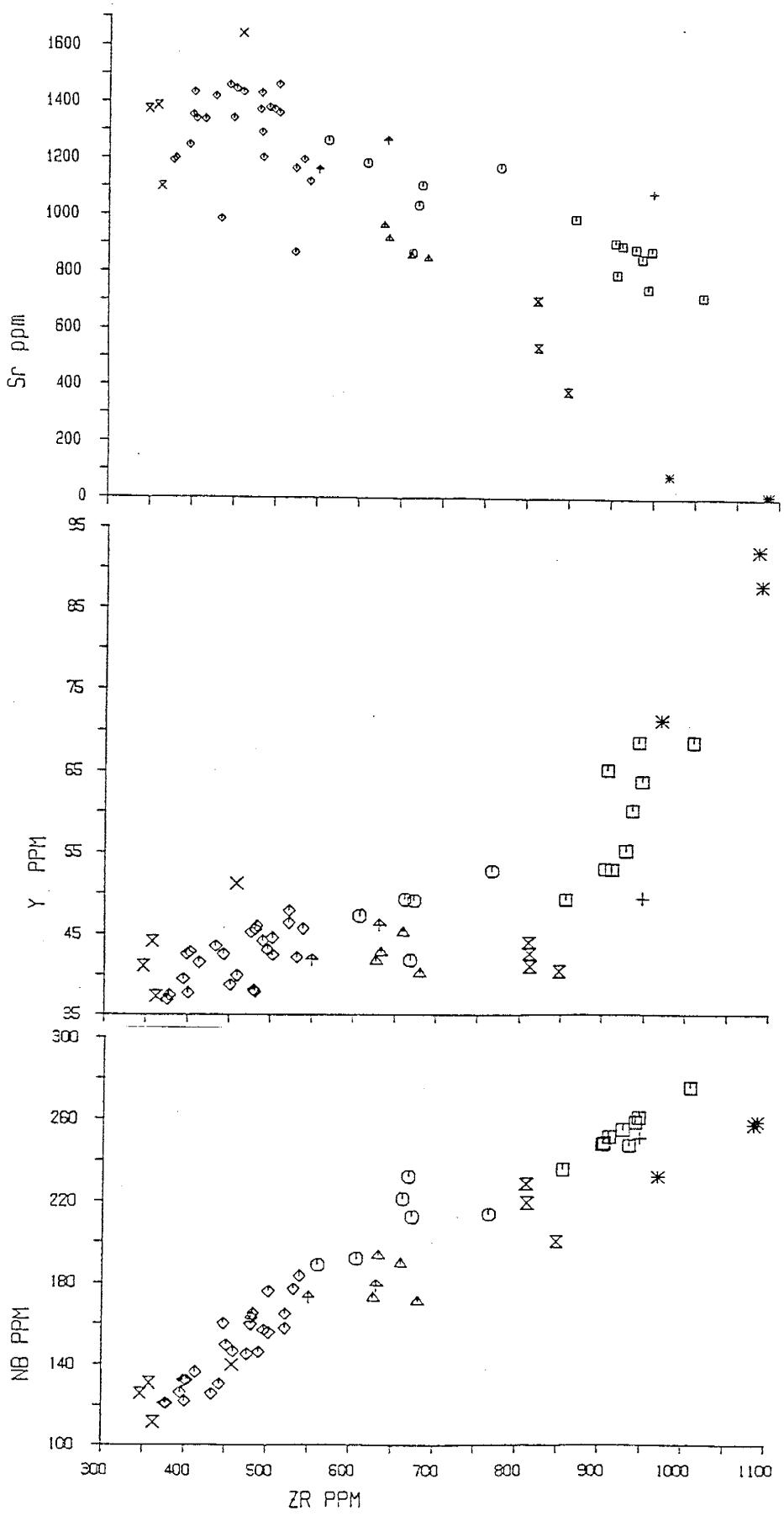

Figure 5.4 continued.

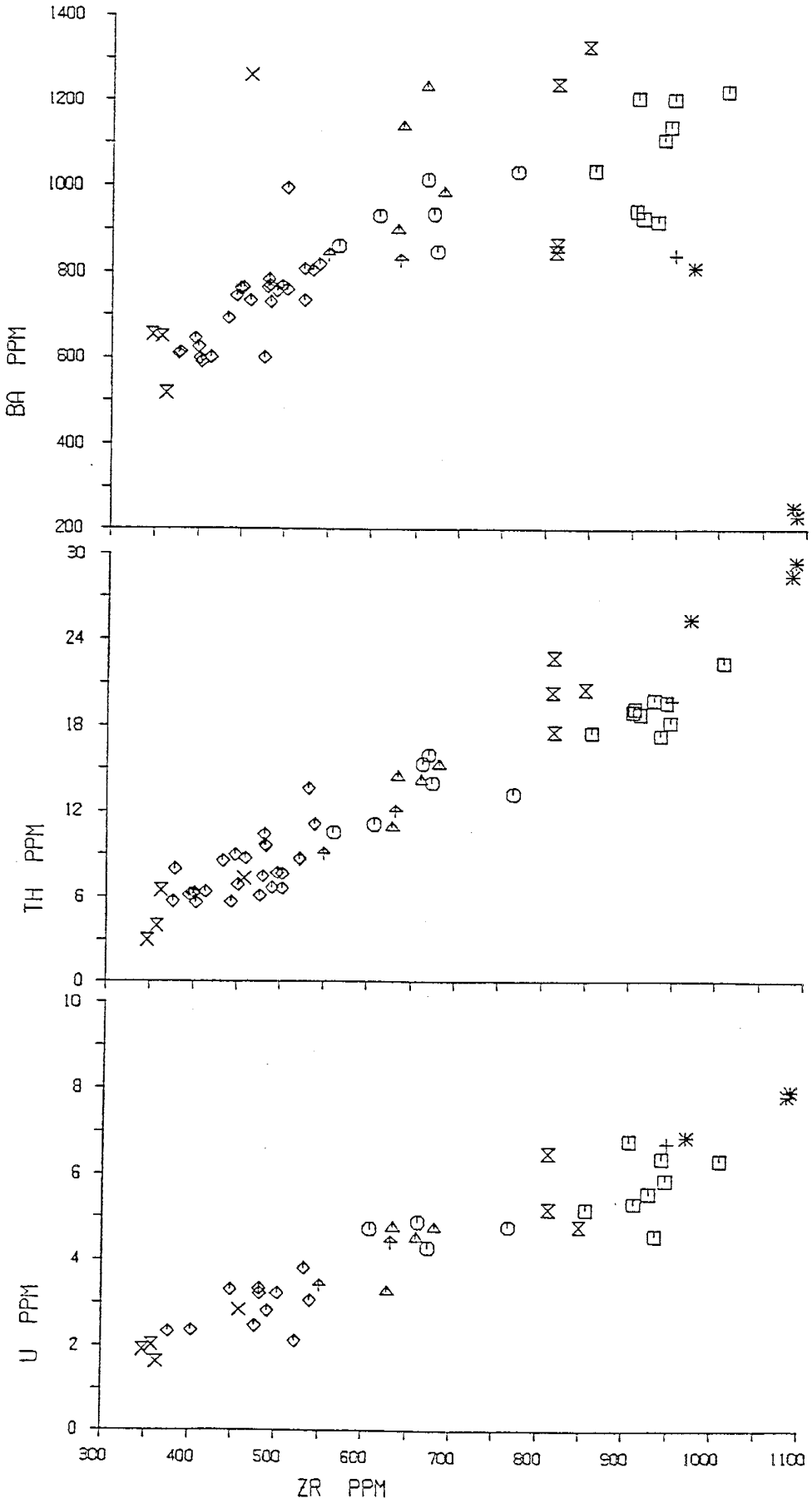

Figure 5.4 continued.

phonolites.

Ga, Hf, Th and U increase steadily with increasing Zr in all the samples. Rb is continuously enriched in EL lavas from basanite through to Ne-benmoreite, then levels out through to anorthoclase phonolite. Nb and Ta also increase strongly with increasing Zr. EL lavas exhibit straight trends for these elements with a slight kink coinciding with the gap in Zr between 670-760 ppm. EFS lavas define a trend with lower Nb and Ta and higher Th than the trend of EL lavas.

Ba increases strongly in EL lavas from basanite to phonolite. The anorthoclase phonolites have a large range in Ba (900-1200 ppm), probably as a result of their anorthoclase-phyric nature. The benmoreites and Inaccessible Island kaersutite phonolites have high Ba contents, while the Bomb Peak kaersutite phonolites and the trachytes are strongly depleted in Ba.

In summary, EL lavas form continuous smooth trends on major and trace elements plots. EFS lavas form distinctly different trends. This is especially obvious in incompatible element plots, such as Zr and Nb against SiO_2 (Fig. 5.5). This figure also shows some Ne-hawaiite and Ne-benmoreite samples and the anorthoclase-pyroxene cumulate as having lower Zr and Nb than the main trend of EL lavas. This is most likely due to the high feldpsar content of these

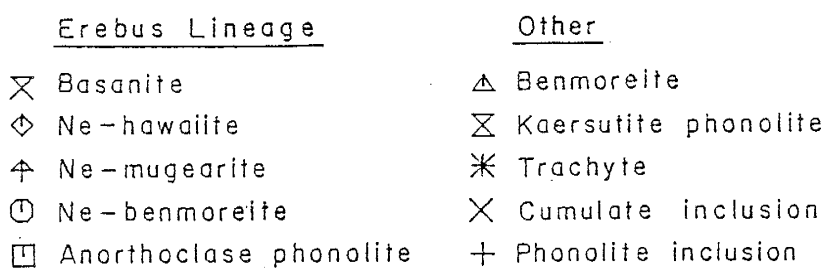
Erebus Lineage
Basanite
Ne-hawaiite
Ne-mugearite
Ne-benmoreite
Anorthoclase phonolite
Other
Benmoreite
Kaersutite phonolite
Trachyte
Cumulate inclusion
Phonolite inclusion

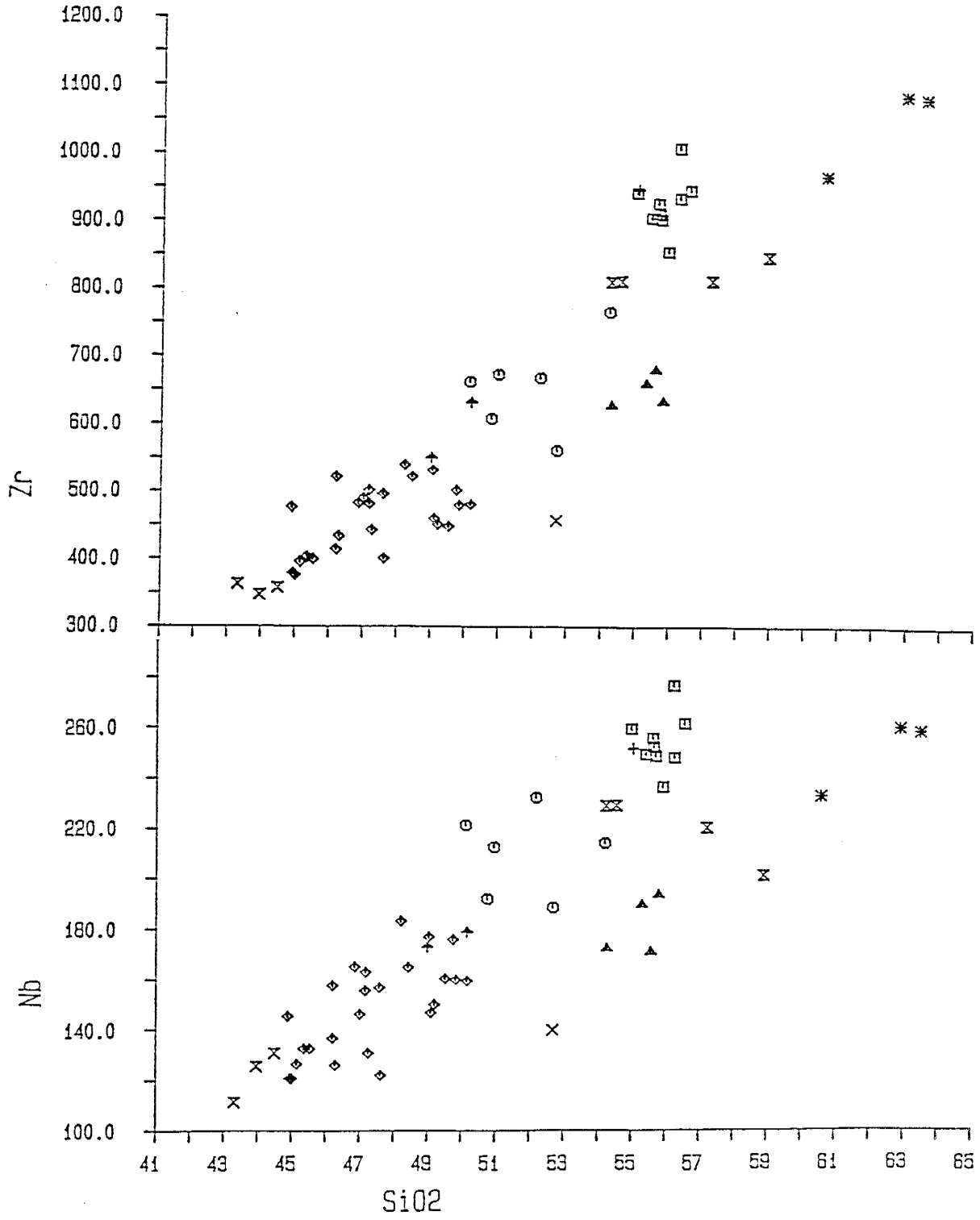

Figure 5.5. Variation of Zr and Nb (in ppm) against silica (wt.%) in Mt. Erebus lavas.

samples which has enriched their silica and Sr contents.

Rare Earth Elements

Typical of alkaline igneous rocks, the samples from Mt. Erebus have high concentrations of REE and are light REE-enriched on chondrite-normalized plots (La_N/Yb_N=13.5-20.2; Figs. 5.6-5.8). In EL lavas, REE show limited nonuniform enrichment from basanite to phonolite. This is best seen in Fig. 5.7, which shows chondrite-normalized REE concentrations of representative EL lavas. The heavy REE (Yb, Lu) show the greatest enrichment and the middle REE (Sm, Eu, Tb) the least. The Ne-hawaiites have a moderate range in REE concentrations, overlapping with the basanites. Some Ne-hawaiite and anorthoclase phonolite samples have slight positive Eu anomaly and the anorthoclase-pyroxene cumulate xenolith (82403) has a strong positive Eu anomaly. REE show a moderate amount of variation and increase with increasing differentiation in the anorthoclase phonolite samples.

The benmoreites have slightly lower light and heavy REE concentrations than the Ne-benmoreites and lower middle REE than all EL lavas (Fig. 5.8). The kaersutite phonolites have approximately the same light REE concentrations but appreciably lower middle and heavy REE concentrations than all EL lavas. The trachytes have the highest concentrations of all REE and show strong negative Eu anomalies.

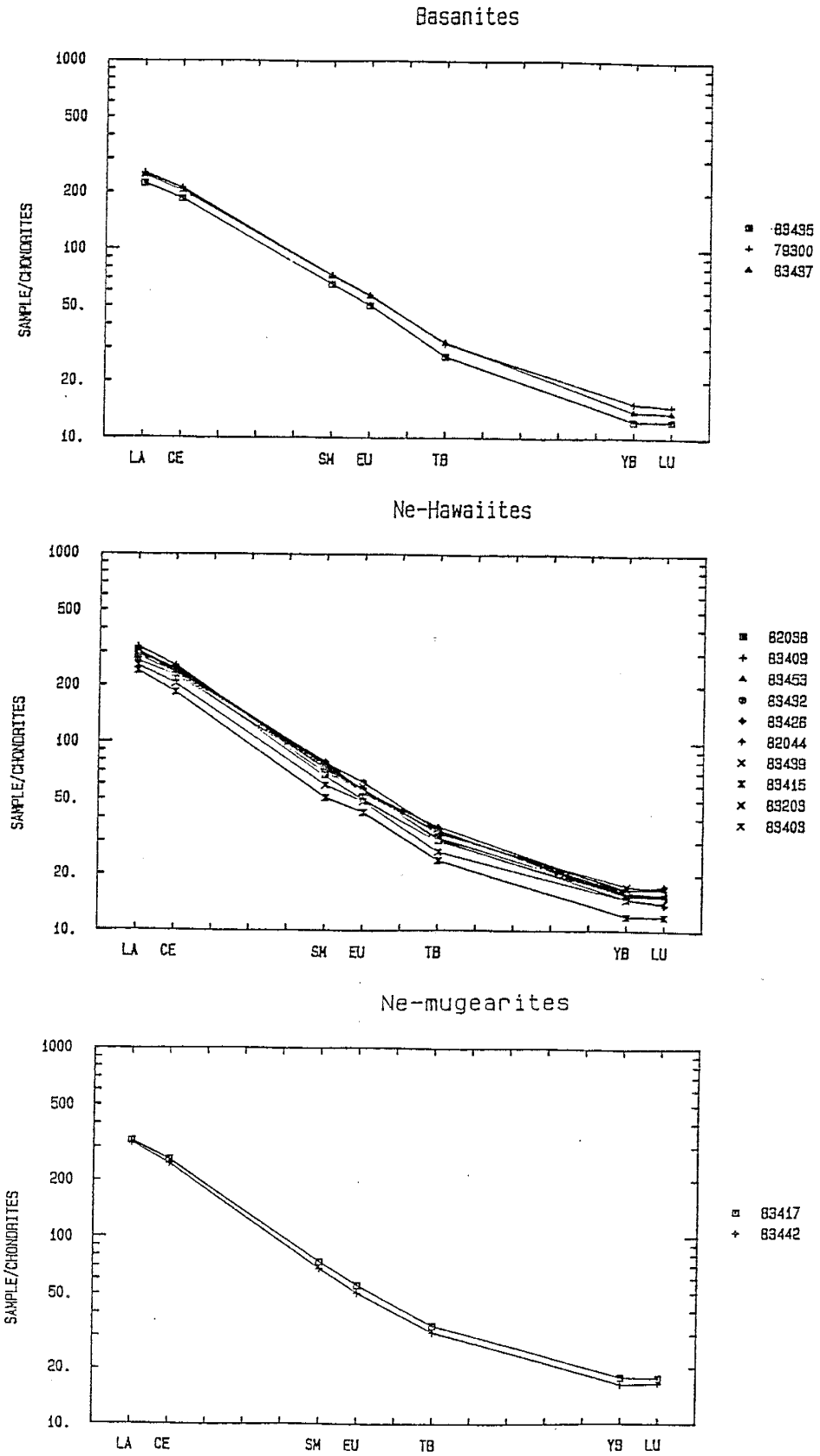

Figure 5.6. Plots of chondrite-normalized rare earth element concentrations (in ppm) of Erebus lineage lavas, using normalization factors of Taylor and Gorton (1977).

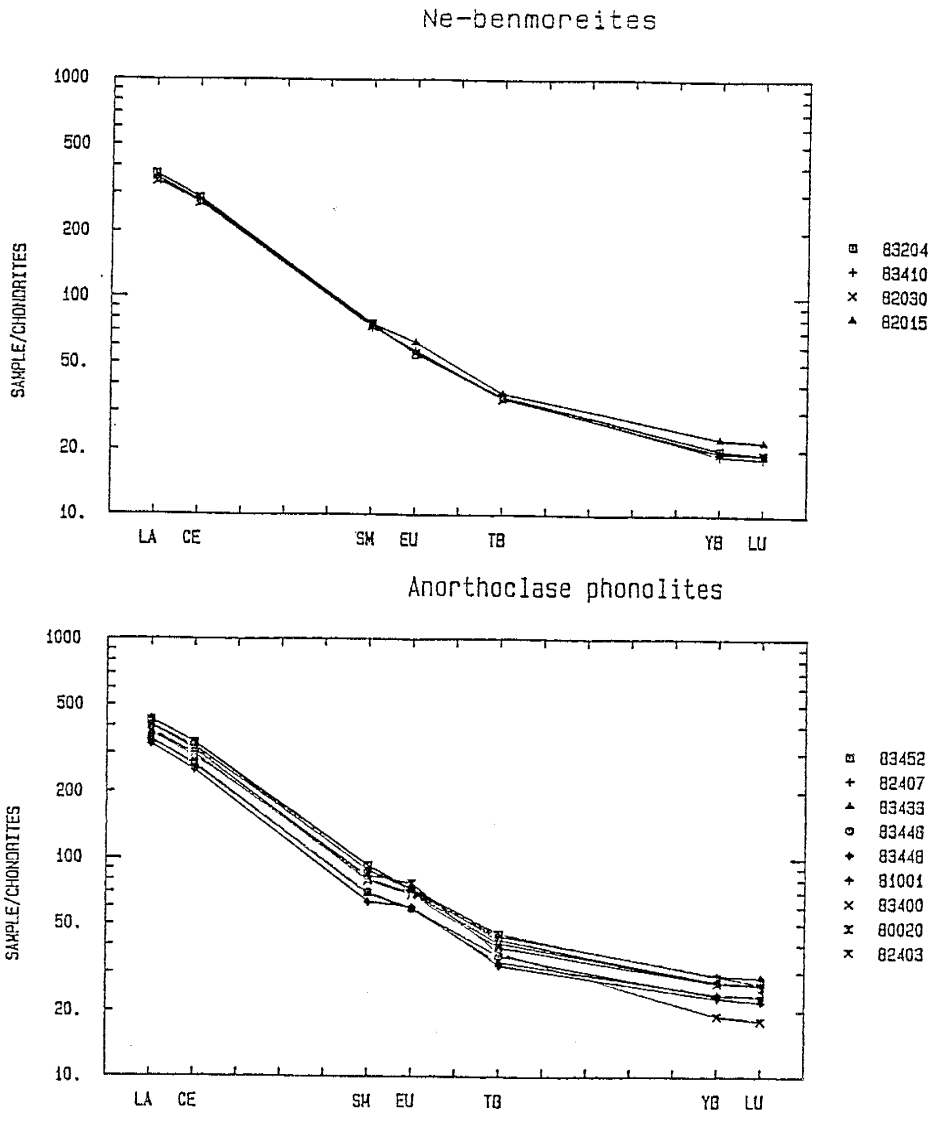

Figure 5.6 continued.

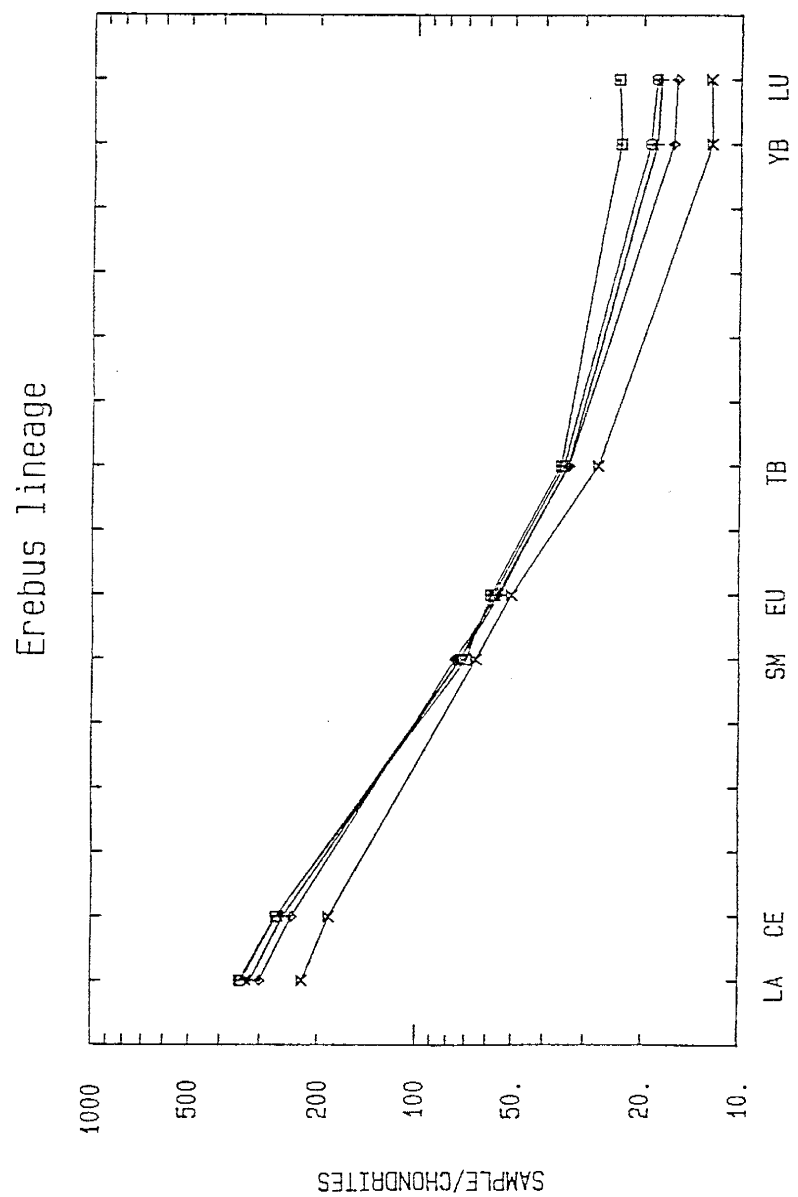

Figure 5.7. Plot of chondrite-normalized rare earth element concentrations (in ppm) in representative samples of Erebus lineage lavas.

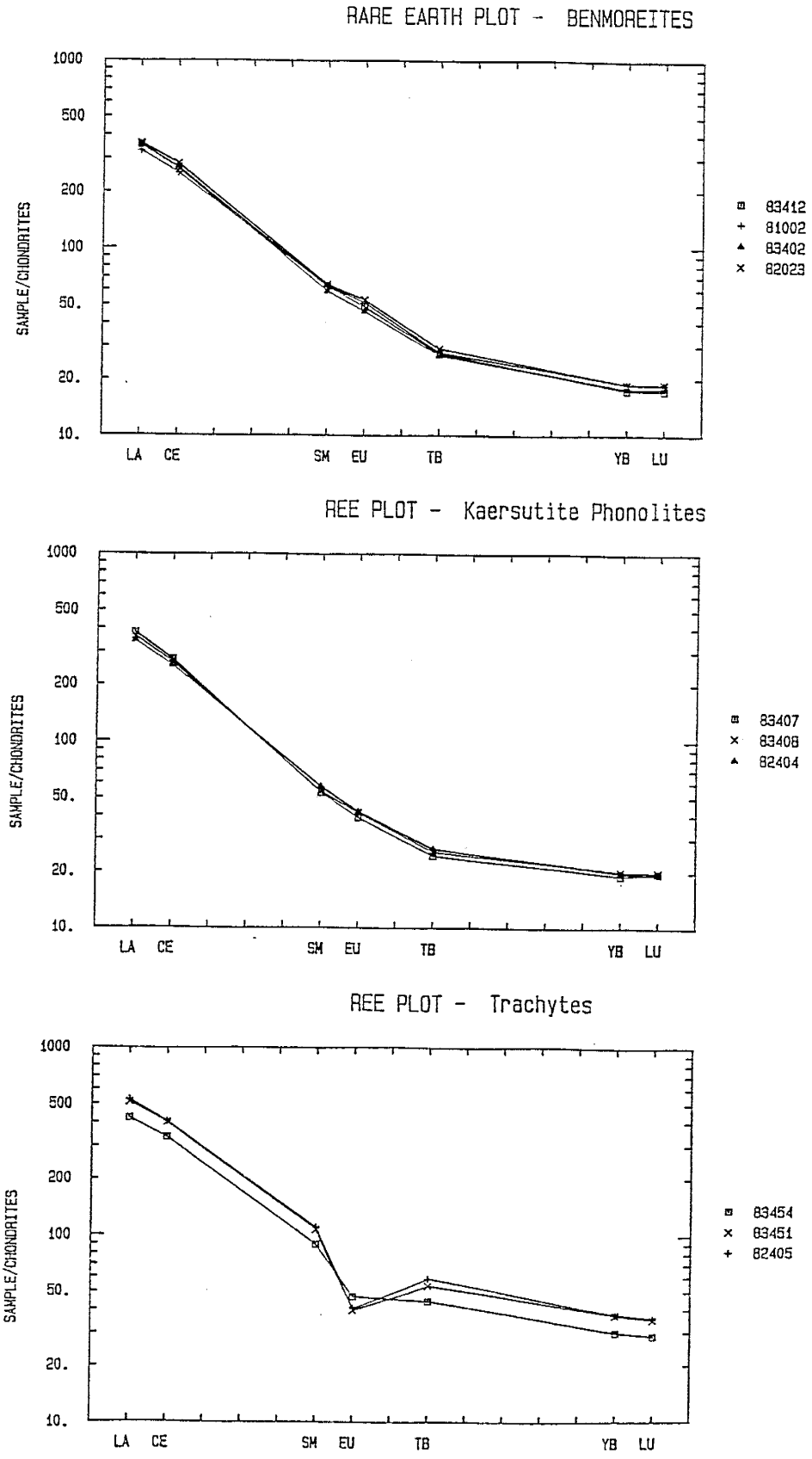

Figure 5.8. Plot of chondrite-normalized rare earth element concentrations (in ppm) in benmoreites, kaersutite phonolites and trachytes.

La/Ce is constant with increasing Zr whereas La/Sm increases slightly in EL lavas from basanite to anorthoclase phonolite (Fig. 5.9). La/Yb stays approximately constant from basanite to Ne-mugearite and decreases slightly from Ne-benmoreite to anorthoclase phonolite. La/Yb and La/Sm ratios are distinctly higher in benmoreites and kaersutite phonolites than Erebus lineage lavas but are similar in anorthoclase phonolites and trachytes.

REE were analyzed in Ne-hawaiite, Ne-mugearite, Ne-benmoreite and phonolite whole rock, groundmass and andesine phenocryst samples from Kyle (1976) (Fig. 5.10). Groundmass samples are uniformly enriched in REE compared to the whole rocks in whole rock-groundmass pairs, in contrast to the trend of the whole rock samples. Slight positive EU anomalies occur in some samples. Some groundmass samples show slight negative Eu anomalies but most exhibit smooth REE variations.

Pb and Sr Isotopes

Sun and Hanson (1975) determined Pb isotopic ratios, and Stuckless and Ericksen (1976) and Jones et al. (1983) determined $^{87}Sr/^{86}Sr$ ratios in samples from Ross Island, including samples from Mt. Erebus (Table 5.2). The Pb isotopic ratios of primary basanites form a geochron which indicates the mantle source of the basanites has been heterogeneous for 1500 m.y. (Sun and Hanson, 1975). The

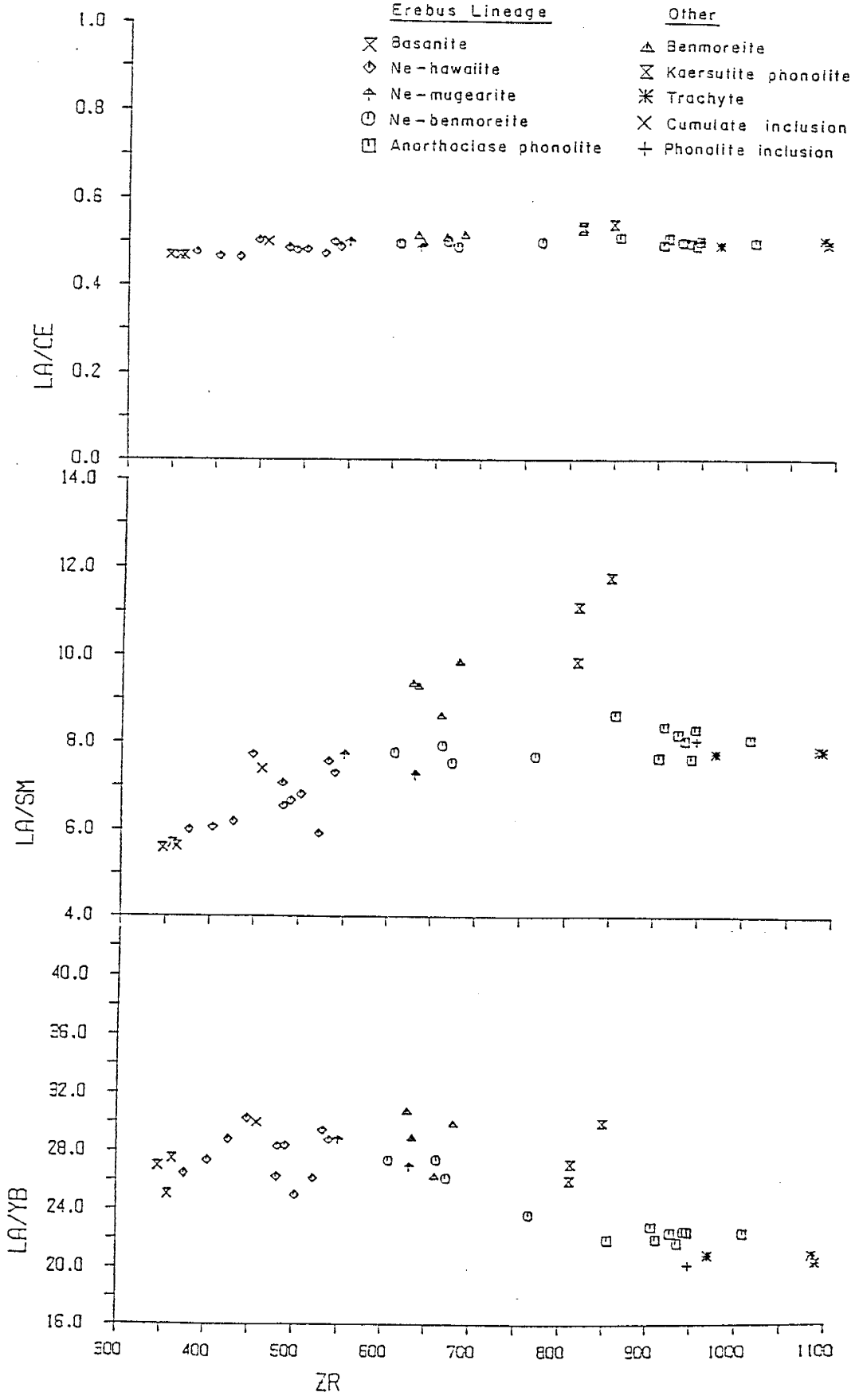

Figure 5.9. Variation of La/Ce, La/Sm, and La/Yb against Zr in Mt. Erebus lavas.

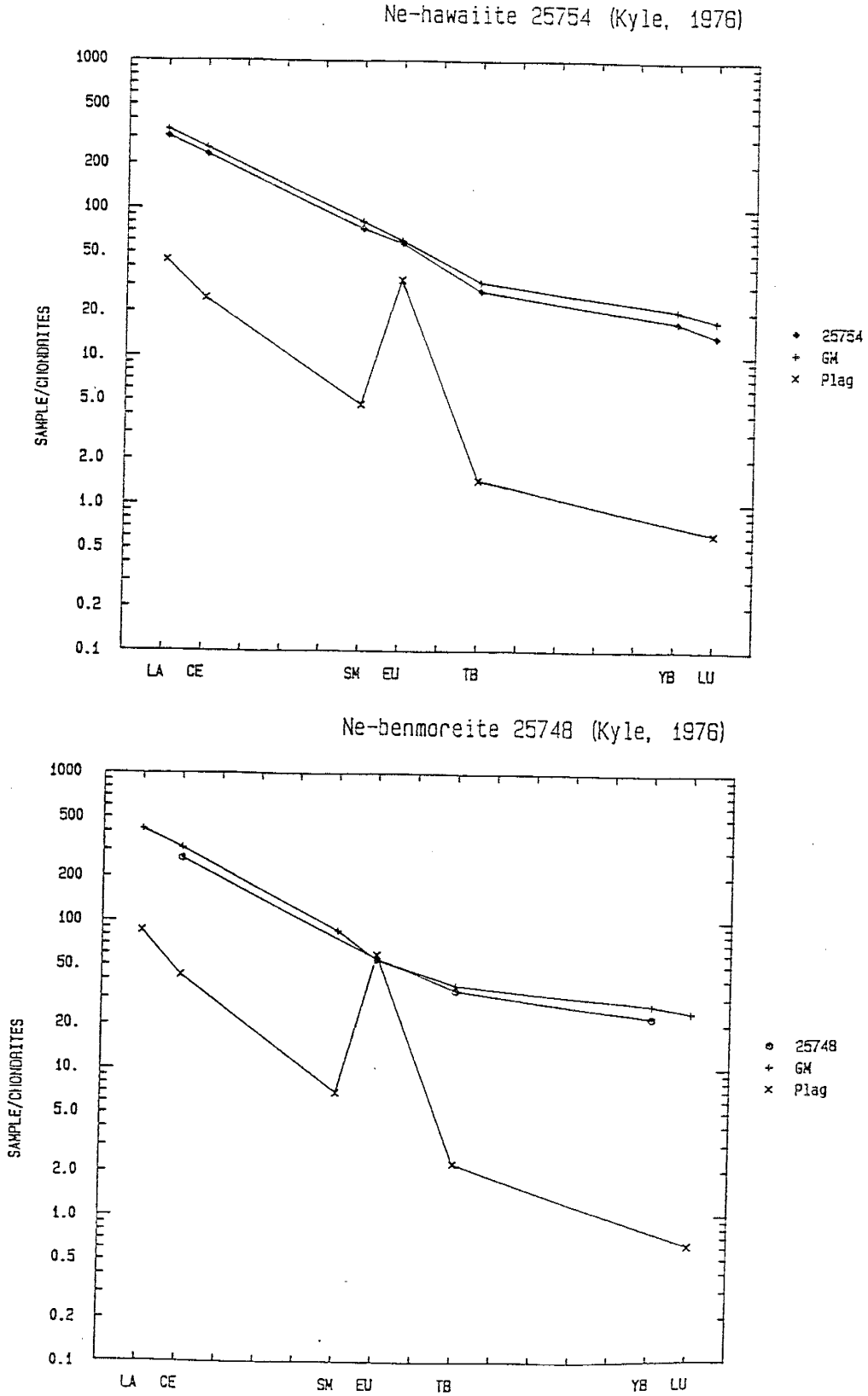

Figure 5.10. Plots of chondrite-normalized rare earth element concentrations (in ppm) in representative Ne-hawaiite and Ne-benmoreite whole rock, groundmass and plagioclase phenocryst samples from Kyle (1976). Normalizing factors of Taylor and Gorton (1977). GM - groundmass; plag - plagioclase phenocrysts.

Table 5.2. Isotopic compositions of lavas of Ross Island and Mt. Erebus

Pb isotopes (Sun and Hanson, 1975

	$^{206}/^{204}Pb$	$^{207}/^{204}Pb$	$^{208}/^{204}Pb$
Basanites (range of 5)	19.523-20.061	15.607-15.653	39.007-39.600
Ne-hawaiite (Cape Barne)	19.902	15.629	39.555
Anorthoclase phonolite (Cape Royds)	19.823 19.821	15.650 15.646	39.407 39.405
Anorthoclase phonolite (Cape Evans)	19.882	15.646	39.484
Trachyte (Mt. Cis)	19.431 19.427	15.632 15.629	39.098 39.146

$^{87}Sr/^{86}Sr$ ratios

1. Stuckless and Ericksen, 1976

Basanite composite (3 samples)	0.70320±0.00002
Anorthoclase phonolite (summit, Mt. Erebus)	0.70321
Anorthoclase (summit, Mt. Erebus)	0.70325
Trachyte (Mt. Cis)	0.70489

2. Jones et al., 1983

Anorthoclase phonolite (Cape Royds)	0.70363±0.00004
Anorthoclase (summit, Mt. Erebus)	0.70330±0.00003

$^{87}Sr/^{86}Sr$ ratios of the samples are low and show a very small range (0.7031-0.7036). Anorthoclase phonolites have virtually the same $^{87}Sr/^{86}Sr$ ratios as the basanites. Anorthoclase phenocrysts in anorthoclase phonolite samples have virtually the same Sr isotopic ratios as the whole rock, indicating they are cognate in origin. The trachytes from Mt. Cis have significantly different Pb isotopic ratios and higher $^{87}Sr/^{86}Sr$ (0.7049) than the rest of the samples from Ross Island.

CHAPTER SIX

PETROGENESIS

Parental Magmas

The strongly undersaturated lavas from Mt. Erebus show a wide range in composition from basanite to anorthoclase phonolite and have been called the Erebus lineage. They form single, continuous trends from basanite to anorthoclase phonolite on geochemical variation diagrams, indicating the lineage evolved from a basanite parental magma.

The basaltic parental magmas of igneous differentiation lineages on oceanic islands are generated by partial melting of peridotite mantle (Kay and Gast, 1973). The basanite lavas of the Erebus lineage are too evolved to be the parental magma. Primary magmas formed as partial melts of peridotite mantle with ~2000 ppm Ni and olivine of Fo_{92-88} should have Mg numbers [$Mg/(Mg+Fe^{2+})$] between 0.68 and 0.77 and 300-400 ppm Ni (Green, 1970; Sun and Hanson, 1975). The basanites from Mt. Erebus have Mg numbers between 0.54 and 0.48 and 10-63 ppm Ni. Thus they must be differentiates of the parental magma. Basanites of the DVDP lineage from the nearby Hut Point Peninsula have an average Mg number of 0.69, 250-276 ppm Ni and 370-477 ppm Cr (Kyle, 1981b), thus are probably very near to primary mantle melts. Because of

the geographic proximity of Mt. Erebus and the Hut Point Peninsula, the EL parental magmas were probably similar to these primary basanites of the DVDP lineage. The DVDP basanites also lie on the extrapolation of EL trends on all variation diagrams as will be shown in a later section.

Sun and Hanson (1975) concluded from the Mg numbers and Ni and Cr contents of DVDP basanites that 10% crystallization of olivine and clinopyroxene had occurred since the basanites were derived, but that the ratios of light REE, Ba, Rb and Sr were not affected. The geochemistry of the primary basanites is therefore indicative of the composition of the mantle source of the basanite parental magmas. Variations in Mg numbers and trace and rare earth element concentrations occur in the primary basanites (Sun and Hanson, 1975), suggesting a spectrum of melts from the mantle due primarily to mantle heterogeneity. Pb isotopic ratios in the basanites suggest 30% variation in trace elements in their mantle source (Sun and Hanson, 1975). The ratios form a linear array which dates the mantle heterogeneity to a 1500 m.y.-old event, probably partial melting (Sun and Hanson, 1975). Sr isotopes (Stuckless and Ericksen, 1976) suggest a homogeneous mantle source but are compatible with 30% variation in the mantle if Rb/Sr has been <0.02 and $^{87}Rb/^{86}Sr$ has been <0.057 for the past 1500 m.y. (Stuckless and Ericksen, 1976).

The $^{87}Sr/^{86}Sr$ ratios in the primary basanites (0.7031-0.7033; Stuckless and Ericksen, 1975) indicates they were derived from a depleted mantle source but less depleted than the mantle source of mid-ocean ridge basalts ($^{87}Sr/^{86}Sr$ c.0.7028; Faure, 1977). The heavy REE depletion of the basanites indicates their peridotite source contains garnet (Kay and Gast, 1973). The basanites therefore were derived at >20kbars pressure, equivalent to 60 km depth (Green, 1973; Merrill and Wyllie, 1975).

Basanite melts were derived experimentally from hydrous garnet peridotite by 7-10% partial melting (Green, 1970). However, incompatible element concentrations were much lower than observed in primary basanites. Partial melting of >1% of garnet peridotite requires incompatible element enrichment of the source in order to match the concentrations of these elements in basanites and alkali basalts (Menzies and Murthy, 1980). Kay and Gast (1973) modeled the generation of alkali basalt by 1-2% partial melting of hydrous garnet peridotite with REE concentrations of 2-5x chondrites. Sun and Hanson (1975) suggested the high concentrations of light REE in basanites ($\geq$200x chondrites) requires greater enrichment of light REE than heavy REE. Therefore Sun and Hanson (1975) concluded that the DVDP basanites were derived by 3-7% melting of chemically-heterogeneous garnet peridotite with La concentrations ~14x chondrite and Yb concentrations ~3x

chondrite.

For partial melts $\leq$5% CO_2 must be present during melting because CaO/Na_2O ratios indicate incongruent melting of clinopyroxene (Frey et al., 1978). Clinopyroxene melting would also enrich the melt in middle REE, and explain the REE pattern of primary basanites. Kyle (1981b) suggested that the primary basanites of Hut Point Peninsula formed by 1-2% partial melting of hydrous, CO_2-containing garnet peridotite with 2-3x chondrite REE contents.

Nd and Sr isotopic ratios in alkaline basalts (O'nions et al., 1979) indicate a long-lived depletion of their source in Rb, light REE and probably other incompatible elements. Enrichment of the source of alkaline basaltic magmas in these elements must therefore precede magma generation by <100 M.y. (Menzies and Murthy, 1980). Metasomatism by light REE and incompatible element-rich fluids from deep in the mantle is suggested to cause the enrichment and to be a necessary precursor to the generation of alkali basaltic magmas (Menzies and Murthy, 1980; Wass and Rogers, 1980).

The model of mantle metasomatism preceding alkaline basaltic magma formation is supported by metasomatic textures in mantle nodules brought up in alkaline magmas. However, evidence suggests that metasomatic textures observed in these mantle nodules may be due to metasomatism

by the alkaline basaltic melts themselves (Roden et al., 1984; Wilshire, 1984). The chemistry of alkaline basalts could be explained by <1% partial melting of garnet peridotite but separation of such small melts from their source was considered unlikely (e.g. Sleep, 1974). However, McKenzie (1985) has recently suggested that low viscosity melts such as carbonatites can separate even when the melt fraction is as low as 0.1%. Therefore the separation of basanitic magmas formed by <1% partial melting is feasible and could explain the incompatible element and isotopic features of primary basanites without invoking recent enrichment of their mantle source.

Evolution of the Erebus Lineage

The range in composition from basanite to phonolite of the lavas of the Erebus lineage could have resulted from a number of processes. These include open system processes such as contamination or magma mixing, and fractionation processes such as liquid immiscibility, volatile transfer, Soret diffusion, boundary layer fractionation and crystal fractionation. In this section, the field, petrographic and geochemical characteristics of igneous differentiation lineages formed by different processes are reviewed and compared to the features of the Erebus lineage to assess the petrogenetic process that most likely formed the lineage.

Open System Processes

Evidence for assimilation includes xenoliths or xenocrysts. Assimilation of continental crustal material gives elevated Sr and $^{207}Pb/^{204}Pb$ ratios. However, Sr isotopes in EL lavas are within the range suggested for uncontaminated mantle-derived basalts from oceanic islands (0.702-0.706; Peterman and Hedge, 1971) and anorthoclase phonolites have the same $^{87}Sr/^{86}Sr$ ratios as primary basanites from the DVDP lineage (Stuckless and Ericksen, 1976). Pb isotopic ratios are also similar to those found in uncontaminated ocean island basalts (Sun and Hanson, 1975). Xenoliths and xenocrysts are absent from EL rocks. Thus contamination is unlikely to have figured in the evolution of the Erebus lineage.

The elevated $^{207}Pb/^{204}Pb$ and $^{87}Sr/^{86}Sr$ of the trachyte occurring at Mt. Cis and numerous crustal xenoliths in this rock indicates that crustal contamination was involved in the evolution of this lava (Goldich et al., 1975; Kyle, 1976; Stuckless and Ericksen, 1976). Sun and Hanson (1975) concluded that since that Mt. Cis trachyte, obviously contaminated with crustal material, plots off the isotopic trends of EL rocks, crustal contamination probably did not take place in the evolution of the Erebus lineage.

Magma mixing yields variegated lavas from incomplete mixing (e.g. Laacher See volcano; Worner, 1984), and completely mixed magmas exhibit linear variation trends on

element-element plots (McBirney, 1984). Magma mixing is also characterized by resorbed, overgrown xenocrysts. EL lavas are not variegated, form smooth curvilinear trends on element-element variation diagrams, and lack resorbed xenocrysts. Therefore mixing of different magmas is unlikely to have caused the compositional range of the Erebus lineage.

Fractionation Processes

Immiscible magmas are known to form under geologically reasonable conditions in two types of systems (McBirney, 1984), highly alkaline magmas rich in CO_2 and very iron-rich tholeiitic magmas. The lavas of Mt. Erebus do not belong to either of these systems.

Experimental work on magmatic differentiation by Soret diffusion indicates large temperature differences are needed, unusual major and trace element enrichment or depletion trends are produced, and incompatible element ratios show strong variation (Baker and McBirney, 1985). However, the mineral chemistry of EL lavas suggests that temperature changed little during differentiation of the magma. Also, no unusual geochemical couplings occur, and incompatible element ratios show little variation. Thus Soret diffusion is not likely to have formed the Erebus lineage. Volatile transfer is still little understood but has not been demonstrated to be of much effect in changing

the bulk composition of magmas. It is a proposed cause of unusual variations in incompatible trace elements (Hildreth, 1979), but no such extraordinary relations exist in EL lavas.

Boundary layer fractionation and the processes listed above are proposed means of forming zoned magma chambers. Zoned magma chambers are evidenced by compositional heterogeneity within individual eruptive units or successive products from an eruption. These eruptive products may show "normal" zoning, where the most evolved magmas were erupted first, or "reverse" zoning, where the more mafic magmas were erupted first. However, Mt. Erebus has had a long history of eruption of anorthoclase phonolite (c.1 m.y.) without significant variation in its composition during that period. This is evidence that the anorthoclase phonolites, and therefore the whole range of EL lavas, were not products of a stratified magma body.

Fractional Crystallization

The evolution of igneous suites by fractional crystallization is characterized by a range of eruptive products which become increasingly felsic with time and exhibit smooth continuous curvilinear trends on elemental variation diagrams. Compatible elements decrease while incompatible elements increase and have approximately constant ratios. A good understanding of the stratigraphy of

Mt. Erebus is not possible because of the lack of overlapping outcrops and age dates. However, within individual outcrops the lavas become more differentiated upward in the sequence. Thus, field relationships and geochemical variation trends of the EL conform with evolution of the lineage by fractional crystallization.

The progressive decrease of TiO_2, FeO*, MgO, CaO and P_2O_5 with increasing evolution of EL lavas is indicative of olivine, clinopyroxene, opaque oxide, and apatite fractionation. The trend of Al_2O_3 is compatible with little feldspar fractionation in lavas from basanite through to Ne-benmoreite, then significant feldspar fractionation in lavas more evolved than Ne-benmoreite. The trends of Na_2O and K_2O also suggest negligible feldspar fractionation until the most evolved compositions.

The trace element trends of the Erebus lineage can also be explained by fractional crystallization. Sc, V, Cr, Ni and Cu decline sharply in the more basic rocks to detection limits, most likely because of olivine, clinopyroxene and opaque oxide fractionation. Sr increases slightly from basanite to Ne-hawaiite, then declines moderately through to anorthoclase phonolite, suggesting apatite and feldspar fractionation from lavas more evolved than basanite. Ga, Y, Zr, Nb, Cs, Ba, Hf, Ta, Th and U increase in concentration in the lavas from basanite through to anorthoclase

phonolite. This fits with fractionation of olivine, clinopyroxene, opaque oxides, feldspar and apatite, in which these elements are incompatible. The trend of Rb increases from basanite through to Ne-benmoreite, then levels out slightly through to anorthoclase phonolite, suggesting fractionation of a Rb-bearing phase in the anorthoclase phonolites. This could be anorthoclase, as Mason et al. (1982) found that anorthoclase in the phonolite is enriched in Rb.

Fractional crystallization also explains the REE patterns of the Erebus lineage. The general enrichment of REE from basanite to phonolite reflects olivine and Fe-Ti oxide fractionation, because REE are strongly incompatible in these minerals. However, the overall enrichment of REE is limited, and this can be attributed to apatite fractionation, because REE are concentrated in apatite. Middle REE show almost no change in concentration, as a result of clinopyroxene fractionation.

The slight positive Eu anomalies in some samples suggests small amounts of cumulate feldspar. However, Eu anomalies are generally absent in the samples and their groundmasses. This suggests that most of the feldspar phenocrysts are not cumulate but crystallized at a late stage. Significant amounts of feldspar fractionation with the REE concentrations of the feldspars measured in this

study would have caused negative Eu anomalies in the samples. Thus feldspar fractionation may have been insignificant in the evolution of the EL lavas. Alternatively, the development of negative Eu anomalies in the samples as a result of feldspar fractionation may have been cancelled out by enrichment of Eu due to clinopyroxene and apatite fractionation. Another possibility is that the feldspar fractionated during evolution of the lineage may have been less enriched in Eu as a result of crystallization at higher oxygen fugacity and temperature, than the late-stage feldspar analyzed in this study (Drake, 1975). Such feldspar would not have formed negative Eu anomalies in the lavas.

Kyle (1981b) showed that K/Rb trends of volcanic lineages depend on whether clinopyroxene or kaersutite was the dominant fractionating phase. This is because Rb has similar distribution coefficients in clinopyroxene and kaersutite, but K is almost twice as compatible in kaersutite as in clinopyroxene. Thus, fractional crystallization of clinopyroxene results in constant K/Rb ratios with increasing differentiation while kaersutite fractionation results in progressively decreasing K/Rb ratios with increasing differentiation. In Fig. 6.1, the Erebus lineage shows almost constant K/Rb from basanite to anorthoclase phonolite, suggesting clinopyroxene and not kaersutite fractionation occurred.

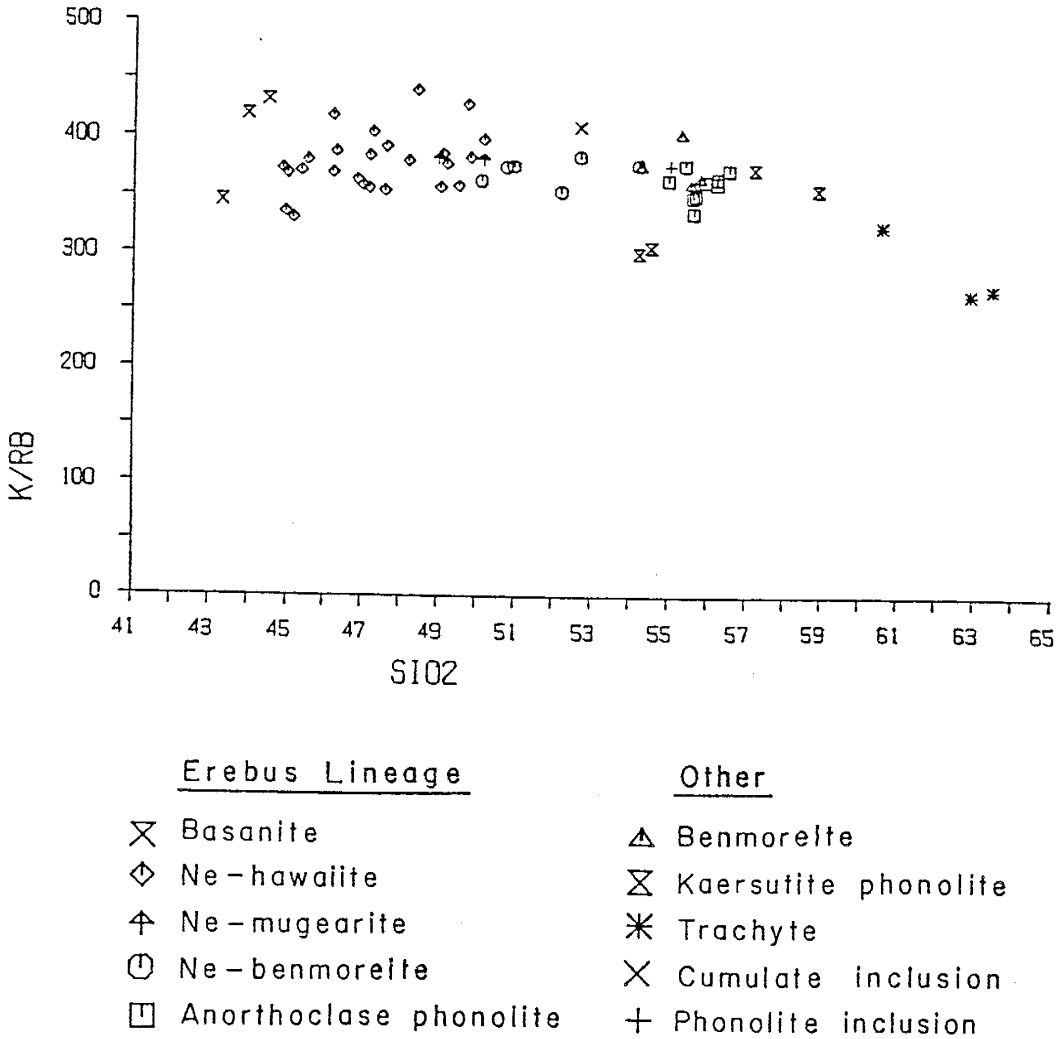

Figure 6.1. Variation in K/Rb (in ppm) against SiO_2 (wt.%) in Mt. Erebus lavas.

The anorthoclase phonolites plot in the low temperature trough close to the ternary minima in the 1 atm normative quartz-nepheline-kalsilite system for evolved igneous rocks (Schairer, 1950) (Fig. 6.2). This suggests the phonolites had reached a natural ternary minima and crystal-liquid equilibria before being erupted. If so, continued fractionation would cause little change in major elements but affect trace elements. This accounts for the narrow range in major element chemistry but moderate range in trace elements in the anorthoclase phonolites.

In summary, the field relationships and geochemical trends of the Erebus lineage strongly support the evolution of the lineage by fractional crystallization. The crystallate implied by the geochemical trends coincides with the observed phenocryst phases of olivine, pyroxene, Fe-Ti oxides, feldspar and apatite.

Fractionation Sequence

Least-squares mass balancing of major elements (Bryan et al. 1969) was used to derive quantitative crystal fractionation models for the Erebus lineage. Microprobe analyses of phenocrysts from the samples were used, with the exception of a chrome spinel analysis from Kyle (1981b), nepheline analyses from Deer et al. (1966), and an apatite analysis from Kyle (unpubl.). Major element analyses of the

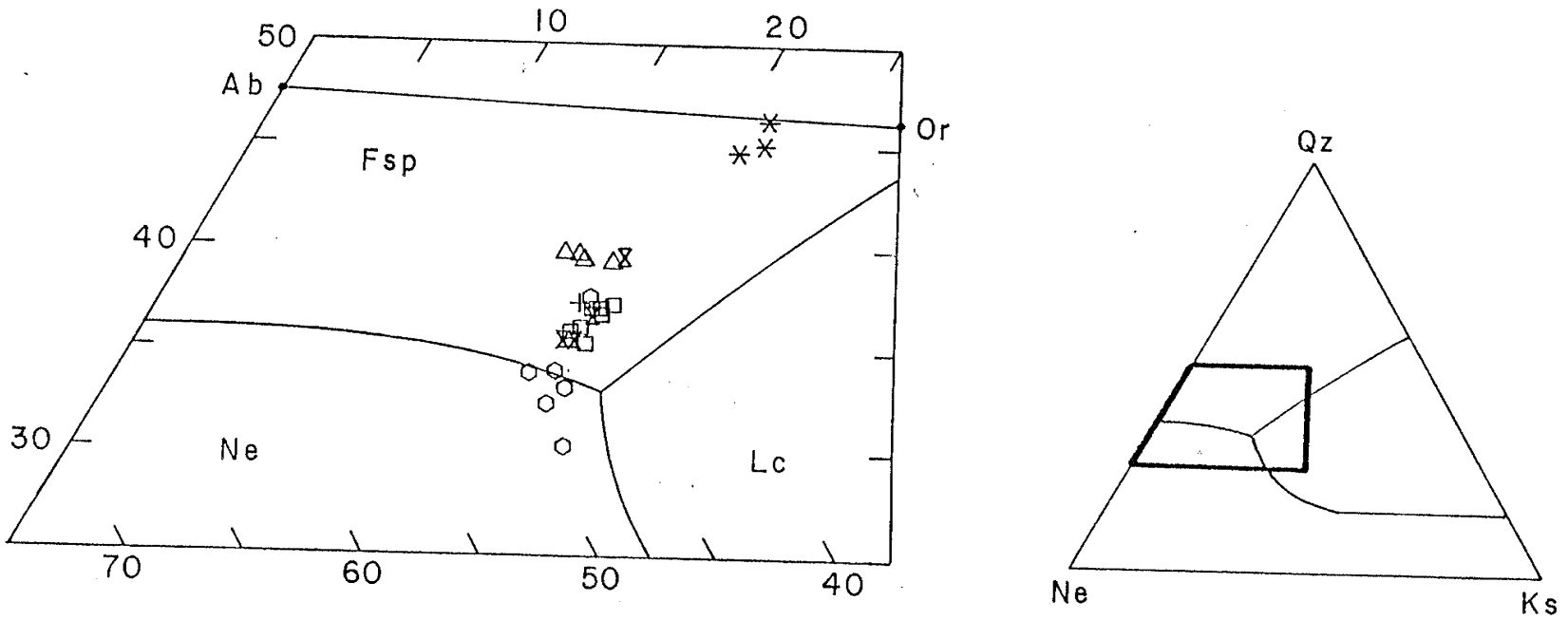

Figure 6.2. Phase equilibrium diagram of the system Ne ($NaAlSiO_4$), Ks ($KAlSiO_4$) and Qz (SiO_2) at P_{H_2O}=1 atm. (Schairer, 1950).

Table 6.1. Mineral compositions used in mass balance modeling.

OLIVINES

	$Fo_{88}B$	$Fo_{65}Nh$	$Fo_{66}Nh$	$Fo_{65}Nm$	$Fo_{58}Ap$
SiO_2	40.28	36.74	37.01	36.48	35.89
FeO*	12.00	30.28	29.54	30.39	35.20
MnO	0.15	0.77	0.83	1.09	1.91
MgO	47.04	31.83	32.29	31.55	27.01
CaO	0.12	0.44	0.33	0.37	0.37

	CLINOPYROXENES				SPINEL	ILMENITE
	$En_{40}B$	$En_{41}B$	$En_{39}Nh$	$En_{39}Ap$		
SiO_2	45.30	44.89	47.70	50.00	0.17	0.09
TiO_2	3.87	4.36	3.39	1.84	3.36	49.48
Al_2O_3	10.05	8.72	5.85	3.69	41.70	0.60
FeO*	7.10	8.44	7.67	9.28	31.60	40.46
MnO	--	0.16	0.21	0.54	0.21	0.72
MgO	12.29	12.62	12.41	12.44	15.10	6.35
CaO	20.72	21.51	21.65	20.89	0.03	--
Na_2O	0.52	0.49	0.75	0.99	--	--

TITANOMAGNETITES

	$Usp_{52}B$	$Usp_{71}Nh$	$Usp_{73}Nh$	$Usp_{61}Nh$	$Usp_{68}Ap$
SiO_2	0.12	0.14	0.12	0.11	0.10
TiO_2	12.69	23.26	23.80	19.67	23.49
Al_2O_3	10.57	4.99	4.94	6.27	2.51
FeO*	60.06	63.26	63.32	65.03	68.16
MnO	0.31	0.66	0.66	0.65	1.71
MgO	7.85	5.58	5.51	5.83	2.83

FELDSPARS

	$An_{64}B$	$An_{72}B$	$An_{52}Nh$	$An_{44}Nm$	$An_{33}Nb$
SiO_2	52.16	50.58	55.68	58.00	59.18
Al_2O_3	30.35	30.98	27.75	26.38	25.47
FeO*	0.60	0.43	0.25	0.21	0.22
CaO	13.19	14.52	10.41	8.69	6.97
Na_2O	3.84	2.99	5.00	5.51	6.98
K_2O	0.31	0.20	0.57	0.89	1.58

Table 6.1 continued.

	NEPHELINE[1]		APATITE[2]
	Ne1	Ne2	
SiO_2	42.41	44.65	0.18
TiO_2	0.05	--	--
Al_2O_3	33.16	32.03	--
FeO*	1.22	0.53	0.34
MnO	--	--	0.13
MgO	0.07	--	0.28
CaO	0.48	0.71	53.69
Na_2O	16.08	17.25	--
K_2O	6.83	3.66	--
P_2O_5	--	--	41.54

Abbreviations: B - basanite; Nh - Ne-hawaiite; Nm - Ne-mugearite; Nb - Ne-benmoreite; AP - anorthoclase phonolite

1-Deer et al. (1966)
2-Kyle (unpubl.)

phenocrysts used in the modeling are given in Table 6.1.

Geologically and mineralogically reasonable models with sums of squares of differences of less than 0.1 were accepted. The models were tested using trace element data and the Rayleigh fractionation equation (Arth, 1976). Measured mineral/melt partition coefficients from the literature and from measurements made on feldspars in this study were used in the trace and rare earth element modeling (Table 6.2). Measured distribution coefficients were used because they take into account inclusions and zoning in natural phenocrysts and are therefore more accurate for crystal fractionation modeling than experimental values (Hart and Brooks, 1974). The distribution coefficients are taken from analyses of phenocryst/matrix pairs in rocks of similar composition as distribution coefficients have been shown to be compositional, temperature and pressure dependent (McIntire, 1963; Philpotts and Schnetzler, 1970; Green and Pearson, 1985).

Models

Sample 2-105.53 from Kyle (1981b), a primitive basanite from DVDP drill core, was used as the parental magma for the Erebus lineage. The evolution of the lineage was modeled in three steps based on the major rock types forming the lineage: basanite to Ne-hawaiite, Ne-hawaiite to Ne-benmoreite, and Ne-benmoreite to anorthoclase phonolite.

Table 6.2. Mineral/melt distribution coefficients used in trace element modeling.

	Olivine	Clinopyroxene			
Step		1	2	3	3
Model		1-3	1,2	1,2	3
Rb	0.010	0.03	0.032	0.032	0.032
Sr	0.014	0.12	0.516	0.516	0.516
Zr	0.01	0.1	0.25	0.25	0.25
Nb	0.01	0.10	0.30	0.30	0.30
Ba	0.010	0.026	0.131	0.131	0.131
La	0.01	0.10	0.10	(0.3)*	0.10
Ce	0.009	0.18	0.18	0.359	0.18
Sm	0.011	0.56	0.56	0.98	0.56
Eu	0.010	0.58	0.58	0.85	0.58
Tb	0.013	0.73	0.73	(1.05)	0.73
Yb	0.023	0.61	0.61	1.05	0.61
Lu	0.010	0.57	0.57	1.12	0.57
Source	1-4	3-5	3-5	3,4,10	3-5

	Spinel, magnetite			
Step	1	2	3	3
Model	1-3	1,2	1,2	3
Rb	0.01	0.01	0.01	0.01
Sr	0.01	0.01	0.01	0.01
Zr	0.1	0.2	0.8	0.2
Nb	0.4	1.0	2.5	1.0
Ba	0.01	0.01	0.01	0.01
La	0.01	0.01	0.01	0.01
Ce	0.01	0.01	0.01	0.01
Sm	0.01	0.01	0.01	0.01
Eu	0.01	0.01	0.01	0.01
Tb	0.01	0.01	0.01	0.01
Yb	0.01	0.01	0.01	0.01
Lu	0.01	0.01	0.01	0.01
Source	4,6	4,6	4,6	4,6

	Feldspar				
Step	1	2	2	3	3
Model	3	1	2	1,2	3
Rb	0.071	0.048	0.048	0.066	0.048
Sr	1.83	2.84	2.84	4.62	2.84
Zr	0.01	0.03	0.03	0.10	0.03
Nb	0.01	0.025	0.025	0.06	0.025
Ba	0.23	0.36	0.36	1.47	0.36
La	0.023	0.023	0.165	0.28	0.165
Ce	0.023	0.023	0.122	0.215	0.122
Sm	0.023	0.023	0.074	0.135	0.074
Eu	0.232	0.232	0.638	1.10	0.638
Tb	(0.018)	(0.018)	0.039	0.10	0.039
Yb	0.030	0.030	0.052	0.062	0.052
Lu	(0.03)	(0.03)	(0.04)	0.060	(0.04)
Source	1,3,4	1,3,4	3,4,11	4,5	3,4,11

Table 2 continued.

	Nepheline		Apatite	
Step		3	3	Others
Model		1,2	1	
Rb	(0.01)	(0.01)	0.01	0.01
Sr	(0.01)	(0.01)	5.0	2.0
Zr	(0.01)	(0.01)	0.01	0.01
Nb	(0.01)	(0.01)	0.01	0.01
Ba	(0.01)	(0.01)	0.10	0.10
La	(0.01)	0.12	15.2	8.0
Ce	(0.01)	0.14	16.6	10.0
Sm	(0.02)	0.22	20.7	14.0
Eu	(0.02)	0.26	14.5	13.0
Tb	(0.03)	0.33	19.8	11.0
Yb	(0.03)	0.33	9.4	7.0
Lu	(0.03)	0.34	7.9	5.0
Source		9	2,6,8	6,7

* values in parantheses extrapolated or interpolated

Sources

1. Schnetzler & Philpotts, 1970
2. Le Roex & Erlank, 1982
3. Arth, 1976
4. Pearce & Norry, 1979
5. Sun & Hanson, 1976
6. Le Roex, 1985
7. Irving & Frey, 1984
8. Nagasawa & Schnetzler, 1971
9. Cullers & Medaris, 1977
10. Nagasawa, 1973
11. This study

Several reasonable models were derived for each step, showing that mass balance calculations are only models and a fractionation step may have a number of satisfactory solutions, as pointed out by Kyle et al. (1979).

Nepheline is fractionated in several of the models derived for the Erebus lineage. Although nepheline phenocrysts are rarely seen, nepheline fractionation is supported by calculation of the one atm liquidus mineralogy using the method of Nathan and Van Kirk (1978). In these calculations nepheline is an early crystallizing phase in lavas of the Erebus lineage. Nepheline phenocrysts may have been resorbed before the magmas were erupted.

Evolution from basanite to Ne-hawaiite gave three reasonable solutions (Table 6.3). In models 1 and 2, Cr spinel was fractionated. In model 2 nepheline was fractionated, and in model 3 nepheline and feldspar were fractionated. Model 1 has predicted trace elements concentrations very similar to the concentrations observed, with the exceptions of Sr and Ba. This may be due to uncertainties in the distribution coefficients for these elements. Predicted trace element concentrations are too high in models 2 and 3, suggesting these models are not applicable.

Table 6.3. Least squares mass balance models for derivation of Ne-hawaiite AW82038 from basanite 2-105.53.

	Observed basanite	Estimated Basanite 1	2	3
SiO_2	42.06	42.10	42.06	42.07
TiO_2	4.21	4.21	4.21	4.21
Al_2O_3	13.08	13.09	13.08	13.07
FeO*	11.46	11.46	11.46	11.46
MnO	0.18	0.21	0.20	0.19
MgO	12.11	12.08	12.11	12.10
CaO	11.50	11.44	11.49	11.49
Na_2O	3.03	2.88	3.08	3.13
K_2O	1.51	1.31	1.38	1.32
P_2O_5	0.87	0.94	0.88	0.88
Wt. fraction Ne-hawaiite		0.4547	0.4133	0.3475
Olivine	$Fo_{88}B$	0.1163	0.1166	0.1299
Clinopyroxene	$En_{41}B$	0.3466	0.3643	0.3473
Cr spinel	Usp_8B	0.0354	0.0261	--
Ti-magnetite	$Usp_{52}B$	0.0124	0.0214	0.0438
Ilmenite		0.0236	0.0226	0.0238
Feldspar	$An_{72}B$	--	--	0.0518
Nepheline	$Ne1^2$	--	0.0272	0.0453
Apatite		0.0092	0.0088	0.0107
Sum		0.9982	1.0002	1.0001
Sum R^2*		0.07	0.02	0.05

Trace element abundances (ppm) in Ne-hawaiite

	Observed	Calculated		
Rb	62	65	71	84
Sr	1295	1663	1822	1829
Nb	163	160	175	207
Ba	721	598	658	766
La	95	99	109	125
Ce	195	194	212	240
Sm	14.5	13.7	14.8	16.4
Eu	4.0	4.3	4.6	5.0
Yb	3.4	3.5	3.8	4.3
Lu	0.5	0.5	0.5	0.6

* R^2 is the square of the residuals.

Two acceptable models were derived for the evolution from Ne-hawaiite to Ne-benmoreite (Table 6.4). The models are very similar except that nepheline is fractionated in model 2. Observed trace element concentrations in the Ne-benmoreite are similar to those predicted by model 1. Trace element concentrations predicted by model 2 are generally too high, suggesting that the fractionation was smaller than calculated by this model.

Evolution from Ne-benmoreite to anorthoclase phonolite gave three reasonable solutions (Table 6.5). The same phases were fractionated in each model, but those in model 3 generally have less evolved compositions than those fractionated in models 1 and 2. In model 1, predicted trace elements are very similar to those measured in the anorthoclase phonolite, with the exceptions of Zr and Sr, which are too low, and Ba, which is too high. In model 2, calculated Rb, Ba, La and Ce are higher than observed, while Sr is too low. These discrepancies suggest that the amount of fractionation calculated in this model is too high, especially for feldspar. In model 3, calculated Zr is lower than observed and calculated Sr, light REE and Ba are high, suggesting the amount of fractionation calculated in this model is too low.

Table 6.4. Least squares mass balance models for derivation of Ne-benmoreite 83410 from Ne-hawaiite AW82038.

	Observed Ne-hawaiite	Estimated Ne-hawaiite 1	Estimated Ne-hawaiite 2
SiO_2	48.03	48.09	48.04
TiO_2	2.76	2.73	2.75
Al_2O_3	18.57	18.51	18.54
FeO*[3]	9.50	9.52	9.51
MnO	0.23	0.22	0.22
MgO	3.19	3.10	3.17
CaO	7.65	7.61	7.65
Na_2O	5.96	5.83	6.09
K_2O	2.88	2.70	2.69
P_2O_5	1.24	1.30	1.24

Wt. fraction Ne-benmoreite		0.7790		0.6880
Olivine	$Fo_{66}Nh$	0.0117	$Fo_{65}Nh$	0.0121
Clinopyroxene	$En_{40}B$	0.0624	$En_{39}Nh$	0.0788
Ti-magnetite	$Usp_{73}Nh$	0.0399	$Usp_{71}Nh$	0.0479
Feldspar	$An_{64}B$	0.0904	$An_{52}Nh$	0.1221
Nepheline		--	$Ne1^2$	0.0377
Apatite		0.0136		0.0144
Sum		0.9970		1.0010
Sum R^2		0.07		0.06

Trace element abundances (ppm) in Ne-benmoreite

	Observed	Calculated	
Rb	72	79	89
Sr	1188	1158	1142
Zr	608	599	674
Nb	192	195	217
Ba	909	879	981
La	108	106	116
Ce	218	210	230
Sm	13.9	14.3	15.5
Eu	4.1	3.9	4.0
Tb	1.7	1.6	1.8
Yb	3.9	3.7	4.1
Lu	0.6	0.6	0.6

* R^2 is the square of the residuals.

Table 6.5. Least squares mass balance models for derivation of anorthoclase phonolite 83446 from Ne-benmoreite 83410.

	Observed anorthoclase phonolite	Calculated anorthoclase phonolite 1	2	3
SiO_2	51.49	51.50	51.49	51.48
TiO_2	1.98	2.00	1.99	2.19
Al_2O_3	19.18	19.16	19.19	19.24
FeO*	7.89	7.89	7.88	7.81
MnO	0.23	0.22	0.21	0.24
MgO	2.23	2.22	2.24	2.31
CaO	5.63	5.61	5.63	5.56
Na_2O	7.00	7.02	6.98	6.91
K_2O	3.43	3.36	3.45	3.47
P_2O_5	0.94	0.96	0.94	1.03
Wt. fraction anorthoclase phonolite		0.6630	0.6112	0.7129
Olivine	$Fo_{58}Ap$	0.0049	$Fo_{58}Ap$ 0.0062	$Fo_{65}Nm$ 0.0151
Clinopyroxene	$En_{39}Ap$	0.0718	$En_{39}Ap$ 0.0743	$En_{40}B$ 0.0617
Ti-magnetite	$Usp_{61}Nh$	0.0550	$Usp_{61}Nh$ 0.0572	$Usp_{68}Ap$ 0.0469
Feldspar	$An_{44}Nm$	0.1262	$An_{33}Nb$ 0.1779	$An_{52}Nh$ 0.1006
Nepheline	Ne2	0.0665	Ne1 0.0589	Ne2 0.0508
Apatite		0.0156	0.0157	0.0168
Sum		1.0029	1.0015	1.0048
Sum R^2		0.01	0.00	0.08

Trace element abundances (ppm) in anorthoclase phonolite

	Observed	Calculated		
Rb	106	110	119	103
Sr	885	767	592	1106
Zr	927	839	897	828
Nb	255	237	252	250
Ba	930	1090	1062	1223
La	109	113	136	126
Ce	219	223	233	245
Sm	13.3	12.5	13.1	14.1
Eu	4.2	3.6	3.6	4.0
Tb	1.7	1.5	1.9	1.8
Yb	4.9	4.3	4.6	4.5
Lu	0.8	0.7	0.7	0.8

* R^2 is the square of the residuals.

In summary, least-squares mass balance modeling has been used successfully to derive quantitative models for the evolution of the Erebus lineage by crystal fractionation. Trace element modeling has been used to test the models. Based on these tests, model 1 is the preferred model for the evolution from basanite to Ne-hawaiite, and suggests that the Ne-hawaiite is a 45% residual liquid of basanite. Model 1 for the evolution from Ne-hawaiite to Ne-benmoreite is preferred, suggesting that Ne-benmoreite is a 78% residual liquid of Ne-hawaiite. Model 1 for the evolution from Ne-benmoreite to anorthoclase phonolite is the most reasonable, suggesting that anorthoclase phonolite is a 66% residual liquid of Ne-benmoreite. These preferred models have been compiled in Fig. 6.3, and suggest that anorthoclase phonolite is a 23.5% residual liquid of basanite. Features of note in each model, as seen in Fig. 6.3, are the importance of olivine, clinopyroxene, opaque oxide and apatite fractionation in each step and the increasing importance of feldspar fractionation. Negative Eu anomalies due to feldspar fractionation were compensated for by Eu enrichment as a result of clinopyroxene and apatite fractionation. Kaersutite fractionation was attempted in the modelling but no reasonable solutions were reached. Thus these quantitative fractionation models fit with the evolution of the Erebus lineage suggested by the geochemical trends and observed phenocrysts.

CRYSTAL FRACTIONATION MODELS FOR EVOLUTION OF EREBUS LINEAGE

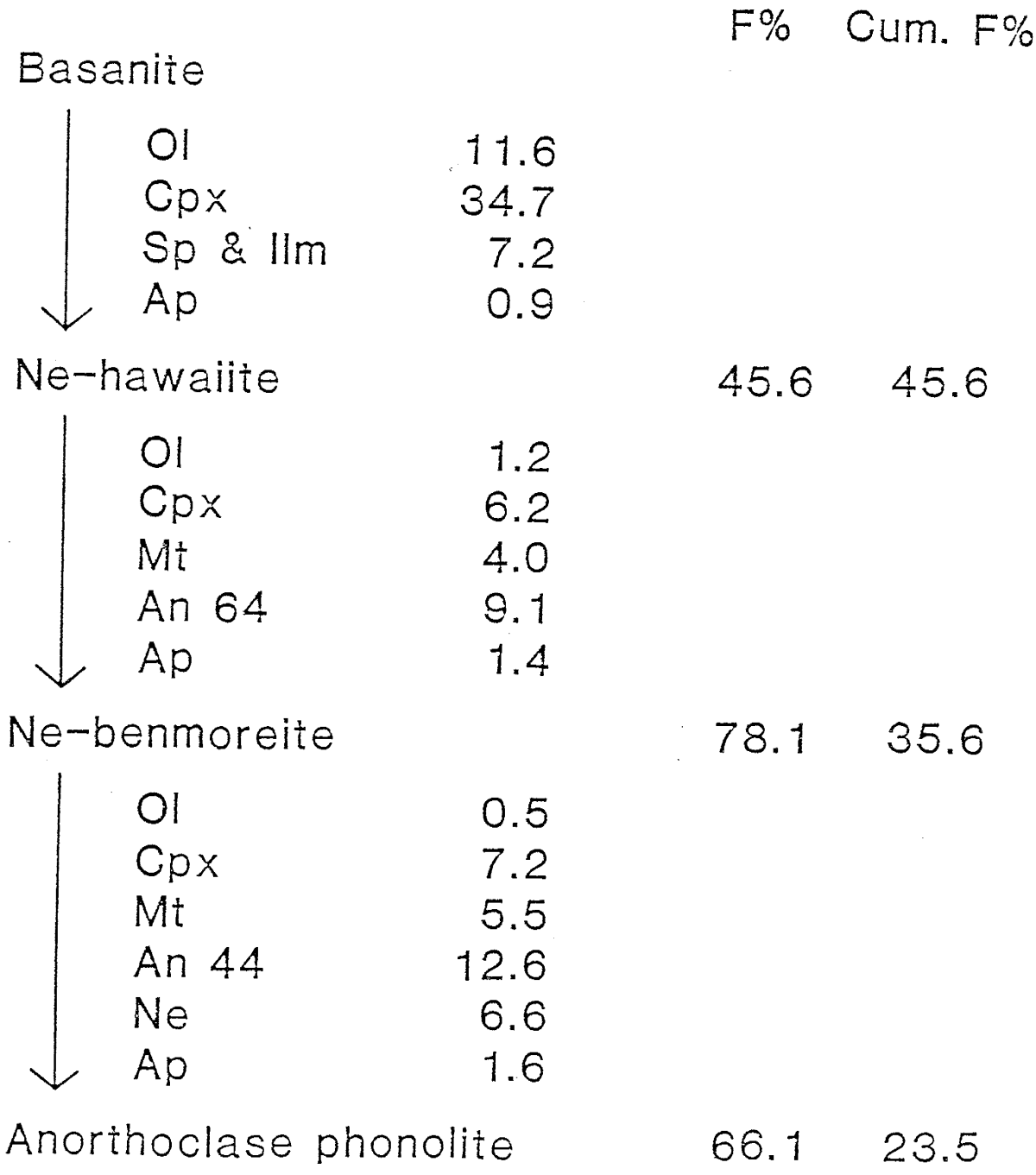

Figure 6.3. Summary of the three mass-balance least squares fractional crystallization models for the Erebus lineage.

Comparison of the Erebus and DVDP Lineages

Introduction

Lavas from Hut Point Peninsula, Ross Island (Fig. 2.1), and core from Dry Valley Drilling Project (DVDP) drill holes 1-3 on Hut Point Peninsula have been investigated by Kyle and Treves (1974a,b & c), Goldich et al. (1975), Sun and Hanson (1975; 1976), Kyle and Rankin (1976), Goldich et al. (1975, 1981), Kyle (1981a & b) and Stuckless et al. (1981). These lavas typically have kaersutite as phenocrysts or in the groundmass. The basic lavas are moderately porphyritic, while the intermediate to felsic lavas are weakly microporphyritic (Kyle, 1981b). Geochemically, the Hut Point Peninsula and DVDP lavas form a lineage consisting of basanite, Ne-hawaiite, Ne-mugearite, Ne-benmoreite and phonolite, termed the DVDP lineage (Kyle, 1981b). This lineage was demonstrated to have evolved by fractional crystallization of olivine, clinopyroxene, kaersutite, opaque oxides, and apatite (Kyle, 1981b).

In contrast to the DVDP lineage, the lavas of the Erebus lineage lack kaersutite and are generally strongly porphyritic. The Erebus lineage consists of the same rock types as the DVDP lineage and evolved by fractional crystallization of similar phases with the exception of kaersutite. The purpose of this section is to compare the geochemistry of the Erebus and DVDP lineages of Ross Island

as it relates to the petrogenesis of the lineages. The data on DVDP lineage rocks comes from Sun and Hanson (1976), Stuckless et al. (1981), and Kyle (1981b).

Fractional Crystallization Models

Kyle (1981b) used least squares mass balance calculations to model the evolution of the DVDP lineage by fractional crystallization. In this section his models are compared to the models for the evolution of the Erebus lineage.

Kyle modeled the evolution from basanite to phonolite in the DVDP lineage in three steps similar to the three steps in which phonolite evolution was modeled in the Erebus lineage (Fig. 6.4). Kaersutite fractionation is important for each evolutionary step in the mass balance models for the DVDP lineage. The total amount of crystallization of the basanite parental magma to derive phonolite is only slightly greater in the petrogenetic model for the Erebus lineage than the model for the DVDP lineage (76.5% and 74.9%, respectively) (Fig. 6.5). However, the total cumulate is composed of slightly greater amounts of olivine and apatite and noticeably greater amounts of clinopyroxene, Fe-Ti oxides, and feldspar in the Erebus lineage model compared to the DVDP lineage model. Also, nepheline is fractionated in the evolution from Ne-bemoreite to anorthoclase phonolite. These models suggest that the phonolite of both lineages

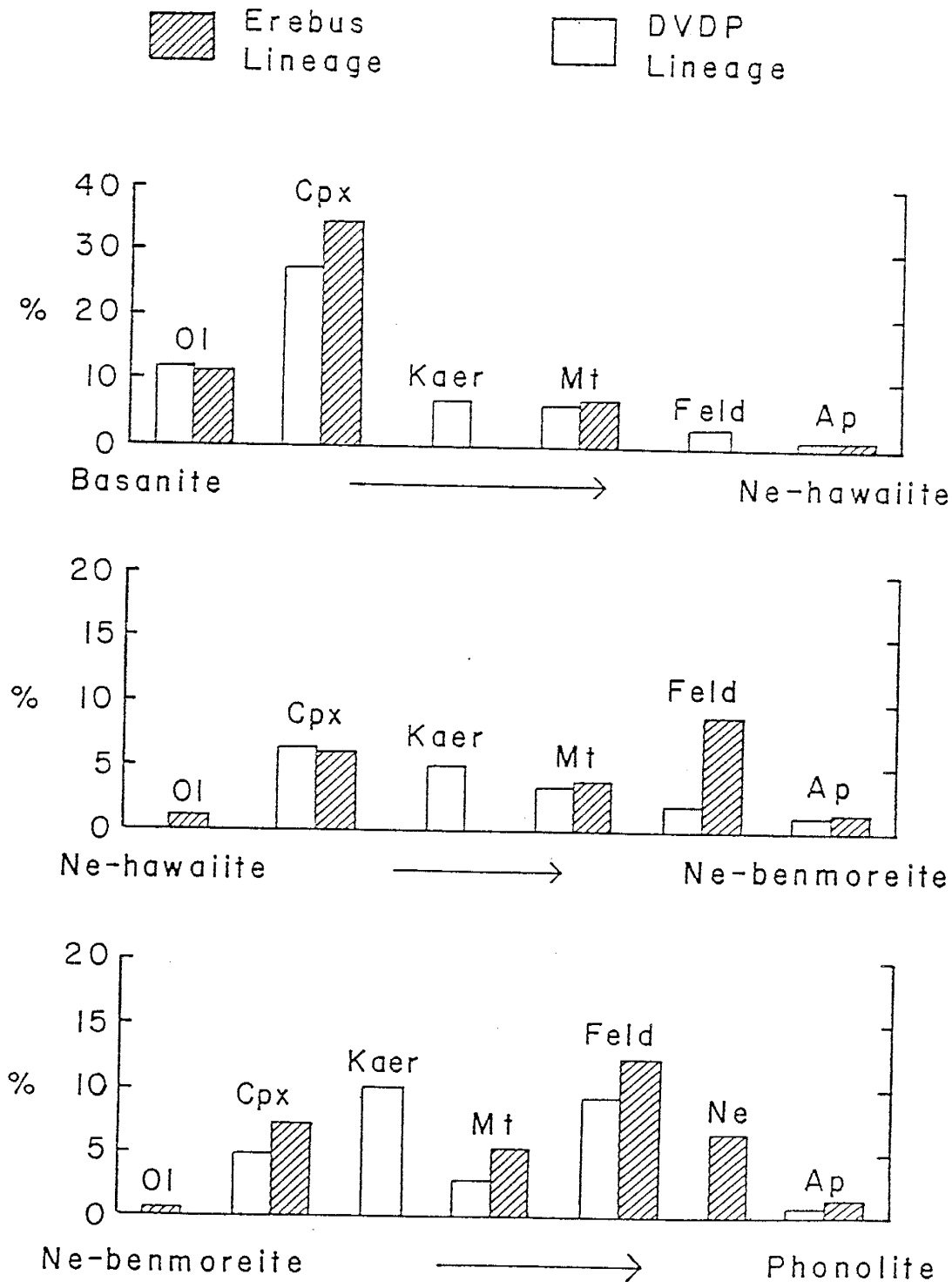

Figure 6.4. The three mass-balance least squares models for the evolution from basanite to phonolite in the Erebus and DVDP lineages.

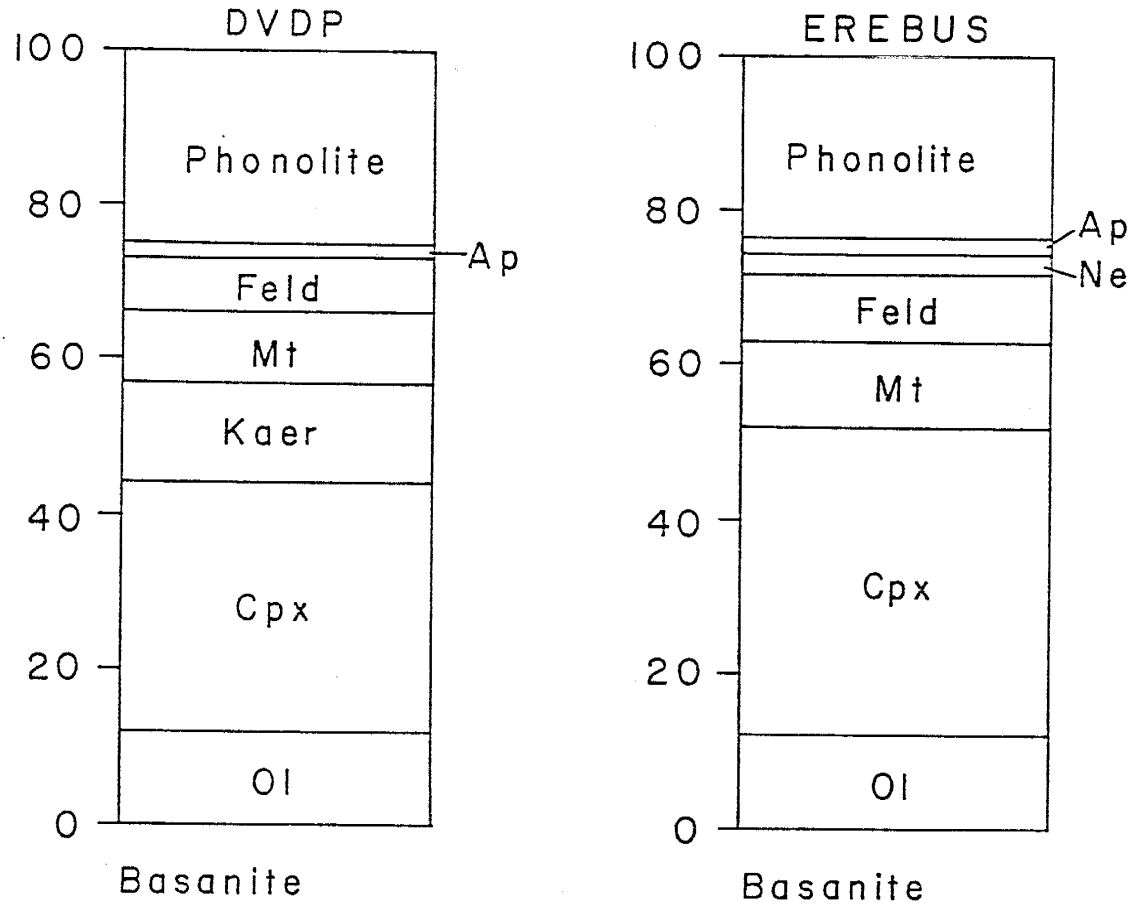

Figure 6.5. Summary of mass balance least squares models for evolution of Erebus and DVDP lineages.

represent similar amounts of residual liquid from fractional crystallization of basanite. The proportionality differences and the fractionation of kaersutite in the evolutionary model for the DVDP lineage suggests, however, that the evolution of the anorthoclase phonolite of Mt. Erebus took place by fractionation of a relatively anhydrous and higher temperature mineral assemblage than that fractionated to form the DVDP lineage phonolite.

Geochemistry

The major element geochemistry of the DVDP and Erebus lineage lavas are very similar. This is consistent with a similar parental magma for both lineages. In the FMA plot (Fig. 6.6) the two lineage form one trend. The primitive basanites of the DVDP lineage extend the trend further toward the MgO apex while the phonolites of the DVDP lineage extend the trend further toward the alkali apex. MgO is slightly higher in most intermediate and evolved rocks of the DVDP lineage, consistent with the greater amounts of olivine and clinopyroxene fractionation from the Erebus lineage. On silica variation diagrams (Fig. 6.7), the Erebus and DVDP lineages fall on the same trends for most major elements. At evolved compositions, the Erebus lineage has slightly lower concentrations of Al_2O_3 and Na_2O. This is consistent with the fractionation of nepheline and greater amounts of feldspar in the Erebus lineage than in the DVDP

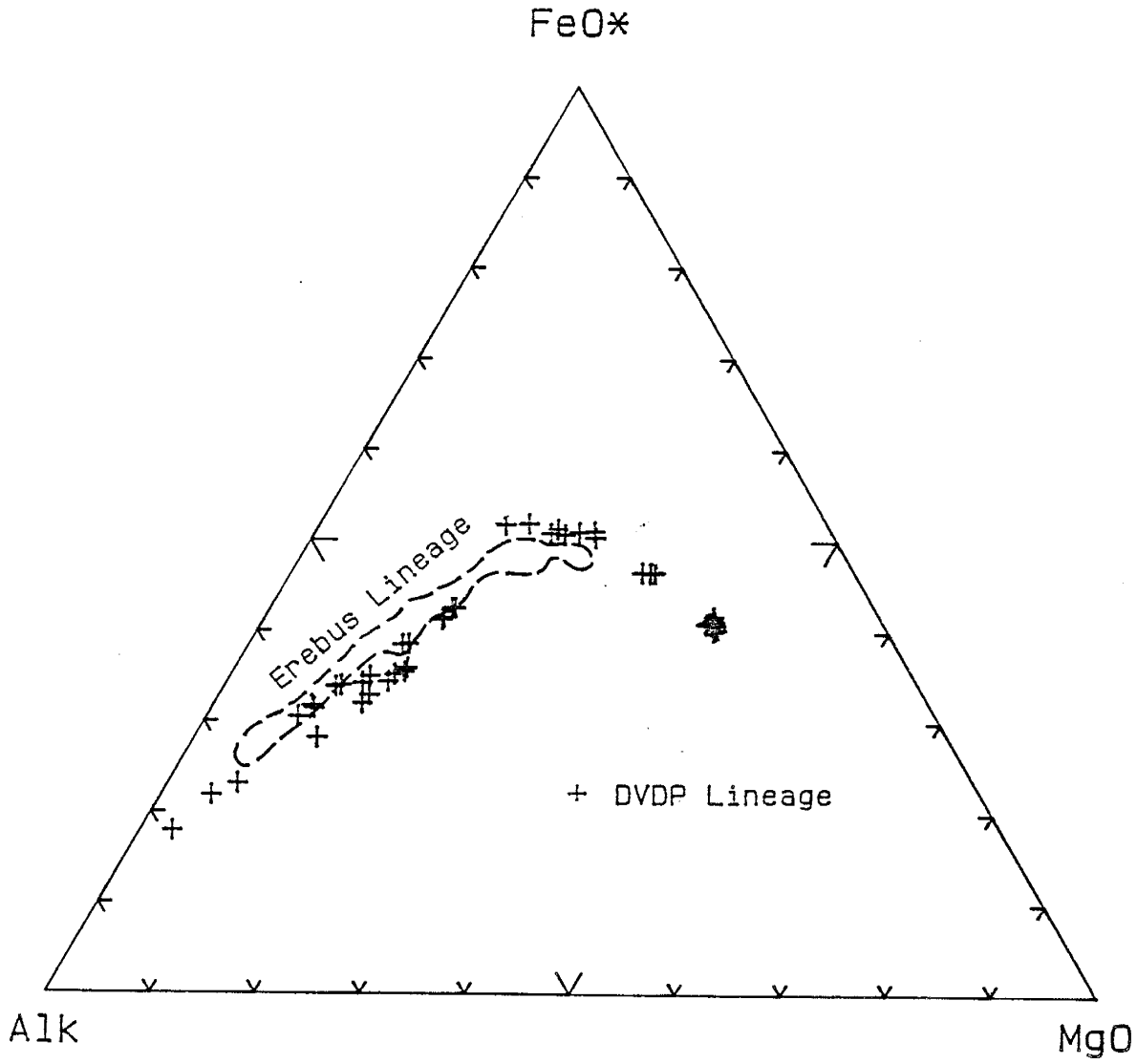

Figure 6.6. Comparison of FeO*-MgO-Alk (Na_2O+K_2O) variation in Erebus and DVDP lineage lavas. Trend of Erebus lineage circled. Values in wt.%.

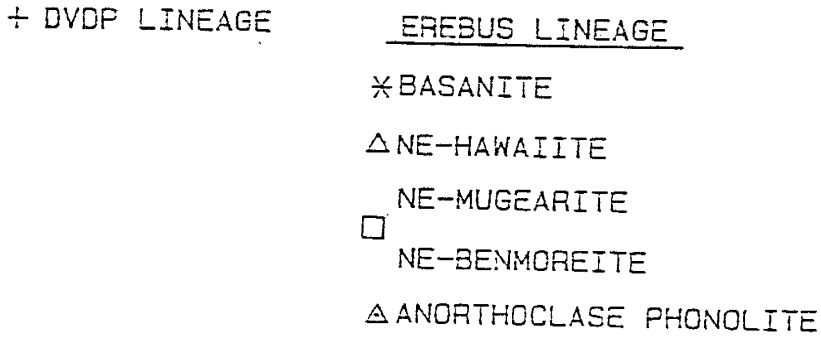

Figure 6.7. Comparison of variation of major elements against silica in Erebus and DVDP lineage lavas. Values in wt.%.

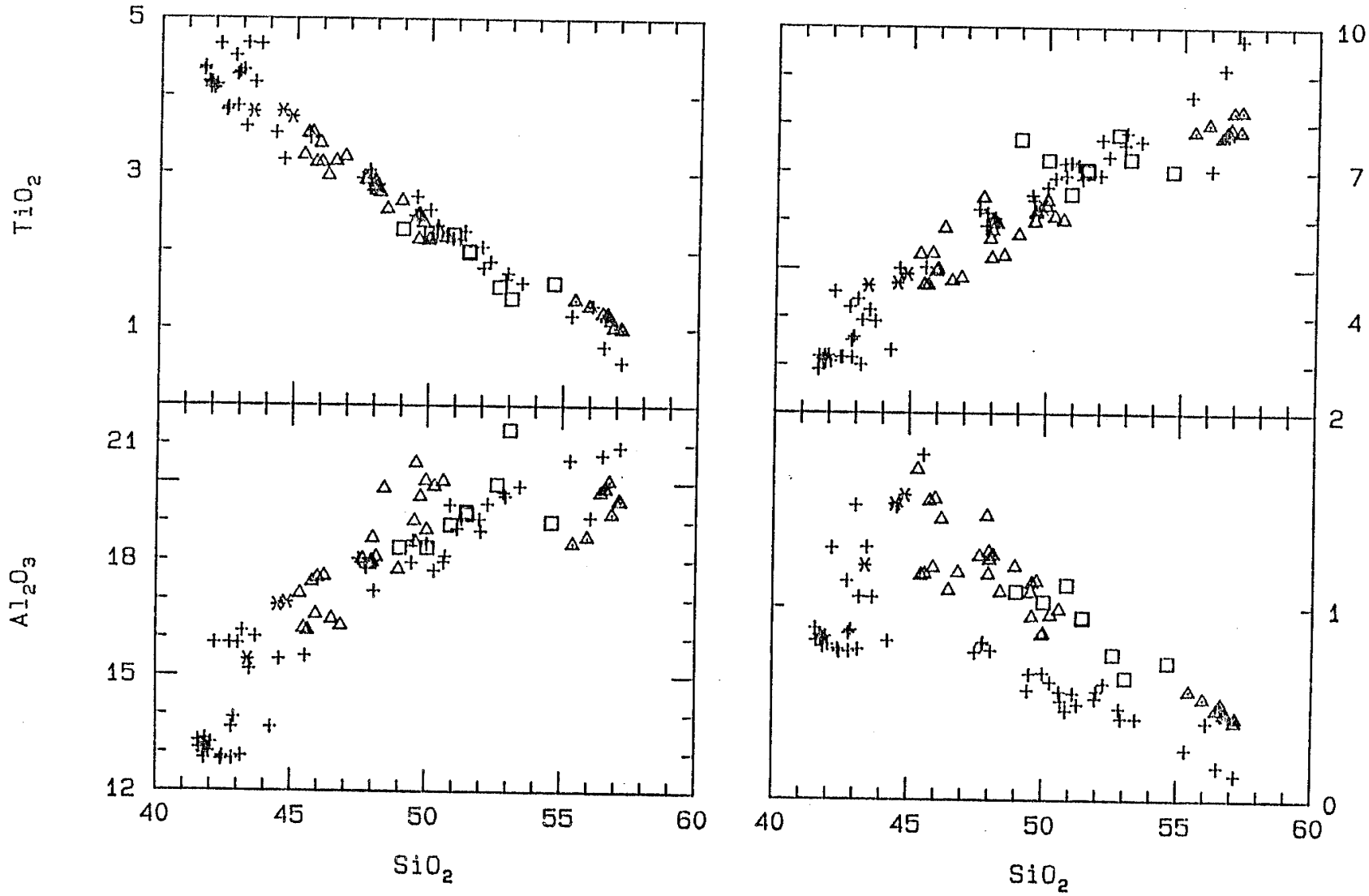
TiO2
Al2O3
SiO2
Na2O
P2O5
SiO2
5
3
1
21
18
15
12
40
45
50
55
60
10
7
4
2
1
0

lineage. TiO_2 and FeO* are slightly lower in most evolved rocks of the DVDP lineage, consistent with kaersutite fractionation.

P_2O_5 increases with increasing SiO_2 in the most basic rocks of the Erebus and DVDP lineages. It shows a moderate decline from evolved basanite through to anorthoclase phonolite in the Erebus lineage, but drops off dramatically between evolved basanite and Ne-hawaiite in the DVDP lineage. This suggests a significant amount of apatite fractionation at this point in the DVDP lineage, but not from the Erebus lineage. Watson (1979) showed that apatite saturation decreases significantly with decreasing temperature. The decline in P_2O_5 may be the result of a significant change in temperature between the evolution from basanite and Ne-hawaiite in the DVDP lineage but not in the Erebus lineage. The large amount of apatite fractionation at this point in the evolution of the DVDP lineage is not seen in the mass balance model because the model steps over the fractionated basanites with enriched P_2O_5 contents. However, it is seen in REE data from the DVDP lineage (Kyle, 1981b). The Ne-hawaiites have similar to slightly depleted light REE concentrations compared to the fractionated basanites as a result of apatite fractionation.

Trace element variation in the Erebus and DVDP lineages is illustrated in representative plots using Rb as the index of differentiation, because Rb is highly incompatible in most rock forming minerals and has been analyzed in all of the DVDP and Erebus lineage samples (Fig. 6.8). For the compatible trace elements Cr, Ni and Cu the two lineages show similar sharp declines in concentrations as the result of olivine, clinopyroxene, kaersutite and Fe-Ti oxide fractionation. Intermediate and evolved rocks of the Erebus lineage are depleted in V relative to DVDP rocks. This is consistent with the greater amount of Fe-Ti oxide fractionation in the Erebus lineage than in the DVDP lineage. Zn increases from basanite to Ne-hawaiite in the DVDP lineage, then decreases slightly from Ne-hawaiite to phonolite, whereas in the Erebus lineage Zn generally increases from basanite to phonolite. These different Zn trends can be attributed to kaersutite fractionation in the DVDP lineage.

Rb variation is illustrated in plots of Rb against SiO_2. Intermediate and evolved lavas in the DVDP lineage have higher Rb concentrations than the Erebus lineage lavas. This can be attributed to the fractionation of a Rb-bearing phase, such as alkali feldspar, from the Erebus lineage. The Erebus and DVDP lineages show different K/Rb trends, as noted by Kyle (1981b). The most basic rocks of both lineage have similar K/Rb ratios, but the ratio decreases with

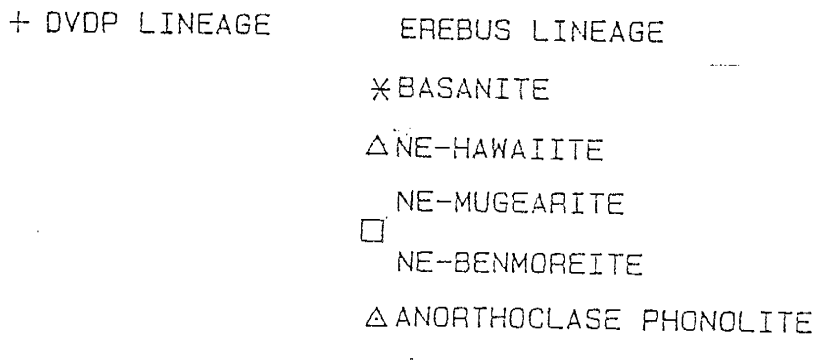
+ DVDP LINEAGE
EREBUS LINEAGE
BASANITE
NE-HAWAIITE
NE-MUGEARITE
NE-BENMOREITE
ANORTHOCLASE PHONOLITE

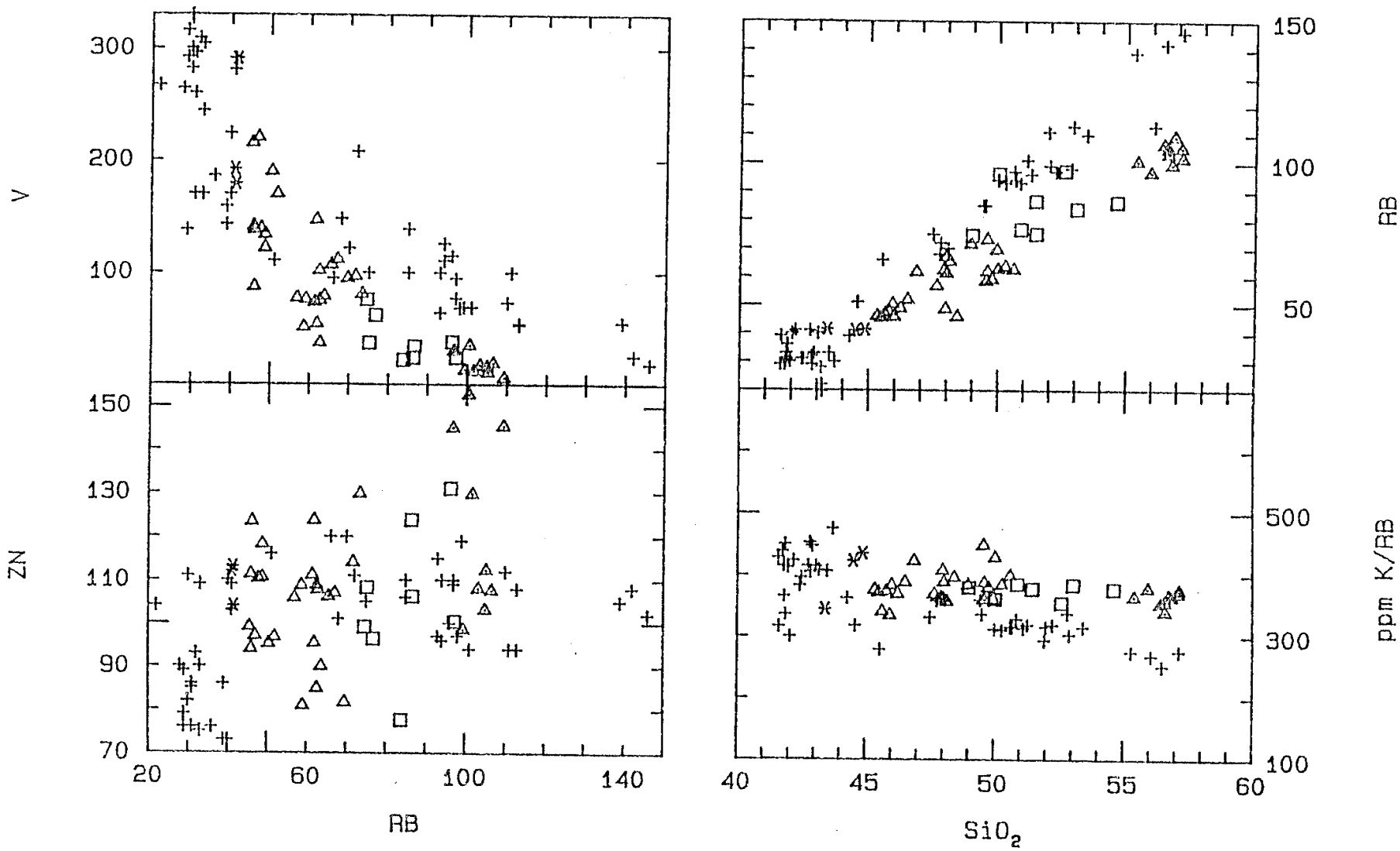

Figure 6.8. Comparison of trace element variation against Rb and silica (wt.%) in Erebus and DVDP lineage lavas. Trace elements in ppm.

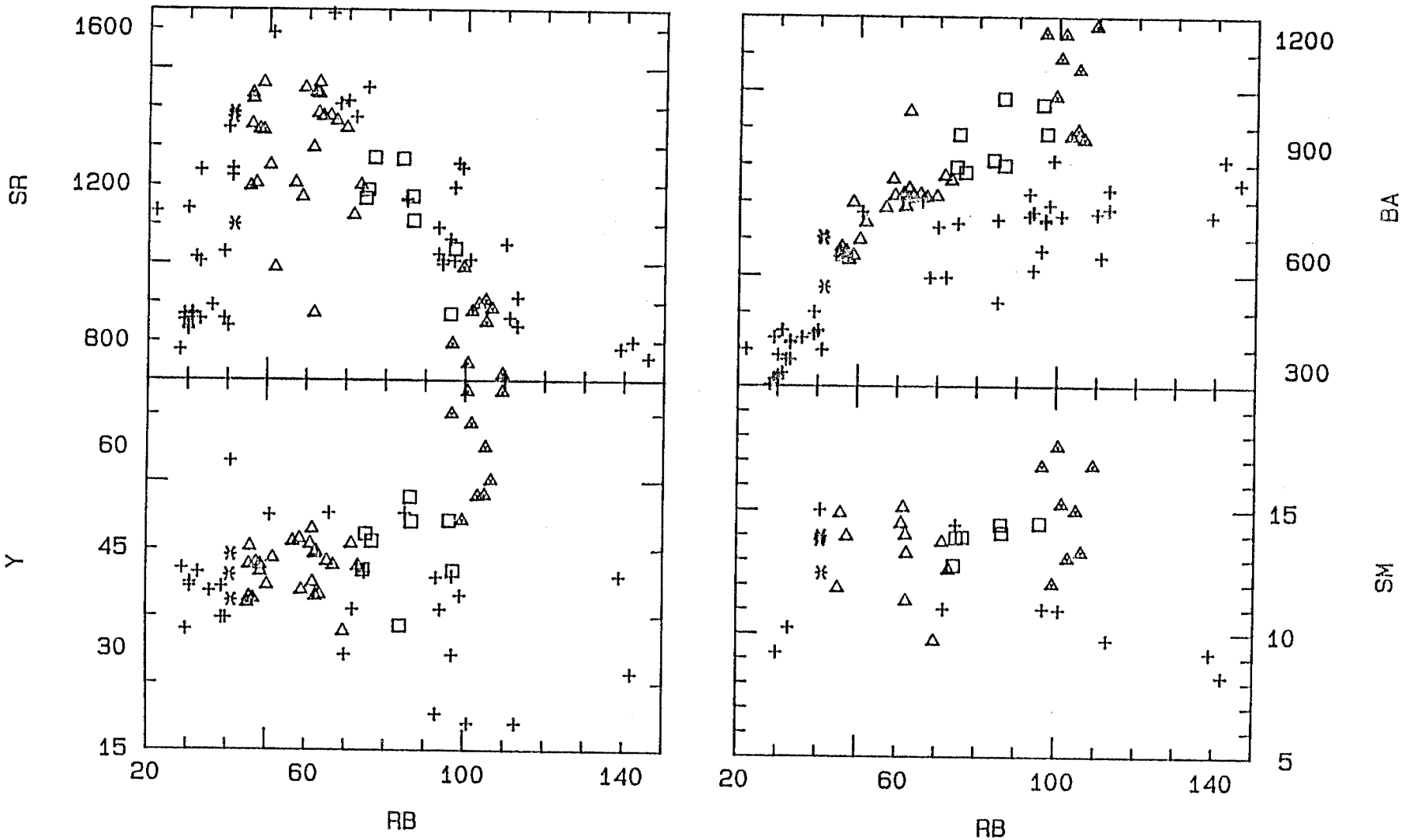

Figure 6.8 continued.

increasing differentiation in the DVDP lineage whereas it remains essentially constant in the Erebus lineage. This is the result of clinopyroxene fractionation in the Erebus lineage and dominantly kaersutite fractionation in the DVDP lineage, as noted by Kyle (1981b).

Sr increases in the Erebus and DVDP lineages from basanite to Ne-hawaiite, then decreases systematically from Ne-hawaiite to phonolite, reflecting apatite and feldspar fractionation in the intermediate and evolved magmas of both lineages. However, Sr decreases more sharply in the Erebus lineage than the DVDP lineage, consistent with the greater amounts of feldspar and apatite fractionation from the Erebus lineage, as seen in the models. The basic rocks of the Erebus and DVDP lineages have similar Y concentrations. However, Y increases in the Erebus lineage with increasing differentiation but declines in the DVDP lineage, consistent with the kaersutite fractionation in the DVDP lineage.

Ba shows a trend of continuing enrichment with differentiation in the Erebus lineage. However, Ba increases in basic rocks and stays approximately constant with increasing differentiation in intermediate and evolved rocks of the DVDP lineage. This implies a bulk distribution coefficient of c.1.0 for Ba in the fractionating crystallate. This may be the result of kaersutite and anorthoclase fractionation from intermediate and evolved

lavas in the DVDP lineage, as shown by Kyle (1981b) and Goldich et al. (1981). Zr, Hf and Th increase uniformly in both the Erebus and DVDP suites, consistent with the high incompatibility of these elements in the fractionating phases of both lineages, and a similar parental magma for both lineages.

Middle rare earth elements, as illustrated in the plot of Sm against Rb, show a systematic depletion with increasing differentiation in the DVDP lineage while in the Erebus lineage, the middle REE show little variation. The phonolites of the Erebus and DVDP lineages show distinctly different REE patterns relative to the same parental basanite (Fig. 6.9). Middle REE are strongly depleted in the DVDP lineage phonolite while the Erebus lineage phonolite is slightly depleted in light REE but enriched in heavy REE relative to the DVDP phonolite. The patterns of middle and heavy REE are consistent with kaersutite fractionation from the DVDP suite but not from the Erebus lineage magma, because kaersutite has higher distribution coefficients for middle and heavy REE than clinopyroxene. The light REE patterns are consistent with the greater amount of apatite fractionation in the evolution of the Erebus lineage.

In summary, the mass balance models for the evolution of the Erebus and DVDP lineages are consistent with the geochemical trends. They both suggest that the DVDP and

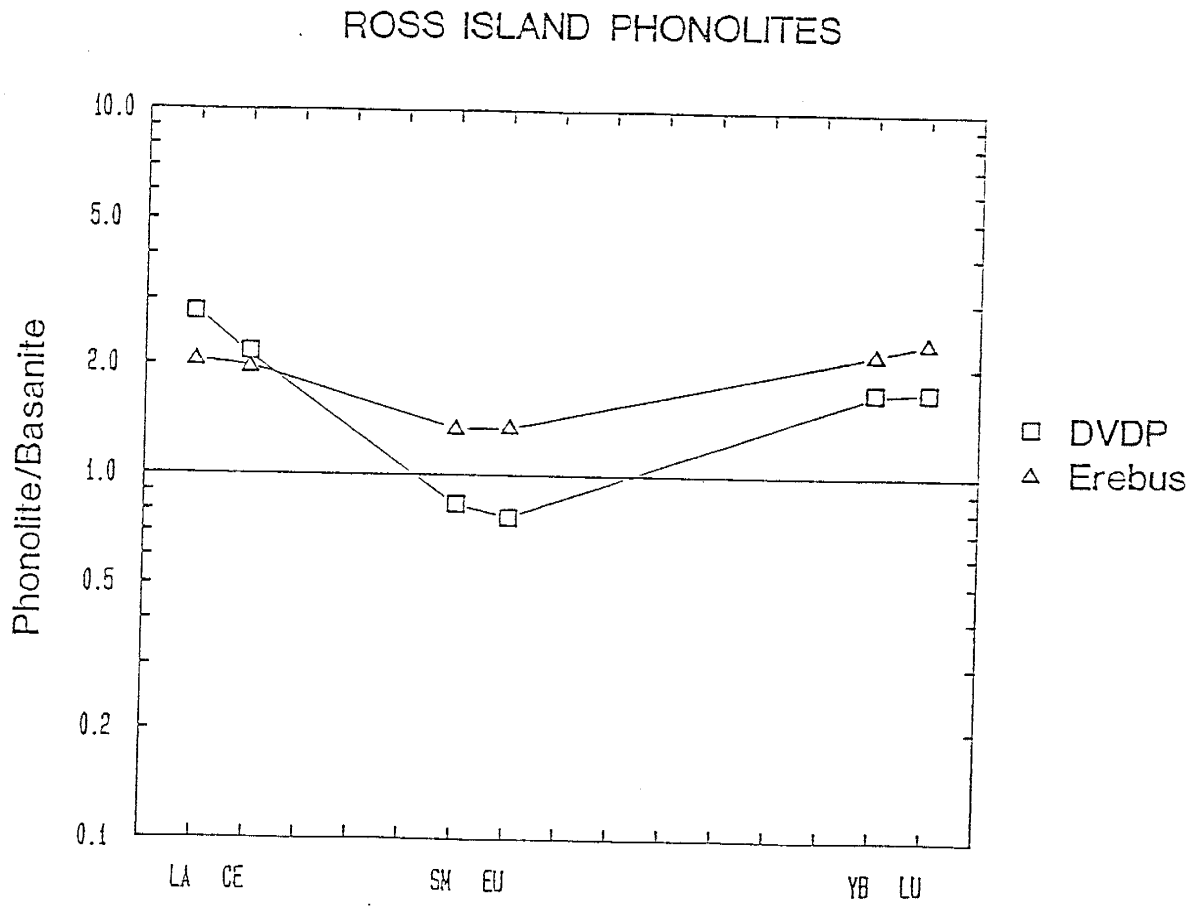

Figure 6.9. Comparison of rare earth element concentrations (in ppm) in Erebus and DVDP lineage phonolites normalized to same parental basanite [sample 2-105.53 (Kyle, 1981b)]. DVDP lineage phonolite: sample 25793 (Kyle, 1981b). Erebus phonolite: sample 83446.

Erebus lineages evolved from a similar basanite parental magma by crystal fractionation of olivine, clinopyroxene, Fe-Ti oxides, feldspar and apatite. Kaersutite was an additional fractionating phase in the DVDP lineage. Greater amounts of olivine, clinopyroxene, Fe-Ti oxide, feldspar and apatite were fractionated from the Erebus lineage than from the DVDP lineage, explaining the differences in geochemistry between the two lineages.

Petrogenesis of Benmoreites, Kaersutite Phonolites, and Trachytes

Introduction

Volumetrically-insignificant amounts of benmoreite, kaersutite phonolite and trachyte occur on Mt. Erebus. Benmoreites occurring at Inaccessible Island and Lewis Bay have feldspar, olivine, opaque oxide, and rare kaersutite microphenocrysts. On Abbott Peak the benmoreite is porphyritic with abundant feldspar, clinopyroxene, opaque oxide and kaersutite phenocrysts. The kaersutite phonolites on Inaccessible Island (II) are weakly porphyritic with feldspar, opaque oxide and accessory kaersutite phenocrysts. The kaersutite phonolites from Bomb Peak (BP) are more porphyritic with abundant feldspar and kaersutite phenocrysts. Trachytes occur at Bomb Peak, the Aurora Glacier, and Mt. Cis and are very weakly porphyritic, with rare phenocrysts of feldspar, sodic pyroxene and opaque

oxides. The petrographic and geochemical distinctiveness of the benmoreites, kaersutite phonolites, and trachytes suggests an evolution separate from the evolution of the Erebus lineage.

Petrogenesis

The benmoreites, II kaersutite phonolites and trachytes form a trend separate from the trend of the Erebus lineage and BP kaersutite phonolites that has been called the enriched iron series (EFS). The distinctive trend of these lavas is seen on the AFM plot, the FeO^*/SiO_2 plot, and on incompatible element plots (e.g. Zr, Nb). This indicates these lavas are not related to the Erebus lineage by crystal fractionation but evolved from a geochemically distinct parental magma. The mineral chemistry of benmoreite AW82023 suggests it evolved from a relatively anhydrous, siliceous parental magma, probably alkali basalt.

Additional evidence for a more siliceous parent comes from the normative Qz-Ne-Ks plot (Fig. 6.2). The EFS lavas plot in the feldspar field on the thermal ridge above the low temperature ternary minimum of the one atmosphere liquidus surface. On the other hand, EL lavas form a trend from the nepheline field to the ternary minimum. This indicates that the more silica-saturated EFS could not have evolved from the more undersaturated Erebus lineage (Gittins, 1979). A more siliceous parental magma is

required. Coombs and Wilkinson (1969) suggested that a volcanic differentiation lineage exists consisting of alkali basalt, hawaiite, benmoreite, and phonolite/trachyte. EFS lavas probably belong to this lineage. The alkali basalt parental magma may have resulted from minor amounts of higher degree partial melting in the mantle below Mt. Erebus. No alkali basalts have been found on Mt. Erebus, but may occur beneath the ice cap or within the volcanic pile.

The geochemical trends of EFS lavas suggests that they could be related by fractional crystallization. A reasonable mass balance model was achieved for the evolution of II kaersutite phonolite from benmoreite by fractionating olivine, clinopyroxene, opaque oxides, feldspar and apatite (Table 6.6).

Table 6.6. Least squares mass balance models for derivation of Inacessible Island and Bomb Peak kaersutite phonolites.

1. Benmoreite (83412) to kaersutite phonolite (83407)

Derivative wt. fract.	Ol	Cpx	Mt	Fsp	Ap	R^2
0.6356	0.0461	0.0180	0.0343	0.2478	0.0130	0.21

2. Ne-benmoreite (83410) to kaersutite phonolite (82404)

Derivative wt. fract.	Kaer	Mt	Fsp	Ap	R^2
0.7050	0.0769	0.0338	0.1620	0.0173	0.38

* R^2 is the square of the residuals.

The high incompatible element concentrations, low concentrations of Sr and Ba, low K/Rb ratios and large negative Eu anomalies of the trachytes suggests they represent residual liquids from extreme fractionation, especially of alkali feldspar. Attempts to model their evolution from benmoreites or kaersutite phonolites were unsuccessful. This suggests another process was involved in their petrogenesis, possibly crustal contamination. The trachytes of Bomb Peak contain xenoliths of anorthoclase phonolite. The trachytes at Mt. Cis contains sandstone and dolerite xenoliths, and have isotopic ratios indicative of crustal contamination. The similar geochemistry of the trachytes suggests they have a similar origin. They may be contaminated residual liquids from fractional crystallization of alkali basalt.

The BP kaersutite phonolites plot on the trends of the DVDP lineage on all major, trace, and rare earth element variation diagrams with the exception of V. This geochemical similarity suggests the BP kaersutite phonolites evolved in a similar way to the DVDP lineage by fractionation of kaersutite. The mineral chemistry of BP kaersutite phonolite 82404 suggests it evolved at higher water contents than the Erebus lineage lavas. A small apophysis of magma must have separated from the main magma chamber of Mt. Erebus. Lower temperatures and higher water pressures in this apophysis resulted in the crystallization of similar mineral phases as

in the DVDP lineage, including kaersutite. Support for this hypothesis comes from mass balance modeling. Reasonable models were achieved for the evolution of BP kaersutite phonolite from Ne-benmoreite by fractionation of kaersutite, opaque oxides, feldspar and apatite (Table 6.6). The BP kaersutite phonolites also have resorbed xenocrysts of labradorite sometimes overgrown by andesine and oligoclase. This suggests that magma mixing may also have been involved in the evolution of these lavas.

CHAPTER SEVEN

CONCLUSIONS

Mt. Erebus is an active, anorthoclase phonolite volcano on Ross Island, Antarctica approximately 1 m.y. in age. The lavas forming Mt. Erebus comprise a strongly undersaturated sodic differentiation lineage consisting of basanite, Ne-hawaiite, Ne-mugearite, Ne-benmoreite and anorthoclase phonolite, termed the Erebus lineage (EL). The lavas generally are strongly porphyritic with cognate phenocrysts of olivine (Mg_{88-51}), clinopyroxene ($Ca_{52-45}Mg_{39-51}Fe^{2+}+Mn_{8-16}$), opaque oxides ($Usp_{51-76}$), feldspar ($An_{72-11}Ab_{27-67}Or_{1-22}$) and apatite. The limited compositional variation in mafic phenocrysts suggests relatively constant temperature and oxygen fugacity during evolution of the EL.

EL lavas show a wide range in geochemistry from basanite to anorthoclase phonolite and form smooth continuous curvilinear trends on major and trace element variation diagrams. They are light REE enriched. REE contents increase slightly with increasing differentiation and there are no significant Eu anomalies. The geology and geochemistry of the EL suggests it evolved from a basanite parental magma. Pb and Sr isotopes suggest the parental magma came from a heterogeneous mantle source, and that

contamination by crustal melts was negligible during evolution of the lineage. The regular geochemical trends indicate the EL evolved by simple fractional crystallization of the observed phenocryst phases. This is confirmed by major element mass balance modeling which suggests that anorthoclase phonolite is a 23.5% residual liquid from fractionation of basanite. The total fractionate was composed of 16% olivine, 52% clinopyroxene, 14% Fe-Ti oxides, 11% feldspar, 3% nepheline, and 3% apatite.

The DVDP volcanic lineage of Hut Point Peninsula and the other volcanic centers of Ross Island surrounding Mt. Erebus consists of similar lava types as the EL. However, the lavas are dominantly basanite with minor amounts of microporphyritic intermediate lavas and phonolites, and contain kaersutite phenocrysts. The DVDP lineage was shown by Kyle (1981b) in mass balance calculations to have evolved by fractional crystallization of similar phases as the Erebus lineage along with 13% kaersutite.

Mass balance modeling indicates the phonolites derived in both the Erebus and DVDP lineages represent a similar amount of residual liquid from a basanite parental magma (c.24%). However, phonolite evolved by fractionation of a higher temperature and relatively anhydrous crystallate in the Erebus lineage. This suggests higher temperatures and lower water contents in the magma chamber where the Erebus lineage evolved than in the DVDP lineage magma chamber.

Minor volumes of benmoreite, kaersutite phonolite and trachyte also occur on Mt. Erebus. The different mineralogy and geochemistry of these lavas suggests evolution independent of the EL. Kaersutite phonolites at Bomb Peak may have evolved by fractionation of kaersutite, similar to the DVDP lineage, in small apophyses off the main Erebus lineage magma chamber. The enriched iron series (EFS) may have evolved from a different parental magma, possibly alkali basalt formed by higher degrees of partial melting in the mantle. The trachytes of Mt. Cis have elevated Pb and Sr isotopic ratios, suggesting crustal contamination, and other trachytes of Mt. Erebus may have a similar origin.

The three-fold radial configuration of volcanic centers at Ross Island may be the result of radial fractures in the crust above a rising mantle diapir (Kyle and Cole, 1974). This diapir may be c.100 km in diameter and centered beneath Mt. Erebus. Low degress of partial melting in this diapir formed the basanite parental magmas of the Erebus and DVDP lineages. EL lavas may have evolved in a large, high temperature magma chamber fed by the main part of the diapir. Basanite at the edges of the diapir may have been at lower temperatures and higher water contents. Leaking upward along the radial fractures in the crust, these basanites may have evolved to form the DVDP lineage. The EFS may have evolved from small batches of alkali basalt formed by higher degrees of partial melting in the mantle diapir.

REFERENCES

Aoki, K., 1964. Clinopyroxenes from alkaline rocks of Japan. Am. Miner. 49, 119-123.

_____ 1968. Petrogenesis of ultrabasic and basic inclusion in alkali basalts, Iki Island, Japan. Am. Miner. 53, 241-256.

_____ 1970. Petrology of kaersutite-bearing ultramafic and mafic inclusions in Iki Island, Japan. Contr. Miner. Petrol. 25, 270-283.

Armstrong, R.L., 1978. K-Ar dating: Late Cenozoic McMurdo Volcanic Group and dry valley glacial history, Victoria Land, Antarctica. N.Z.J. Geol. Geophys. 21, 685-698.

Arth, J.G., 1976. Behavior of trace elements during magmatic processes - A summary of theoretical models and their applications. J. Res. U.S. Geol. Surv. 4, 41-47.

Baker, B.H., and McBirney, A.R., 1985. Liquid fractionation. Part III: Geochemistry of zoned magmas and the compositional effects of liquid fractionation. J. Volc. Geotherm. Res. 24,55-81.

Barker, D.S., and Hodges, F.N., 1977. Mineralogy of intrusions in the Diablo Plateau, northern Trans Pecos magmatic province, Texas and New Mexico. Bull. Geol. Soc. Am. 88, 1428-1436.

Barrett, P.J., 1965. Geology of the area between the Axel Heiberg and Shackleton Glaciers, Queen Maud Range, Antarctica. Part 2 - Beacon Group. N.Z.J. Geol. Geophys. 8, 344-370.

Berlin, R., and Henderson, C.M.B., 1969. The distribution of Sr and Ba between the alkali feldspar, plagioclase and groundmass phases of porphyritic trachytes and phonolites. Geochim. Cosmochim. Acta, 33, 247-255.

Boudette, D.L., and Ford, A.B., 1966. Physical properties of anorthoclase from Antarctica. Am. Miner. 51, 1374-1387.

Brey, G.P., and Green, D.H., 1975. The role of CO_2 in the genesis of olivine melilite. Contr. Miner. Petrol. 49, 93-103

Brooks, C.K., and Printzlau, I., 1978. Magma mixing in mafic alkaline volcanic rocks: The evidence from relict phenocryst phases and other inclusions. J. Volcanol. Geotherm. Res. 4, 315-31.

Bryan, W.B., Finger, L.W., and Chayes, F., 1969. Estimating proportions in petrograpic mixing equations by least-squares approximation. Science, 163, 926-7.

Carmichael, I.S.E., 1962. Pantelleritic liquids and their phenocrysts. Miner. Mag. 33, 86-113.

_____ 1963. The crystallization of feldspar in volcanic acid liquids. Q. J. Geol. Soc. London, 119, 95-131.

_____ 1964. Natural liquids and the phonolite minimum. Geol.J. 4, 55-60.

_____ 1967. The iron-titanium oxides of salic volcanic rocks and their associated ferromagnesian silicates. Contr. Miner. Petrol. 14, 36-64.

_____ and MacKenzie, W.S., 1964. The lattice parameters of high-temperature triclinic sodic feldspar. Miner. Mag. 33, 949-962.

Coombs, P.S., and Wilkinson. J.F.G., 1969. Lineages and fractionation trends in undersaturated volcanic rocks from the East Otago Volcanic Province (New Zealand) and related rocks. J. Petrology, 10, 440-501.

Cooper, A.K., and Davey, F.J., 1985. Episodic rifting of phanerozioc rocks in the Victoria Land Basin, western Ross Sea, Antarctica. Science, 229, 1085-1087.

Cox, K.G., Bell, J.D., and Pankhurst, R.J., 1979. The Interpretation of Igneous Rocks. London: George Allen and Urwin.

Craddock, C., 1983. Antarctica and Gondwanaland. In: Craddock, C. (ed.) Antarctic Geoscience. Madison: The University of Wisconsin Press, 3-13.

Cullers, Rl.L., and Medaris, G. Jr., 1977. Rare earth elements in carbonatite and cogenetic alkaline rocks: Examples from Seabrook Lake and Callander Bay, Ontario. Contr. Miner. Petrol. 65, 143-153.

Debenham, F., 1923. The physiography of the Ross Archipalego. Brit. Antarctic ("Terra Nova") Exped. 1910-1913. London: Harrison.

Deer, W.A., Howie, R.A., and Zussman, J., 1963. Rock-Forming Minerals, Vol. 4, Framework Silicates. London: Longmans.

_____ _____ _____ 1966. An Introduction to the Rock-forming minerals. London: Longmans.

Drake, M.J., 1975. The oxidation state of europium as an indicator of oxygen fugacity. Geochim. Cosmochim. Acta, 39, 55-64.

Duda, A., and Schmincke, H.-U., 1985. Polybaric differentiation of alkali basaltic magmas: Evidence from green core clinopyroxenes (Eifel, FRG). Contrib. Mineral. Petrol. 91, 340-53.

Duke, J.M., 1974. The effect of oxidation on the crystallization of an alkali basalt from the Azores. J. Geol. 82, 524-8.

Faure, G., 1977. Principles of Isotope Geology. New York: Wiley.

Forbes, R.B., Turner, D.L., and Carden. J.R., 1974. Age of trachyte from Ross Island, Antarctica. Geology, 2, 297-8.

Ford, A.B., and Barrett, P.J., 1975. Basement rocks of the south-central Ross Sea, Site 270, DSDP Leg 28. Initial Rep. Deep Sea Drilling Project, 28, 861-8.

_____ and Boudette, E.L., 1968. On the staining of anorthoclase. Am. Miner. 53, 331-4.

Frey, F.A., Green, D.H., and Roy, S.D., 1978. Integrated model of basalt petrogenesis: A study of quartz tholeiites to olivine melilites from southeastern Australia using geochemical and experimental petrological data. J. Petrology, 19, 463-513.

Gibb, F.G.F., 1973. The zoned clinopyroxenes of the Shiant Isles sill, Scotland. J. Petrology 14, 203-230.

Gittins, J., 1979. The feldspathoidal alkaline rocks. In: Yoder, H.S. (ed.) The Evolution of the Igneous Rocks. Princeton: Princeton University Press, 351-90.

Gladney, E.S., Burns, C.E., and Roelandts, I., 1983. 1982 compilation of elemental concentrations in eleven United States Geological Survey rock standards. Geostandards Newsletter, 7, 3-226.

Goldich, S.S., Treves, S.B., Suhr, N.H., and Stuckless, J.S., 1975. Geochemistry of the Cenozoic volcanic rocks of Ross Island and vicinity, Antarctica. J. Geol. 83, 415-435.

_____ Stuckless, J.S., Suhr, N.H., Bodkin, J.B., and Wamser, R.C., 1981. Some trace element relationships on the Cenozioc volcanic rocks from Ross Island and vicinity. In: McGinnis, L.D. (ed.) Antarctic Research Ser., vol. 33, Dry Valley Drilling Project. Washington, D.C.: Am. Geophys. Un., 215-28.

Green, D.H., 1970. The origin of basaltic and nephelinitic magmas. Trans. Leicester Lit. Phil. Soc. 64, 28-54.

_____ 1973. Experimental melting studies on a model upper mantle composition at high pressure under water saturated and water undersaturated conditions. Earth Planet. Sci. Lett. 19, 37-53.

_____ and Pearson, N.J., 1985. Rare earth element partitioning between clinopyroxene and silicate liquid at moderate to high pressure. Contr. Miner. Petrol. 91, 24-36.

Haggerty, S.E., 1976. Opaque mineral oxides in terrestrial igneous rocks. In: Rumble, D. III (ed.) Oxide Minerals, Miner. Soc. Am. Short Course Notes, 3, Hg101-Hg300.

Hart, S.R., and Brooks, C., 1974. Clinopyroxene-matrix partitioning of K, Rb, Cs, Sr, and Ba. Geochim.Cosmochim. Acta, 38, 1799-1806.

Hayes, D.E., and Davey, F.J., 1975. A geophysical study of the Ross Sea. Initial Rep. Deep Sea Drilling Project, 28, 887-907.

Heming, R.F., and Carmichael, I.S.E., 1973. High temperature pumice flows from the Rabaul Caldera, Papua, New Guinea. Contr. Miner. Petrol. 38, 1-20.

Hildreth, W., 1979. The Bishop Tuff: Evidence for the origin of compositional zonation in silicic magma chambers. Geol. Soc. Am. Spec. Pap. 180, 43-75.

Hill, R., and Roeder, P., 1974. The crystallization of spinel from basaltic liquid as a function of oxygen fugacity. J. Geol. 82,709-729.

Holloway, J.R., and Ford, C.E., 1973. The effect of fluorine on hornblende: Fluid-absent melting of F-OH pargasite to 35 Kb. EOS Trans. Am. Geophys. Un. 54, 478.

Irvine, T.N., 1965. Chromian spinels as a petrogenetic indicator. Part 1. Theory. Can. J. Earth Sci. 2, 648-72.

Irving, A.J., and Frey, F.A., 1984. Trace element abundances in megacrysts and their host basalts: Constraints on partition coefficients and megacryst genesis. Geochim. Cosmochim. Acta, 48, 1201-1221.

Jakobsson, S.P., Pedersen, A.K., Ronsbo, J.G., and Larsen, L.M., 1973. Petrology of mugearite-hawaiite: Early extrusives in the 1973 Heimaey eruption, Iceland. Lithos, 6, 203-14.

Jensen, H.I., 1916. Report on the petrology of the alkaline rocks of Mt. Erebus, Antarctica. Rep. Brit. Antarctic Exped. 1907-09, Geol. 2, 93-128.

Jones, L., and Walker, R.L., 1972. Geochemistry of the McMurdo volcanics, Victoria Land. Part I. Strontium isotope composition. Antarctic J. U.S., 7, 142-144.

_____ Faure, G., Taylor, K.S., and Corbato, C.E., 1983. The origin of salts on Mount Erebus and along the coast of Ross Island, Antarctica. Isotope Geoscience, 1, 57-64.

Kay, R.W., and Gast, P.W., 1973. The rare earth content and origin of alkali-rich basalts. J. Geol. 81, 653-82.

Keil, K., Fodor, R.V., and Bunch, T.E., 1972. Contributions to the mineral chemistry of Hawaiian rocks. II. Feldspars and interstitial material in rocks from Haleakala and West Maui Volcanoes, Maui, Hawaii. Contr. Miner. Petrol. 49, 67-81.

Kerr, P.F., 1977. Optical Mineralogy. New York: McGraw-Hill.

Kyle, P.R., 1976. Geology, mineralogy, and geochemistry of the Late Cenozoic McMurdo Volcanic Group, Victoria Land, Antarctica. Unpubl. Ph.D. thesis, Dept.of Geology, Victoria University of Wellington.

_____ 1977. Mineralogy and glass chemistry of recent volcanic ejecta from Mt. Erebus, Ross Island, Antarctica. N.Z.J. Geol. Geophys. 20, 1123-1146.

____ 1981a. Geologic history of Hut Point Peninsula as inferred from DVDP 1, 2, and 3 drillcores and surface mapping. In: McGinnis, L.D. (ed.) Dry Valley Drilling Project. Washington, D.C.: A.G.U., 427-445.

_____ 1981b. Mineralogy and geochemistry of a basanite to phonolite sequence at Hut Point Peninsula, Antarctica, based on core from Dry Valley Drilling Project drillholes 1, 2, and 3. J. Petrology, 22, 451-500.

_____ 1986. Volcanic activity of Mt. Erebus: 1972-1984. International Volcanological Congress, NewZealand, 1986, Abstracts, 250.

_____ (in press). Mineral chemistry of Late Cenozoic McMurdo Volcanic Group rocks from The Pleiades, northern Victoria Land. Antarctic Res. Ser. Washington, D.C.: Am. Geophys. Un.

_____ Adams, J., and Rankin, P.C., 1979. Geology and petrology of the McMurdo Volcanic Group at Rainbow Ridge, Brown Peninsula, Antarctica. Bull. Geol. Soc.Am. 90, 676-88.

_____ and Cole, J.W., 1974. Structural control of volcanism in the McMurdo Volcanic Group, Antarctica. Bull. Volcanol. 38, 16-25.

_____ Dibble, R.R., Giggenbach, W.F., and Keys, J., 1982. Volcanic activity associated with the anorthoclase phonolite lava lake, Mt. Erebus, Antarctica. In: Craddock, C. (ed.) Antarctic Geoscience. Madison: Univ. Wisconsin Press, 735-45.

_____ and Muncy, H.L., 1978. Volcanic geology of the lower slopes of Mt. Morning. Antarctic J. U.S. 13, 34-36.

_____ and Rankin, P.C., 1976. Rare earth elememt geochmistry of Late Cenozoic alkaline lavas of the McMurdo Volcanic Group, Antarctica. Geochim. Cosmochim. Acta, 40, 1497-1507.

_____ and Treves, S.B., 1974a. Geology of DVDP 3, Hut Point Peninsula, Ross Island, Antarctica. Dry Valley Drilling Project Bull. 3, 13-48.

_____ _____ 1974b. Geology of DVDP 3, Hut Point Peninsula, Ross Island. Antarctic J. U.S. 9,127-9.

_____ _____ 1974c. Geology of Hut Point Peninsula, Ross Island. Antarctic J. U.S. 9, 232-4.

Le Maitre, R.W., 1984. A proposal by the IUGS Subcommission on the Systematics of Igneous Rocks for a chemical classification of volcanic rocks based on the total alkali silica (TAS) diagram. Australian J. Earth Sci. 31, 243-255.

Le Masurier, W.E. and Wade, F.A., 1976. Volcanic history of Marie Byrd Land: implications with regard to southern hemisphere tectonic reconstructions. In: Gonzales-Ferran, O. (ed.) Andean and Antarctic Volcanology Problems. Rome: Intl. Assoc. Volcanol. Chem. Earth's Interior, 398-424.

Le Roex, A.P., 1985. Geochemistry, mineralogy, and magmatic evolution of the basaltic and trachytic lavas from Gough Island., South Atlantic. J. Petrology, 26, 149-86.

_____ and Erlank, A.J., 1982. Quantitative evolution of fractional crystallization in Bouvet Island lavas. J. Volcanol. Geotherm. Res. 13, 309-38.

Lofgren, G., 1974. An experimental study of plagioclase crystal morphology; isothermal crystallization. Am. J. Sci. 274, 243-73.

Luckman, P.C., 1974. Products of submarine volcanism in the McMurdo Sound region, Ross Island, Antarctica. Unpubl. B.Sc. (Hons.) Project, Dept. of Geology, Victoria Univ. of Wellington.

MacDonald, R., 1974. Nomenclature and petrochemistry of the peralkaline oversaturated extrusive rocks. Bull. Volcanol. 38, 498-516.

_____ and Katsura, T., 1964. Chemical composition of Hawaiian lavas. J. Petrology, 5, 82-133.

MacKenzie, W.S., Donaldson, C.H., and Guilford, C., 1982. Atlas of Igneous Rocks and Their Textures. Essex: Longman.

Mason, R.A., Smith, J.V., Dawson, J.B., and Treves, S.B., 1982. A reconnaissance of trace elements in anorthoclase megacrysts. Miner. Mag. 46, 7-11.

Mawson, D., 1916. Petrology of rocks collected from the mainland of south Victoria Land. Rep. Brit. Antarctic Exped. 1907-9, Geol. 2, 201-37.

McBirney, A.R., 1984. Igneous Petrology. San Francisco: Freeman, Cooper and Company.

McGinnis, L.D., Bowen, R.H., Erickson, J.M., Allred, B.J., and Kreamer, J.L., 1985. East-West Antarctic boundary in McMurdo Sound. Tectonophys. 114, 341-56.

_____ _____ and Kreamer, J., 1983. Deep seismic soundings along the boundary between East and West Antarctica. Antarctic J. U.S. 18, 32-34.

_____ Clark, C.C., Pederson, D.T., Wong, H.K., Ervin. C.P., and Montgomery, G.E., 1974. Aeromagnetic and refraction seismic studies for the Dry Valley Drilling Project (DVDP). Dry Valley Drilling Project Bull. 4, 34-6.

McIntire, W.L., 1963. Trace element partition coefficients - a review of theory and application to geology. Geochim. Cosmochim. Acta, 27, 1209-64.

McKenzie, D., 1985. The extraction of magma from the crust and mantle. Earth Planet. Sci. Lett. 74, 81-91.

Menzies, M., and Murthy, V.R., 1980. Mantle metasomatism as a precursor to the genesis of alkaline magmas - isotopic evidence. Am. J. Sci. 280A, 622-38.

Merrill, R.B., and Wyllie, P.J., 1975. Kaersutite and kaersutite ecologite from Kakanui, New Zealand - Water-excess and water-deficient melting to 30 kilobars. Bull. Geol. Soc. Am. 86, 555-70.

Mountain, E.D., 1925. Potash-oligoclase from Mt. Erebus, Antarctica and anorthoclase from Mt. Kenya, East Africa. Miner. Mag. 29, 331-45.

Muncy, H.L., 1979. Geologic history and petrogenesis of alkaline volcanic rocks, Mt. Morning, Antarctica. Unpubl. M. Sci. thesis, The Ohio State Univ.

Mysen, B.O., 1983. The solubility mechanisms of volatiles in silicate melts and their relations to crystal-andesite liquid equilibria. J. Volcanol. Geotherm. Res. 18, 361-85.

Nagasawa, H., 1973. Rare-earth distribution in alkali rocks from Oki-Dogo Island, Japan. Contr. Miner. Petrol. 39, 301-8.

_____ and Schnetzler, C.C., 1971. Partitioning of rare-earth, alkali and alkaline earth elements between phenocryst and acidic igneous magma. Geochim. Cosmochim. Acta, 35, 953-68.

Nash, W.P., and Wilkinson, J.F.G., 1970. Shonkin Sag laccolith, Montana. I. Mafic minerals and estimates of temperature, pressure, oxygen fugacity and silica activity. Contr. Miner. Petrol. 25, 241-69.

____ Carmichael, I.S.E., and Johnson, R.W., 1969. The mineralogy and petrology of Mt. Suswa, Kenya. J. Petrology 10, 409-39.

Nathan, H.D., and Van Kirk, C.K., 1978. A model of magmatic crystallization. J. Petrology 19, 66-94.

Nicholls, J., Carmichael, I.S.E. , and Stormer, J.C., 1971. Silica activity and P_{Total} in igneous rocks. Contr. Miner. Petrol. 33, 1-20.

Norrish, K., and Hutton, J.T., 1969. An accurate X-ray spectrographic method for the analysis of a wide range of geological samples. Geochim. Cosmochim. Acta, 34, 307-22.

O'Nions, R.K., Carter, S.R., Evensen, N.M., and Hamilton, P.J., 1979. Geochemical and cosmochemical applications of Nd isotope analysis. Ann. Rev. Earth Planet. Sci. 7, 11-38.

Papike, J.J., Cameron, K.L., and Baldwin, K., 1974. Amphiboles and pyroxenes: Characterization of other than quadrilateral components and estimates of ferric iron from microprobe data. Abstr. Progrm. Geol. Soc.Am. 6, 1053-4.

Pearce, J.A., and Norry, M.J., 1979. Petrogenetic implications of Ti, Zr, Y, and Nb variations in volcanic rocks. Contr. Miner. Petrol. 69, 33-47.

Peterman, Z.E., and Hedge, C.E., 1971. Related strontium isotopic and chemical variation in oceanic basalts. Bull. Geol. Soc. Am. 82, 493-500.

Philpotts, J.A., and Schnetzler, C.C., 1970. Phenocryst-matrix partition coefficients for K, Rb, Sr and Ba with applications to anorthosite and basalt genesis. Geochim. Cosmochim. Acta, 34, 307-22.

Price, R.C., Johnson, R.W., Gray, C.M., and Frey, F.A., 1985. Geochemistry of phonolites and trachytes from the summit region of Mt. Kenya. Contrib. Mineral. Petrol. 89, 394-409.

Prior, G.T., 1898. Petrographical notes on the rock-specimens collected in Antarctic regions during the voyage of H.M.S. Erebus and Terror under Sir James Ross in 1839-43. Miner. Mag. 12, 69-91.

_____ 1902. Report on rock specimens collected by the Southern Cross Antarctic Expedition. Rep. Southern Cross Collections (British Museum), 321-32.

_____ 1907. Report of the rock specimens collected during the Discovery Antarctic Expedition, 1901-4. National Antarctic Exped. 1901-4, Nat. Hist. 1, 101-60.

Reichen, L.E., and Fahey, J.J., 1962. An improved method for the determination of FeO in rocks and minerals including garnet. U.S. Geol. Surv Bull. 1144-B, B1-B5.

Roden, M.K., Hart, S.R., Frey, F.A., and Melson, W.G., 1984. Sr, Nd, and Pb isotopic and REE geochemistry of St. Paul's Rocks: The metamorphic and metasomatic development of an alkali basalt mantle source. Contr. Miner. Petrol. 85, 376-90.

Ross, J., 1847. Voyage to the Southern Seas, vol. 1. London: John Murray.

Schairer, J.F., 1950. The alkali-feldspar join in the system $NaAlSiO_4$-$KAlSiO_4$-SiO_2. J. Geol. 58, 512-17.

Schnetzler, C.C., and Philpotts, J.A., 1970. Partition coefficients of rare earth elements between igneous matrix material and rock-forming mineral phenocrysts II. Geochim. Cosmochim. Acta, 34, 331-40.

Sigurdsson, H., and Schilling, J.-G., 1976. Spinels in Mid-Atlantic Ridge basalts: Chemistry and occurrence. Earth Planet. Sci. Lett. 29, 7-20.

Sleep, N.H., 1974. Segregation of magma from a mostly crystalline mush. Bull. Geol. Soc. Am. 85, 1225-32.

Smith, J.V., 1974. Feldspar Minerals, 1, Crystal Structure and Physical Properties. Heidelberg: Springer-Verlag.

Smith, W.C., 1954. The volcanic rocks of the Ross Archipalego. Brit. Antarctic Exped., 1910, Natural Hist. Rep., Geol. 2, 1-107.

Smithson, S.B., 1972. Gravity interpretation in the Transantarctic Mountains near McMurdo Sound. Bull. Geol. Soc. Am. 83, 3437-42.

Stephenson, D., 1972. Alkali clinopyroxenes from nepheline syenites of the South Qoroq centre, South Greenland. Lithos, 187-201.

Stewart, D., 1956. On the petrology of Antarctica. Geophys. Mono. Ser. (Am. Geophys. Un.) 1, 52-74.

Stormer, J.C. Jr., 1973. Calcium zoning in olivine and its relationship to silica activity and pressure. Geochim. Cosmochim. Acta, 37, 1815-21.

_____ 1983. The effects of recalculation on estimates of temperature and oxygen fugacity of multicomponent iron-titanium oxides. Am. Miner. 68, 586-94.

Stuckless, J.S., and Ericksen, R.L., 1976. Sr isotope geochemistry of the volcanic rocks and associated megacrysts and inclusions from Ross Island and vicinity, Antarctica. Contr. Miner. Petrol. 58, 111-26.

_____ Miesch, A.T., Goldich, S.S., and Weiblen, P.W., 1981. A Q-mode factor for the petrogenesis of the volcanic rocks from Ross Island and vicinity, Antarctica. In: McGinnis, L.D. (ed.) Antarctic Research Ser., vol. 33, Dry Valley Drilling Project. Washington, D.C.: Am. Geophys. Un., 257-280.

Sun, S.S., and Hanson, G.N., 1975. Origin of Ross Island basanitoids and limitations upon the heterogeneity of mantle sources for alkali basalts and nephelinites. Contr. Miner. Petrol. 52, 77-106.

_____ _____ 1976. Rare earth evidence of differentiation of McMurdo Volcanics, Ross Island, Antarctica. Contr. Miner. Petrol. 54, 139-55.

Takahashi, E., 1978. Partitioning of Ni^{2+}, Fe^{2+}, Mn^{2+} and Mg^{2+} between olivine and silicate melts: Compositional dependence of partition coefficients. Geochim. Cosmochim. Acta, 42, 1829-44.

Taylor, S.R., and Gorton, M.P., 1977. Geochemical application of spark source mass spectrography - III. Element sensitivity, precision and accuracy. Geochim. Cosmochim. Acta, 41, 1375-80.

Thompson, R.N., Esson, J., and Dunham, A.C., 1972. Major element chemical variation in the Eocene lavas of the Isle of Skye, Scotland. J. Petrology, 13, 219-53.

Thomson, J.A., 1916. Report on the inclusions of the volcanic rocks of the Ross Archipalego (with Appendix by F. Cohen). Rep. Brit. Antarctic Exped. 1907-9, Geol. 2, 129-51.

Toulmin, P. III, and Barton, P.B., 1964. A thermodynamic study of pyrite and pyrrhotite. Geochim. Cosmochim Acta, 28, 641-71.

Treves, S.B., 1962. The geology of Cape Evans and Cape Royds, Ross Island, Antarctica. Geophys. Mono. Ser. (Am. Geophys. Un.) 7, 40-6.

_____ 1968. Volcanic rocks of the Ross Island area. Antarctic J. U.S. 3, 108-9.

Tuttle, O.F., and Bowen. N.L., 1958. Origin of granite in the light of experimental studies in the system $NaAlSi_3O_8$-$KAlSi_3O_8$-H_2O. Mem. Geol. Soc. Am. 74.

Veiten, K., 1980. The minerals of the volcanic rock association of the Siebengebirge. I. Clinopyroxenes. 2. Variation of chemical composition of Ca-rich clinopyroxenes (salites) in the course of crystallization. N. Jb. Miner. Abh. 140, 54-88.

Warren, G., 1969. Geology of the Terra Nova Bay-McMurdo Sound area, Victoria Land. In: Bushnell, V.C. (ed.) "Geological Map of Antarctica 1:1,000,000" Antarctic Map Folio Ser. New York: Am. Geographical Soc.

Wass, S.Y., 1979. Multiple origins of clinopyroxenes in alkali basaltic rocks. Lithos, 12, 115-32.

_____ and Rogers, N.W., 1980. Mantle metasomatism - Precursor to continental alkaline volcanism. Geochim. Cosmochim. Acta, 44, 1811-23.

Watson, E.B., 1977. Partitioning of manganese between forsterite and silicate liquid. Geochim. Cosmochim. Acta, 41, 1363-74.

_____ 1979. Apatite saturation in basic and intermediate magmas. Geophys. Res. Lett. 6, 937-40.

Weiblen, P.W., Hunter, W.C., Stuckless, J.S., Schulz, K.J., and Mudrey, M.G. Jr., 1981. Correlation of clinopyroxene composition with environment of formation basd on data from Ross Island Volcanics, Antarctica. In: McGinnis, L.D. (ed.) Antarctic Research Ser., vol. 33, Dry Valley Drilling Project. Washington, D.C.: Am. Geophys. Un., 229-46.

Wilkinson, J.F.G., 1956. Clinopyroxenes of alkali olivine-basalt magma. Am. Miner. 42, 724-43.

Wilshire, H.G., 1984. Mantle metasomatism; The REE story. Geology, 12, 395-8.

Wong, H.K., and Christoffel, D.A., 1981. A reconnaissance seismic survey of McMurdo Sound and Terra Nova Bay, Ross Sea. In: McGinnis, L.D. (ed.) Antarctic Research Ser., vol. 33, Dry Valley Drilling Project. Washington, D.C.: Am. Geophys. Un., 37-62.

Worner, G., and Wright, T.L., 1984. Evidence for magma mixing within the Laacher See magma chamber (East Eifel, Germany). J. Volcanol. Geotherm. Res. 22, 301-327.

Wright, A.C., Kyle, P.R., McIntosh, W.C., and Klich, I, 1984. Geological field investigations of volcanic rocks at Mount Discovery and Mason Spur, McMurdo Sound. Antarctic J. U.S., 19, 1984 Review, 20.

_____ McIntosh, W., and Ellerman, P., 1983. Volcanic geology of Turks Head, Tryggve Point, and Minna Bluff, southern Victoria Land. Antarctic J. U.S., 18, 1983 Review, 35-36.

Yagi, K., and Onuma, K., 1967. The join $CaMgSi_2O_6$-$CaTiAl_2O_6$ and its bearing on the titanaugites. J. Fac. Sci. Hokkaido Univ., Ser. IV, 8, 463-83.

_____ Hariya, Y., Onuma, K., and Fukushima, N., 1975. Stability relation of kaersutite. J. Fac. Sci. Hokkaido Univ., Ser. IV, 16, 331-42.

APPENDIX A

Classification of Mt. Erebus lavas in proposed I.U.G.S. total alkali silica (TAS) classification

The I.U G.S. Subcommission on the Systematics of Igneous Rocks has proposed a classification for volcanic rocks based on the total alkali silica (TAS) plot (Le Maitre, 1984). The subcommission chose a classification based on chemical parameters because of problems in determining the modes of volcanic rocks. Systems based on normative minerals were considered unsuitable because of the complicated calculations involved and problems in dividing Ab between plagioclase and alkali feldspar. The TAS plot was chosen because of its simplicity, widespread acceptance and usefulness in separating various rock types.

The proposed classification is purely descriptive and strictly for fresh volcanic rocks. Analyses must be recalculated to 100% on a volatile-free basis before plotting on the diagram. FeO and Fe_2O_3 must be determined or calculated using a suitable method. Fe_2O_3 was standardized using the method of Thompson et al. (1972) for classifying the lavas of Mt. Erebus in the TAS system. Table A.1 contains a listing of samples from this study and their equivalent TAS nomenclature.

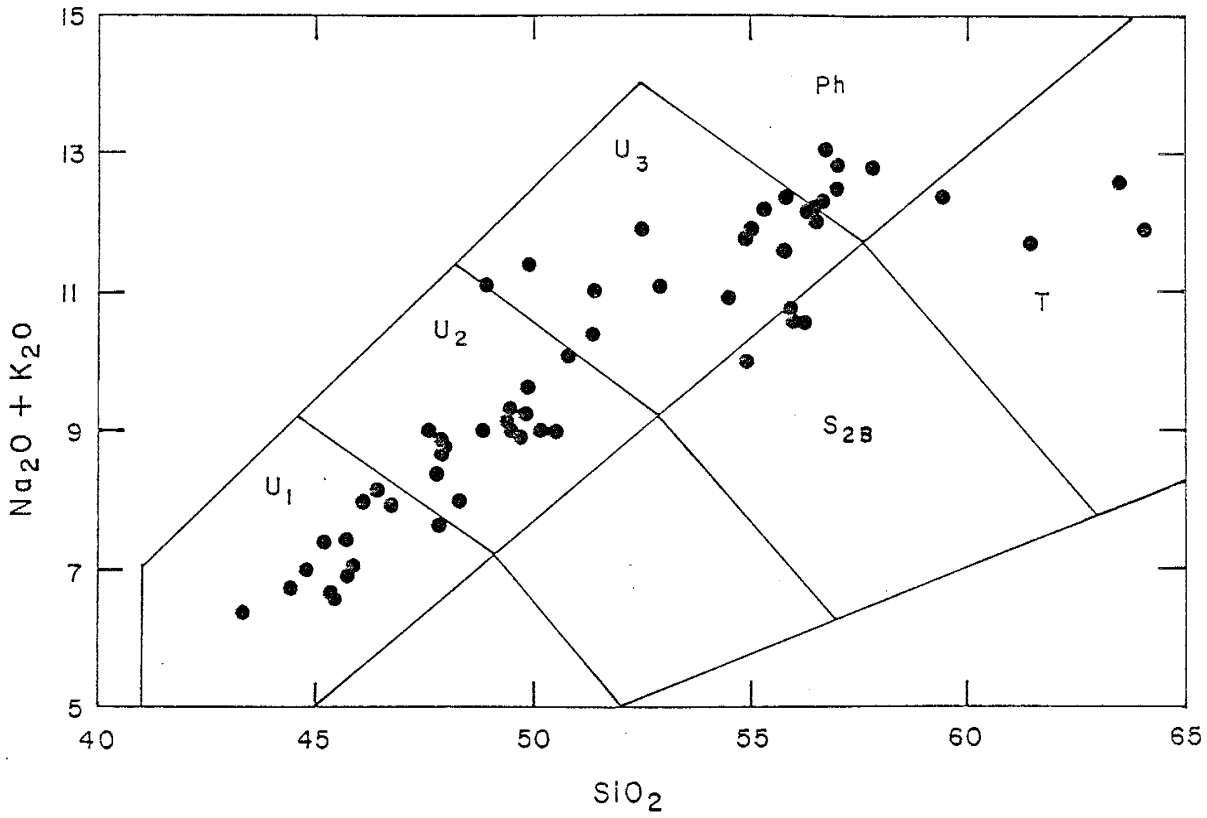

Figure A.1. Total alkalis against silica plot of Mt. Erebus lavas showing TAS classification. Nomenclature: U_1-basanite [ol (normative olivine)>10%), tephrite (ol<10%); U_2-phonotephrite; U_3-tephriphonolite; S_{2B}-benmoreite (sodic), latite (potassic); Ph-phonolite; T-trachyte [P.I. (peralkaline index)<1], alkali trachyte (P.I.>1).

Table A.1. Comparison of sample nomenclature used in this study and TAS nomenclature.

	Nomenclature	
Sample	This study	TAS
83435	basanite	basanite
83437	basanite	basanite
83405	Ne-hawaiite	basanite
83404	Ne-hawaiite	basanite
83406	Ne-hawaiite	basanite
AW82044	Ne-hawaiite	basanite
AW82032	Ne-hawaiite	basanite
79300	basanite	tephrite
83432	Ne-hawaiite	tephrite
83426	Ne-hawaiite	tephrite
83428	Ne-hawaiite	tephrite
83427	Ne-hawaiite	tephrite
83418	Ne-hawaiite	tephrite

Table A.1 continued

	Nomenclature	
Sample	This study	TAS
AW82029	Ne-hawaiite	phonotephrite
83439	Ne-hawaiite	phonotephrite
83438	Ne-hawaiite	phonotephrite
AW82038	Ne-hawaiite	phonotephrite
83441	Ne-hawaiite	phonotephrite
83436	Ne-hawaiite	phonotephrite
83409	Ne-hawaiite	phonotephrite
AW82041	Ne-hawaiite	phonotephrite
83453	Ne-hawaiite	phonotephrite
83440	Ne-hawaiite	phonotephrite
83401	Ne-hawaiite	phonotephrite
83415	Ne-hawaiite	phonotephrite
83203	Ne-hawaiite	phonotephrite
83411	Ne-hawaiite	phonotephrite
83403	Ne-hawaiite	phonotephrite
83417	Ne-mugearite	phonotephrite
83442	Ne-mugearite	tephriphonolite
83204	Ne-benmoreite	tephriphonolite
83410	Ne-benmoreite	tephriphonolite
AW82030	Ne-benmoreite	tephriphonolite
83202	Ne-benmoreite	tephriphonolite
83421	Ne-benmoreite	tephriphonolite
AW82015	Ne-benmoreite	tephriphonolite
83452	phonolite	tephriphonolite
82407	phonolite	tephriphonolite
83446	phonolite	tephriphonolite
83433	phonolite	tephriphonolite
83447	phonolite	tephriphonolite
82431	phonolite	tephriphonolite
80018	phonolite	tephriphonolite
82404	phonolite	tephriphonolite
83448	phonolite	phonolite
81001	phonolite	phonolite
83400	phonolite	phonolite
80020	phonolite	phonolite
83408	phonolite	phonolite
83412	benmoreite	benmoreite
81002	benmoreite	benmoreite
83402	benmoreite	benmoreite
AW82023	benmoreite	benmoreite
83407	phonolite	trachyte
83454	trachyte	alkali trachyte
83451	comenditic trachyte	alkali trachyte
82405	comenditic trachyte	alkali trachyte

APPENDIX B

DETAILED PETROGRAPHIC DESCRIPTIONS

In this section, detailed petrographic descriptions of the samples from Mt. Erebus are given. The descriptions are grouped by rock type first, then sample location. The modes given are visual estimates, and the petrographic terminology used is generally from MacKenzie et al., 1982. Feldspar compositions were determined by the Michel-Levy method (Kerr, 1977), using A-normal sections when observed.

Samples 83404 and 83405 lie in the basanite field but were classified as Ne-hawaiites because their coarsely porphyritic texture and moderately evolved trace element concentrations are more characteristic of the Ne-hawaiites.

BASANITES

83435

Seriate porphyritic. Vesicles rare, <0.5 mm. About 10 vol.% phenocrysts of clinopyroxene (5%), olivine (3%), feldspar (1%) and opaque oxides (1%). Clinopyroxene: 0.5-1.5 mm; pale brown; oscillatory, sector and discontinuous zoning; euhedral; rare pyrrhotite inclusions; rare sieved, embayed pale greenish cores. Olivine: 0.1-1.5 mm; euhedral, sometimes anhedral, embayed; opaque inclusions. Feldspar: An_{70}; 0.1-1.5 mm; weak continuous zoning; euhedral; rarely sieved. Opaque oxides: 0.1-0.3 mm; rare grains up to 1.0 mm; embayed; clots with olivine and clinopyroxene. Groundmass: holocrystalline; pilotaxitic; weakly flow-banded. Clinopyroxene (30%), feldspar (25%), opaque oxides (14%), olivine (5%), apatite (1%). 5% interstitial material, possibly nepheline.

79300

Seriate porphyritic. Trachytoid. Glomeroporphyritic. Vesicles common, 0.1-0.6 mm. 20% phenocrysts of feldspar (15%), olivine (4%), opaque oxides (1%) and rare clinopyroxene and apatite. Feldspar: An_{50-75}; 0.1-2 mm; subhedral-euhedral; continuous and rare oscillatory zoning; sometimes cores sieved; some embayed anhedral grains with thin overgrowths. Olivine: 0.5-1 mm; subhedral-euhedral, sometimes embayed; rare olivine-opaque clots with interstitial feldspar. Opaque oxides: 0.1-0.5 mm; anhedral-euhedral; sometimes embayed. Clinopyroxene: one microphenocryst 0.5 mm; pale brown; subhedral; partly enclosing feldspar microphenocrysts; opaque inclusions. Apatite: 0.1-0.3 mm; subhedral-euhedral. Groundmass: hypocrystalline; pilotaxitic; intersertal; 30% feldspar, 25% opaque oxides, 25% olivine, 10% glass, 10% possible interstitial nepheline.

83437

Moderately vesicular, vesicles <1 mm. Glomeroporphyritic. Seriate porphyritic. Trachytoid. 25% phenocrysts of feldspar (17%), olivine (5%), opaque oxides (2%), and clinopyroxene (1%). Feldspar: An_{67}; 0.1-4 mm; euhedral; cores sometimes sieved; sometimes thin discontinuous oligoclase rims (An_{29}); clinopyroxene inclusions. Olivine: 0.1-1 mm; subhedral. Opaque oxides: 0.1-0.6 mm; anhedral-subhedral. Clinopyroxene: 0.1-0.25 mm; subhedral. Groundmass: holocrystalline, pilotaxitic, intersertal; 40% opaque oxides, 40% feldspar, 10% olivine, 5% clinopyroxene. Rare nepheline.

NEPHELINE HAWAIITES

83426, 83427

These sections are similar and not warranting separate descriptions. Moderately vesicular, vesicles <2 mm; seriate microporphyritic and glomeroporphyritic, c. 20% microphenocrysts of feldspar (15%), olivine (2%), opaque oxides (2%), clinopyroxene (1%), and rare apatite. Feldspar: An_{60-70}; 0.1-1.4 mm; subhedral-euhedral; oscillatory and continuous zoning; olivine inclusions. Olivine: 0.1-0.6 mm; subhedral-euhedral; sometimes embayed; opaque oxide inclusions. Opaque oxides: 0.1-0.4 mm; anhedral, embayed. Clinopyroxene: pale purplish-brown, pleochroic; 0.1-0.3 mm; anhedral-subhedral; sector zoning. Apatite: 0.1-0.2 mm; anhedral-subhedral. Groundmass: hypocrystalline, intersertal, pilotaxitic, c. 5% glass, 50% feldspar, 33%

clinopyroxene, 10% opaque oxides, 5% olivine, 2% apatite.

83428

Weakly vesicular, vesicles <3 mm; seriate microporphyritic, c. 30% microphenocrysts of feldspar (23%), olivine (3%), opaque oxides (3%), clinopyroxene (1%) and rare apatite. Feldspar: An_{57}; 0.1-1.4 mm; subhedral-euhedral; some albite twinning, but generally weakly twinned; boundaries intergrown with groundmass; oscillatory and discontinuous zoning. Olivine: 0.1-0.3 mm; subhedral-euhedral; opaque oxide inclusions. Opaque oxides: 0.1-0.3 mm; anhedral-subhedral; embayed; apatite inclusions. Clinopyroxene: purplish brown, pleochroic; 0.1-0.2; subhedral; discontinuous zoning sometimes. Apatite: 0.1-0.2 mm; euhedral. Groundmass: slightly spherulitic; holocrystalline; felty; equigranular. 60% feldspar, 25% clinopyroxene, 10% opaque oxides, 5% olivine, accessory apatite.

83432

Moderately vesicular, vesicles <1 mm. Seriate microporphyritic, c. 20% microphenocrysts of feldspar (15%), olivine (3%), opaque oxides (1%), clinopyroxene (1%), and rare apatite. Feldspar: An_{63}; 0.1-0.5mm; euhedral; continuously zoned. Olivine: 0.1-0.3 mm; subhedral-euhedral; opaque inclusions. Opaque oxides: 0.1-0.3 mm; anhedral-subhedral, embayed; one 1.4 mm phenocryst with apatite microphenocrysts adhered to edges. Clinopyroxene: pale brown; 0.1-0.3 mm; euhedral; opaque inclusions. Apatite: 0.2-0.3 mm; euhedral. Groundmass: slightly devitrified; intersertal, pilotaxitic; flow-banded; 45% feldspar, 40% glass, 10% opaque oxides, 5% olivine.

AW82029

Moderately vesicular, vesicles <2 mm. Seriate porphyritic and glomeroporphyritic. 25% phenocrysts of feldspar (19%), olivine (5%), and opaque oxides (1%). Feldspar: An_{59}; 2-15 mm; anhedral-subhedral; commonly broken, sieved or embayed; edges corroded; oscillatory zoned; olivine and apatite inclusions. Olivine: 0.2-1 mm; anhedral-subhedral; apatite, opaque and rare olivine inclusions; commonly embayed; Opaque oxides: 0.1-0.6 mm; anhedral-subhedral; commonly embayed. Groundmass: holocrystalline; intersertal; weakly spherulitic; felty; 45% feldspar (An_{23} and interstitial alkali feldspar), 30% clinopyroxene, 10% opaque oxides, 10% interstitial material, possibly nepheline, 5% olivine.

AW82032

Weakly vesicular, vesicles <1 mm. Porphyritic; slightly glomeroporphyritic; 25 vol.% seriate phenocrysts of feldspar (9%), clinopyroxene (9%), olivine (5%), opaque oxides (2%) and apatite (1%). Feldspar: An_{43}; 1.4-8mm; anhedral-subhedral; sometimes embayed; rims commonly corroded, sometimes sieved; oscillatory and convolute zoning. Clinopyroxene: 1-4mm; purplish-brown; anhedral-euhedral; oscillatory zoning; opaque oxide and olivine inclusions; sometimes rims sieved and embayed. Olivine: 0.2-4mm; anhedral-euhedral; sometimes embayed; slightly iddingsitized. Opaque oxides: anhedral, embayed; 0.2-1mm; slightly oxidized. Groundmass: holocrystalline, intersertal, felty, slightly spherulitic; 35% feldspar (An_{57}), 20% clinopyroxene, 20% opaques, 5% olivine, 15% interstitial alkali feldspar and possibly nepheline.

AW82038

Vesicles rare. Trachytoid. Seriate porphyritic. Glomeroporphyritic. C. 20% phenocrysts of feldspar (15%), olivine (3%), opaque oxides (2%), apatite (1%), and rare clinopyroxene. Feldspar: An_{58-70}; 2-10 mm; subhedral-euhedral, sometimes broken; oscillatory zoned; outer rims continuously zoned to c. An_{20}; apatite, opaque oxide and glass inclusions. Olivine: 0.2-0.5 mm; subhedral-euhedral; magnetite and apatite inclusions; one embayed phenocryst with reaction rim possibly of clinopyroxene. Opaque oxides: 0.1-0.5 mm; anhedral; apatite inclusions. Clinopyroxene: pale brown; 0.1-0.2 mm; anhedral. Apatite: 0.1-0.3 mm; subhedral-euhedral. Groundmass: hypocrystalline, intersertal, felty, spherulitic, moderately devitrified; 45% glass, 30% feldspar (c. An_{55}), 10% opaque oxides, 10% low birefringent mineral, possibly nepheline, 5% olivine, 3% clinopyroxene, 2% apatite.

AW82041

Slightly vesicular, vesicles 0.3-0.5 mm. Seriate porphyritic and glomeroporphyritic; 15% phenocrysts of feldspar (10%), olivine (3%), opaque oxides (2%) and apatite (1%). Feldspar: An_{59}; 3-20 mm; anhedral-euhedral; broken fragments common; oscillatory zoned; inclusions of olivine, apatite and opaque oxides; sometimes sieved. Olivine: 0.1-0.8 mm; anhedral-euhedral; inclusions of apatite and opaque oxides. Opaque oxides: 0.1-0.7 mm; anhedral, embayed; glass inclusions; slightly oxidized. Apatite: 0.1-0.3 mm; subhedral; Groundmass: hypocrystalline, weakly spherulitic, intersertal, mostly devitrified. 45% feldspar (An_{44} and alkali feldspar), 10% olivine, 20% opaque oxides, 3%

clinopyroxene, 10% glass, 2% apatite. 10% interstitial material, probably nepheline, partly altered to zeolites, and calcite. Vesicles and fractures commonly filled or lined with zeolites.

AW82044

Weakly vesicular, vesicles <0.5 mm. Glomeroporphyritic. Seriate porphyritic. 25% phenocrysts of clinopyroxene (10%), feldspar (8%), olivine (4%), opaque oxides (2%) and apatite (1%). Clinopyroxene: 0.3-3 mm; pale brown-purplish brown, pleochroic; subhedral-euhedral, sometimes embayed; discontinuous, convolute and oscillatory zoning; olivine, opaque, apatite and sometimes clinopyroxene inclusions. Feldspar: An_{43}; 0.4-4 mm; anhedral-euhedral; sometimes sieved; commonly embayed, resorbed; sometimes discontinuously overgrown by alkali feldspar; incipient replacement by calcite. Olivine: 0.1-1 mm; anhedral-subhedral; opaque, apatite and rare clinopyroxene inclusions; incipient alteration to saponite. Opaque oxides: 0.1-0.6 mm; anhedral-subhedral; commonly embayed; moderately oxidized to hematite. Apatite: 0.1-0.3 mm; anhedral. Groundmass: holocrystalline, pilotaxitic, intersertal, devitrified, weakly spherulitic; 35% feldspar (An_{36}), 20% clinopyroxene, 20% opaques, 5% olivine, 5% calcite, 15% interstitial material, possibly nepheline.

83401

Vesicles rare, <1 mm. Seriate porphyritic and glomeroporphyritic. 30% phenocrysts of feldspar (22%), olivine (5%), opaque oxides (2%), and apatite (1%). Feldspar: An_{37}; 2-10 mm; anhedral-subhedral, corroded; oscillatory zoning; commonly sieved; inclusions of olivine, apatite, opaques. Olivine: 0.2-0.7 mm; subhedral-euhedral; inclusions of apatite and opaque oxides. Opaque oxides: 0.1-0.5 mm; anhedral-subhedral; embayed; apatite inclusions. Apatite: 0.2-0.4 mm; subhedral. Groundmass: holocrystalline; intersertal, slightly spherulitic; devitrified; 52% feldspar (An_{30} and alkali feldspar), 20% clinopyroxene, 10% opaques, 5% olivine, 2% apatite, 15% interstitial material, possibly nepheline.

83403

Vesicles scarce, <0.2 mm. Seriate porphyritic and glomeroporphyritic. 50% phenocrysts of feldspar (40%), olivine (8%), opaque oxides (5%), clinopyroxene (1%) and apatite (1%). Feldspar: An_{51}; 2-15 mm; anhedral-subhedral, commonly embayed, sieved; some broken fragments; inclusions

of olivine and opaques; oscillatory zoned. Olivine: 0.2-0.7 mm; anhedral-euhedral, sometimes embayed; inclusions of apatite and opaques; infrequent olivine-clinopyroxene clots. Opaque oxides: 0.2-0.7 mm; anhedral, commonly embayed. Clinopyroxene: 0.1-0.4 mm; anhedral; pale purplish brown. Apatite: 0.1-0.4 mm; anhedral-subhedral, sometimes embayed. Groundmass: hypocrystalline, intersertal, pilotaxitic; moderately devitrified; 35% glass, 40% feldspar (An_{39}), 15% opaque oxides, 10% olivine.

83404, 83405, 83406

These samples are similar and do not warrant separate descriptions. Moderately vesicular, vesicles 0.1-7 mm. Seriate porphyritic. 40% phenocrysts of feldspar (15%), clinopyroxene (10%), olivine (7-8%), opaque oxides (7%), and apatite (<1%). Feldspar: An_{61-67}; 0.1-8 mm; anhedral-euhedral; sometimes sieved; continuous and oscillatory zoning; clinopyroxene, opaque and apatite inclusions; slightly to moderately altered to epidote. Clinopyroxene: 0.1-5 mm; purplish brown, pleochroic; subhedral-euhedral; discontinuous, continuous, oscillatory and sector zoning; sometimes twinned; clots with and inclusions of opaque oxides and apatite; slightly altered to iddingsite. Olivine: 0.1-2.5 mm; anhedral-euhedral; sometimes embayed, glomerocrysts of olivine, opaques and apatite, sometimes with clinopyroxene and interstitial feldspar; inclusions of opaques, apatite and sometimes clinopyroxene; sometimes overgrown by clinopyroxene; slightly to moderately iddingsitized. Opaque oxides: 0.1-2 mm; anhedral; embayed; clotted with apatite; slightly-moderately oxidized. Apatite: 0.1-0.6 mm; subhedral-euhedral. Groundmass: holocrystalline, devitrified, slightly spherulitic; pilotaxitic, intersertal; 50% feldspar, 10-15% clinopyroxene, 10% olivine, 20-25% opaques, 1% apatite. Slightly to moderately altered to hematite, epidote, iddingsite, chlorite.

83409

Slightly vesicular, vesicles 0.2-0.6 mm. Seriate porphyritic and glomeroporphyritic. 20% phenocrysts of feldspar (10%), olivine (5%), opaque oxides (3%), clinopyroxene (1%) and apatite (1%). Feldspar: An_{44}; 2-10 mm; anhedral-euhedral; commonly embayed, resorbed, sieved; olivine inclusions; oscillatory zoned. Olivine: 0.2-1 mm; anhedral-subhedral; embayed; inclusions of opaques and apatite; slightly altered to iddingsite. Opaque oxides: 0.2-1.2 mm; anhedral-subhedral; heavily embayed, sieved; apatite inclusions; slightly altered to hematite. Clinopyroxene: 0.3-3 mm; anhedral-euhedral; purplish brown, pleochroic;

sometimes embayed; discontinuously zoned; opaque and apatite inclusions. Apatite: 0.2-0.5 mm; anhedral-subhedral. Groundmass: holocrystalline, pilotaxitic; flow banded; intersertal. 30% feldspar, 20% opaques, 10% olivine, 10% clinopyroxene, 30% interstitial material, possibly nepheline. Slightly altered to calcite.

83411

Scarce vesicles <0.2 mm. Seriate porphyritic and glomeroporphyritic; 40% phenocrysts of feldspar (30%), opaque oxides (4%), olivine (3%), clinopyroxene (2%) and apatite (1%). Feldspar: andesine; 2-15 mm; anhedral-subhedral, sometimes embayed; occasional broken pieces; inclusions of opaque oxides, apatite, olivine; oscillatory zoned; slightly altered to epidote, calcite. Opaque oxides: 0.15-1.5 mm; anhedral-subhedral; generally embayed; slightly altered to hematite. Olivine: 0.1-2 mm; anhedral-euhedral; embayed; inclusions of apatite and opaques; slightly to extensively iddingsitized. Clinopyroxene: 0.3-4.0 mm; anhedral-subhedral; purplish or greenish brown; inclusions of olivine, opaques and apatite; oscillatory and continuous zoning. Apatite: 0.1-0.4 mm; subhedral-euhedral; sometimes embayed. Groundmass: holocrystalline, pilotaxitic, intersertal. 44% feldspar (An_{31}), 35% opaque oxides, 5% olivine, 5% clinopyroxene, 1% apatite, 10% interstitial material, possibly nepheline.

83415

Vesicles scarce, <1 mm. Seriate porphyritic and glomeroporphyritic; c. 50% phenocrysts of feldspar (30%), clinopyroxene (8%), olivine (7%), opaque oxides (3%), and apatite (2%). Feldspar: An_{52}; 1-6 mm; anhedral-subhedral, many broken fragments <1mm; commonly sieved; corroded contacts; apatite, opaque oxide, glass and olivine inclusions. Clinopyroxene: pale brown-purplish brown pleochroism; 0.5-4 mm; anhedral, rounded; sometimes embayed, oscillatory zoning, reaction rims; apatite, opaque oxide, glass and, rarely, feldspar inclusions; sometimes consertally intergrown with olivine; one phenocryst show exsolution of opaque oxides along internal cleavage planes. Olivine: 0.1-2 mm; anhedral-subhedral; commonly embayed; smaller phenocrysts generally euhedral; apatite and opaque oxide inclusions; sometimes consertally intergrown with opaque oxides. Opaque oxides: 0.1-1 mm; anhedral-subhedral; embayed. Apatite: 0.1-0.3 mm; subhedral-euhedral. Groundmass: hyalo-ophitic; pilotaxitic; 30% glass, 33% feldspar (c. An_{47}), 30% opaque oxides, 5% olivine, 2% apatite.

83418

Moderately vesicular, vesicles 1-5 mm. Seriate porphyritic. 40% phenocrysts of feldspar (20%), opaque oxides (10%), olivine (5%), clinopyroxene (3%), apatite (2%) and rare nepheline. Feldspar: An_{55}; 1-6 mm; anhedral-euhedral, commonly embayed, resorbed; some broken fragments; discontinuously zoned; some oscillatory zoning; apatite, opaque and clinopyroxene inclusions; some grains recrystallized to aggregates of smaller anhedral grains. Opaque oxides: 0.2-1 mm; anhedral-subhedral; commonly embayed and resorbed. Olivine: 0.5-0.8 mm; subhedral, embayed; inclusions of apatite and opaques; some phenocrysts show exsolution of opaques from cores. Clinopyroxene: 0.3-4 mm; greenish or purplish brown pleochroism; anhedral-euhedral; sometimes sieved, embayed, or opaque rims; rare oscillatory or discontinuous zoning. Apatite: 0.2-0.4 mm; anhedral-subhedral. Nepheline: occurs in ~2 mm diameter glomeroporphyritic clots; anhedral; extensively altered to feldspar. Groundmass: holocrystalline, pilotaxitic, intersertal. 40% clinopyroxene, 40% feldspar (An_{60} and alkali feldspar), 14% opaques, 5% olivine, 1% apatite. Possible interstitial nepheline.

83203

Weakly vesicular, vesicles <0.5 mm. Seriate porphyritic and glomeroporphyritic. 40% phenocrysts of feldspar (20%), clinopyroxene (8%), olivine (5%), opaque oxides (5%), and apatite (2%). Feldspar: An_{60}; 0.1-4.5 mm; subhedral-euhedral; broken fragments common; commonly sieved and resorbed; apatite and opaque inclusions; oscillatory zoning. Clinopyroxene: 0.2-4 mm; euhedral; purplish brown pleochroism; some embayed, resorbed phenocrysts; convolute and sector zoning; sometimes twinned; rare opaque rims. Olivine: 0.1-0.5 mm; anhedral-subhedral, commonly embayed. Opaque oxides: 0.1-1 mm; anhedral-euhedral; commonly embayed. Groundmass: intersertal, holocrystalline, equigranular. Concentrations of microlitic opaque oxides. 55% feldspar, 35% opaques, 5% olivine, 5% clinopyroxene.

83436

Moderately vesicular, vesicles <0.5 mm. Slightly trachytoid. Seriate porphyritic and glomeroporphyritic, c. 30% phenocrysts of feldspar (20%), olivine (5%), opaque oxides (5%), and rare clinopyroxene and apatite. Feldspar: An_{54-60}; 0.5-10 mm; subhedral-euhedral; many broken fragments; sometimes embayments, reaction rims; oscillatory zoned; olivine, opaque oxide and apatite inclusions; rare consertal intergrowths with clinopyroxene. Olivine: 0.1-0.7 mm;

subhedral-euhedral; sometimes larger grains embayed; opaque oxide and apatite inclusions; sometimes slightly oxidized. Opaque oxides: 0.1-1.2 mm; anhedral-subhedral, embayed. Clinopyroxene: colorless to pale purplish brown; 0.1-2mm; subhedral-euhedral; sector zoning; apatite inclusions. Apatite: 0.1-0.2 mm; anhedral-subhedral. Groundmass: holocrystalline, intersertal, pilotaxitic. 45% feldspar, 30% opaque oxides, 15% clinopyroxene, 10% olivine.

83438, 83439

These sections are similar and not warranting separate descriptions. Vesicles rare, <0.5 mm. Trachytoid. Seriate porphyritic and glomeroporphyritic, c. 50% phenocrysts of feldspar (25%), clinopyroxene (10%), opaque oxides (7%), olivine (6%), and apatite (2%). Feldspar: An_{50-58}; 0.1-7 mm; anhedral-euhedral; sometimes embayed, sieved; generally corroded edges; oscillatory and sometimes convolute zoning; olivine, apatite and opaque inclusions. Clinopyroxene: brown-purplish brown, slightly pleochroic; 0.3-3.5 mm; anhedral to euhedral, sometimes broken; sometimes twinned; oscillatory, sector and discontinuous zoning; apatite, olivine and opaque inclusions, sometimes geometrically arranged along internal cleavage planes. Opaque oxides: 0.1-0.7 mm; anhedral-subhedral; embayed. Olivine: 0.1-1mm; anhedral-subhedral; sometimes embayed. Apatite: 0.1-0.3 mm; subhedral-euhedral; embayed sometimes. Groundmass: holocrystalline, intersertal, pilotaxitic; 65% feldspar, 23% opaques, 5% olivine, 5% clinopyroxene, 2% apatite.

83440

Moderately vesicular, vesicles <2 mm. Seriate porphyritic and glomeroporphyritic, c. 35% phenocrysts of feldspar (25%), olivine (5%), opaque oxides (3%), apatite (2%), and rare clinopyroxene. Feldspar: An_{52}; 0.1-9 mm; anhedral-euhedral; many broken fragments; oscillatory zoning; commonly embayed; sometimes thin discontinuous overgrowths; olivine, opaque oxide and apatite inclusions. Olivine: 0.2-1 mm; subhedral-euhedral; sometimes embayed; slightly iddingsitized sometimes; clinopyroxene, apatite, and opaque oxide inclusions; rare zoned, embayed phenocrysts with opaque oxide exsolution along internal cleavage planes. Opaque oxides: 0.1-0.7 mm; anhedral-subhedral; embayed; apatite inclusions; sometimes slightly oxidized. Apatite: 0.1-0.4 mm; anhedral-subhedral; embayed. Clinopyroxene: purplish-brown; c. 1 mm; embayed, anhedral; corroded boundaries; sector zoning and twinning; opaque oxide and apatite inclusions. Groundmass: holocrystalline, intersertal, pilotaxitic, slightly oxidized. 65% feldspar, 25% opaque oxides, 5% olivine, 5% apatite.

83441

Moderately vesicular, vesicles <1 mm. Seriate porphyritic and glomeroporphyritic; c. 50% phenocrysts of feldspar (20%), clinopyroxene (16%), opaque oxides (7%), olivine (5%), and apatite (2%). Feldspar: An_{53}; 0.1-8 mm; anhedral-euhedral; sometimes embayed, sieved, corroded, and broken; oscillatory zoned; olivine, apatite and opaque inclusions. Clinopyroxene: 0.3-3.5 mm; brown-purplish brown, slightly pleochroic; anhedral-euhedral; may be rounded, sieved, embayed; sector and fine oscillatory zoning in largest phenocrysts, smaller phenocrysts may show discontinuous zoning; geometrically-arranged opaque and apatite inclusions. Opaque oxides: 0.1-0.8 mm; anhedral-subhedral, embayed. Olivine: 0.1-1mm; anhedral-euhedral; sometimes embayed. Apatite: 0.1-0.2 mm; anhedral and embayed to euhedral. Groundmass: Pilotaxitic, holocrystalline, intersertal. 70% feldspar (An_{41}), 20% opaques, 7% olivine, accessory clinopyroxene and apatite. Microlitic opaques concentrated around phenocrysts.

83453

Extremely vesicular, vesicles <8 mm. Microporphyritic; c. 5% microphenocrysts of feldspar (2%), opaque oxides (1%), olivine (1%), accessory clinopyroxene and apatite, and rare kaersutite. Feldspar: An_{57}; 0.1-1.4 mm; euhedral; oscillatory zoned; larger phenocrysts somewhat resorbed, sieved, embayed; sometimes glomerocrystic. Opaque oxides: 0.1-0.4 mm; subhedral, embayed; slightly oxidized. Olivine: 0.1-0.6 mm; anhedral-euhedral; sometimes embayed; apatite and opaque oxide inclusions; slightly iddingsitized. Clinopyroxene: pale brown; 0.1-0.2 mm; euhedral; sometimes polysynthetic twinning and discontinuous zoning. Apatite: 0.1 mm; subhedral. Kaersutite: c. 1 mm; extensively oxidized. Groundmass: hyalo-ophitic, slightly devitrified; pilotaxitic; 40% glass, 40% feldspar, 10% opaque oxides, 7% olivine, 2% apatite, 1% clinopyroxene.

NEPHELINE MUGEARITES

83417

Porphyritic. Rare vesicles <0.1mm. 30 vol.% phenocrysts of feldspar (15%), olivine (5%), opaque oxides (5%), clinopyroxene (3%), and apatite (2%). Feldspar: An_{48}; 1-11 mm; anhedral-euhedral; corroded edges; sieved, embayed; discontinuous, continuous, and oscillatory zoning; inclusions of olivine, clinopyroxene and opaques. Olivine: 0.2-1.6 mm; slightly iddingsitized; apatite and opaque

inclusions; sometimes embayed; rare phenocrysts with opaque oxide exsolution along internal cleavage planes. Opaque oxides: 0.1-0.8 mm; embayed; oxidized; abundant ilmenite lamellae. Clinopyroxene: 0.2-1 mm; corroded, subhedral, embayed; sometimes oscillatory zoned; rims greenish, sometimes have dusty opaque inclusions. Apatite: 0.1-0.5 mm; subhedral-euhedral; resorbed cores sometimes. Groundmass: intersertal, equigranular, mosaic-textured; 60% alkali feldspar, 20% clinopyroxene, 15% opaques, 3% olivine, 1% apatite.

83442

Scarce vesicles 0.1-0.3 mm; seriate porphyritic and glomeroporphyritic; 20% phenocrysts of feldspar (7%), clinopyroxene (5%), opaque oxides (3%), olivine (3%), and apatite (2%). Feldspar: An_{60}; 0.2-5 mm; anhedral-euhedral; broken fragments common; olivine, opaque and apatite inclusions; cores continuously zoned, rims oscillatory zoned; sometimes weakly altered; cores or rims sometimes sieved. Clinopyroxene: 0.3-2.5 mm; anhedral-euhedral; sometimes embayed; inclusions of opaques and apatite; sometimes twinned; discontinuous zoning; sometimes sieved; sometimes partly altered to chlorite and opaques. Opaque oxides: 0.1-0.9 mm; anhedral-subhedral; commonly embayed; apatite inclusions; moderately oxidized to hematite. Olivine: 0.1-0.4 mm; anhedral-subhedral; inclusions of apatite and opaques; sometimed embayed; partly to extensively iddingsitized. Apatite: 0.2-1 mm; anhedral-euhedral; embayed; sometimes glass cores; partly altered to calcite. Groundmass: holocrystalline, intersertal; felty; 65% feldspar (An_{46}), 25% opaque oxides, 7% olivine, 3% apatite. Slightly altered to hematite, iddingsite, kaolinite, epidote and chlorite.

NEPHELINE BENMOREITES

AW82015

Moderately vesicular, vesicles 0.5-2.5 mm. Seriate porphyritic. 42% phenocrysts of anorthoclase (30%), olivine (5%), opaques (3%), clinopyroxene (3%) and apatite (1%). Anorthoclase: 1-20 mm; subhedral-euhedral; broken fragments common; corroded edges; opaque, olivine, apatite inclusions; microcline, carlsbad and pericline twinning; continuously zoned. Olivine: 0.1-1.4 mm; anhedral-euhedral; embayed; clots with and inclusions of opaques, apatite; sometimes intergrown with clinopyroxene. Opaque oxides: 0.1-0.8 mm; anhedral-subhedral; embayed; apatite inclusions. Clinopyroxene: 0.3-2.0 mm; anhedral-subhedral; sometimes

embayed; clots with opaques and apatite; pale greenish brown; apatite, opaque and glass inclusions. Apatite: 0.1-0.8 mm; subhedral-euhedral; glass inclusions in cores. Groundmass: intersertal, hypocrystalline, mostly devitrified, 65% feldspar, 15% glass, 10% clinopyroxene, 5% opaque oxides, 3% olivine, 1% apatite.

AW82030

Vesicles scarce, 0.1-0.4 mm. Trachytoid, porphyritic. 20% phenocrysts of feldspar (10%), olivine (4%), opaque oxides (2%), apatite (2%), and clinopyroxene (2%). Feldspar: An_{49}; 1-18mm; anhedral-subhedral; some broken fragments; embayed, sieved; corroded edges; olivine, apatite and opaque inclusions; discontinuous and oscillatory zoning. Olivine: 0.1-1 mm; anhedral-euhedral; sometimes embayed; inclusions of apatite and opaques; clots with opaques, clinopyroxene and apatite. Opaque oxides: 0.1-0.8 mm; anhedral-subhedral; embayed; slight oxidation to hematite. Clinopyroxene: 0.2-0.8 mm; anhedral; pale purplish brown pleochroism; apatite and opaque inclusions; clots with apatite, opaques, and olivine; discontinuous zoning. Apatite: 0.3-1 mm; subhedral-euhedral. Groundmass: holocrystalline, intersertal, felty, equigranular, devitrified, slightly spherulitic; 45% feldspar (andesine), 34% clinopyroxene, 15% opaques, 3% olivine, 3% apatite. Some calcite.

25748

Moderately vesicular, vesicles 0.02-0.1 mm. Seriate porphyritic; 50% phenocrysts of feldspar (38%), olivine (5%), opaque oxides (3%), clinopyroxene (2%) and apatite (2%). Glass inclusions common in feldspar, olivine, and clinopyroxene phenocrysts. Feldspar: An_{32}; 0.1-10 mm; anhedral-subhedral; many broken fragments; commonly embayed; apatite and olivine inclusions; commonly fractured; oscillatory zoning; sometimes thin discontinuous overgrowths. Olivine: 0.1-1 mm; anhedral-subhedral; embayed; clots with and inclusions of apatite and opaques; rare consertal intergrowths with apatite. Opaque oxides: 0.06-0.6 mm; anhedral-euhedral; commonly embayed; rare clinopyroxene overgrowths. Clinopyroxene: 0.2-2.6 mm: anhedral-subhedral; embayed; clots with and inclusions of apatite, opaque oxides; sector and oscillatory zoning; cores usually homogeneous; commonly twinned. Apatite: 0.1-0.5 mm; subhedral-euhedral; slightly embayed; glass inclusions in cores common. Groundmass: hyalo-ophitic; slightly devitrified; pilotaxitic; 75% glass, 15% feldspar (An_{20}), 5% opaques, 3% olivine, 2% olivine, <1% pyrrhotite.

83421

Extremely vesicular, vesicles 0.2-2 mm. Seriate porphyritic and glomeroporphyritic; 50% phenocrysts of feldspar (37%), opaque oxides (7%), olivine (5%) and apatite (1%). Feldspar: An_{57}; 0.1-10 mm; anhedral-euhedral; small broken fragments common; commonly embayed, sieved; inclusions of opaque oxides, olivine, apatite; oscillatory and sometimes convolute zoning; sometimes thin discontinuous overgrowths, opaque rims or bulbous colloidal-looking overgrowths. Opaque oxides: 0.1-0.4 mm; anhedral-euhedral; sometimes embayed. Olivine: 0.1-0.8 mm; anhedral-euhedral; sometimes embayed; inclusions of opaques and apatite. Apatite: 0.1-0.2 mm; anhedral-subhedral. Groundmass: holocrystalline, pilotaxitic, intersertal; 65% feldspar, 25% opaques, 5% olivine, 5% apatite.

83410

Weakly vesicular, vesicles <0.1 mm. Seriate porphyritic and glomeroporphyritic; c. 30% phenocrysts of feldspar (20%), olivine (5%), opaque oxides (2%), apatite (2%), and clinopyroxene (1%). Feldspar: An_{49}; 1-11 mm; anhedral-subhedral, broken fragments <1mm; commonly embayed, sieved; olivine, apatite, opaque oxide inclusions; discontinuous and oscillatory zoning. Olivine: 0.1-1 mm; anhedral-euhedral; embayed; apatite, opaque oxide and rare clinopyroxene inclusions. Opaque oxides: 0.1-0.6 mm; anhedral-subhedral; embayed. Apatite: 0.2-0.5 mm; subhedral-euhedral. Clinopyroxene: pale brown-purplish brown pleochroism; 0.2-1 mm; anhedral; discontinuous and oscillatory zoning; opaque oxide and apatite inclusions. Groundmass: holocrystalline; pilotaxitic; intersertal; 65% feldspar, 23% opaque oxides, 5% olivine, 5% clinopyroxene, 2% apatite.

83202

Highly vesicular, vesicles 0.1-2 mm; porphyritic; 35% phenocrysts of feldspar (20%), olivine (7%), opaque oxides (5%), clinopyroxene (2%), and apatite (1%). Feldspar: An_{50}; 2-7 mm; broken fragments common; anhedral-subhedral; commonly embayed, sieved; opaque and olivine inclusions; oscillatory and sometimes convolute zoning; opaque rims common. Olivine: 0.1-1.9 mm; anhedral-subhedral; embayed; clots with apatite and opaques. Opaque oxides: 0.1-0.8 mm; anhedral-subhedral; embayed. Clinopyroxene: 0.2-0.5 mm; anhedral, embayed; purplish brown, pleochroic; opaque rims common; clots with and inclusions of opaque oxides and apatite; sometimes continuously zoned, twinned. Apatite: 0.1-0.8 mm; anhedral-subhedral; glass inclusions in cores

common. Groundmass: holocrystalline, devitrified, felty; 50% feldspar, 40% opaques, 10% olivine. Rare nepheline euhedral.

83204

Vesicles common, 0.1-2 mm; seriate porphyritic, slightly glomeroporphyritic; 20 vol.% phenocrysts of feldspar (11%), olivine (5%), opaque oxides (3%), and apatite (1%). Feldspar: An_{49}; 0.1-2.5 mm; euhedral; oscillatory and discontinuous zoning. Olivine: 0.1-0.8 mm; euhedral; sometimes embayed; apatite and opaque inclusions. Opaque oxides: 0.1-0.5 mm; embayed to euhedral. Apatite: 0.1-0.4 mm; commonly euhedral; sometimes glass inclusions in cores. Groundmass: hyalo-ophitic; slightly devitrified; pilotaxitic; 85% glass, 10% feldspar (An_{41}), 3% olivine, 2% opaques; rare euhedral nepheline microlites.

ANORTHOCLASE PHONOLITES

83400

Vesicles uncommon, 0.4-3 mm; seriate porphyritic; 40% phenocrysts of anorthoclase (30%), olivine (4%), opaque oxides (3%), apatite (2%) and clinopyroxene (1%). Anorthoclase: 2-20 mm; subhedral-euhedral; smaller phenocrysts clotted with olivine and opaques; inclusions of olivine, opaque oxides, clinopyroxene and apatite; fractured; zonal sieving and arrangement of inclusions; overgrowths continuous with groundmass feldspar; crosshatched and carlsbad twinning; cores homogeneous or show coarse, diffuse oscillatory zoning. Olivine: 0.3-1 mm; anhedral-subhedral; embayed; clots with and inclusions of opaque oxides and apatite; one phenocrysts 1.3 mm, subhedral, containing inclusions of nepheline and biotite partly altered to chlorite. Opaque oxides: 0.3-1 mm; anhedral-euhedral; sometimes embayed; apatite and rare biotite inclusions. Apatite: 0.2-0.6 mm; anhedral-subhedral; sometimes embayed; glass inclusions in cores common. Clinopyroxene: 0.8-2.5 mm; anhedral; embayed; clots with and inclusions of opaque oxides and apatite; continuously zoned from brown cores to bright green rims. Groundmass: hypocrystalline, intersertal, fine grained; 75% alkali feldspar, 10% clinopyroxene, 5% opaques, 3% green hornblende, 2% apatite, 2% aenigmatite, 2% yellowish-green glass, 1% pyrrhotite. Groundmass clinopyroxene continuously zoned to bright green rims like phenocryst clinopyroxenes. Green hornblende: interstitial or sometimes overgrowing olivine or groundmass clinopyroxene. Aenigmatite: interstitial or rimming groundmass opaques.

83433, 83446, 83447, 83448

These sections are similar and do not warrant separate descriptions. Vesicles moderately common, 0.5-4 mm. Seriate porphyritic; 30-40 vol.% phenocrysts of anorthoclase (25-30%), olivine (2-5%), opaque oxides (2-4%), clinopyroxene (1-3%), and apatite (1%). Anorthoclase: 0.5-20 mm; euhedral; broken fragments common; corroded edges; inclusions of olivine, opaque oxides, apatite, sometimes clinopyroxene; fractured; sometimes slightly sieved; sometimes thin overgrowths or opaque rims; microphenocrysts sometimes sieved; sometimes weak continuous, oscillatory or discontinuous zoning; pericline, crosshatched and carlsbad twinning common. Olivine: 0.2-1.4 mm; anhedral-subhedral; embayed; clots with and inclusions of apatite, opaques oxides; sometimes opaque rims, glass inclusions. Opaque oxides: 0.1-1 mm; anhedral-euhedral; sometimes embayed; apatite inclusions. Clinopyroxene: 0.15-3 mm; greenish brown to brown pleochroism; anhedral-euhedral, embayed; apatite and opaque oxide inclusions; continuous zoning sometimes. Apatite: 0.15-0.4 mm, subhedral-euhedral, sometimes embayed; sometimes glass inclusions in cores. Pyrrhotite: commonly clotted with magnetite; rare microphenocrysts 0.25 mm; . Groundmass: hypocrystalline, felty, intersertal; 55-60% alkali feldspar, 7-15% opaque oxides, 10-25% yellowish-brown glass, 5-7% feldspathoids, 3-5% interstitial to subhedral kaersutite, 2% green clinopyroxene, 1-2% apatite, 1% olivine, 1% pyrrhotite. Feldspathoids: interstitial or discrete grains 0.1 mm, subhedral, rounded, commonly full of inclusions.

80020

Extremely vesicular, vesicles 0.03-5 mm. Seriate porphyritic, glomeroporphyritic, trachytoid; 50% phenocrysts of feldspar (40%), olivine (5%), opaque oxides (3%), clinopyroxene (1%) and apatite (1%). Glass inclusions common in phenocrysts. Feldspar: anorthoclase and oligoclase (An_{16-24}); 1-30 mm; subhedral-euhedral; inclusions of other phenocryst phases; thin overgrowths discontinuous with rims; zonal arrangement of groundmass constituents in overgrowths; fractured; microcline, pericline, albite and carlsbad twins; coarse, faint oscillatory zoning. Olivine: 0.25-1.5 mm; anhedral-euhedral; commonly embayed; inclusions of opaques, apatite and olivine. Opaque oxides: 0.1-1 mm; anhedral-subhedral; commonly embayed; apatite inclusions. Clinopyroxene: 0.7-1.4 mm; subhedral-euhedral; brownish-green; inclusions of apatite, opaque oxides, clinopyroxene, olivine. Apatite: 0.1-0.6 mm; subhedral-euhedral; glass inclusions in cores. Groundmass: vitrophyric, pilotaxitic. 80% glass, 9% alkali feldspar, 3% opaque oxides and pyrrhotite, 3% pale green clinopyroxene, 3% olivine, 1%

apatite, 1% sodalite (euhedral, <0.02 mm).

81001

Moderately vesicular, vesicles 0.2-2 mm. Seriate porphyritic. Glass inclusions common in phenocrysts. 35% phenocrysts of anorthoclase (28%), opaque oxides (3%), olivine (3%), apatite (1%) and rare clinopyroxene. Anorthoclase: 6-20 mm; subhedral-euhedral; apatite, olivine, clinopyroxene and opaque inclusions; sometimes opaque rims; fractured; rarely sieved; rare clots with olivine; generally unzoned; carlsbad and pericline twins. Opaque oxides: 0.1-0.5 mm; anhedral-euhedral; sometimes embayed; apatite inclusions. Olivine: 0.2-0.5 mm; anhedral-euhedral, sometimes embayed; clots with and inclusions of apatite, opaques, clinopyroxene; rare phenocrysts ~1 mm, anhedral, corroded and embayed. Apatite: 0.2-0.3 mm; subhedral-euhedral; glass inclusions in cores sometimes. Clinopyroxene: ~2 mm; greenish brown, pleochroic; anhedral-subhedral; embayed; clots with opaques and olivine; inclusions of opaques and apatite. Groundmass: vitrophyric. Pilotaxitic. Slightly devitrified. 80% glass, 10% feldspar, 4% clinopyroxene, 3% olivine, 3% opaques.

82407

Extremely vesicular, vesicles stretched, 0.1-5 mm. Seriate porphyritic, glomeroporphyritic; 52% phenocrysts of anorthoclase (48%), olivine (5%), opaques (4%), clinopyroxene (2%), and apatite (1%). Glass inclusions common in phenocrysts. Anorthoclase: 0.3-15 mm; generally euhedral; some broken fragments and embayed, anhedral grains; inclusions of feldspar, opaques, olivine, clinopyroxene, apatite, and sometimes olivine-opaque-apatite clots; commonly fractured; microcline, carlsbad and pericline twinning; faint continuous, oscillatory and convolute zoning. Olivine: 0.1-0.8 mm; anhedral-subhedral; embayed; clots with opaque oxides, apatite and clinopyroxene; inclusions of apatite and opaques; sometimes embayed. Opaques: 0.1-0.6 mm: anhedral; commonly embayed. Clinopyroxene: 0.25-1.5 mm; subhedral-euhedral; greenish brown, pleochroic; opaque inclusions; sometimes sieved. Apatite: 0.1-0.4 mm; euhedral. Groundmass: vitrophyric; flow banded; pilotaxitic; 87% glass, 3% alkali feldspar, 3% olivine, 3% opaques, 3% clinopyroxene, 1% apatite.

83452

Extremely vesicular, vesicles 0.03-1.1 mm; seriate porphyritic; 50% phenocrysts of anorthoclase (40%), olivine

(5%), opaque oxides (3%), clinopyroxene (1%), and apatite (1%). Anorthoclase: 3-15 mm; euhedral; opaque, apatite, olivine, clinopyroxene, glass inclusions; opaque rims common; sometimes thin discontinuous overgrowths; microcline, pericline and carlsbad twinning; slight, faint continuous and oscillatory zoning. Olivine: 0.2-0.9 mm; anhedral-euhedral; sometimes embayed; clots with and inclusions of opaques and apatite. Opaques: 0.1-0.3 mm; anhedral-euhedral; sometimes embayed. Clinopyroxene: 0.1-0.5 mm; subhedral-euhedral; greenish brown, pleochroic; clots with opaques, olivine; opaque and glass inclusions. Apatite: 0.1-0.5 mm; euhedral. Groundmass: vitrophyric; flow banded; pilotaxitic. 87% glass, 3% feldspar, 3% olivine, 3% clinopyroxene, 3% opaques, 1% apatite.

BENMOREITES

83402

Microporphyritic, glomeroporphyritic. 10% microphenocrysts of feldspar (5%), opaque oxides (2%), olivine (2%), kaersutite (1%), and apatite (<1%). Rare feldspar and clinopyroxene xenocrysts (?). Feldspar: An_{43}; 0.2-0.5 mm; subhedral-euhedral; continuous and oscillatory zoning; carlsbad, albite, pericline twins; kaersutite inclusions. Feldspar xenocrysts: 1.0-1.3 mm, composition undetermined; anhedral, corroded, resorbed, sieved; oscillatory zoned. Opaque oxides: 0.1-0.15 mm; anhedral; embayed. Olivine: 0.1-0.3 mm; anhedral-euhedral; embayed; opaque inclusions. Kaersutite: 0.1-0.2 mm; anhedral-subhedral; slightly to moderately oxidized to opaque oxides. Apatite: ~0.1 mm; embayed, subhedral. Clinopyroxene xenocrysts: 0.6 mm, green, anhedral, glomeroporphyritic with opaque oxides; opaque inclusions; altered to kaersutite. Groundmass: holocrystalline; trachytic; kinked foliation; 80% alkali feldspar, 10% opaques, 5% olivine, 3% kaersutite, 2% apatite.

83412

Microporphyritic. Vesicles rare, <0.5 mm. Glomeroporphyritic. 15% microphenocrysts of feldspar (9%), olivine (3%), opaque oxides (2%) and apatite (1%). Feldspar: 0.1-0.8 mm; euhedral; inclusions of olivine, opaques; largest grains slightly sieved; discontinuously and continuously zoned from cores of An_{65} to rims of An_{49}. Olivine: 0.1-0.5 mm; subhedral-euhedral; sometimes embayed; inclusions of opaques and apatite; rare phenocrysts ~1 mm, subhedral, embayed, with opaque oxide exsolution along internal cleavage planes and in rims. Opaque oxides: 0.1-0.4

mm; anhedral-euhedral; sometimes embayed. Apatite: 0.1-0.4 mm; anhedral-euhedral. Groundmass: holocrystalline, trachytic; 75% feldspar, 15% opaques, 9% olivine, 1% interstitial phase, possibly kaersutite.

AW82023

Vesicles scarce, 0.1-0.2 mm. Microporphyritic, glomeroporphyritic. 20% microphenocrysts of feldspar (10%), opaque oxides (5%), olivine (3%), clinopyroxene (2%) and rare apatite. Feldspar: An_{45}; 0.2-1 mm; subhedral-euhedral; oscillatory or continuously zoned rims and homogeneous cores; largest phenocrysts generally embayed and resorbed. Opaque oxides: 0.1-0.4 mm; anhedral-subhedral; apatite inclusions. Olivine: 0.1-0.5 mm; anhedral-subhedral; slightly embayed. Clinopyroxene: 0.1-1 mm; pale green; subhedral-euhedral; opaque and apatite inclusions. Apatite: 0.2-0.3 mm; subhedral-euhedral; glass inclusions in cores sometimes. Groundmass: holocrystalline, trachytic; kinked foliation. 65% feldspar, 15% opaque oxides, 15% clinopyroxene, 5% olivine.

81002

Highly vesicular, vesicles 0.2-4 mm. Seriate porphyritic, glomeroporphyritic; 60% phenocrysts of feldspar (43%), opaque oxides (5%), clinopyroxene (5%), kaersutite (3%), olivine (3%), and apatite (1%). Feldspar: An_{44}; 0.1-4 mm; subhedral-euhedral; sometimes embayed; inclusions of all other phenocryst phases; some heavily sieved and embayed grains; discontinuously or continuously zoned; rare oscillatory zoning. Opaque oxides: 0.1-0.5 mm; anhedral-euhedral; commonly embayed, corroded; apatite and glass inclusions. Clinopyroxene: 0.1-0.8 mm; subhedral-euhedral; pale green; inclusions of opaques and apatite; twinned; slight continuous zoning;. Kaersutite: 0.1-1.4 mm; subhedral-euhedral; slight to moderate alteration to opaques; opaque and apatite inclusions; occasional consertal intergrowths with feldspar. Olivine: 0.1-0.4 mm; anhedral-euhedral; apatite, opaque and sometimes glass inclusions; slightly iddingsitized. Apatite: 0.1-0.3 mm; subhedral-euhedral. Groundmass: hyalo-ophitic; mostly devitrified; pilotaxitic. 90% alkali feldspar, 10 % glass.

KAERSUTITE PHONOLITES

83407

Rare vesicles 0.05-0.2 mm; seriate porphyritic, glomeroporphyritic; 3% phenocrysts of feldspar (2%), opaque oxides (0.5%), kaersutite (0.5%) and rare olivine and clinopyroxene. Feldspar: 0.4-3 mm; subhedral-euhedral; inclusions of opaques; sometimes sieved; Carlsbad, albite, pericline and microcline twinning; cores oscillatory or continuously zoned or homogeneous; discontinuous rims. Opaque oxides: 0.1-0.8 mm; anhedral-subhedral, embayed, sieved. Kaersutite: 0.6-1.8 mm; subhedral; extensively altered to opaques. Olivine: one phenocryst 1.4 mm; anhedral, embayed, sieved, opaque inclusions. Clinopyroxene: one phenocryst 0.2 mm; subhedral, embayed; yellowish-green. Groundmass: holocrystalline, trachytic; 72% feldspar, 12% clinopyroxene, 10% opaque oxides, 6% olivine. Mafics moderately altered to chlorite.

83408

Vesicles rare, <0.2 mm. Seriate porphyritic; 10% phenocrysts of feldspar (4%), olivine (2%), opaque oxides (25%), kaersutite (1%), clinopyroxene (1%), and rare apatite. Feldspar: 0.1-2.5 mm; euhedral; some anhedral corroded phenocrysts; zoned from embayed and corroded cores of An_{40} to discontinuous thin alkali feldspar rims. Olivine: 0.2-1.2 mm; anhedral; usually embayed; sometimes opaque rims; inclusions of apatite and opaques. Opaque oxides: 0.1-0.6 mm; anhedral-euhedral; commonly embayed. Kaersutite: 0.5-2.5 mm; anhedral; generally completely oxidized to opaques. Clinopyroxene: 0.4-0.6 mm; anhedral-subhedral; embayed; opaque inclusions. Apatite:0.1-0.2 mm; euhedral. Groundmass: holocrystalline, trachytic; 82% alkali feldspar, 10% yellowish-green clinopyroxene, 5% opaques, 2% olivine, 1% apatite.

82404

Moderately vesicular, vesicles 0.05-4 mm. Porphyritic, weakly glomeroporphyritic. 10% phenocrysts of feldspar (5%), kaersutite (2%), olivine (1%), magnetite (1%), and rare clinopyroxene and apatite. Feldspar: 1.0-3.5 mm; subhedral-euhedral; inclusions of clinopyroxene, opaque oxides, and kaersutite; sometimes embayed; discontinuously zoned from sieved, homogeneous cores of An_{49} to continuous or oscillatory zoned rims. Kaersutite: 0.1-1 mm; subhedral-euhedral; apatite, opaque and glass inclusions; slightly to extensively oxidized to opaques and

clinopyroxene. Olivine: 0.2-0.7 mm; anhedral-subhedral; inclusions of opaque oxides. Magnetite: 0.1-0.6 mm; anhedral-euhedral; embayed; pyrrhotite and apatite inclusions; incipient ilmenite exsolution. Clinopyroxene: 0.1-0.8 mm; pale brown-brownish green; anhedral-euhedral; continuous and sector zoning; some large, embayed subhedral grains. Groundmass: hyalo-ophitic. Slightly devitrified and spherulitic; pilotaxitic; glomeroporphyritic; 50% feldspar, 25% glass, 15% leucite, 6% clinopyroxene, 3% opaques, 1% olivine, <1% pyrrhotite. Leucite: up to 0.15 mm; subhedral-euhedral; inclusions common.

80018

Seriate porphyritic, glomeroporphyritic; 15% phenocrysts of feldspar (7%), kaersutite (3%), opaque oxides (2%), clinopyroxene (1%) and apatite (1%). Feldspar: 0.8-10 mm; euhedral; olivine and apatite inclusions; convolute, colloform, oscillatory and continuous zoning; sometimes discontinuously zoned from homogeneous, sieved and embayed cores of An_{50} to oscillatory or continuously zoned rims to thin discontinuous alkali feldspar outer rims; largest phenocrysts generally anhedral, embayed, sieved, corroded and sometimes recrystallized. Kaersutite: 0.2-1.5 mm; subhedral-euhedral; commonly embayed; sometimes slightly oxidized; apatite and opaque oxide inclusions; cores sometimes sieved. Opaque oxides: 0.1-0.4 mm; anhedral-subhedral, embayed. Olivine: 0.2-1.1 mm; anhedral-subhedral, embayed; reaction rims sometimes; opaque oxide and apatite inclusions. Clinopyroxene: 0.1-0.8 mm; euhedral; pale green; sector twinning. Apatite: 0.1-0.5 mm; euhedral; glass inclusions in cores. Groundmass: holocrystalline, trachytic. 60% feldspar, 29% leucite, 5% clinopyroxene, 5% opaques, 2% olivine, 1% apatite. Leucite: <0.1 mm, subhedral.

TRACHYTES

83454

Moderately vesicular, vesicles 0.1-1.0 mm. Seriate porphyritic, glomeroporphyritic; 5% phenocrysts of feldspar (3%), clinopyroxene (1%), opaque oxides (1%), and rare olivine. Feldspar: 0.6-3 mm; untwinned; subhedral-euhedral, sometimes embayed; clinopyroxene and opaque inclusions; discontinuous and continuous zoning. Clinopyroxene: 0.1-0.6 mm; subhedral-euhedral, sometimes embayed; opaque and apatite inclusions; pale green; sometimes thin discontinuous rims. Opaque oxides: 0.1-0.3 mm; anhedral-euhedral; sometimes embayed. Olivine: one phenocryst 0.8 mm;

subhedral; apatite, opaque and glass inclusions. Groundmass: hyalo-ophitic; slightly devitrified, spherulitic; pilotaxitic; flow-banded phenocrysts; vesicle layering; 45% feldspar, 40% glass, 10% clinopyroxene, 5% opaques, 5% olivine.

83451

Rare microphenocrysts of olivine, opaque oxides and clinopyroxene. Olivine: ~1 mm, subhedral, embayed, apatite and opaque oxide inclusions. Opaque oxides: ~0.25 mm; anhedral, embayed; clots with clinopyroxene. Clinopyroxene: ~0.5 mm; euhedral; green; apatite inclusions. Groundmass: hypocrystalline, trachytic, weakly spherulitic. 60% alkali feldspar, 20% reddish-brown glass, 10% yellowish-green clinopyroxene, 5% opaque oxides, 5% olivine.

82405

Moderately vesicular, vesicles 0.05-0.5 mm. Weakly porphyritic and glomeroporphyritic; 3% phenocrysts of feldspar (2%), opaque oxides (1%) and clinopyroxene (1%). Feldspar: untwinned; 1.2-2 mm; anhedral-subhedral, embayed, corroded. Opaque oxides: 0.25-0.4 mm; anhedral-euhedral, embayed. Clinopyroxene: 0.25-3.0 mm; subhedral-euhedral; yellow to green. Groundmass: holocrystalline, trachytic, flow banded, devitrified, spherulitic; 90% alkali feldspar, 5% opaque oxides, 5% yellowish-green clinopyroxene.

INCLUSIONS

Microxenolith in AW82044

6 mm in diameter, round. Holocrystalline, porphyritic. 5% pyroxene phenocrysts: 0.3-0.5 mm; pale green to brown pleochroism; anhedral, corroded; sieved, poikilitic with opaque oxides; Groundmass: equigranular, mosaic-textured; 65% pale green to greenish brown clinopyroxene, 25% nepheline, 10% opaque oxides. Nepheline: moderately altered to calcite. Strongly altered to feldspar at edge of microxenolith.

Microxenolith in 83411

2 mm in diameter. Weakly porphyritic. Mostly alkali feldspar with lesser amount of opaque oxides, olivine, and apatite. Minerals generally have corroded edges.

Microxenolith in VUW25748

2 mm in diameter. Subangular. Hypidiomorphic granular. 74% feldspar, 10% pyroxene, 10% opaque oxides, 3% apatite, 3% nepheline (?).

82431

Seriate porphyritic. Glomeroporphyritic. 30% phenocrysts of feldspar (26%), opaque oxides (2%), apatite (1%), and clinopyroxene (1%). Feldspar: 0.2-10 mm; euhedral; rhombic; discontinuous edges intergrown with groundmass; opaque inclusions; inclusions of groundmass constituents zonally arranged in outer rims; continuous and weak oscillatory zoning; sometimes pericline or microcline twinning; larger phenocrysts fractured and strongly replaced by leucite in cores and along fractures; larger phenocrysts show albite twinning. Opaque oxides: 0.2-1.8 mm; anhedral-subhedral, embayed; corroded edges; completely oxidized to consertal intergrowths of maghemite and ilmenite. Apatite: 0.1-0.7 mm; subhedral; commonly broken; corroded contacts. Clinopyroxene: 0.2-0.7 mm; subhedral; completely altered to acmitic pyroxene and opaque oxides. Groundmass: hypocrystalline, equigranular, fine grained, mosaic-textured, weakly spherulitic. 53% alkali feldspar, 20% glass, 15% opaque oxides, 10% yellowish green pyroxene, 2% apatite. Glass patches 0.4-6 mm in diameter, brownish-yellow, inclusions of groundmass constituents along edges of patches.

82403

Hypidiomorphic granular; weakly layered; trachytoid; 80% anorthoclase, 6% clinopyroxene, 5% opaque oxides, 4% kaersutite, 2% apatite, 2% biotite, 1% olivine. Anorthoclase: 0.5-15 mm; anhedral; recrystallized lobate contacts; fractured; undulatory extinction; sometimes completely recrystallized; opaque oxide, clinopyroxene, biotite and apatite inclusions. Clinopyroxene: 0.3-2.5 mm; anhedral-euhedral; colorless to pale brown; sometimes embayed; lobate contacts; biotite, apatite and opaque oxide inclusions. Opaque oxides: magnetite and rare corroded pyrrhotite; 0.2-1 mm; anhedral, embayed, corroded contacts; apatite inclusions; many magnetite and pyrrhotite blebs <0.1 mm scattered throughout section. Kaersutite: intercumulus and alteration rims on clinopyroxene; dark red brown to yellowish brown pleochroism; anhedral. Apatite: 0.1-1.4 mm; euhedral; clots with clinopyroxene and opaques. Biotite: intercumulus and alteration rims on opaque oxides; dark brown to medium reddish brown pleochroism; serrate contacts. Olivine: 0.2-1 mm; anhedral; embayed; lobate contacts

sometimes; weakly sieved; apatite and opaque inclusions; sometimes opaque rims.

APPENDIX C

ANALYTICAL PROCEDURES

Electron Microprobe Analysis

Phenocryst and groundmass minerals in the samples from Mt. Erebus were analyzed in polished thin sections on an ARL-EMX electron microprobe at the University of New Mexico. The electron accelerating potential was 15 kV and the sample current was about 0.02 microamps. The sections were carbon-coated for analysis and the electron beam diameter was 1-2 microns. Natural mineral standards and empirical correction factors (Bence and Albee, 1968) were used.

Geochemistry

Sample Preparation

Most of the samples were broken into 1-3 cm chips with a rock hammer on a steel plate. Chips showing alteration and secondary mineralization were discarded. The sample size selected for analysis ranged from 0.5-1 kg for fine grained samples, 2 kg for coarse grained samples, and 4 kg for very coarse grained samples. The anorthoclase phonolite samples were crushed in plastic bags to avoid loss of feldspar due to preferential crushing. Several samples were too small to obtain a representative sample of by chipping. Therefore slabs were cut from these samples on water-cooled rock saws

to obtain a representative section for analysis.

Samples from near the coast and sawed samples were thoroughly washed before crushing. These samples were repeatedly soaked in distilled water, then dried at 110°C until no salts precipitated on them. For several samples this washing process required 3 days. The effects of washing on sample chemistry was tested on splits of sample 83447. One split was washed and dried three times while the other split was washed and dried several times more. No significant differences in the chemistry of the splits occurs, suggesting the washing technique did not alter the chemistry of the samples.

The coarse grained samples were crushed in a small jaw crusher with Al2O3 plates to c.0.5 cm size and split to obtain smaller representative samples. All samples were ground in a high-speed TEMA mill with a tungsten-carbide head. Approximately 100 g of sample at a time were ground for 45-60 secs., yielding a powder of c. 10 microns. The powders from large samples were split using the cone-and-quarter method on clean sheets of paper to obtain a sample size of 400-500 g.

X-ray Fluorescence Spectrometry

Major elements and most trace elements in the samples were analyzed on a Rigaku XRF spectrometer with a Rh tube. Major elements were analyzed using the technique of Norrish and Hutton (1969). Approximately 0.5 g of each sample was mixed with a Li tetraborate-Li carbonate-La oxide flux, fused in a Pt-Au crucible, and pressed into a disc. Calibration was made using a large suite of international rock standards. Determinations of analytical and machine error, thus the precision of the data, are given in Table C.1.

Trace elements were analyzed in pressed powder discs made with 5.5 g of sample for the basanites, 6.5 g of sample for the intermediate lavas, and 7 g of sample for the phonolites and trachytes. For most trace elements mass absorption corrections were made using the Rh compton peak. For Cr, V and Ba major element compositions were used to calculate mass absorption coefficients. Calibration curves were generated using international rock standards. The precision of the data is based on the machine error, given in Table C.2. Analytical error using this technique is within the range of the machine error because of the large sample size.

Instrumental Neutron Activation Analysis

Rare earth elements and some trace elements were analyzed by INAA made on c.0.1 g of sample placed in ultrapure quartz vials and irradiated for c.40 hours. Samples were counted for 3 hours after 7 days and 3 hours after 40 days. Calibration was made using several international geochemical standards. Aliquots of G-2 and BCR-1 were analyzed at the same time to provide a measurement of precision and accuracy (Table C.3).

Ferrous Iron Analysis

Fe^{2+} was analyzed in a few samples by wet chemistry using the back titration method of Reichen and Fahey (1962). Powdered sample aliquots of 0.5-1.0 g were dissloved in HF and mixed with standard potassium dichromate solution. The sample solution was titrated with ferrous ammonium sulfate solution, and then backtitrated with dichromate solution.

Table C.1. XRF major element analytical and machine error.

A. Analytical error

Example of analytical error: major element composition of three discs of sample 83447A

	1	2	3	Average	C.V.*
SiO2	55.68	55.82	55.77	55.76	0.099
TiO2	1.14	1.13	1.12	1.13	0.805
Al2O3	19.46	19.61	19.55	19.54	0.305
Fe2O3	5.47	5.40	5.38	5.42	0.699
MnO	0.19	0.19	0.19	0.19	0.000
MgO	1.18	1.23	1.27	1.23	3.240
CaO	3.21	3.21	3.21	3.21	0.059
Na2O	7.54	7.77	7.63	7.65	1.248
K2O	4.40	4.43	4.42	4.42	0.347
P2O5	0.45	0.46	0.46	0.46	0.842
Total	98.79	99.31	99.81		

	Range in C.V. for samples analyzed in duplicate and triplicate	Average C.V.
SiO2	0.09-0.39	0.26
TiO2	0.05-0.81	0.41
Al2O3	0.03-0.46	0.24
Fe2O3	0.08-0.70	0.41
MnO	0.00-2.80	1.32
MgO	0.02-3.86	1.88
CaO	0.06-0.54	0.20
Na2O	0.74-2.93	1.40
K2O	0.14-0.35	0.27
P2O5	0.41-0.84	0.61

B. Machine Error

	Range in C.V. from multiple analyses of same discs	Average C.V.
SiO2	0.08-0.12	0.10
TiO2	0.32-0.43	0.39
Al2O3	0.06-0.15	0.10
Fe2O3	0.24-0.35	0.27
MnO	0.87-1.58	1.25
MgO	0.95-3.16	2.14
CaO	0.08-0.32	0.21
Na2O	0.47-0.84	0.68
K2O	0.07-0.24	0.14
P2O5	0.25-0.56	0.42

* C.V.: coefficient of variation
[(standard deviation (1 sigma)/mean)100]

Table C.2. XRF Trace Element Machine Error

	Range in C.V. from multiple analyses of same discs	Average C.V.*
V	1.67-32.01	7.59
Cr	1.34-26.28	9.53
Ni	6.40-16.70	11.42
Cu	2.67-15.06	6.10
Zn	0.37-1.19	0.62
Ga	1.13-4.43	2.89
Rb	0.36-2.21	1.01
Sr	0.06-0.63	0.21
Y	0.10-1.46	0.72
Zr	0.05-0.29	0.17
Nb	0.01-0.39	0.13
Ba	0.37-1.43	0.74
Pb	4.27-27.74	18.55
Th	2.98-16.23	8.98

* C.V.: coefficient of variation
[(standard deviation (1 sigma)/mean)100]

Table C.3: Average INAA data from 10 analyses of G-2 and BCR-1.

A. G-2

	Average	S.D.[1]	C.V.*	Consensus[2]
FeO*%	2.38	0.03	1.26	2.41±0.08
Sc	3.30	0.048	1.45	3.5±0.4
Cr	8.02	0.56	6.98	9±2
Co	4.33	0.11	2.54	4.6±0.4
Rb	166	3	1.8	170±3
Sb	0.04	0.02	50	0.078±0.032
Cs	1.31	0.04	3.05	1.33±0.14
Ba	1848	30	1.6	1880±20
La	85.3	0.99	1.16	86±5
Ce	163.2	1.8	1.10	159±11
Nd	55.0	1.6	2.9	53±8
Sm	7.35	0.15	2.04	7.2±0.6
Eu	1.33	0.03	2.26	1.41±0.12
Tb	0.47	0.02	4.26	0.48±0.07
Yb	0.70	0.05	7.14	0.78±0.14
Lu	0.108	0.007	6.48	0.113±0.024
Hf	8.33	0.21	2.52	7.9±0.7
Ta	0.776	0.02	2.60	0.88±0.12
Th	23.62	0.26	1.10	24.6±1.5
U	2.07	0.29	14.01	2.04±0.17

Table C.3 continued.

B. BCR-1

	Average	S.D.[1]	C.V.*	Consensus[2]
FeO*%	12.14	0.086	0.71	12.11±0.16
Sc	31.95	0.094	0.29	32.8±1.7
Cr	10.6	0.58	5.47	16±4
Co	37.2	0.28	0.75	36.3±1.6
Rb	49	1.1	2.2	47.1±0.6
Sb	0.57	0.069	12.1	0.62±0.10
Cs	0.98	0.036	3.67	0.97±0.13
Ba	674	16	2.37	678±16
La	24.43	0.21	0.86	25.0±0.08
Ce	52.7	0.7	1.33	53.7±0.8
Nd	28.8	1.0	3.47	28.7±0.6
Sm	6.68	0.07	1.05	6.58±0.17
Eu	1.90	0.02	1.05	1.96±0.05
Tb	1.07	0.03	2.8	1.05±0.09
Yb	3.38	0.05	1.48	3.39±0.08
Lu	0.516	0.006	1.16	0.512±0.025
Hf	5.12	0.05	0.98	4.9±0.3
Ta	0.77	0.02	2.6	0.79±0.09
Th	5.69	0.10	1.76	6.04±0.60
U	1.7	0.1	5.88	1.71±0.16

[1] Standard deviation (1 sigma).
[2] Gladney *et al.* (1983).
* C.V.: coefficient of variation
[(standard deviation (1 sigma)/mean)100]

APPENDIX D

MINERAL CHEMISTRY

Part 1. Electron microprobe analyses of minerals in Mt. Erebus lavas

Table D.1. Olivine

Table D.2. Pyroxene

Table D.3. Opaque oxides

Table D.4. Feldspar

Table D.1. Olivines

	83435-1	83435-2	83435-3	83435-4	83435-5	83435-6	83435-7	83435-8	83435-9	83435-10
SIO2	40.23	39.13	40.28	39.83	38.95	39.01	39.09	39.05	38.91	39.15
FEOT*	13.72	17.63	12.00	12.48	18.97	20.03	19.03	18.13	18.75	17.00
MNO	0.16	0.33	0.15	0.17	0.34	0.42	0.27	0.23	0.30	0.22
MGO	46.34	42.72	47.04	46.68	41.53	41.43	42.20	42.37	41.82	42.80
CAO	0.18	0.33	0.12	0.14	0.28	0.32	0.30	0.30	0.35	0.29
TOTAL	100.63	100.12	99.57	99.29	100.06	101.21	100.89	100.07	100.13	99.46
FO+	85.8	81.2	87.5	87.0	79.6	78.7	79.8	80.6	79.9	81.8
FA x	14.2	18.8	12.5	13.0	20.4	21.3	20.2	19.4	20.1	18.2

*** ALL ZERO VALUES PRINTED AS BLANKS. ***

SAMPLE DESCRIPTION :

83435-1	INTERMEDIATE
83435-2	EXTREME EDGE
83435-3	CORE
83435-4	INTERMEDIATE
83435-5	CORE
83435-6	RIM
83435-7	CORE
83435-8	EDGE
83435-9	GROUNDMASS
83435-10	CORE

	83435-11	79300-12	79300-13	79300-14	79300-15	79300-16	79300-17	79300-18	79300-P1	79300-P2
SIO2	38.59	37.29	37.71	38.20	38.27	37.88	37.90	37.88	37.71	38.09
FEOT	19.60	25.76	24.37	22.13	22.45	23.15	22.90	23.64	23.84	23.80
MNO	0.29	0.58	0.62	0.40	0.47	0.50	0.47	0.54	0.46	0.46
MGO	40.66	35.69	36.52	38.40	38.39	38.56	38.17	37.51	37.89	38.70
CAO	0.31	0.37	0.50	0.37	0.45	0.35	0.36	0.48	0.49	0.40
TOTAL	99.44	99.70	99.72	99.50	100.04	100.45	99.80	100.05	100.58	101.56
FO	78.7	71.2	72.8	75.6	75.3	74.8	74.8	73.9	73.9	74.3
FA	21.3	28.8	27.2	24.4	24.7	25.2	25.2	26.1	26.1	25.7

*** ALL ZERO VALUES PRINTED AS BLANKS. ***

SAMPLE DESCRIPTION :

83435-11	RIM
79300-12	CORE
79300-13	EDGE
79300-14	INTERMEDIATE
79300-15	INTERMEDIATE
79300-16	EDGE
79300-17	CORE
79300-18	GROUNDMASS
79300-P1	GROUNDMASS
79300-P2	GROUNDMASS

* Total Fe analyzed as FeO
\+ Mg cations on basis of 4 (O)
x Fe cations on basis of 4 (O)

Table D.1. cont.

	79300-P3	AW82038-1	AW82038-3	AW82038-4	AW82038-5	AW82038-6	AW82038-7	AW82038-8	AW82038-9	AW82038-10
SIO2	37.12	36.72	36.84	36.66	36.94	36.74	36.60	36.81	37.24	36.74
FEOT	23.39	29.81	30.15	29.67	30.17	30.28	31.22	29.90	30.62	28.62
MNO	0.52	0.70	0.69	0.66	0.85	0.77	0.76	0.76	0.80	0.76
MGO	37.80	32.19	31.91	32.51	31.76	31.83	31.94	31.91	31.62	33.24
CAO	0.47	0.46	0.47	0.40	0.41	0.44	0.45	0.43	0.43	0.46
TOTAL	99.43	99.87	100.07	99.90	100.12	100.06	100.97	99.80	100.70	99.81
FO	74.2	65.8	65.4	66.1	65.2	65.2	64.6	65.5	64.8	67.4
FA	25.8	34.2	34.6	33.9	34.8	34.8	35.4	34.5	35.2	32.6

*** ALL ZERO VALUES PRINTED AS BLANKS. ***

SAMPLE DESCRIPTION :

79300-P3	:	GROUNDMASS
AW82038-1	:	EDGE
AW82038-3	:	INTERMEDIATE
AW82038-4	:	EDGE
AW82038-5	:	EXTREME EDGE
AW82038-6	:	CORE
AW82038-7	:	INTERMEDIATE
AW82038-8	:	INTERMEDIATE
AW82038-9	:	INCLUSION IN FELDSPAR
AW82038-10	:	GROUNDMASS

	83415-1	83415-2	83415-3	83415-4	83415-5	83415-6	83415-7	83415-A	83417-1	83417-2
SIO2	36.68	37.01	37.26	36.92	36.98	37.10	36.95	36.99	36.27	36.75
FEOT	28.93	29.54	29.14	28.86	29.42	28.87	29.32	29.15	30.06	29.76
MNO	0.92	0.83	0.77	0.81	0.84	0.98	0.78	0.85	1.05	1.10
MGO	32.10	32.29	33.45	33.14	32.83	33.14	33.28	32.89	30.99	32.06
CAO	0.47	0.33	0.34	0.32	0.38	0.36	0.34	0.36	0.33	0.36
TOTAL	99.11	100.01	100.97	100.04	100.44	100.46	100.67	100.24	98.71	100.04
FO	66.4	66.1	67.2	67.2	66.5	67.2	66.9	66.8	64.8	65.8
FA	33.6	33.9	32.8	32.8	33.5	32.8	33.1	33.2	35.2	34.2

*** ALL ZERO VALUES PRINTED AS BLANKS. ***

SAMPLE DESCRIPTION :

83415-1	:	EDGE
83415-2	:	CORE
83415-3	:	EDGE
83415-4	:	CORE
83415-5	:	INTERMEDIATE
83415-6	:	INTERMEDIATE
83415-7	:	INTERMEDIATE
83415-A	:	AVERAGE
83417-1	:	CORE
83417-2	:	EDGE

Table D.1. cont.

	83417-3	83417-4	83417-5	83417-7	83417-9	83417-10	25748-K46@	25748-K47	25748-K49	25748-50
SIO2	36.41	36.77	36.60	36.48	36.38	36.64	35.75	35.68	35.16	35.21
FEOT	30.59	30.58	29.45	30.39	30.18	30.87	34.99	34.12	35.30	35.28
MNO	0.94	1.02	1.15	1.09	1.14	1.19	1.21	1.22	1.09	1.17
MGO	31.77	31.08	31.04	31.55	30.97	30.87	29.18	30.15	28.45	28.64
CAO	0.35	0.33	0.30	0.37	0.37	0.39	0.40	0.41	0.41	0.38
TOTAL	100.06	99.77	98.54	99.88	99.05	99.95	101.53	101.58	100.41	100.68
FO	64.9	64.4	65.3	64.9	64.7	64.1	58.9	60.3	58.2	58.3
FA	35.1	35.6	34.7	35.1	35.3	35.9	41.1	39.7	41.8	41.7

*** ALL ZERO VALUES PRINTED AS BLANKS. ***

SAMPLE DESCRIPTION :

83417-3	:	INTERMEDIATE
83417-4	:	INTERMEDIATE
83417-5	:	INTERMEDIATE
83417-7	:	INTERMEDIATE
83417-9	:	INTERMEDIATE
83417-10	:	INTERMEDIATE
25748-K46	:	INTERMEDIATE
25748-K47	:	EDGE
25748-K49	:	CORE
25748-50	:	EDGE

	25748-1	25748-3	25748-4	25748-5	25748-6	25748-7	25748-8	25748-9	25748-10	25748-11
SIO2	36.07	36.35	36.44	36.02	36.18	36.41	36.16	36.21	35.95	36.07
FEOT	34.21	34.19	35.32	34.26	34.55	33.99	34.67	33.48	34.18	34.10
MNO										
MGO	27.69	27.84	28.97	27.59	28.07	28.42	28.43	28.10	29.18	28.91
CAO	0.38	0.38	0.43	0.43	0.42	0.43	0.37	0.44	0.46	0.49
TOTAL	98.35	98.76	101.16	98.30	99.22	99.25	99.63	98.23	99.76	99.57
FO	59.1	59.2	59.4	58.9	59.1	59.8	59.4	59.9	60.3	60.2
FA	40.9	40.8	40.6	41.1	40.9	40.2	40.6	40.1	39.7	39.8

*** ALL ZERO VALUES PRINTED AS BLANKS. ***

SAMPLE DESCRIPTION :

25748-1	:	CORE
25748-3	:	RIM
25748-4	:	CORE
25748-5	:	RIM
25748-6	:	CORE
25748-7	:	RIM
25748-8	:	CORE
25748-9	:	RIM
25748-10	:	CORE
25748-11	:	RIM

@K: Kyle (unpubl.)

Table D.1. cont.

	25748-12	25748-13	25748-14	25748-16	25748-17	25748-18	25748-19	25748-20	25748-21	25748-22
SIO2	36.16	36.36	36.14	36.23	36.12	36.31	36.63	36.02	36.57	36.28
FEOT	34.06	33.66	34.25	35.80	36.16	34.52	34.24	34.44	35.45	34.68
MNO										
MGO	28.48	29.26	27.24	28.15	28.18	28.45	28.18	28.17	28.98	28.13
CAO	0.48	0.48	0.40	0.37	0.37	0.40	0.34	0.32	0.40	0.38
TOTAL	99.18	99.76	98.04	100.55	100.83	99.68	99.38	98.96	101.40	99.48
FO	59.8	60.8	58.6	58.4	58.1	59.5	59.5	59.3	59.3	59.1
FA	40.2	39.2	41.4	41.6	41.9	40.5	40.5	40.7	40.7	40.9

*** ALL ZERO VALUES PRINTED AS BLANKS. ***

SAMPLE DESCRIPTION :

25748-12	:	RIM
25748-13	:	CORE
25748-14	:	CORE
25748-16	:	RIM
25748-17	:	CORE
25748-18	:	RIM
25748-19	:	CORE
25748-20	:	RIM
25748-21	:	RIM
25748-22	:	CORE

	25748-23	25748-24	25748-25	25748-26	25748-27	25748-28	25748-29	25748-30	83448-1	83448-3
SIO2	37.81	37.66	37.48	37.77	35.84	36.44	36.23	36.13	35.89	36.10
FEOT	26.37	25.77	25.48	24.69	35.34	34.44	35.16	35.41	35.20	35.78
MNO									1.91	1.72
MGO	35.66	35.64	36.53	36.87	28.20	28.70	28.25	28.36	27.01	27.49
CAO	0.31	0.26	0.22	0.29	0.40	0.44	0.46	0.43	0.37	0.41
TOTAL	100.14	99.32	99.70	99.60	99.78	100.01	100.10	100.33	100.38	101.49
FO	70.7	71.1	71.9	72.7	58.7	59.8	58.9	58.8	57.8	57.8
FA	29.3	28.9	28.1	27.3	41.3	40.2	41.1	41.2	42.2	42.2

*** ALL ZERO VALUES PRINTED AS BLANKS. ***

SAMPLE DESCRIPTION :

25748-23	:	XENOCRYST CORE
25748-24	:	XENOCRYST RIM
25748-25	:	XENOCRYST RIM
25748-26	:	XENOCRYST CORE
25748-27	:	CORE
25748-28	:	RIM
25748-29	:	CORE
25748-30	:	RIM
83448-1	:	INTERMEDIATE
83448-3	:	RIM

Table D.1. cont.

	83448-4	83448-6	83448-7	83448-9	83400-1	83400-2	83400-3	83400-5	83400-6	83400-9
SIO2	36.29	36.02	36.10	36.40	34.53	35.27	34.97	34.86	34.67	34.87
FEOT	35.96	35.39	35.66	35.36	38.99	40.32	39.83	39.55	39.16	38.76
MNO	1.88	1.83	1.88	1.67	2.31	2.34	2.44	2.48	2.34	2.35
MGO	27.36	27.46	27.26	27.30	22.68	23.55	23.22	22.84	22.93	23.01
CAO	0.41	0.47	0.40	0.35	0.47	0.46	0.48	0.52	0.56	0.44
TOTAL	101.89	101.17	101.29	101.08	98.98	101.46	100.94	100.25	99.66	99.42
FO	57.6	58.0	57.7	57.9	50.9	51.0	51.0	50.7	51.1	51.4
FA	42.4	42.0	42.3	42.1	49.1	49.0	49.0	49.3	48.9	48.6

*** ALL ZERO VALUES PRINTED AS BLANKS. ***

SAMPLE DESCRIPTION :

83448-4	:	CORE
83448-6	:	INTERMEDIATE
83448-7	:	INTERMEDIATE
83448-9	:	INTERMEDIATE
83400-1	:	INTERMEDIATE
83400-2	:	RIM
83400-3	:	CORE
83400-5	:	CORE
83400-6	:	INTERMEDIATE
83400-9	:	INTERMEDIATE

	80020-21	80020-22	80020-23	80020-25	80020-26	80020-27	80020-28	AW82023-13	AW82023-14	AW82023-15
SIO2	34.97	35.39	35.02	34.22	34.77	34.71	34.45	34.18	33.99	34.11
FEOT	38.03	38.47	37.22	37.92	37.61	37.38	38.08	41.62	43.26	41.25
MNO	2.56	2.32	2.33	2.44	2.43	2.48	2.56	1.62	1.94	1.60
MGO	24.10	24.17	23.85	23.70	24.09	23.64	23.66	21.86	19.76	22.61
CAO	0.47	0.56	0.40	0.46	0.45	0.44	0.45	0.34	0.36	0.32
TOTAL	100.12	100.91	98.81	98.73	99.36	98.65	99.19	99.62	99.31	99.90
FO	53.0	52.8	53.3	52.7	53.3	53.0	52.5	48.4	44.9	49.4
FA	47.0	47.2	46.7	47.3	46.7	47.0	47.5	51.6	55.1	50.6

*** ALL ZERO VALUES PRINTED AS BLANKS. ***

SAMPLE DESCRIPTION :

80020-21	:	INTERMEDIATE
80020-22	:	CORE
80020-23	:	EDGE
80020-25	:	INTERMEDIATE
80020-26	:	INTERMEDIATE
80020-27	:	INCLUSION IN FELDSPAR
80020-28	:	INCLUSION IN FELDSPAR
AW82023-13	:	CORE
AW82023-14	:	GROUNDMASS
AW82023-15	:	GROUNDMASS

Table D.1. cont.

	AW82023-16	AW82023-17	AW82023-20
SIO2	34.10	34.23	33.75
FEOT	42.73	42.81	44.22
MNO	2.02	1.83	2.44
MGO	19.49	20.22	18.67
CAO	0.37	0.38	0.39
TOTAL	98.71	99.46	99.47
FO	44.8	45.7	42.9
FA	55.2	54.3	57.1

*** ALL ZERO VALUES PRINTED AS BLANKS. ***

SAMPLE DESCRIPTION :

AW82023-16 : CORE
AW82023-17 : EDGE
AW82023-20 : GROUNDMASS

Table D.2. Pyroxene

	83435-1	83435-3	83435-4	83435-5	83435-6	83435-9	83435-10	83435-11	83435-12	83435-14
SIO2	45.05	46.50	48.87	45.20	43.35	48.74	45.30	47.68	46.79	48.86
TIO2	4.45	2.84	2.26	3.47	5.15	2.61	3.87	2.86	3.19	2.79
AL2O3	9.53	7.79	6.14	9.32	11.16	6.07	10.05	7.80	8.48	5.98
FEOT*	7.64	9.91	7.07	7.69	7.12	6.73	7.10	6.58	6.52	6.61
MNO	0.15	0.25	0.18			0.14		0.11		
MGO	12.19	11.09	14.14	11.99	11.77	14.34	12.29	13.46	13.25	14.13
CAO	21.58	20.25	21.66	20.83	22.17	21.82	20.72	20.71	22.12	21.99
NA2O	0.50	0.83	0.48	0.67	0.54	0.36	0.52	0.53	0.44	0.51
K2O		0.18		0.02						
TOTAL	101.09	99.64	100.81	99.19	101.26	100.81	99.85	99.72	100.79	100.87
FE2O3 +	1.80	1.89	2.18	1.89	2.82	1.59	0.35	0.10	1.89	1.56
FEO +	6.02	8.21	5.10	5.99	4.58	5.30	6.78	6.49	4.82	5.21
NTOT×	101.27	99.83	101.02	99.38	101.54	100.97	99.89	99.74	100.98	101.03
SI[1]	1.66	1.75	1.79	1.69	1.60	1.79	1.69	1.77	1.72	1.79
TI[1]	0.12	0.08	0.06	0.10	0.14	0.07	0.11	0.08	0.09	0.08
AL[1]	0.41	0.35	0.27	0.41	0.48	0.26	0.44	0.34	0.37	0.26
FE3[1]	0.05	0.05	0.06	0.05	0.08	0.04	0.01	0.00	0.05	0.04
FE2[1]	0.19	0.26	0.16	0.19	0.14	0.16	0.21	0.20	0.15	0.16
MN[1]	0.01	0.01	0.01			0.00		0.00		
MG[1]	0.67	0.62	0.77	0.67	0.65	0.78	0.68	0.74	0.73	0.77
CA[1]	0.85	0.82	0.85	0.84	0.87	0.86	0.83	0.82	0.87	0.86
NA[1]	0.04	0.06	0.03	0.05	0.04	0.03	0.04	0.04	0.03	0.04
MGI[2]	0.78	0.70	0.83	0.78	0.82	0.82	0.76	0.78	0.83	0.83
WO[3]	49.77	47.89	47.64	49.38	52.64	47.41	48.06	46.45	49.91	48.10
EN[3]	39.12	36.49	43.28	39.55	38.88	43.36	39.66	42.00	41.60	43.01
FS[3]	11.12	15.61	9.08	11.08	8.49	9.23	12.28	11.55	8.49	8.89
RWO[4]					43.70					
REN[4]					46.10					
RFS[4]					10.10					

*Total Fe analyzed as FeO
+Recalculated Fe_2O_3 and FeO
×New total
[1]No. of cations on the basis of 6 (O)
[2]Mg index ($(Mg/(Mg+Fe^{2+}+Mn))$
[3]Pyroxene endmembers
[4]Recalculated pyroxene endmembers

SAMPLE DESCRIPTION :

83435-1	RIM
83435-3	CORE
83435-4	RIM
83435-5	CORE
83435-6	CORE
83435-9	RIM
83435-10	INTERMEDIATE
83435-11	CORE
83435-12	RIM
83435-14	INTERMEDIATE

Table D.2. cont.

	83435-15	83435-16	83435-17	83415-4	83415-5	83415-6	83415-7	83417-1	83417-5	83417-6
SIO2	44.89	46.40	44.91	47.75	47.70	47.32	48.35	50.34	48.91	50.73
TIO2	4.36	4.08	4.05	3.83	3.39	3.86	3.16	2.45	2.48	2.24
AL2O3	8.72	7.26	8.97	6.30	5.85	6.11	5.60	4.90	4.74	3.81
FEOT	8.44	8.14	7.36	8.09	7.67	7.84	7.51	8.84	9.16	8.73
MNO	0.16	0.16		0.24	0.21	0.27	0.23	0.36	0.26	0.37
MGO	12.62	12.86	12.49	11.88	12.41	12.10	12.39	12.44	12.62	13.05
CAO	21.51	22.41	22.27	21.30	21.65	21.23	21.80	21.16	21.95	21.21
NA2O	0.49	0.39	0.54	0.80	0.75	0.77	0.68	1.07	0.96	0.83
K2O		0.02	0.02	0.02						0.02
TOTAL	101.19	101.72	100.61	100.22	99.64	99.50	99.73	101.57	101.08	100.99
FE2O3	3.70	2.90	3.70		1.26	0.44	0.28	1.17	4.20	0.81
FEO	5.11	5.53	4.03	8.09	6.54	7.44	7.25	7.79	5.38	8.00
NTOT	101.56	102.01	100.98	100.21	99.76	99.54	99.75	101.68	101.50	101.07
SI	1.66	1.70	1.66	1.78	1.78	1.78	1.81	1.85	1.80	1.87
TI	0.12	0.11	0.11	0.11	0.09	0.11	0.09	0.07	0.07	0.06
AL	0.38	0.31	0.39	0.28	0.26	0.27	0.25	0.21	0.21	0.17
FE3	0.10	0.08	0.10		0.04	0.01	0.01	0.03	0.12	0.02
FE2	0.16	0.17	0.12	0.25	0.21	0.23	0.23	0.24	0.17	0.25
MN	0.01	0.01		0.01	0.01	0.01	0.01	0.01	0.01	0.01
MG	0.69	0.70	0.69	0.66	0.69	0.68	0.69	0.68	0.69	0.72
CA	0.85	0.88	0.88	0.85	0.87	0.85	0.87	0.83	0.87	0.84
NA	0.04	0.03	0.04	0.06	0.05	0.06	0.05	0.08	0.07	0.06
MGI	0.81	0.80	0.85	0.72	0.77	0.74	0.75	0.73	0.80	0.73
WO	49.81	50.08	52.04	48.20	49.00	48.15	48.57	47.20	49.98	46.20
EN	40.66	39.99	40.61	37.50	39.08	38.19	38.41	38.61	39.98	39.55
FS	9.53	9.93	7.35	14.30	11.92	13.66	13.02	14.19	10.03	14.24
RWO	42.20				45.50					
REN	46.80				42.60					
RFS	11.10				11.90					

*** ALL ZERO VALUES PRINTED AS BLANKS. ***

SAMPLE DESCRIPTION :

83435-15	:	CORE
83435-16	:	GROUNDMASS
83435-17	:	GROUNDMASS
83415-4	:	RIM
83415-5	:	CORE
83415-6	:	RIM
83415-7	:	CORE
83417-1	:	INCLUSION IN FELDSPAR
83417-5	:	CORE
83417-6	:	INTERMEDIATE

Table D.2. cont.

	83417-7	83417-8	25748K-1#	25748K-2	25748K-4	25748K-5	25748K-6	25748K-7	25748K-8	25748-1
SIO2	49.99	50.16	48.90	47.60	48.80	48.60	47.60	49.70	49.40	50.60
TIO2	2.54	2.79	1.60	2.19	2.30	2.06	2.64	1.84	1.83	1.69
AL2O3	4.80	4.65	3.49	4.88	4.62	4.52	5.43	4.10	4.17	3.20
FEOT	9.06	8.79	8.81	9.03	9.28	8.85	9.30	8.20	9.12	8.48
MNO	0.39	0.35	0.36	0.40	0.36	0.38	0.38	0.40	0.41	0.42
MGO	12.61	12.79	12.90	12.10	12.60	12.40	11.80	12.90	12.60	12.60
CAO	20.79	20.64	21.30	21.40	21.10	21.00	20.90	20.70	20.90	22.00
NA2O	1.01	0.90	0.96	0.93	1.09	1.09	1.06	1.02	1.01	0.85
K2O	0.02									
TOTAL	101.21	101.08	98.32	98.53	100.15	98.90	99.11	98.86	99.44	99.84
FE2O3	1.34	0.08	4.44	4.27	4.19	3.70	3.47	1.96	3.04	1.63
FEO	7.85	8.72	4.81	5.18	5.51	5.52	6.18	6.43	6.38	7.01
NTOT	101.34	101.08	98.77	98.96	100.57	99.27	99.46	99.06	99.74	100.00
SI	1.84	1.85	1.85	1.80	1.81	1.83	1.79	1.87	1.85	1.89
TI	0.07	0.08	0.05	0.06	0.06	0.06	0.08	0.05	0.05	0.05
AL	0.21	0.20	0.16	0.22	0.20	0.20	0.24	0.18	0.18	0.14
FE3	0.04	0.00	0.13	0.12	0.12	0.11	0.10	0.06	0.09	0.05
FE2	0.24	0.27	0.15	0.16	0.17	0.17	0.20	0.20	0.20	0.22
MN	0.01	0.01	0.01	0.01	0.01	0.01	0.01	0.01	0.01	0.01
MG	0.69	0.70	0.73	0.68	0.70	0.70	0.66	0.72	0.70	0.70
CA	0.82	0.82	0.86	0.87	0.84	0.85	0.84	0.83	0.84	0.88
NA	0.07	0.06	0.07	0.07	0.08	0.08	0.08	0.07	0.07	0.09
MGI	0.73	0.72	0.82	0.79	0.79	0.79	0.76	0.77	0.77	0.75
WO	46.43	45.34	49.20	50.24	48.82	48.99	49.24	47.06	47.79	48.53
EN	39.19	39.10	41.46	39.52	40.57	40.25	38.68	40.80	40.09	38.67
FS	14.38	15.56	9.33	10.24	10.61	10.75	12.08	12.14	12.13	12.80
RWO	43.90									
REN	42.60									
RFS	13.50									

*** ALL ZERO VALUES PRINTED AS BLANKS. ***
#K: Kyle (unpubl.)

SAMPLE DESCRIPTION :

83417-7	:	CORE
83417-8	:	CORE
25748K-1	:	CORE
25748K-2	:	INTERMEDIATE
25748K-4	:	INTERMEDIATE
25748K-5	:	RIM
25748K-6	:	CORE
25748K-7	:	INTERMEDIATE
25748K-8	:	RIM
25748-1	:	CORE

Table D.2. cont.

	25748-4	25748-5	25748-6	25748-7	25748-9	25748-10	25748-11	25748-12	25748-13	25748-15
SIO2	49.90	48.28	49.80	49.30	49.40	50.10	49.50	50.60	49.90	49.30
TIO2	1.95	2.56	1.99	2.10	2.29	1.86	2.30	1.76	1.90	1.99
AL2O3	3.78	4.92	3.99	4.62	4.44	3.81	4.24	3.49	4.18	3.63
FEOT	9.00	8.92	8.82	9.08	8.55	8.80	8.90	8.60	9.09	8.35
MNO	0.48	0.32	0.45	0.53	0.49	0.48	0.43	0.47	0.49	0.51
MGO	12.20	12.00	12.10	12.00	12.10	12.10	12.20	12.80	12.20	12.40
CAO	21.41	22.40	22.00	21.30	21.80	21.60	21.30	20.40	20.40	23.10
NA2O	0.96	0.82	0.92	1.02	0.99	0.95	0.97	0.88	1.01	0.70
K2O										
TOTAL	99.68	100.22	100.07	99.95	100.06	99.70	99.84	99.00	99.17	99.98
FE2O3	1.88	3.45	2.18	2.43	2.23	1.50	1.79	0.02	0.86	3.41
FEO	7.31	5.82	6.86	6.89	6.54	7.45	7.29	8.58	8.31	5.28
NTOT	99.87	100.57	100.29	100.19	100.28	99.85	100.02	99.00	99.26	100.32
SI	1.87	1.80	1.86	1.84	1.84	1.88	1.85	1.90	1.88	1.84
TI	0.06	0.07	0.06	0.06	0.06	0.05	0.07	0.05	0.05	0.06
AL	0.17	0.22	0.18	0.20	0.20	0.17	0.19	0.15	0.19	0.16
FE3	0.05	0.10	0.06	0.07	0.06	0.04	0.05	0.00	0.02	0.10
FE2	0.23	0.18	0.21	0.21	0.20	0.23	0.23	0.27	0.26	0.16
MN	0.02	0.01	0.01	0.02	0.02	0.02	0.01	0.02	0.02	0.02
MG	0.68	0.67	0.67	0.67	0.67	0.68	0.68	0.72	0.69	0.69
CA	0.86	0.90	0.88	0.85	0.87	0.87	0.85	0.82	0.82	0.92
NA	0.07	0.06	0.07	0.07	0.07	0.07	0.07	0.06	0.07	0.05
MGI	0.74	0.78	0.75	0.74	0.75	0.73	0.74	0.72	0.71	0.79
WO	48.15	51.04	49.39	48.63	49.40	48.40	48.08	45.06	46.10	51.47
EN	38.17	38.04	37.79	38.12	38.15	37.72	38.32	39.34	38.36	38.45
FS	13.68	10.92	12.82	13.24	12.45	13.87	13.61	15.61	15.54	10.08
RWO					46.60					
REN					40.60					
RFS					12.80					

*** ALL ZERO VALUES PRINTED AS BLANKS. ***

SAMPLE DESCRIPTION :

25748-4	:	INTERMEDIATE
25748-5	:	RIM
25748-6	:	INTERMEDIATE
25748-7	:	CORE
25748-9	:	CORE
25748-10	:	RIM
25748-11	:	CORE
25748-12	:	RIM
25748-13	:	CORE
25748-15	:	RIM

Table D.2. cont.

	25748-16	83448-21	83448-22	83448-23	82431-11	82431-12	82431-14	82431-16	82431-17	82431-18
SIO2	49.50	50.53	50.00	49.95	49.73	51.69	51.15	47.95	50.08	50.05
TIO2	2.17	1.52	1.84	1.91	1.68	1.27	1.33	1.96	1.47	1.64
AL2O3	4.65	3.22	3.69	4.14	3.89	3.22	3.14	5.14	4.19	4.68
FEOT	8.95	9.05	9.28	8.99	7.23	6.25	6.31	7.59	6.38	7.08
MNO	0.43	0.51	0.54	0.72	0.61	0.72	0.69	0.63	0.69	0.73
MGO	12.00	12.67	12.44	12.49	13.40	14.27	14.24	12.84	13.84	13.49
CAO	20.80	20.51	20.89	20.62	20.10	19.81	20.44	20.45	20.30	20.38
NA2O	1.04	0.83	0.99	1.01	1.83	1.72	1.64	1.50	1.53	1.53
K2O							0.03	0.03	0.06	0.03
TOTAL	99.54	98.84	99.67	99.83	98.48	98.96	98.97	98.09	98.54	99.61
FE2O3	1.23	0.54	2.13	1.82	5.55	3.13	4.28	5.77	4.10	4.19
FEO	7.84	8.56	7.37	7.35	2.24	3.43	2.46	2.40	2.69	3.31
WTOT	99.66	98.89	99.88	100.01	99.03	99.26	99.40	98.67	98.95	100.03
SI	1.86	1.91	1.87	1.87	1.86	1.91	1.89	1.80	1.86	1.85
TI	0.06	0.04	0.05	0.05	0.05	0.04	0.04	0.06	0.04	0.05
AL	0.21	0.14	0.16	0.18	0.17	0.14	0.14	0.23	0.18	0.20
FE3	0.04	0.02	0.06	0.05	0.16	0.09	0.12	0.16	0.12	0.12
FE2	0.25	0.27	0.23	0.23	0.07	0.11	0.08	0.08	0.08	0.10
MN	0.01	0.02	0.02	0.02	0.02	0.02	0.02	0.02	0.02	0.02
MG	0.67	0.71	0.70	0.70	0.74	0.79	0.79	0.72	0.77	0.74
CA	0.84	0.83	0.84	0.83	0.80	0.78	0.81	0.82	0.81	0.81
NA	0.08	0.06	0.07	0.07	0.13	0.12	0.12	0.11	0.11	0.11
MGI	0.72	0.71	0.74	0.73	0.89	0.86	0.89	0.98	0.88	0.86
WO	47.32	45.35	47.07	46.54	49.06	46.16	47.84	50.27	48.10	48.17
EN	37.98	38.98	39.01	39.22	45.51	46.27	46.38	43.91	45.63	44.36
FS	14.70	15.67	13.92	14.24	5.44	7.56	5.78	5.82	6.26	7.47
RWO			44.80							44.70
REN			41.30							47.30
RFS			14.00							8.00

*** ALL ZERO VALUES PRINTED AS BLANKS. ***

SAMPLE DESCRIPTION :

25748-16	:	CORE
83448-21	:	CORE
83448-22	:	INTERMEDIATE
83448-23	:	CORE
82431-11	:	GROUNDMASS
82431-12	:	GROUNDMASS
82431-14	:	GROUNDMASS
82431-16	:	GROUNDMASS
82431-17	:	GROUNDMASS
82431-18	:	GROUNDMASS

Table D.2. cont.

	83400-36	83400-1	83400-42	83400-44	83400-48	83400-49	83400-50	82403-2	82403-3	82403-5
SIO2	50.21	50.21	50.26	50.52	50.72	51.40	50.44	51.57	50.23	52.06
TIO2	1.60	1.95	1.06	1.21	1.52	1.15	2.21	1.59	2.24	0.38
AL2O3	3.41	1.79	0.93	1.10	2.96	0.75	3.67	2.89	4.02	1.14
FEOT	10.09	16.08	17.02	16.48	10.10	17.09	10.81	8.01	8.41	12.77
MNO	0.68	0.92	0.98	0.96	0.76	0.90	0.68	0.49	0.39	0.83
MGO	11.37	7.37	6.78	7.35	11.69	6.93	11.07	12.67	12.36	11.12
CAO	20.75	20.22	18.73	19.52	21.39	18.04	21.41	22.62	21.68	21.70
NA2O	1.02	1.40	1.80	1.41	0.77	2.15	0.83	0.66	0.89	0.45
K2O		0.03	0.03	0.03	0.02	0.06	0.02			
TOTAL	99.13	99.98	97.59	98.58	99.94	98.47	101.16	100.51	100.22	100.46
FE2O3	0.98	0.36	1.57	0.69	0.76	2.07	0.25	0.04	0.74	0.81
FEO	9.21	15.30	15.61	15.85	9.42	15.23	10.59	7.97	7.75	12.04
NTOT	99.23	100.06	97.75	98.65	100.01	98.68	101.16	100.50	100.29	100.53
SI	1.90	1.94	1.99	1.98	1.91	2.01	1.88	1.92	1.87	1.97
TI	0.05	0.06	0.03	0.04	0.04	0.03	0.06	0.04	0.06	0.01
AL	0.15	0.08	0.04	0.05	0.13	0.04	0.16	0.13	0.18	0.05
FE3	0.03	0.02	0.05	0.02	0.02	0.06	0.01	0.00	0.02	0.02
FE2	0.29	0.50	0.52	0.52	0.30	0.50	0.33	0.25	0.24	0.38
MN	0.02	0.03	0.03	0.03	0.02	0.03	0.02	0.02	0.01	0.03
MG	0.64	0.43	0.40	0.43	0.66	0.40	0.62	0.70	0.69	0.63
CA	0.84	0.84	0.80	0.82	0.86	0.76	0.86	0.90	0.87	0.88
NA	0.08	0.11	0.14	0.11	0.06	0.16	0.06	0.05	0.06	0.03
MGI	0.67	0.45	0.42	0.44	0.67	0.43	0.64	0.73	0.73	0.61
WO	46.84	46.86	45.55	45.52	46.90	44.78	46.94	48.27	47.93	45.95
EN	35.72	23.77	22.94	23.85	35.66	23.94	33.77	37.62	38.02	32.76
FS	17.44	29.37	31.51	30.63	17.43	31.28	19.29	14.11	14.05	21.29
RWO				46.80	45.60					45.40
REN				25.00	37.60					33.40
RFS				28.20	16.90					21.20

*** ALL ZERO VALUES PRINTED AS BLANKS. ***

SAMPLE DESCRIPTION :

83400-36	:	INTERMEDIATE
83400-1	:	GROUNDMASS CORE
83400-42	:	GROUNDMASS RIM
83400-44	:	GROUNDMASS RIM
83400-48	:	CORE
83400-49	:	GROUNDMASS RIM
83400-50	:	GROUNDMASS CORE
82403-2	:	CORE
82403-3	:	CORE
82403-5	:	RIM

Table D.2. cont.

	82403-6	82403-7	AW82023-2	AW82023-3	AW82023-4	AW82023-8	AW82023-9	82404-1A	82404-1B	82404-3
SIO2	52.03	51.65	49.92	51.07	51.05	49.55	48.51	51.15	52.03	51.42
TIO2	0.51	1.78	0.88	0.86	0.67	0.96	1.86	1.55	0.75	1.00
AL2O3	1.51	2.65	2.26	2.03	1.52	2.78	4.37	3.74	1.99	1.98
FEOT	11.32	8.33	15.83	15.23	15.28	13.66	12.08	9.95	10.21	10.61
MNO	0.70	0.46	0.78	0.89	1.01	0.69	0.62	0.49	0.46	0.59
MGO	11.53	13.15	8.76	9.34	9.53	9.57	10.54	12.29	12.34	12.03
CAO	21.74	22.03	21.44	21.35	21.04	20.58	20.55	22.17	21.95	22.54
NA2O	0.50	0.76	0.56	0.57	0.44	0.56	0.56	0.60	0.55	0.45
K2O			0.02				0.02		0.02	0.03
TOTAL	99.84	100.81	100.44	101.34	100.54	98.35	99.11	101.94	100.30	100.65
FE2O3	0.09	0.69	2.04	1.04	0.71	0.30	0.84	1.09	0.52	1.39
FEO	11.24	7.71	14.00	14.29	14.64	13.39	11.32	8.97	9.74	9.36
NTOT	99.85	100.88	100.65	101.44	100.61	98.38	99.19	102.05	100.35	100.79
SI	1.97	1.91	1.92	1.94	1.95	1.92	1.86	1.88	1.95	1.92
TI	0.02	0.05	0.02	0.02	0.02	0.03	0.05	0.04	0.02	0.03
AL	0.07	0.12	0.10	0.09	0.07	0.13	0.20	0.16	0.09	0.09
FE3	0.00	0.02	0.06	0.03	0.02	0.01	0.02	0.03	0.02	0.04
FE2	0.36	0.24	0.45	0.45	0.47	0.43	0.36	0.28	0.30	0.29
MN	0.02	0.01	0.02	0.03	0.03	0.02	0.02	0.02	0.02	0.02
MG	0.65	0.73	0.50	0.53	0.54	0.55	0.60	0.67	0.69	0.67
CA	0.88	0.87	0.88	0.87	0.86	0.86	0.84	0.87	0.88	0.90
NA	0.04	0.06	0.04	0.04	0.03	0.04	0.04	0.04	0.04	0.03
MGI	0.63	0.74	0.51	0.52	0.52	0.55	0.61	0.70	0.68	0.68
WO	46.15	47.17	47.46	46.21	45.22	45.84	46.14	47.52	46.62	47.91
EN	34.05	39.18	26.98	28.13	28.50	29.66	32.92	36.65	36.47	35.58
FS	19.80	13.66	25.55	25.67	26.28	24.50	20.94	15.83	16.92	16.51
RWO				45.20						
REN				29.10						
RFS				25.80						

*** ALL ZERO VALUES PRINTED AS BLANKS. ***

SAMPLE DESCRIPTION :

82403-6	:	RIM
82403-7	:	CORE
AW82023-2	:	RIM
AW82023-3	:	RIM
AW82023-4	:	CORE
AW82023-8	:	GROUNDMASS
AW82023-9	:	GROUNDMASS
82404-1A	:	CORE
82404-1B	:	CORE
82404-3	:	RIM

Table D.2. cont.

	82404-10	82404-11	82404-1C
SIO2	51.42	50.58	51.19
TIO2	1.02	1.56	1.27
AL2O3	2.44	3.18	2.57
FEOT	9.47	9.56	9.31
MNO	0.44	0.40	0.39
MGO	13.00	11.75	12.91
CAO	23.18	22.99	23.63
NA2O	0.59	0.65	0.51
K2O		0.02	
TOTAL	101.57	100.69	101.78
FE2O3	3.30	1.68	2.80
FEO	6.50	8.05	6.79
NTOT	101.89	100.86	102.06
SI	1.89	1.89	1.88
TI	0.03	0.04	0.04
AL	0.11	0.14	0.11
FE3	0.09	0.05	0.08
FE2	0.20	0.25	0.21
MN	0.01	0.01	0.01
MG	0.71	0.65	0.71
CA	0.91	0.92	0.93
NA	0.04	0.05	0.04
MGI	0.77	0.71	0.76
WO	49.65	50.05	50.06
EN	38.74	35.59	38.06
FS	11.61	14.37	11.88
RWO		48.10	
REN		37.00	
RFS		14.90	

*** ALL ZERO VALUES PRINTED AS BLANKS. ***

SAMPLE DESCRIPTION :

82404-10 : CORE
82404-11 : CORE
82404-1C : CORE

Table D.3. Opaque oxides

		83435-1	83435-2	83435-3	83435-4	83435-5	83435-6	83435-7	83435-8	83435-9	83435-10
SIO2		0.13	0.12	0.11	0.12	0.12	0.12	0.14	0.13	0.14	0.14
TIO2		15.30	15.56	15.08	15.22	15.43	12.69	16.12	15.96	16.59	13.83
AL2O3		9.56	9.31	9.36	9.63	9.22	10.57	8.43	9.32	9.32	9.76
CR2O3		1.12	2.05	2.25	2.23	2.24	7.40	0.71	3.04	3.00	4.60
FEOT	*	64.56	64.38	64.28	64.10	64.76	60.06	65.01	63.91	64.03	62.38
MNO		0.33	0.38	0.34	0.33	0.34	0.31	0.40	0.46	0.48	0.41
MGO		7.82	7.29	7.23	7.95	7.48	7.85	7.62	4.53	4.56	5.92
CAO											
TOTAL		99.34	99.11	98.66	99.59	99.61	99.02	98.44	97.36	98.12	97.03
FE2O3	o	31.74	31.08	31.46	31.93	31.74	29.86	32.15	26.25	25.55	28.96
FEO	o	36.00	36.41	35.97	35.37	36.20	33.19	36.08	40.29	41.04	36.32
NTOT	x	102.50	102.20	101.80	102.78	102.77	101.99	101.65	99.98	100.68	99.94
SI	'	0.00	0.00	0.00	0.00	0.00	0.00	0.01	0.00	0.01	0.01
TI	'	0.40	0.39	0.38	0.38	0.39	0.32	0.41	0.42	0.43	0.36
AL	'	0.38	0.37	0.37	0.38	0.36	0.41	0.34	0.38	0.38	0.40
CR	'	0.03	0.05	0.06	0.06	0.06	0.20	0.02	0.08	0.08	0.13
FE3	'	0.80	0.78	0.80	0.80	0.80	0.75	0.82	0.69	0.66	0.75
FE2	'	1.00	1.02	1.01	0.98	1.01	0.92	1.02	1.17	1.19	1.05
MN	'	0.01	0.01	0.01	0.01	0.01	0.01	0.01	0.01	0.01	0.01
MG	'	0.39	0.36	0.36	0.39	0.37	0.39	0.38	0.23	0.23	0.30
CA	'										
FE	2	1.80	1.81	1.81	1.78	1.81	1.67	1.84	1.86	1.85	1.80
USP	@	0.52	0.53	0.52	0.51	0.52	0.52	0.51	0.63	0.65	0.55

*Total Fe analyzed as FeO
°Recalculated Fe_2O_3 and FeO
xNew total
'No. of cations on the basis of 32 (0)
²Total Fe cations on basis of 32 (0)
@Ulvospinel ($2FeO \cdot TiO_2$). Mol. proportion.

SAMPLE DESCRIPTION :

83435-1	: CORE
83135-2	: RIM
83435-3	: RIM
83435-4	: CORE
83435-5	: CORE
83435-6	: CORE
83435-7	: INCLUSION IN CPX
83435-8	: INCLUSION IN OLIVINE
83435-9	: INCLUSION IN OLIVINE
83435-10	: INCLUSION. IN OLIVINE - AVE.

Table D.3. cont.

	83435-12	83435-14	83435-15	83435-16	83435-17	83435-0	83435-00	83435-1A	83435-2A	79300-1
SIO2	0.13	0.15	0.14	0.13	0.11	0.11	0.11	0.13	0.11	0.10
TIO2	22.42	22.61	24.49	25.73	22.75	15.03	15.32	15.12	15.10	21.07
AL2O3	7.50	7.52	5.99	4.37	7.48	9.04	9.07	9.04	8.99	6.79
CR2O3	0.46	0.42	0.37	0.07	0.33	2.48	2.47	2.52	2.07	0.36
FEOT	62.87	63.29	63.99	64.97	64.15	63.32	63.15	64.48	65.11	64.44
MNO	0.73	0.71	0.85	0.87	0.67	0.40	0.46	0.41	0.36	0.59
MGO	3.72	3.74	3.30	2.72	3.86	6.67	6.77	6.67	6.25	5.79
CAO										
TOTAL	97.83	98.43	99.13	98.87	99.36	97.07	97.35	98.37	98.02	99.15
FE2O3	17.86	17.89	16.27	15.56	18.60	30.21	29.86	30.91	31.03	23.91
FEO	46.80	47.19	49.35	50.97	47.41	36.14	36.28	36.67	37.19	42.93
NTOT	99.82	100.23	100.76	100.43	101.21	100.08	100.34	101.47	101.10	101.54
SI	0.01	0.01	0.01	0.01	0.00	0.00	0.00	0.00	0.00	0.00
TI	0.59	0.60	0.65	0.69	0.59	0.39	0.39	0.39	0.39	0.55
AL	0.31	0.31	0.25	0.18	0.31	0.37	0.37	0.36	0.36	0.27
CR	0.01	0.01	0.01	0.00	0.01	0.07	0.07	0.07	0.06	0.01
FE3	0.48	0.47	0.43	0.42	0.49	0.78	0.77	0.79	0.80	0.62
FE2	1.38	1.39	1.46	1.53	1.38	1.04	1.04	1.04	1.06	1.23
MN	0.02	0.02	0.02	0.03	0.02	0.01	0.01	0.01	0.01	0.02
MG	0.20	0.20	0.17	0.14	0.20	0.34	0.35	0.34	0.32	0.30
CA										
FE	1.86	1.86	1.89	1.94	1.87	1.82	1.81	1.83	1.86	1.85
USP	0.78	0.79	0.81	0.81	0.78	0.54	0.54	0.53	0.53	0.67

*** ALL ZERO VALUES PRINTED AS BLANKS. ***

SAMPLE DESCRIPTION :

83435-12	:	GROUNDMASS
83435-14	:	GROUNDMASS
83435-15	:	GROUNDMASS
83435-16	:	GROUNDMASS
83435-17	:	GROUNDMASS
83435-0	:	CORE
83435-00	:	CORE
83435-1A	:	RIM
83435-2A	:	CORE
79300-1	:	CORE

Table D.3. cont.

	79300-2	79300-3	79300-4	79300-5	79300-6	79300-7	79300-8	79300-9	79300-10	79300-11
SIO2	0.12	0.10	0.11	0.13	0.11	0.10	0.13	0.12	0.13	0.10
TIO2	22.35	21.40	22.09	21.95	21.11	22.14	20.94	21.31	22.01	24.68
AL2O3	5.57	6.72	5.92	5.04	6.10	5.38	6.88	6.43	5.38	4.12
CR2O3	0.30	0.45	0.01	0.05	0.19	0.07	0.14	0.26	0.12	0.01
FEOT	65.04	64.61	65.48	65.15	64.92	65.13	65.23	65.04	64.68	63.67
MNO	0.73	0.58	0.72	0.69	0.58	0.69	0.63	0.63	0.73	0.88
MGO	5.25	5.40	5.49	5.34	5.88	5.60	5.96	5.63	5.30	5.14
CAO										
TOTAL	99.36	99.27	99.84	98.35	98.90	99.12	99.91	99.42	98.36	98.61
FE2O3	22.66	23.07	23.58	23.71	24.72	23.65	24.89	24.04	23.06	19.40
FEO	44.65	43.85	44.26	43.82	42.68	43.85	42.83	43.41	43.93	46.21
NTOT	101.63	101.57	102.18	100.73	101.37	101.48	102.39	101.83	100.66	100.54
SI	0.00	0.00	0.00	0.01	0.00	0.00	0.00	0.00	0.00	0.00
TI	0.58	0.55	0.57	0.58	0.55	0.58	0.54	0.55	0.58	0.65
AL	0.23	0.27	0.24	0.21	0.25	0.22	0.28	0.26	0.22	0.17
CR	0.01	0.01		0.00	0.01	0.00	0.00	0.01	0.00	
FE3	0.59	0.60	0.61	0.63	0.64	0.62	0.64	0.62	0.61	0.51
FE2	1.29	1.26	1.27	1.28	1.23	1.27	1.22	1.25	1.29	1.36
MN	0.02	0.02	0.02	0.02	0.02	0.02	0.02	0.02	0.02	0.03
MG	0.27	0.28	0.28	0.28	0.30	0.29	0.30	0.29	0.28	0.27
CA										
FE	1.39	1.86	1.88	1.91	1.88	1.89	1.86	1.87	1.89	1.88
USP	0.69	0.69	0.68	0.67	0.65	0.67	0.66	0.67	0.68	0.74

*** ALL ZERO VALUES PRINTED AS BLANKS. ***

SAMPLE DESCRIPTION :

79300-2	:	RIM
79300-3	:	CORE
79300-4	:	CORE
79300-5	:	EDGE
79300-6	:	CORE
79300-7	:	RIM
79300-8	:	CORE
79300-9	:	INTERMEDIATE
79300-10	:	RIM
79300-11	:	MICROPHENOCRYST

Table D.3. cont.

	79300-12	79300-13	AW82038-1A	AW82038-2A	AW82038-1B	AW82038-2B	AW82038-3B	AW82038-1C	AW82038-2C	AW82038-3C
SIO2	0.12	0.14	0.13	0.15	0.14	0.14	0.11	0.12	0.12	0.10
TIO2	24.95	24.50	23.29	23.26	23.09	23.26	23.60	23.26	23.19	23.34
AL203	3.95	3.80	5.05	4.99	4.95	4.99	5.21	5.12	4.49	5.14
CR203	0.01	0.01	0.01	0.01		0.01	0.01	0.01	0.01	0.01
FEOT	64.45	64.32	63.10	62.99	63.92	63.26	62.65	64.24	64.41	63.79
MNO	0.89	0.86	0.69	0.67	0.68	0.66	0.70	0.70	0.82	0.75
MGO	5.08	4.73	5.33	5.28	5.32	5.58	5.30	5.43	4.97	5.41
CAO										
TOTAL	99.45	98.37	97.63	97.33	98.11	97.91	97.61	98.91	98.04	98.56
FE203	19.60	19.66	20.40	20.27	21.29	20.88	19.57	21.40	21.44	21.00
FEO	46.81	46.63	44.74	44.75	44.76	44.47	45.04	44.98	45.12	44.89
NTOT	101.41	100.33	99.64	99.38	100.23	99.99	99.54	101.01	100.16	100.64
SI	0.00	0.01	0.01	0.01	0.01	0.01	0.00	0.00	0.00	0.00
TI	0.66	0.65	0.62	0.62	0.61	0.62	0.63	0.61	0.62	0.61
AL	0.16	0.16	0.21	0.21	0.21	0.21	0.22	0.21	0.19	0.21
CR										
FE3	0.52	0.52	0.54	0.54	0.56	0.55	0.52	0.56	0.57	0.55
FE2	1.37	1.38	1.32	1.33	1.32	1.31	1.33	1.31	1.33	1.31
MN	0.03	0.03	0.02	0.02	0.02	0.02	0.02	0.02	0.02	0.02
MG	0.27	0.25	0.28	0.28	0.28	0.29	0.28	0.28	0.26	0.28
CA										
FE	1.89	1.91	1.86	1.87	1.88	1.86	1.85	1.87	1.91	1.87
USP	0.73	0.73	0.72	0.72	0.71	0.71	0.74	0.71	0.70	0.71

*** ALL ZERO VALUES PRINTED AS BLANKS. ***

SAMPLE DESCRIPTION :

79300-12	MICROPHENOCRYST
79300-13	GROUNDMASS
AW82038-1A	CORE
AW82038-2A	CORE
AW82038-1B	CORE
AW82038-2B	CORE
AW82038-3B	CORE
AW82038-1C	CORE
AW82038-2C	CORE
AW82038-3C	CORE

Table D.3. cont.

	AW82038-4C	AW82038-5C	AW82038-9C	AW82038-11D	AW82038-12D	AW82038-10D	AW82038-IA	83415	83415	83415
SIO2	0.10	0.12	0.11	0.25	0.25	0.26	0.09	0.11	0.25	0.21
TIO2	23.36	23.80	24.40	23.35	23.58	23.74	49.48	24.63	25.74	26.16
AL2O3	4.78	4.94	4.41	5.04	5.37	4.87	0.60	4.34	4.48	4.16
CR2O3	0.01		0.01	0.12	0.01	0.01	0.01	0.07	0.01	
FEOT	63.91	63.32	63.32	62.46	62.73	62.37	40.46	64.60	62.73	62.87
MNO	0.78	0.66	0.78	0.78	0.82	0.65	0.72	0.90	1.05	0.98
MGO	4.97	5.51	5.21	5.56	5.51	5.35	6.35	4.65	4.88	4.92
CAO				0.06	0.06	0.09	0.11		0.07	0.02
TOTAL	97.92	98.35	98.25	97.63	98.38	97.33	97.81	99.29	99.31	99.22
FE2O3	20.69	20.18	19.36	20.03	19.74	19.21	8.93	19.37	16.68	16.43
FEO	45.29	45.16	45.90	44.44	44.97	45.09	32.42	47.17	47.72	48.09
NTOT	99.97	100.37	100.18	99.63	100.35	99.26	98.70	101.24	100.89	100.97
SI	0.00	0.00	0.00	0.01	0.01	0.01	0.00	0.00	0.01	0.01
TI	0.62	0.63	0.65	0.62	0.62	0.63	0.91	0.65	0.68	0.69
AL	0.20	0.20	0.18	0.21	0.22	0.20	0.02	0.18	0.19	0.17
CR				0.00				0.00		
FE3	0.55	0.53	0.51	0.53	0.52	0.51	0.16	0.51	0.44	0.43
FE2	1.34	1.32	1.35	1.31	1.31	1.34	0.66	1.38	1.40	1.41
MN	0.02	0.02	0.02	0.02	0.02	0.02	0.02	0.03	0.03	0.03
MG	0.26	0.29	0.27	0.29	0.29	0.28	0.21	0.24	0.25	0.26
CA				0.00	0.00	0.00	0.00		0.00	0.00
FE	1.89	1.86	1.87	1.84	1.83	1.85	0.83	1.89	1.84	1.84
USP	0.72	0.73	0.74	0.72	0.73	0.74	0.90	0.74	0.78	0.79

*** ALL ZERO VALUES PRINTED AS BLANKS. ***

SAMPLE DESCRIPTION :

AW82038-4C	:	CORE
AW82038-5C	:	INCLUSION IN FELDSPAR
AW82038-9C	:	GROUNDMASS
AW82038-11D	:	RIM
AW82038-12D	:	CORE
AW82038-10D	:	GROUNDMASS
AW82038-IA	:	ILMENITE AVE.
83415	:	4/12 CORED MT AVE.
83415	:	5/1-8 - CORED MT
83415	:	5/1-9 - CORED MT

Table D.3. cont.

	83415	83415	83415	83415	83415	83415	83415	83415	83415	83415
SIO2	0.10	0.11	0.10	0.22	0.22	0.12	0.12	0.12	0.11	0.10
TIO2	23.07	21.98	21.66	22.21	22.56	22.67	20.52	21.71	19.67	20.62
AL2O3	4.25	5.56	5.89	5.44	5.31	4.66	6.04	5.10	6.27	6.21
CR2O3				0.01		0.01	0.06	0.07	0.01	0.01
FEOT	64.81	64.98	64.54	64.11	63.87	65.54	65.62	65.48	65.03	65.38
MNO	0.89	0.79	0.74	0.79	0.93	0.86	0.78	0.88	0.65	0.65
MGO	4.49	5.04	5.61	4.97	4.88	4.00	5.29	4.47	5.83	5.93
CAO				0.06	0.06					
TOTAL	97.61	98.46	98.54	97.81	97.83	97.87	98.43	97.83	97.59	98.91
FE2O3	20.61	23.00	23.66	21.88	21.29	21.63	25.46	23.38	26.68	25.86
FEO	45.42	44.28	43.25	44.42	44.71	46.08	42.71	44.23	41.02	42.11
NTOT	100.21	100.77	100.91	100.01	99.95	100.03	100.98	99.66	100.24	101.49
SI	0.00	0.00	0.00	0.01	0.01	0.00	0.00	0.00	0.00	0.00
TI	0.62	0.58	0.57	0.59	0.60	0.61	0.54	0.58	0.52	0.53
AL	0.18	0.23	0.24	0.23	0.22	0.20	0.25	0.21	0.26	0.25
CR							0.00	0.00		
FE3	0.58	0.61	0.62	0.58	0.57	0.58	0.67	0.62	0.70	0.67
FE2	1.36	1.30	1.26	1.31	1.32	1.37	1.24	1.32	1.20	1.21
MN	0.03	0.02	0.02	0.02	0.03	0.03	0.02	0.03	0.02	0.02
MG	0.24	0.26	0.29	0.26	0.26	0.21	0.27	0.24	0.30	0.30
CA				0.00	0.00					
FE	1.93	1.90	1.88	1.89	1.89	1.95	1.91	1.94	1.90	1.89
USP	0.72	0.68	0.67	0.70	0.71	0.70	0.64	0.67	0.61	0.63

*** ALL ZERO VALUES PRINTED AS BLANKS. ***

SAMPLE DESCRIPTION :

83415	:	4/12-BLEBBED MT EDGE AVE.
83415	:	4/12-BLEBBED MT INTERMEDIATE AVE
83415	:	4/12-BLEBBED MT CORE AVE.
83415	:	5/1-2:BLEBBED MT CORE
83415	:	5/1-3: BLEBBED MT CORE
83415	:	4/12-10B:INCLUSION IN CPX
83415	:	4/12-12B:CORE
83415	:	4/12 13&14B AVE.;RIM
83415	:	4/12-15B
83415	:	4/12-16B

Table D.3. cont.

	83415	83415	83415	83415	83415	83415	83415	83415	83415	25748K-15 #
SIO2	0.12	0.12	0.16	0.17	0.05	0.06	0.17	0.20	0.05	
TIO2	23.21	22.68	51.09	51.46	50.45	49.73	51.09	51.16	49.04	25.63
AL2O3	3.82	3.60	0.41	0.40	0.48	0.43	0.59	0.53	0.60	4.30
CR2O3	0.14	0.15					0.01			0.20
FEOT	64.37	65.03	39.59	39.38	40.44	40.30	40.60	40.88	41.74	63.28
MNO	1.02	1.07	0.84	1.02	0.83	0.85	0.82	0.98	0.83	1.30
MGO	3.80	3.71	6.33	6.50	6.28	6.31	5.85	5.83	5.78	4.30
CAO			0.17	0.13			0.06	0.20		
TOTAL	96.51	96.37	98.59	99.04	98.52	97.68	99.21	99.78	98.04	99.01
FE2O3	20.29	21.52	6.45	6.31	7.82	8.46	6.43	6.97	9.69	17.12
FEO	46.11	45.67	33.79	33.70	33.40	32.68	34.81	34.61	33.02	47.89
NTOT	98.52	98.53	99.24	99.68	99.30	98.53	99.85	100.48	99.01	100.71
SI	0.00	0.00	0.00	0.00	0.00	0.00	0.00	0.01	0.00	
TI	0.63	0.62	0.93	0.93	0.92	0.91	0.93	0.92	0.90	0.68
AL	0.16	0.15	0.01	0.01	0.01	0.01	0.02	0.02	0.02	0.18
CR	0.00	0.00								0.01
FE3	0.55	0.59	0.12	0.12	0.14	0.16	0.12	0.13	0.18	0.45
FE2	1.40	1.39	0.69	0.68	0.68	0.67	0.70	0.70	0.67	1.42
MN	0.03	0.03	0.02	0.02	0.02	0.02	0.02	0.02	0.02	0.04
MG	0.21	0.20	0.23	0.23	0.23	0.23	0.21	0.21	0.21	0.23
CA			0.00	0.00			0.00	0.01		
FE	1.96	1.98	0.80	0.79	0.82	0.82	0.82	0.82	0.85	1.87
USP	0.72	0.70	0.93	0.93	0.92	0.91	0.93	0.93	0.90	0.78

*** ALL ZERO VALUES PRINTED AS BLANKS. ***

#K: Kyle (unpubl.)

SAMPLE DESCRIPTION :

83415	:	4/12-18: GROUNDMASS
83415	:	4/12-19: GROUNDMASS
83415	:	5/1-4: ILM BLEB
83415	:	5/1-5: ILM BLEB
83415	:	4/12 - ILM BLEBS AVE
83415	:	4/12-ILM BLEBS AVE.
83415	:	5/1-6:ILM CORE
83415	:	5/1-7: ILM CORE
83415	:	4/12- ILM CORE AVE.
25748K-15	:	INCLUSION IN CPX; CORE

Table D.3. cont.

	25748-K16	25748-K17	25748-K18	25748-K19	25748-K51	83448-1	83448-4	83448-5	83448-6	83448-8
SIO2						0.10	0.11	0.09	0.10	0.10
TIO2	25.21	26.06	25.34	25.45	25.43	23.49	24.08	24.24	22.89	24.11
AL2O3	3.70	4.00	3.80	3.80	3.80	2.51	2.63	2.43	2.61	2.72
CR2O3	0.20	0.20	0.20	0.20	0.22		0.01			0.01
FEOT	64.26	64.53	64.52	64.29	64.87	68.16	68.39	68.30	67.84	68.38
MNO	1.30	1.30	1.30	1.30	1.30	1.71	1.56	1.62	1.54	1.46
MGO	4.40	4.60	4.40	4.30	4.40	2.83	3.03	2.66	3.05	3.07
CAO										
TOTAL	99.02	99.75	99.59	99.33	100.02	98.80	99.82	99.33	98.02	99.86
FE2O3	18.84	19.23	18.81	18.39	18.96	22.73	22.18	21.60	23.40	22.08
FEO	47.34	47.19	47.58	47.75	47.84	47.71	48.43	48.86	46.78	48.51
NTOT	100.99	101.63	101.38	101.14	101.92	101.08	102.03	101.49	100.36	102.06
SI						0.00	0.00	0.00	0.00	0.00
TI	0.67	0.66	0.67	0.67	0.67	0.63	0.64	0.65	0.62	0.64
AL	0.15	0.17	0.16	0.16	0.16	0.11	0.11	0.10	0.11	0.11
CR	0.01	0.01	0.01	0.01	0.01					
FE3	0.50	0.51	0.50	0.49	0.50	0.62	0.59	0.58	0.64	0.59
FE2	1.40	1.38	1.40	1.41	1.40	1.44	1.44	1.47	1.41	1.44
MN	0.04	0.04	0.04	0.04	0.04	0.05	0.04	0.05	0.05	0.04
MG	0.23	0.24	0.23	0.22	0.23	0.15	0.16	0.14	0.16	0.16
CA										
FE	1.90	1.89	1.90	1.90	1.90	2.05	2.03	2.05	2.05	2.03
USP	0.75	0.74	0.75	0.76	0.75	0.68	0.69	0.70	0.67	0.70

*** ALL ZERO VALUES PRINTED AS BLANKS. ***

SAMPLE DESCRIPTION :

25748-K16	:	INCLUSION. IN CPX; RIM
25748-K17	:	CORE
25748-K18	:	CORE
25748-K19	:	CORE
25748-K51	:	INCLUSION IN OLIVINE
83448-1	:	CORE
83448-4	:	CORE
83448-5	:	RIM
83448-6	:	CORE
83448-8	:	INCLUSION IN OLIVINE

Table D.3. cont.

	83448-9	83448-10	83448-11	83448-12	83448-7	80020-1	80020-2	80020-3	80020-4	80020-5
SIO2	0.10	0.10	0.11	0.10	0.09	0.12	0.11	0.11	0.11	0.11
TIO2	24.25	23.58	23.25	23.36	23.69	23.23	23.77	23.33	23.78	24.14
AL2O3	2.49	2.74	2.53	2.60	2.51	2.34	2.49	2.36	2.44	2.23
CR2O3									0.01	
FEOT	68.22	67.49	67.70	67.53	68.10	68.41	68.66	68.31	67.46	68.42
MNO	1.54	1.39	1.69	1.45	1.69	1.78	1.75	1.79	1.83	1.79
MGO	2.95	3.53	2.99	3.25	3.00	2.46	2.67	2.45	2.44	2.85
CAO										
TOTAL	99.55	98.84	98.27	98.29	99.09	98.34	99.45	98.35	98.06	99.54
FE2O3	21.80	22.68	22.88	22.75	22.65	22.88	22.54	22.67	21.42	22.27
FEO	48.60	47.08	47.11	47.06	47.72	47.82	48.38	47.91	48.19	48.38
NTOT	101.72	101.10	100.56	100.57	101.36	100.63	101.71	100.62	100.22	101.77
SI	0.00	0.00	0.00	0.00	0.00	0.00	0.00	0.00	0.00	0.00
TI	0.65	0.63	0.63	0.63	0.64	0.63	0.64	0.64	0.65	0.65
AL	0.11	0.12	0.11	0.11	0.11	0.10	0.11	0.10	0.11	0.09
CR							0.00	0.00		
FE3	0.59	0.61	0.62	0.62	0.61	0.62	0.61	0.62	0.59	0.60
FE2	1.45	1.41	1.42	1.42	1.43	1.45	1.45	1.45	1.47	1.45
MN	0.05	0.04	0.05	0.04	0.05	0.06	0.05	0.06	0.06	0.54
MG	0.16	0.19	0.16	0.17	0.16	0.13	0.14	0.13	0.13	0.15
CA										
FE	2.04	2.02	2.04	2.03	2.04	2.07	2.06	2.07	2.05	2.05
USP	0.70	0.68	0.67	0.68	0.68	0.68	0.69	0.68	0.70	0.69

*** ALL ZERO VALUES PRINTED AS BLANKS. ***

SAMPLE DESCRIPTION :

83448-9	:	RIM
83448-10	:	INCLUSION IN FELDSPAR
83448-11	:	CORE
83448-12	:	INCLUSION IN CPX
83148-7	:	CORE
80020-1	:	CORE
80020-2	:	CORE
80020-3	:	RIM
80020-4	:	CORE
80020-5	:	INCLUSION IN CPX

Table D.3. cont.

	80020-6	80020-7	80020-8	83400-2	83400-3	83400-4	83400-5	83400-6	83400-7	83400-8
SIO2	0.12	0.11	0.11	0.10	0.11	0.12	0.12	0.09	0.10	0.10
TIO2	23.98	22.88	23.67	24.31	24.38	24.75	25.95	24.78	24.76	24.33
AL2O3	2.40	2.26	2.29	1.80	2.10	1.99	0.81	2.00	1.76	2.25
CR2O3		0.01				0.01	0.01	0.01	0.01	0.01
FEOT	68.64	68.26	68.10	69.56	69.59	69.58	70.39	70.15	69.83	68.56
MNO	1.79	1.72	1.91	1.79	1.84	1.86	1.92	1.85	1.68	1.63
MGO	2.42	2.42	2.36	1.09	0.81	0.70	0.42	0.43	0.49	2.26
CAO										
TOTAL	99.34	97.67	98.44	98.66	98.85	99.01	99.62	99.33	98.63	99.15
FE2O3	21.97	23.19	22.07	20.81	20.23	19.64	18.93	19.70	19.55	21.23
FEO	48.87	47.39	48.24	50.84	51.39	51.91	53.36	52.42	52.24	49.46
NTOT	101.55	99.98	100.65	100.74	100.86	100.98	101.52	101.28	100.59	101.27
SI	0.00	0.00	0.00	0.00	0.00	0.00	0.00	0.00	0.00	0.00
TI	0.65	0.63	0.65	0.67	0.67	0.68	0.72	0.68	0.69	0.66
AL	0.10	0.10	0.10	0.08	0.09	0.09	0.04	0.09	0.08	0.10
CR										
FE3	0.59	0.64	0.60	0.57	0.56	0.54	0.52	0.54	0.54	0.58
FE2	1.47	1.45	1.46	1.56	1.57	1.59	1.64	1.61	1.61	1.49
MN	0.06	0.05	0.06	0.06	0.06	0.06	0.06	0.06	0.05	0.05
MG	0.13	0.13	0.13	0.06	0.04	0.04	0.02	0.02	0.03	0.12
CA										
FE	2.06	2.09	2.07	2.13	2.13	2.13	2.16	2.15	2.15	2.07
USP	0.89	0.67	0.89	0.71	0.73	0.73	0.74	0.73	0.73	0.71

*** ALL ZERO VALUES PRINTED AS BLANKS. ***

SAMPLE DESCRIPTION :

80020-6	:	CORE
80020-7	:	RIM
80020-8	:	RIM
83400-2	:	RIM
83400-3	:	CORE
83400-4	:	CORE
83400-5	:	RIM
83400-6	:	CORE
83400-7	:	CORE
83400-8	:	CORE

Table D.3. cont.

	83400-9	83400-10	83400-12	83400-13	83400-14	83400-1	82403-1	82403-2	82403-3	82403-4
SIO2	0.09	0.10	0.11	0.11	0.10	0.10	0.10	0.09	0.11	0.09
TIO2	23.81	26.06	25.22	25.31	25.77	23.04	26.76	26.36	26.03	26.65
AL2O3	2.46	0.20	0.19	0.18	0.19	2.05	1.61	1.66	1.77	1.79
CR2O3	0.01		0.01		0.01	0.01	0.01			
FEOT	68.41	69.96	69.48	69.87	69.97	69.34	68.40	68.22	67.55	68.03
MNO	1.62	2.15	2.19	2.09	2.11	1.73	1.79	1.68	1.68	1.65
MGO	1.99	0.04	0.11	0.06	0.16	1.06	1.40	1.55	2.11	1.32
CAO										
TOTAL	98.42	98.51	97.33	97.63	98.29	97.36	100.07	99.55	99.23	99.55
FE2O3	21.35	18.49	19.36	19.40	19.01	22.12	17.19	17.70	18.29	16.78
FEO	49.20	53.32	52.08	52.41	52.86	49.44	52.93	52.29	51.09	52.93
NTOT	100.53	100.35	99.25	99.56	100.20	99.55	101.79	101.33	101.08	101.21
SI	0.00	0.00	0.00	0.00	0.00	0.00	0.00	0.00	0.00	0.00
TI	0.65	0.73	0.72	0.72	0.73	0.64	0.73	0.72	0.71	0.73
AL	0.11	0.01	0.01	0.01	0.01	0.09	0.07	0.07	0.08	0.08
CR										
FE3	0.59	0.52	0.55	0.55	0.53	0.62	0.47	0.48	0.50	0.46
FE2	1.50	1.67	1.64	1.65	1.65	1.53	1.60	1.59	1.55	1.61
MN	0.05	0.07	0.07	0.07	0.07	0.05	0.06	0.05	0.05	0.05
MG	0.11	0.00	0.01	0.00	0.01	0.06	0.08	0.08	0.11	0.07
CA										
FE	2.08	2.19	2.19	2.20	2.19	2.15	2.07	2.07	2.05	2.07
USP	0.70	0.73	0.72	0.72	0.73	0.69	0.77	0.76	0.75	0.77

*** ALL ZERO VALUES PRINTED AS BLANKS. ***

SAMPLE DESCRIPTION :

83400-9	:	INCLUSION IN FELDSPAR
83400-10	:	GROUNDMASS
83400-12	:	GROUNDMASS
83400-13	:	GROUNDMASS
83400-14	:	GROUNDMASS
83400-1	:	CORE
82403-1	:	CORE
82403-2	:	INTERMEDIATE
82403-3	:	RIM
82403-4	:	CORE

Table D.3. cont.

	82403-6	82403-7	82403-8	82403-9	82403-11	82403-5	82403-10	82404-1	82404-2	82404-3
SIO2	0.09	0.08	0.07	0.09	0.09	0.08	0.07	0.13	0.12	0.11
TIO2	26.84	26.55	26.92	25.62	25.98	25.44	25.83	21.34	21.89	21.96
AL2O3	1.50	1.55	1.54	1.56	1.57	1.54	1.55	2.27	2.24	2.40
CR2O3		0.01	0.01	0.01			0.01	0.01		0.01
FEOT	68.24	68.11	68.29	68.00	67.27	67.51	67.23	70.93	70.74	70.16
MNO	1.78	1.76	1.75	1.72	1.65	1.70	1.68	1.50	1.43	1.39
MGO	1.23	1.26	1.22	1.28	1.42	1.22	1.37	2.11	2.29	2.26
CAO										
TOTAL	99.68	99.32	99.84	98.27	97.97	97.48	97.73	98.31	98.70	98.30
FE2O3	16.81	17.11	16.71	18.25	17.36	18.06	17.52	26.61	25.96	25.30
FEO	53.11	52.71	53.25	51.58	51.65	51.26	51.46	46.99	47.38	47.40
NTOT	101.36	101.02	101.48	100.11	99.72	99.30	99.50	100.96	101.31	100.84
SI	0.00	0.00	0.00	0.00	0.00	0.00	0.00	0.01	0.00	0.00
TI	0.73	0.73	0.74	0.71	0.72	0.71	0.72	0.58	0.59	0.60
AL	0.06	0.07	0.07	0.07	0.07	0.07	0.07	0.10	0.09	0.10
CR										
FE3	0.46	0.47	0.46	0.51	0.48	0.51	0.49	0.73	0.71	0.69
FE2	1.62	1.61	1.62	1.59	1.59	1.59	1.59	1.43	1.43	1.44
MN	0.06	0.05	0.05	0.05	0.05	0.05	0.05	0.05	0.04	0.04
MG	0.07	0.07	0.07	0.07	0.08	0.07	0.08	0.11	0.12	0.12
CA										
FE	2.08	2.08	2.07	2.09	2.07	2.10	2.08	2.15	2.14	2.13
USP	0.77	0.77	0.77	0.75	0.76	0.75	0.76	0.62	0.63	0.64

*** ALL ZERO VALUES PRINTED AS BLANKS. ***

SAMPLE DESCRIPTION :

82403-6	CORE
82403-7	CORE
82403-8	CORE
82403-9	INTERMEDIATE
82403-11	RIM
82403-5	CORE
82403-10	RIM
82404-1	CORE
82404-2	CORE
82404-3	CORE

Table D.3. cont.

	82404-4	82404-6	82404-5	AW82023-2	AW82023-3	AW82023-4	AW82023-5	AW82023-7	AW82023-9	AW82023-10
SIO2	0.12	0.12	0.12	0.11	0.12	0.13	0.10	0.12	0.13	0.12
TIO2	21.54	21.73	21.09	21.41	21.76	21.39	20.98	21.19	21.89	21.31
AL2O3	3.35	2.75	3.24	2.30	1.75	1.38	2.23	2.55	2.54	2.14
CR2O3	0.01					0.01	0.01	0.01		
FEOT	69.43	70.03	69.44	72.41	73.11	72.45	71.76	71.25	71.77	72.08
MNO	1.36	1.47	1.32	1.43	1.44	1.43	1.48	1.41	1.39	1.43
MGO	2.45	2.22	2.25	1.25	0.82	0.91	1.15	1.57	1.66	1.38
CAO										
TOTAL	98.27	98.34	97.47	98.90	99.01	97.71	97.73	98.07	99.34	98.45
FE2O3	25.03	25.32	25.40	26.45	26.21	26.50	26.49	26.14	25.68	26.57
FEO	46.91	47.25	46.58	48.61	49.53	48.61	47.92	47.73	48.66	48.17
NTOT	100.77	100.87	100.01	101.56	101.63	100.35	100.36	100.72	101.95	101.12
SI	0.00	0.00	0.00	0.00	0.00	0.01	0.00	0.00	0.01	0.00
TI	0.58	0.59	0.58	0.59	0.60	0.60	0.58	0.58	0.59	0.59
AL	0.14	0.12	0.14	0.10	0.08	0.06	0.10	0.11	0.11	0.09
CR										
FE3	0.68	0.69	0.70	0.72	0.72	0.74	0.73	0.72	0.70	0.73
FE2	1.42	1.43	1.42	1.48	1.51	1.51	1.47	1.46	1.47	1.47
MN	0.04	0.04	0.04	0.04	0.04	0.04	0.05	0.04	0.04	0.04
MG	0.13	0.12	0.12	0.07	0.04	0.05	0.06	0.08	0.09	0.08
CA										
FE	2.10	2.12	2.12	2.20	2.23	2.25	2.21	2.18	2.16	2.20
USP	0.65	0.64	0.64	0.63	0.63	0.62	0.63	0.63	0.64	0.63

*** ALL ZERO VALUES PRINTED AS BLANKS. ***

SAMPLE DESCRIPTION :

82404-4	:	CORE
82404-6	:	CORE
82404-5	:	CORE
AW82023-2	:	CORE
AW82023-3	:	CORE
AW82023-4	:	CORE
AW82023-5	:	CORE
AW82023-7	:	CORE
AW82023-9	:	CORE
AW82023-10	:	RIM

Table D.3. cont.

	AW82023-11	AW82023-12	AW82023-13	AW82023-1	AW82023-6	AW82023-8
SIO2	0.14	0.14	0.13	0.11	0.14	0.20
TIO2	21.58	21.27	21.63	20.94	20.45	20.66
AL2O3	1.50	1.60	1.56	2.58	1.71	2.33
CR2O3	0.01		0.01	0.01	0.01	
FEOT	72.63	72.69	72.67	71.68	72.01	70.83
MNO	1.39	1.48	1.45	1.29	1.47	1.33
MGO	0.74	0.93	0.70	1.39	0.90	1.41
CAO						
TOTAL	97.99	98.11	98.13	97.98	96.69	96.74
FE2O3	26.04	26.77	25.98	26.46	27.25	26.24
FEO	49.20	48.60	49.29	47.87	47.49	47.22
NTOT	100.60	100.79	100.74	100.64	99.42	99.40
SI	0.01	0.01	0.01	0.00	0.01	0.01
TI	0.60	0.59	0.60	0.58	0.57	0.58
AL	0.07	0.07	0.07	0.11	0.08	0.10
CR						
FE3	0.73	0.74	0.72	0.73	0.77	0.73
FE2	1.52	1.50	1.52	1.46	1.48	1.46
MN	0.04	0.05	0.04	0.04	0.05	0.04
MG	0.04	0.05	0.04	0.08	0.05	0.08
CA						
FE	2.25	2.24	2.24	2.19	2.25	2.20
USP	0.63	0.62	0.63	0.63	0.61	0.62

*** ALL ZERO VALUES PRINTED AS BLANKS. ***

SAMPLE DESCRIPTION :

AW82023-11	:	GROUNDMASS
AW82023-12	:	GROUNDMASS
AW82023-13	:	GROUNDMASS
AW82023-1	:	CORE
AW82023-6	:	CORE
AW82023-8	:	CORE

Table D.4. Feldspar

	83435-1	83435-2	83435-3	83435-4	83435-5	83435-6	83435-7	83435-8	83435-9	83435-10
SIO2	51.98	51.39	51.74	51.44	52.01	51.36	53.76	52.28	52.16	51.61
AL203	30.31	29.69	30.68	30.49	30.01	30.31	28.88	30.37	30.35	30.68
FEOT *	0.70	0.57	0.65	0.66	0.56	0.63	0.56	0.64	0.60	0.59
CAO	13.64	13.05	13.89	13.58	12.59	13.40	11.85	13.57	13.19	13.99
NA2O	3.48	3.58	3.45	3.45	4.03	3.65	4.53	3.54	3.84	3.23
K2O	0.27	0.32	0.30	0.29	0.37	0.27	0.40	0.29	0.31	0.28
TOTAL	100.38	98.61	100.70	99.91	99.58	99.62	99.98	100.69	100.46	100.38
SI '	9.44	9.48	9.37	9.38	9.50	9.40	9.75	9.46	9.46	9.37
AL '	6.48	6.46	6.55	6.56	6.46	6.54	6.18	6.47	6.48	6.56
FE '	0.11	0.09	0.10	0.10	0.09	0.10	0.08	0.10	0.09	0.09
CA '	2.65	2.58	2.69	2.65	2.47	2.63	2.30	2.63	2.56	2.72
NA '	1.22	1.28	1.21	1.22	1.43	1.30	1.59	1.24	1.35	1.14
K '	0.06	0.08	0.07	0.07	0.09	0.06	0.09	0.07	0.07	0.07
AN x	67.30	65.60	67.80	67.40	61.90	65.90	57.70	66.70	64.30	69.40
AB x	31.10	32.50	30.50	31.00	35.90	32.50	40.00	31.50	33.90	29.00
OR x	1.60	1.90	1.70	1.70	2.20	1.60	2.30	1.70	1.80	1.70

*Total Fe analyzed as FeO

' No. of cations on the basis of 32 (0).

x Feldspar endmembers (mol. %)

SAMPLE DESCRIPTION :

83435-1	MICROPHENOCRYST
83435-2	GROUNDMASS CORE
83435-3	GROUNDMASS RIM
83435-4	GROUNDMASS CORE
83435-5	GROUNDMASS EDGE
83435-6	GROUNDMASS CORE
83435-7	GROUNDMASS RIM
83435-8	MICROPHENOCRYST RIM
83435-9	MICROPHENOCRYST INT.
83435-10	MICROPHENOCRYST CORE

Table D.4. cont.

	83435-11	83435-12	83435-13	83435-14	83435-15	83435-16	83435-17	83435-18	79300-1	79300-2
SIO2	51.76	52.82	51.16	52.01	52.10	51.54	51.97	53.06	52.85	51.02
AL2O3	30.49	29.66	30.13	30.23	29.90	30.50	30.24	30.16	30.56	30.74
FEOT	0.71	0.61	0.76	0.80	0.83	0.66	0.58	0.59	0.45	0.38
CAO	13.56	12.56	13.51	12.99	13.52	13.98	13.63	12.70	13.33	14.24
NA2O	3.46	3.93	3.59	3.68	3.59	3.37	3.48	3.89	3.60	3.26
K2O	0.28	0.37	0.30	0.34	0.31	0.27	0.27	0.37	0.27	0.23
TOTAL	100.27	99.94	99.47	100.04	100.23	100.32	100.18	100.76	101.07	99.88
SI	9.41	9.60	9.39	9.47	9.48	9.37	9.45	9.56		
AL	6.53	6.35	6.52	6.48	6.41	6.54	6.48	6.41		
FE	0.11	0.09	0.12	0.12	0.13	0.10	0.09	0.09		
CA	2.64	2.44	2.66	2.53	2.63	2.72	2.65	2.45		
NA	1.22	1.39	1.28	1.30	1.27	1.19	1.23	1.36		
K	0.07	0.08	0.07	0.08	0.07	0.06	0.06	0.08		
AN	67.30	62.40	66.30	64.80	66.30	68.50	67.30	62.90	66.10	69.70
AB	31.10	35.40	31.90	33.20	31.90	29.90	31.10	34.90	32.30	28.90
OR	1.70	2.20	1.80	2.00	1.80	1.60	1.60	2.20	1.60	1.30

*** ALL ZERO VALUES PRINTED AS BLANKS. ***

SAMPLE DESCRIPTION :

83435-11	:	MICROPHENOCRYST CORE
83435-12	:	MICROPHENOCRYST RIM
83435-13	:	GROUNDMASS
83435-14	:	GROUNDMASS
83435-15	:	GROUNDMASS
83435-16	:	MICROPHENOCRYST CORE
83435-17	:	MICROPHENOCRYST INT.
83435-18	:	MICROPHENOCRYST EDGE
79300-1	:	EXTREME EDGE
79300-2	:	INTERMEDIATE

Table D.4. cont.

	79300-3	79300-4	79300-5	79300-6	79300-7	79300-8	79300-10	79300-11	79300-12	79300-13
SIO2	51.11	51.40	51.08	50.97	51.65	51.39	50.58	50.88	51.93	51.95
AL2O3	31.02	31.23	31.03	31.01	30.47	30.48	30.98	30.58	30.76	30.31
FEOT	0.50	0.40	0.43	0.41	0.44	0.49	0.43	0.41	0.52	0.55
CAO	14.11	13.90	14.22	14.01	13.84	13.98	14.52	13.97	13.55	13.26
NA2O	3.15	3.27	3.10	3.26	3.09	3.22	2.99	3.27	3.48	3.56
K2O	0.23	0.20	0.20	0.22	0.21	0.25	0.20	0.24	0.25	0.31
TOTAL	100.12	100.40	100.05	99.89	99.71	99.81	99.70	99.34	100.48	99.95
AN	70.3	69.3	70.9	69.5	70.3	69.6	72.0	69.3	67.3	66.1
AB	28.4	29.5	28.0	29.2	28.4	29.0	26.8	29.3	31.2	32.1
OR	1.4	1.2	1.2	1.3	1.3	1.5	1.2	1.4	1.5	1.8

*** ALL ZERO VALUES PRINTED AS BLANKS. ***

SAMPLE DESCRIPTION :

79300-3	CORE
79300-4	INTERMEDIATE
79300-5	INTERMEDIATE
79300-6	INTERMEDIATE
79300-7	INTERMEDIATE
79300-8	EDGE
79300-10	INTERMEDIATE
79300-11	CORE
79300-12	EXTREME EDGE
79300-13	GROUNDMASS

	79300-14	79300-15	79300-17	79300-18	79300-19	AW82038-1	AW82038-2	AW82038-3	AW82038-4	Aw82038-5
SIO2	52.57	51.50	52.46	52.73	51.92	51.98	51.38	54.65	54.84	56.63
AL2O3	29.56	29.56	29.80	29.31	29.35	30.27	29.13	29.05	29.00	27.67
FEOT	0.89	0.68	1.83	0.68	0.60	0.24	0.20	0.26	0.30	0.27
CAO	12.46	12.70	11.91	12.56	13.08	13.10	11.77	11.81	11.48	10.19
NA2O	4.09	3.90	4.46	3.95	3.69	3.36	4.28	4.38	4.47	5.03
K2O	0.34	0.34	1.31	0.33	0.27	0.33	0.49	0.50	0.53	0.70
TOTAL	99.92	98.69	101.76	99.57	98.91	99.28	100.24	100.64	100.63	100.49
AN	61.5	63.0	55.3	62.5	65.2	66.9	58.5	58.1	56.8	50.6
AB	36.5	35.0	37.5	35.5	33.2	31.1	38.6	39.0	40.0	45.2
OR	2.0	2.0	7.2	2.0	1.6	2.0	2.9	2.9	3.1	4.1

*** ALL ZERO VALUES PRINTED AS BLANKS. ***

SAMPLE DESCRIPTION :

79300-14	GROUNDMASS
79300-15	GROUNDMASS
79300-17	GROUNDMASS
79300-18	GROUNDMASS CORE
79300-19	GROUNDMASS RIM
AW82038-1	CORE
AW82038-2	INTERMEDIATE
AW82038-3	INTERMEDIATE
AW82038-4	INTERMEDIATE
AW82038-5	RIM

Table D.4. cont.

	AW82038-6	AW82038-7	AW82038-8	AW82038-10	AW82038-11	AW82038-12	AW82038-13	AW82038-14	AW82038-15	AW82038-16
SIO2	56.00	54.85	53.61	54.49	54.38	54.75	55.83	56.32	55.90	55.00
AL2O3	27.73	28.06	29.33	28.92	28.22	28.22	27.92	27.26	27.50	28.49
FEOT	0.41	0.22	0.31	0.20	0.28	0.29	0.50	0.53		
CAO	10.30	10.82	11.94	11.73	11.00	10.89	10.46	9.80	10.17	11.00
NA2O	4.69	4.65	4.36	4.28	4.68	4.74	4.96	5.09	5.04	4.76
K2O	0.98	0.57	0.49	0.50	0.56	0.59	0.65	0.68	0.82	0.81
TOTAL	100.12	99.16	100.04	100.13	99.11	99.49	100.31	99.68	99.42	100.05
AN	51.6	54.3	58.5	58.5	54.6	54.0	51.8	49.5	50.2	53.5
AB	42.5	42.3	38.6	38.6	42.1	42.6	44.4	46.4	45.0	41.8
OR	5.9	3.4	2.9	2.9	3.3	3.5	3.8	4.1	4.8	4.7

*** ALL ZERO VALUES PRINTED AS BLANKS. ***

SAMPLE DESCRIPTION :

AW82038-6	:	EXTREME EDGE
AW82038-7	:	RIM
AW82038-8	:	INTERMEDIATE
AW82038-10	:	INTERMEDIATE
AW82038-11	:	INCLUSION RIM
AW82038-12	:	INCLUSION CORE
AW82038-13	:	GROUNDMASS
AW82038-14	:	GROUNDMASS
AW82038-15	:	CORE
AW82038-16	:	EDGE

	AW82038-18	AW82038-19	AW82038-20	83415-5	83415-2	83415-3	83415-4	83415-5	83415-6	83415-7
SIO2	55.50	55.40	56.02	59.84	57.70	56.30	55.85	54.83	55.55	57.25
AL2O3	28.04	27.38	27.69	24.92	27.48	27.23	27.29	27.90	27.68	26.77
FEOT	0.50	0.35	0.32	0.31	0.41	0.29	0.19	0.31	0.23	0.22
CAO	10.83	10.42	10.47	7.27	9.51	9.48	9.88	10.11	10.37	9.03
NA2O	4.70	4.87	4.94	6.39	5.39	5.31	5.40	5.06	5.20	5.51
K2O	0.58	0.65	0.66	0.92	0.67	0.72	0.72	0.62	0.65	0.76
TOTAL	100.15	99.08	100.10	99.64	101.13	99.34	99.33	98.82	99.67	99.54
AN	54.1	52.1	51.9	36.5	47.4	47.5	48.2	50.5	50.4	45.4
AB	42.5	44.1	44.3	58.0	48.6	48.2	47.6	45.8	45.8	50.1
OR	3.4	3.9	3.9	5.5	4.0	4.3	4.2	3.7	3.8	4.6

*** ALL ZERO VALUES PRINTED AS BLANKS. ***

SAMPLE DESCRIPTION :

AW82038-18	:	GROUNDMASS
AW82038-19	:	MICROPHENOCRYST
AW82038-20	:	MICROPHENOCRYST
83415-5	:	EXTREME EDGE
83415-2	:	INTERMEDIATE
83415-3	:	INTERMEDIATE
83415-4	:	INTERMEDIATE
83415-5	:	INTERMEDIATE
83415-6	:	INTERMEDIATE
83415-7	:	INTERMEDIATE

Table D.4. cont.

	83415-8	83415-9	83415-10	83415-AVE	83415-1B	83415-2B	83415-AVE	83415-1C	83415-2C	83415-3C
SIO2	57.56	58.90	57.05	57.08	56.17	58.06	57.12	56.08	55.90	55.06
AL2O3	26.61	26.29	26.91	26.91	27.28	26.46	26.87	28.14	27.13	27.97
FEOT	0.26	0.24	0.17	0.26	0.37	0.29	0.33	0.18	0.21	0.37
CAO	9.07	8.34	9.23	9.23	10.03	8.94	9.48	10.18	10.50	10.54
NA2O	5.54	5.68	5.41	5.49	5.03	5.37	5.20	4.97	5.04	4.98
K2O	0.79	0.96	0.76	0.76	0.61	0.70	0.66	0.57	0.67	0.47
TOTAL	99.84	100.41	99.53	99.73	99.48	99.82	99.65	100.11	99.45	99.40
AN	45.2	42.2	46.3	46.0	50.5	45.8	48.2	51.3	51.5	52.4
AB	50.0	52.0	49.1	49.5	45.8	49.9	47.8	45.3	44.7	44.8
OR	4.7	5.8	4.6	4.5	3.7	4.3	4.0	3.4	3.9	2.8

*** ALL ZERO VALUES PRINTED AS BLANKS. ***

SAMPLE DESCRIPTION :

83415-8	: CORE
83415-9	: CORE
83415-10	: CORE
83415-AVE	: PHENOCRYST AVE.
83415-1B	: GROUNDMASS EDGE
83415-2B	: GROUNDMASS CORE
83415-AVE	: GROUNDMASS AVE.
83415-1C	: CORE
83415-2C	: INTERMEDIATE
83415-3C	: EDGE

	83415-AVE	83415-1D	83415-2D	83415-3D	83415-4D	83415-AVE	83417-1	83417-1B	83417-3	83417-4
SIO2	55.68	56.10	57.55	55.59	55.66	56.23	57.63	58.17	59.30	59.57
AL2O3	27.75	27.34	26.58	27.97	27.70	27.40	26.29	25.61	25.29	25.48
FEOT	0.25	0.35	0.43	0.51	0.45	0.44	0.34	0.18	0.26	0.24
CAO	10.41	9.91	8.95	10.28	10.02	9.79	8.59	7.79	7.58	7.36
NA2O	5.00	5.17	5.53	4.98	5.10	5.20	5.76	5.94	6.19	6.14
K2O	0.57	0.63	0.70	0.57	0.63	0.63	0.58	0.96	0.99	1.15
TOTAL	99.65	99.51	99.75	99.90	99.57	99.68	99.19	98.63	99.58	99.92
AN	51.7	49.5	45.2	51.5	50.1	49.1	43.6	39.6	38.0	37.1
AB	44.9	46.7	50.6	45.1	46.2	47.1	52.9	54.6	56.1	56.0
OR	3.4	3.8	4.2	3.4	3.7	3.8	3.5	5.8	5.9	6.9

*** ALL ZERO VALUES PRINTED AS BLANKS. ***

SAMPLE DESCRIPTION :

83415-AVE	: PHENOCRYST AVE.
83415-1D	: GROUNDMASS
83415-2D	: GROUNDMASS
83415-3D	: GROUNDMASS
83415-4D	: GROUNDMASS
83415-AVE	: GROUNDMASS AVE
83417-1	: EXTREME EDGE
83417-1B	: INTERMEDIATE
83417-3	: CORE
83417-4	: INTERMEDIATE

Table D.4. cont.

	83417-5	83417-6	83417-7	83417-8	83417-9	83417-AVE	83417-3C	83417-5C	83417-6C	83417-7C
SIO2	60.33	57.30	59.75	58.36	59.14	58.99	65.29	58.50	58.23	58.58
AL2O3	24.62	26.42	25.35	25.52	25.54	25.48	19.12	25.95	26.51	26.56
FEOT	0.34	0.31	0.22	0.23	0.22	0.25	0.29	0.41	0.27	0.24
CAO	6.34	8.80	7.31	7.78	7.61	7.57	0.66	8.54	8.88	8.85
NA2O	7.14	5.57	6.13	5.94	6.24	6.16	5.43	6.25	5.80	5.68
K2O	0.56	0.80	1.07	0.92	0.87	0.91	7.52	0.49	0.66	0.78
TOTAL	99.32	99.22	99.82	98.74	99.61	99.37	98.29	100.14	100.34	100.68
AN	31.8	44.4	37.2	39.6	38.2	39.2	3.4	41.8	44.0	44.1
AB	64.8	50.8	56.4	54.8	56.6	56.3	50.6	55.3	52.0	51.2
OR	3.3	4.8	6.4	5.6	5.2	5.5	46.1	2.9	3.9	4.6

*** ALL ZERO VALUES PRINTED AS BLANKS. ***

SAMPLE DESCRIPTION :

83417-5	: EXTREME EDGE
83417-6	: EDGE
83417-7	: INTERMEDIATE
83417-8	: CORE
83417-9	: CORE
83417-AVE	: PHENOCRYST AVE.
83417-3C	: GROUNDMASS
83417-5C	: GROUNDMASS
83417-6C	: EDGE
83417-7C	: INTERMEDIATE

	83417-8C	83417-9C	83417-10C	83417-13C	25748-K27°	25748-K28	25748-K29	25748-K30	25748-K31	25748-K32
SIO2	58.00	57.73	64.92	58.11	59.54	59.92	58.90	59.29	60.17	59.76
AL2O3	26.38	26.57	20.25	26.45	25.19	25.18	25.78	26.10	25.63	25.81
FEOT	0.21	0.18	0.28	0.18	0.35	0.36	0.39	0.36	0.29	0.37
CAO	8.69	8.61	0.42	8.57	7.02	6.72	7.60	7.65	7.02	7.25
NA2O	5.51	5.74	4.57	5.91	6.60	6.69	6.47	6.42	6.67	6.59
K2O	0.89	0.91	9.98	0.74	1.37	1.38	1.19	1.16	1.33	1.22
TOTAL	99.68	99.74	100.41	99.96	100.07	100.25	100.33	100.98	101.11	101.00
AN	44.1	42.8	2.0	42.6	34.1	32.8	36.7	37.1	33.9	35.2
AB	50.5	51.7	40.2	53.1	58.0	59.1	56.5	56.3	58.4	57.8
OR	5.4	5.4	57.8	4.4	7.9	8.0	6.9	6.7	7.7	7.0

*** ALL ZERO VALUES PRINTED AS BLANKS. ***

°Kyle (unpubl.)

SAMPLE DESCRIPTION :

83417-8C	: INTERMEDIATE
83417-9C	: CORE
83417-10C	: GROUNDMASS
83417-13C	: MICROPHENOCRYST
25748-K27	: CORE
25748-K28	: INTERMEDIATE
25748-K29	: INTERMEDIATE
25748-K30	: RIM
25748-K31	: CORE
25748-K32	: INTERMEDIATE

Table D.4. cont.

	25748-K33	25748-K34	25748-K35	25748-K36	25748-K37	25748-K39	25748-K40	25748-41	25748-K42	25748-K43
SIO2	59.16	59.82	59.92	60.63	60.56	62.09	62.43	60.91	60.40	60.18
AL2O3	25.74	25.49	25.44	25.00	25.54	23.32	23.10	24.19	24.79	24.98
FEOT	0.35	0.46	0.36	0.39	0.53	0.38	0.35	1.08	0.38	0.41
CAO	7.10	6.79	6.65	6.12	6.52	4.59	4.33	5.42	6.43	6.62
NA2O	6.55	6.67	6.66	6.69	6.54	7.03	7.02	6.67	6.83	6.62
K2O	1.31	1.30	1.46	1.73	1.57	2.80	3.08	2.08	1.63	1.53
TOTAL	100.21	100.53	100.49	100.56	101.26	100.21	100.31	100.35	100.46	100.34
AN	34.6	33.3	32.6	30.2	32.2	22.2	20.9	27.1	31.0	32.4
AB	57.8	59.2	59.0	59.7	58.5	61.6	61.3	60.5	59.6	58.7
OR	7.6	7.6	8.5	10.1	9.2	16.1	17.7	12.4	9.4	8.9

*** ALL ZERO VALUES PRINTED AS BLANKS. ***

SAMPLE DESCRIPTION :

25748-K33	: INTERMEDIATE
25748-K34	: RIM
25748-K35	: RIM
25748-K36	: CORE
25748-K37	: RIM
25748-K39	: CORE
25748-K40	: INTERMEDIATE
25748-41	: RIM
25748-K42	: CORE
25748-K43	: INTERMEDIATE

	25748-K44	25748-1	25748-3	25748-4	25748-5	25748-6	25748-7	25748-8	25748-9	25748-10
SIO2	60.46	59.86	59.18	58.08	58.39	58.77	58.18	59.32	57.79	58.07
AL2O3	24.68	25.28	25.47	26.07	26.73	26.28	26.59	26.55	26.72	26.34
FEOT	0.50	0.24	0.22	0.20	0.27	0.23	0.25	0.16	0.24	0.18
CAO	6.69	6.48	6.97	7.61	8.40	7.77	8.08	7.96	8.55	8.11
NA2O	6.63	6.91	6.98	6.26	6.30	6.56	6.23	6.56	6.45	6.48
K2O	1.32	1.72	1.58	1.26	1.09	1.18	1.11	1.17	1.09	1.16
TOTAL	100.28	100.47	100.38	99.47	101.19	100.78	100.44	101.72	100.84	100.33
AN	33.0	30.8	32.5	37.2	39.8	36.9	39.0	37.5	39.7	38.2
AB	59.2	59.5	58.8	55.4	54.1	56.4	54.5	55.9	54.3	55.3
OR	7.8	9.7	8.7	7.4	6.1	6.7	6.4	6.6	6.0	6.5

*** ALL ZERO VALUES PRINTED AS BLANKS. ***

SAMPLE DESCRIPTION :

25748-K44	: RIM
25748-1	: EDGE
25748-3	: INTERMEDIATE
25748-4	: INTERMEDIATE
25748-5	: INTERMEDIATE
25748-6	: CORE
25748-7	: INTERMEDIATE
25748-8	: INTERMEDIATE
25748-9	: INTERMEDIATE
25748-10	: INTERMEDIATE

Table D.4. cont.

	25748-11	25748-12	25748-13	25748-15	25748-20	25748-21	25748-24	25748-25	25748-26	25748-27
SIO2	58.76	59.90	60.65	60.58	61.58	61.29	58.69	58.33	58.16	57.60
AL2O3	26.89	25.17	24.99	25.18	23.93	23.83	25.47	26.99	27.01	26.94
FEOT	0.22	0.25	0.23	0.19	0.24	0.21	0.30	0.22	0.24	0.20
CAO	8.61	6.62	6.55	6.31	4.91	5.06	7.26	8.82	8.84	8.67
NA2O	6.39	6.99	6.64	6.85	7.35	7.24	6.97	6.29	6.19	6.11
K2O	1.04	1.62	1.60	1.66	2.77	2.75	1.29	0.94	0.93	0.99
TOTAL	101.91	100.55	100.65	100.74	100.76	100.37	99.97	101.51	101.38	100.50
AN	40.2	31.2	32.0	30.5	22.8	23.6	33.9	41.4	41.8	41.5
AB	54.0	59.7	58.7	59.9	61.9	61.1	58.9	53.4	53.0	52.9
OR	5.8	9.1	9.3	9.5	15.3	15.3	7.2	5.3	5.2	5.6

*** ALL ZERO VALUES PRINTED AS BLANKS. ***

SAMPLE DESCRIPTION :

25748-11	INTERMEDIATE
25748-12	INTERMEDIATE
25748-13	INTERMEDIATE
25748-15	INTERMEDIATE
25748-20	EDGE
25748-21	EDGE
25748-24	CORE
25748-25	INTERMEDIATE
25748-26	INTERMEDIATE
25748-27	INTERMEDIATE

	25748-28	25748-29	25748-30	25748-34	25748-35	25748-36	25748-38	25748-39	25748-40	25748-48
SIO2	58.56	59.79	58.46	57.80	58.00	59.60	59.17	59.48	58.06	58.87
AL2O3	26.80	26.08	26.09	25.94	26.40	25.32	25.72	25.47	26.26	25.41
FEOT	0.25	0.25	0.28	0.24	0.26	0.24	0.27	0.29	0.37	0.38
CAO	8.27	7.34	7.82	7.44	7.84	6.93	7.48	6.82	7.89	6.69
NA2O	6.67	6.91	6.55	6.56	6.55	6.65	6.77	6.90	6.50	7.29
K2O	1.10	1.31	1.21	1.28	1.21	1.46	1.40	1.53	1.14	1.49
TOTAL	101.66	101.67	100.40	99.25	100.23	100.19	100.79	100.48	100.20	100.11
AN	38.2	34.3	37.0	35.7	37.1	33.5	35.0	32.3	37.6	30.9
AB	55.7	58.4	56.1	57.0	56.1	58.1	57.2	59.1	56.0	60.9
OR	6.1	7.3	6.8	7.3	6.8	8.4	7.8	8.6	6.5	8.2

*** ALL ZERO VALUES PRINTED AS BLANKS. ***

SAMPLE DESCRIPTION :

25748-28	INTERMEDIATE
25748-29	EDGE
25748-30	CORE
25748-34	GROUNDMASS CORE
25748-35	GROUNDMASS CORE
25748-36	GROUNDMASS CORE
25748-38	GROUNDMASS RIM
25748-39	GROUNDMASS
25748-40	GROUNDMASS
25748-48	GROUNDMASS

Table D.4. cont.

	83448-1	83448-2	83448-3	83448-4	83448-5	83448-6	83448-7	83448-AVE.	83448-8	83449-9
SIO2	62.22	63.22	63.79	63.35	63.24	62.40	62.75	63.13	63.30	63.02
AL2O3	23.19	22.30	22.19	22.41	22.36	23.04	22.52	22.47	22.19	22.37
FEOT	0.22	0.12	0.24	0.15	0.16	0.16	0.15	0.16	0.34	0.29
CAO	4.89	3.64	3.59	3.88	3.99	4.52	3.81	3.90	3.29	3.64
NA2O	7.37	7.51	7.31	7.33	7.30	7.15	7.27	7.31	7.26	7.08
K2O	1.92	2.87	2.75	2.56	2.49	2.20	2.74	2.60	3.04	2.82
TOTAL	99.80	99.65	99.84	99.67	99.53	99.46	99.23	99.58	99.41	99.21
AN	23.8	17.6	17.9	19.2	19.8	22.5	18.8	19.3	16.4	18.4
AB	65.0	65.8	65.8	65.7	65.5	64.5	65.1	65.4	65.5	64.7
OR	11.1	16.5	16.3	15.1	14.7	13.0	16.1	15.3	18.1	16.9

*** ALL ZERO VALUES PRINTED AS BLANKS. ***

SAMPLE DESCRIPTION :

83448-1	EDGE
83448-2	INTERMEDIATE
83448-3	INTERMEDIATE
83448-4	INTERMEDIATE
83448-5	INTERMEDIATE
83448-6	INTERMEDIATE
83448-7	CORE
83448-AVE.	PHENOCRYST AVE.
83448-8	GROUNDMASS
83449-9	GROUNDMASS

	83448-10	83448-11	83448-12	83448-13	83448-14	83448-15	83448-16	83448-20	83448-21	83400-1
SIO2	65.03	63.71	63.73	66.10	61.69	63.06	62.67	63.09	65.11	62.76
AL2O3	19.54	22.50	22.16	19.50	23.44	22.85	23.14	22.28	20.15	21.83
FEOT	0.20	0.33	0.31	0.21	0.30	0.21	0.13	0.28	0.26	0.15
CAO	0.82	3.62	3.28	1.05	5.12	4.36	4.71	3.48	1.55	3.82
NA2O	6.25	7.48	7.32	6.47	7.26	7.29	7.35	7.59	6.70	7.05
K2O	6.77	2.34	3.04	6.31	1.73	2.18	2.07	2.64	5.02	2.54
TOTAL	98.59	99.97	99.83	99.62	99.52	99.93	100.06	99.35	98.77	98.15
AN	4.0	10.2	10.3	5.2	25.2	21.7	23.0	17.1	7.9	19.5
AB	56.0	67.9	65.8	57.8	64.7	65.5	65.0	67.5	61.7	65.1
OR	39.9	14.0	18.0	37.1	10.1	12.9	12.0	15.4	30.4	15.4

*** ALL ZERO VALUES PRINTED AS BLANKS. ***

SAMPLE DESCRIPTION :

83448-10	GROUNDMASS
83448-11	GROUNDMASS
83448-12	GROUNDMASS
83448-13	PHENOCRYST OVERGROWTH
83448-14	EDGE
83448-15	INTERMEDIATE
83448-16	CORE
83448-20	GROUNDMASS
83448-21	GROUNDMASS
83400-1	CORE

Table D.4. cont.

	83400-2	83400-3	83400-4	83400-5	83400-6	83400-11	83400-8	83448-9	83400-10	83400-11
SIO2	62.72	63.91	63.34	63.90	64.14	66.73	67.37	65.10	64.02	66.81
AL2O3	22.07	22.01	21.97	22.35	21.99	19.46	19.14	21.51	22.08	19.95
FEOT	0.14	0.18	0.13	0.16	0.15	0.22	0.09	0.35	0.27	0.17
CAO	3.78	3.38	3.66	3.53	3.57	0.69	0.64	2.55	3.30	1.26
NA2O	7.34	7.41	7.59	7.44	7.85	6.36	6.56	7.92	8.29	7.42
K2O	2.69	2.66	2.57	2.58	1.81	6.23	6.06	2.14	1.44	4.47
TOTAL	98.74	99.59	99.25	99.95	99.51	99.67	99.86	99.56	99.41	100.07
AN	18.6	16.9	17.9	17.6	17.9	3.5	3.3	13.1	16.5	6.3
AB	65.6	67.2	67.2	67.1	71.3	58.7	60.2	73.7	74.9	67.1
OR	15.8	15.9	14.9	15.3	10.8	37.8	36.6	13.1	8.6	26.6

*** ALL ZERO VALUES PRINTED AS BLANKS. ***

SAMPLE DESCRIPTION :

83400-2	:	CORE
83400-3	:	INTERMEDIATE
83400-4	:	INTERMEDIATE
83400-5	:	INTERMEDIATE
83400-6	:	EDGE
83400-11	:	OVERGROWTH
83400-8	:	GROUNDMASS
83448-9	:	MICROPHENOCRYST RIM
83400-10	:	MICROPHENOCRYST CORE
83400-11	:	GROUNDMASS

	83400-15	83400-1B	83400-2B	83400-4B	80020-1	80020-2	83400-3	80020-4	80020-5	80020-6
SIO2	67.56	68.04	67.21	67.86	64.72	63.31	64.09	66.02	63.47	64.75
AL2O3	19.73	20.77	18.70	19.20	20.86	21.50	21.29	21.16	21.95	20.82
FEOT	0.42	0.25	0.23	0.26	0.16	0.25	0.16	0.15	0.13	0.28
CAO	0.74	1.87	0.56	0.14	2.22	2.94	2.64	2.54	3.48	1.95
NA2O	7.34	6.27	4.75	5.62	7.31	7.28	7.55	7.54	7.37	7.21
K2O	4.97	3.66	8.97	7.94	3.71	3.22	3.49	3.28	2.50	4.17
TOTAL	100.75	100.85	100.41	101.03	98.98	98.99	99.21	100.69	98.89	99.18
AN	3.7	10.6	2.8	0.7	11.2	14.7	12.9	12.6	17.6	9.8
AB	66.6	64.6	43.3	51.5	66.6	66.0	66.8	67.9	67.4	65.3
OR	29.7	24.8	53.9	47.8	22.2	19.2	20.3	19.5	15.0	24.9

*** ALL ZERO VALUES PRINTED AS BLANKS. ***

SAMPLE DESCRIPTION :

83400-15	:	GROUNDMASS
83400-1B	:	GROUNDMASS
83400-2B	:	GROUNDMASS
83400-4B	:	GROUNDMASS
80020-1	:	CORE
80020-2	:	CORE
83400-3	:	INTERMEDIATE
80020-4	:	INTERMEDIATE
80020-5	:	RIM
80020-6	:	EXTREME EDGE

Table D.4. cont.

	83400-7	80020-8	80020-9	80020-10	80020-11	80020-12	80020-13	80020-14	82403-1	82403-2
SIO2	65.29	64.12	64.01	65.64	64.75	63.88	63.66	62.18	63.99	62.44
AL2O3	21.23	22.04	22.39	20.83	22.17	21.88	22.08	23.46	22.35	23.07
FEOT	0.13	0.24	0.20	0.19	0.55	0.39	0.35	0.38	0.15	0.03
CAO	2.67	3.47	3.49	2.06	3.39	3.36	3.20	4.38	3.88	4.76
NA2O	7.48	7.46	7.58	7.39	7.53	7.55	7.64	7.32	7.91	7.59
K2O	3.34	2.77	2.80	4.10	2.58	3.03	2.71	2.34	1.61	1.24
TOTAL	100.23	100.09	100.45	100.20	100.96	100.07	99.63	100.03	99.87	99.12
AN	13.2	17.1	17.0	10.1	16.9	16.3	15.8	21.5	19.3	23.8
AB	67.1	66.6	66.8	65.8	67.9	66.2	68.2	64.9	71.2	68.8
OR	19.7	16.3	16.2	24.0	15.3	17.5	16.0	13.6	9.5	7.4

*** ALL ZERO VALUES PRINTED AS BLANKS. ***

SAMPLE DESCRIPTION :

83400-7	INTERMEDIATE
80020-8	CORE
80020-9	INTERMEDIATE
80020-10	EDGE
80020-11	INTERSTITIAL IN OL PHENOCRYST
80020-12	GROUNDMASS
80020-13	GROUNDMASS
80020-14	GROUNDMASS
82403-1	EDGE
82403-2	INTERMEDIATE

	82403-3	82403-5	82403-6	82403-7	82403-9	82403-10	82403-12	82431-5	82431-6	82431-8
SIO2	63.12	62.15	62.30	62.29	62.50	62.16	64.33	59.09	58.92	58.72
AL2O3	23.00	23.37	23.38	23.84	23.46	23.87	22.40	25.33	25.28	25.16
FEOT	0.09	0.08	0.06	0.11	0.10	0.14	0.14	0.29	0.30	0.42
CAO	4.59	4.43	4.73	5.45	5.15	5.54	3.73	7.12	7.46	7.42
NA2O	7.51	7.56	7.46	7.28	7.27	7.37	7.70	6.55	6.36	6.52
K2O	1.29	1.27	1.09	1.00	1.08	0.97	1.67	0.86	0.84	0.86
TOTAL	99.58	98.84	99.01	99.95	99.56	100.02	99.96	99.22	99.15	99.09
AN	23.3	22.6	24.2	27.5	26.3	27.7	19.0	35.6	37.4	36.7
AB	68.9	69.7	69.1	66.5	67.1	66.6	70.9	59.2	57.6	58.3
OR	7.8	7.7	6.6	6.0	6.6	5.7	10.1	5.1	5.0	5.0

*** ALL ZERO VALUES PRINTED AS BLANKS. ***

SAMPLE DESCRIPTION :

82403-3	CORE
82403-5	EDGE
82403-6	INTERMEDIATE
82403-7	INTERMEDIATE
82403-9	EDGE
82403-10	INTERMEDIATE
82403-12	MICROPHENOCRYST
82431-5	CORE
82431-6	INTERMEDIATE
82431-8	RIM

Table D.4. cont.

	82431-9	82431-16	82431-19	82431-20	82431-21	82431-22	82431-23	82431-24	AW82023-1	AW82023-2
SIO2	63.16	59.67	58.99	63.91	62.62	63.19	61.31	64.04	59.57	58.89
AL2O3	21.83	24.97	25.26	21.99	22.43	21.37	23.04	21.35	25.73	25.43
FEOT	2.01	0.62	0.50	0.82	0.89	0.74	0.53	0.73	0.33	0.35
CAO	1.83	7.29	7.45	4.09	4.17	3.79	5.15	3.45	7.74	7.40
NA2O	6.87	6.34	6.34	7.44	7.17	7.34	7.22	7.44	6.37	6.41
K2O	3.04	0.90	0.87	2.24	2.47	2.50	1.56	2.58	0.61	0.63
TOTAL	98.72	99.78	99.39	100.47	99.74	98.92	98.81	99.58	100.33	99.10
AN	10.2	36.8	37.3	20.2	20.8	18.9	25.7	17.3	38.7	37.5
AB	69.5	57.9	57.5	66.6	64.6	66.3	65.1	67.4	57.7	58.7
OR	20.2	5.4	5.2	13.2	14.6	14.8	9.3	15.4	3.6	3.8

*** ALL ZERO VALUES PRINTED AS BLANKS. ***

SAMPLE DESCRIPTION :

82431-9	EDGE
82431-16	RIM
82431-19	INTERMEDIATE
82431-20	GROUNDMASS
82431-21	GROUNDMASS
82431-22	GROUNDMASS
82431-23	GROUNDMASS
82431-24	GROUNDMASS
AW82023-1	CORE
AW82023-2	EDGE

	AW82023-3	AW82023-4	AW82023-5	AW82023-6	AW82023-7	AW82023-8	AW82023-9	AW82023-10	AW82023-11	AW82023-12
SIO2	59.79	59.14	58.25	58.88	59.56	58.80	65.26	63.51	61.74	59.79
AL2O3	25.03	25.46	25.98	25.61	25.41	25.92	21.12	22.57	23.75	25.36
FEOT	0.34	0.30	0.27	0.37	0.27	0.34	0.53	0.57	0.58	0.53
CAO	7.45	7.64	7.93	7.41	6.99	7.89	3.34	4.14	6.08	7.52
NA2O	6.25	6.54	6.29	6.35	6.71	6.16	7.95	7.96	7.18	6.48
K2O	0.62	0.64	0.58	0.67	0.70	0.59	1.17	1.04	0.45	0.53
TOTAL	99.46	99.70	99.28	99.28	99.35	99.68	99.36	99.78	99.78	100.20
AN	38.2	37.8	39.7	37.6	35.0	40.0	17.4	20.9	31.0	37.9
AB	58.0	58.5	56.9	58.3	60.8	56.5	75.2	72.8	66.3	59.0
OR	3.8	3.8	3.4	4.1	4.1	3.5	7.3	6.3	2.7	3.2

*** ALL ZERO VALUES PRINTED AS BLANKS. ***

SAMPLE DESCRIPTION :

AW82023-3	CORE
AW82023-4	EDGE
AW82023-5	CORE
AW82023-6	EDGE
AW82023-7	CORE
AW82023-8	RIM
AW82023-9	GROUNDMASS
AW82023-10	GROUNDMASS
AW82023-11	GROUNDMASS
AW82023-12	GROUNDMASS

Table D.4. cont.

	AW82023-13	AW82023-14	AW82023-15	82404-1A	82404-1	82404-2	82404-3	82404-4	82404-5	82404-6
SIO2	59.05	59.58	66.96	58.44	59.40	59.57	59.71	54.73	55.73	58.80
AL2O3	25.87	24.74	19.60	25.18	25.62	25.54	25.41	28.40	28.05	25.81
FEOT	0.37	0.48	0.32	0.29	0.30	0.27	0.19	0.33	0.27	0.17
CAO	7.80	6.28	0.56	7.35	7.53	7.35	7.19	10.84	10.28	7.68
NA2O	6.25	6.88	6.61	6.24	6.46	6.54	6.40	4.83	5.12	6.15
K2O	0.58	1.28	6.08	0.82	0.70	0.76	0.76	0.40	0.41	0.68
TOTAL	99.91	99.22	100.13	98.31	99.99	100.02	99.64	99.53	99.87	99.27
AN	39.4	31.0	2.8	37.5	37.5	36.6	36.5	54.0	51.3	39.1
AB	57.1	61.5	60.5	57.6	58.3	58.9	58.8	43.6	46.2	56.7
OR	3.5	7.5	36.6	5.0	4.1	4.5	4.6	2.4	2.5	4.1

*** ALL ZERO VALUES PRINTED AS BLANKS. ***

SAMPLE DESCRIPTION :

AW82023-13	GROUNDMASS
AW82023-14	GROUNDMASS
AW82023-15	INTERSTITIAL
82404-1A	EXTREME EDGE
82404-1	EDGE
82404-2	INTERMEDIATE
82404-3	INTERMEDIATE
82404-4	CORE
82404-5	CORE
82404-6	INTERMEDIATE

	82404-7	82404-8	82404-9	82404-10	82404-12	82404-13A	82404-13B	82404-14	82404-15	82404-16
SIO2	55.56	57.06	58.89	59.19	59.13	60.21	60.93	63.25	65.53	61.11
AL2O3	28.14	26.26	25.45	25.25	25.62	24.06	24.16	23.52	21.16	24.07
FEOT	0.38	0.27	0.22	0.23	0.31	0.29	0.33	0.49	0.31	0.41
CAO	10.46	8.44	7.73	7.37	7.38	5.71	6.02	4.84	2.42	5.76
NA2O	4.98	6.12	6.40	6.38	6.24	6.86	6.67	7.20	7.07	6.93
K2O	0.40	0.62	0.75	0.73	0.76	1.16	1.23	1.71	3.54	1.10
TOTAL	99.91	98.74	99.43	99.13	99.42	98.28	99.32	101.00	100.01	99.36
AN	52.4	41.7	38.2	37.2	37.7	29.3	30.8	24.3	12.5	29.4
AB	45.2	54.7	57.3	58.4	57.7	63.6	61.7	65.5	65.9	63.9
OR	2.4	3.6	4.4	4.4	4.6	7.1	7.5	10.2	21.7	6.7

*** ALL ZERO VALUES PRINTED AS BLANKS. ***

SAMPLE DESCRIPTION :

82404-7	CORE
82404-8	INTERMEDIATE
82404-9	INTERMEDIATE
82404-10	INTERMEDIATE
82404-12	EXTREME EDGE
82404-13A	GROUNDMASS CORE
82404-13B	GROUNDMASS EDGE
82404-14	GROUNDMASS EDGE
82404-15	GROUNDMASS
82404-16	GROUNDMASS

Table D.4. cont.

	82404-17	82404-18	82404-19	82404-6B	82404-7B	82404-11 B	82404-12 B
SIO2	60.63	63.90	61.51	60.40	58.98	51.43	54.52
AL2O3	24.14	22.97	24.20	24.32	25.59	30.35	28.38
FEUT	0.49	0.43	0.31	0.38	0.29	0.36	0.36
CAO	6.29	4.39	5.53	6.03	7.50	13.03	11.01
NA2O	6.93	7.42	7.02	7.04	6.48	3.74	4.85
K2O	1.17	1.70	1.14	1.14	0.75	0.26	0.39
TOTAL	99.63	100.80	99.71	99.29	99.58	99.17	99.50
AN	31.1	22.1	28.2	29.9	37.3	64.8	54.4
AB	62.0	67.6	64.8	63.3	58.3	33.7	43.3
OR	6.9	10.2	6.9	6.7	4.4	1.5	2.3

*** ALL ZERO VALUES PRINTED AS BLANKS. ***

SAMPLE DESCRIPTION :

82404-17	: GROUNDMASS
82404-18	: GROUNDMASS
82404-19	: GROUNDMASS
82404-6B	: MICROPHENOCRYST EDGE
82404-7B	: MICROPHENOCRYST CORE
82404-11B	: XENOCRYST CORE
82404-12B	: XENOCRYST RIM

APPENDIX D continued

Part 2. Analyses of feldspars in Mt. Erebus lavas from Kyle (1976).

Table D.5. Feldspar analyses. Major elements and some trace elements by XRF (Kyle, 1976). FeO* is total Fe analyzed as FeO. Trace and rare earth elements by INAA. Analyses of FeO*, Na_2O, Cr, Rb, Ba and Th by INAA prefixed by I. Undetermined elements represented by zeros.

Sample	25754	25758	25778	25748
SiO_2	53.57	53.63	53.96	58.31
TiO_2	0.25	0.29	0.13	0.18
Al_2O_3	28.57	28.56	28.82	25.82
FeO*[3]	0.54	0.72	0.34	0.32
MnO	0.00	0.01	0.00	0.00
MgO	0.12	0.17	0.10	0.00
CaO	10.77	10.78	10.84	7.23
Na_2O	4.90	4.84	4.85	6.20
K_2O	0.66	0.70	0.50	1.34
H_2O+[1]	0.07	0.03	0.04	0.00
Total	99.45	99.73	99.58	99.40
IFeO*	0.54	0.65	0.35	0.32
INa_2O	4.86	5.85	5.02	6.46
Sc	0.3	0.3	0.1	0.1
V	0	0	0	<2[2]
Cr	0	0	0	<2[2]
ICr	<1	<1	<1	1
Ni	0	0	0	<5[2]
Cu	0	0	0	10[2]
Zn	0	0	0	8[2]
Rb	0	0	0	<1[2]
IRb	3	4	<3	5
Sr	0	0	0	2913[2]
Sb	0.02	<0.02	<0.02	0.09
Cs	0.04	0.07	<0.04	<0.04
Ba	0	0	0	518[2]
IBa	514	505	639	1365
La	14.0	16.0	15.0	27.1
Ce	20	25	21	35
Sm	0.9	1.2	0.8	1.3
Eu	2.39	2.42	3.16	4.26
Tb	0.07	0.09	0.06	0.11
Yb	<0.2	0.2	<0.2	<0.2
Lu	0.02	<0.02	<0.02	0.02
Hf	0.3	0.4	0.1	0.3
Ta	0.4	0.4	0.1	0.2
ITh	0.3	0.5	0.1	0.4
U	<1.0	<1.0	<1.0	<1.0
Feldspar endmembers (mol. %)				
An	52.7	52.9	53.6	36.1
Ab	43.4	43.0	43.4	56.0
Or	3.9	4.1	2.9	8.0

[1] LOI.
[2] Kyle (1976).

25754: Ne-hawaiite, Turks Head.
25758: Ne-hawaiite, Tryggve Point.
25778: Ne-hawaiite, Fang Ridge.
25748: Ne-benmoreite, Tent Island.

APPENDIX E

GEOCHEMISTRY

Part 1. Analyses of Mt. Erebus lavas

Geochemical analyses of the samples from Mt. Erebus are given in Table E.1. The analyses are recalculated on a dried basis, i.e. excluding H_2O-. The Erebus lineage samples appear first in the table, in order of increasing differentiation and SiO_2. The benmoreites, kaersutite phonolites and trachytes are given next, in order of increasing SiO_2. The nomenclature and location of the samples are given at the end of the table.

Major elements are given in oxide weight per cent. FeO* is total Fe analyzed as Fe_2O_3, multiplied by 0.899811 to convert to FeO. INAA determinations of total Fe as FeO, and Na_2O are given the prefix I. LOI is the loss on ignition at 1000°C. Negative LOIs are due to oxidation of Fe^{2+}. Negative H_2O-s are within analytical error. Trace elements are given in parts per million. V, Ni, Cu, Zn, Ga, Sr, Y, Zr, Nb, and Pb were determined by XRF. Sc, As, Sb, Cs, La, Ce, Nd, Sm, Eu, Tb, Yb, Lu, Hf, Ta and U were determined by INAA. Cr, Rb, Ba and Th were determined by XRF and INAA. The INAA determination of these elements have the prefix I.

Elements not determined in samples are represented by zeros. The detection limits of certain elements are prefixed by less-than symbols.

TABLE E.1. ANALYSES OF LAVAS FROM MT. EREBUS

SMPL#	83435	83437	79300	83405	83404	83432	83406	83426
SIO2	43.32	43.97	44.50	44.95	45.01	44.89	45.16	45.37
TIO2	3.78	3.75	3.69	3.46	3.47	3.20	3.32	3.10
AL203	15.38	16.65	16.77	15.93	16.06	16.96	16.31	17.27
FEO*	12.08	11.44	11.04	11.46	11.57	11.23	11.29	10.98
MNO	0.22	0.24	0.23	0.23	0.23	0.25	0.23	0.24
MGO	6.77	4.92	4.69	5.40	5.42	4.21	4.98	4.13
CAO	10.66	9.62	9.71	9.44	9.41	9.28	8.98	9.05
NA20	4.63	4.64	4.84	4.58	4.61	5.24	4.85	5.26
K20	1.72	2.07	2.15	1.90	2.02	2.07	2.01	2.13
P205	1.21	1.51	1.56	1.15	1.15	1.69	1.18	1.53
LOI	0.03	-0.44	-0.56	-0.30	-0.48	-0.13	-0.31	-0.27
TOTAL	99.82	98.36	98.61	98.19	98.47	98.88	97.99	98.78
H20-	0.18	0.01	-0.02	0.03	0.06	0.03	-0.03	0.02
IFEO	12.33	11.65	11.35	0.00	11.63	11.48	0.00	11.05
INA_2O	3.94	4.64	4.60	0.00	4.56	4.93	0.00	4.87
SC	20.30	11.13	11.18	0.00	15.46	8.82	0.00	8.15
V	291	192	179	220	215	138	190	139
CR	139	34	24	81	89	12	67	13
ICR	130	27	9	0	93	2	0	3
NI	63	13	10	34	32	<5	30	<5
CU	43	23	22	41	36	19	36	16
ZN	104	112	113	97	99	123	95	110
GA	21	22	21	22	23	22	22	23
AS	<1.0	<1.0	<1.0	0.0	<1.0	1.6	0.0	1.1
RB	41	41	41	47	46	46	50	48
IRB	44	36	41	0	44	43	0	47
SR	1100	1374	1386	1203	1195	1421	1249	1342
Y	37	41	44	38	37	45	40	43
ZR	363	347	358	379	377	427	396	403
NB	111	126	131	121	121	145	127	133
SB	0.1	0.1	0.1	0.0	0.2	0.1	0.0	0.1
CS	0.38	0.40	0.40	0.00	0.38	0.44	0.00	0.43
BA	517	654	650	614	610	602	646	591
IBA	485	653	682	0	560	593	0	606
LA	70.0	77.0	79.3	0.0	71.1	92.0	0.0	84.4
CE	149.8	164.5	170.1	0.0	149.4	198.4	0.0	181.3
ND	67	76	85	0	68	98	0	88
SM	12.45	13.80	13.93	0.00	11.84	14.87	0.00	13.94
EU	3.630	4.070	4.120	0.000	3.340	4.420	0.000	4.080
TB	1.33	1.57	1.55	0.00	1.37	1.68	0.00	1.49
YB	2.55	2.86	3.17	0.00	2.69	3.20	0.00	3.09
LU	0.400	0.440	0.480	0.000	0.400	0.490	0.000	0.450
HF	8.49	7.65	7.87	0.00	8.39	9.19	0.00	8.78
TA	6.57	7.32	7.50	0.00	7.29	8.27	0.00	7.75
PB	<4	<4	<4	<4	<4	<4	<4	<4
TH	6	3	4	8	6	6	6	6
ITH	7.2	6.6	7.1	0.0	7.6	8.4	0.0	8.3
U	1.6	1.9	2.0	0.0	2.3	2.5	0.0	2.4

TABLE E.1. ANALYSES OF LAVAS FROM MT. EREBUS

SMPL#	83428	AW82044	83427	AW82032	AW82029	83439	83438	AW82038
SIO2	45.54	46.20	46.21	46.29	46.86	47.01	47.17	47.19
TIO2	3.10	3.16	2.96	3.13	2.83	2.77	2.76	2.72
AL203	17.37	16.07	17.57	16.39	17.72	17.53	17.63	18.24
FEO*	10.94	11.11	10.57	10.89	9.76	9.96	9.68	9.33
MNO	0.24	0.25	0.25	0.23	0.23	0.24	0.24	0.22
MGO	4.11	4.74	4.11	5.34	3.46	3.66	3.68	3.13
CAO	9.14	8.05	8.82	9.01	7.36	7.30	7.29	7.52
NA2O	4.93	4.74	5.83	4.72	6.35	5.52	5.67	5.89
K2O	2.10	3.11	2.17	2.42	2.49	2.70	2.88	2.83
P2O5	1.54	1.16	1.45	1.08	1.24	1.44	1.26	1.22
LOI	-0.34	0.33	-0.09	-0.24	0.61	0.10	-0.21	0.78
TOTAL	98.67	98.91	99.84	99.26	98.90	98.21	98.04	99.05
H2O-	0.00	0.10	0.02	0.12	0.16	0.01	0.04	0.17
IFEO	0.00	11.10	0.00	0.00	0.00	10.05	0.00	9.52
INA_2O	0.00	4.80	0.00	0.00	0.00	5.49	0.00	5.75
SC	0.00	13.15	0.00	0.00	0.00	7.13	0.00	6.42
V	141	147	134	170	77	102	112	73
CR	13	59	18	71	23	<10	10	26
ICR	0	61	0	0	0	2	0	2
NI	5	27	<5	39	9	7	10	10
CU	17	46	20	49	39	20	28	56
ZN	111	124	118	97	106	109	107	111
GA	24	24	20	23	21	25	24	22
AS	0.0	<1.0	0.0	0.0	0.0	2.0	0.0	1.2
RB	46	62	49	52	57	63	67	61
IRB	0	67	0	0	0	60	0	62
SR	1354	871	1339	988	1205	1383	1364	1295
Y	43	48	42	44	46	44	43	46
ZR	400	522	414	434	483	491	503	482
NB	132	158	137	126	165	146	156	163
SB	0.0	0.0	0.0	0.0	0.0	0.1	0.0	0.1
CS	0.00	0.53	0.00	0.00	0.00	0.52	0.00	0.62
BA	626	736	602	693	732	757	761	771
IBA	0	686	0	0	0	720	0	721
LA	0.0	89.5	0.0	0.0	0.0	93.4	0.0	94.7
CE	0.0	189.5	0.0	0.0	0.0	194.7	0.0	195.3
ND	0	85	0	0	0	89	0	86
SM	0.00	15.11	0.00	0.00	0.00	14.00	0.00	14.46
EU	0.000	3.960	0.000	0.000	0.000	3.930	0.000	4.010
TB	0.00	1.75	0.00	0.00	0.00	1.53	0.00	1.64
YB	0.00	3.43	0.00	0.00	0.00	3.30	0.00	3.35
LU	0.000	0.570	0.000	0.000	0.000	0.500	0.000	0.510
HF	0.00	10.61	0.00	0.00	0.00	10.21	0.00	9.78
TA	0.00	8.92	0.00	0.00	0.00	8.96	0.00	9.46
PB	<4	<4	<4	4	<4	<4	<4	<4
TH	6	9	6	9	10	7	8	10
ITH	0.0	10.0	0.0	0.0	0.0	9.9	0.0	11.3
U	0.0	2.1	0.0	0.0	0.0	2.8	0.0	3.2

TABLE E.1. ANALYSES OF LAVAS FROM MT. EREBUS

SMPL#	83418	83441	83436	83409	AW82041	83453	83440	83401
SIO2	47.26	47.59	47.62	48.22	48.44	49.05	49.11	49.21
TIO2	2.84	2.72	2.49	2.60	2.38	2.44	2.13	2.34
AL203	17.70	17.86	19.51	17.49	18.58	18.25	20.31	19.41
FEO*	10.09	9.45	8.34	9.58	8.67	8.85	7.72	7.74
MNO	0.23	0.24	0.19	0.23	0.21	0.23	0.19	0.20
MGO	3.78	3.84	2.98	3.47	2.59	3.30	2.33	2.81
CAO	7.95	7.22	8.78	6.79	6.88	6.42	7.31	7.21
NA2O	5.14	5.86	5.18	5.61	5.83	6.08	6.09	6.13
K2O	2.36	2.79	2.16	3.27	3.10	3.15	2.87	2.68
P2O5	1.15	1.25	1.06	1.19	1.05	1.11	0.94	1.12
LOI	-0.44	-0.18	0.07	0.17	1.12	-0.16	0.33	-0.09
TOTAL	98.07	98.64	98.38	98.63	98.85	98.72	99.33	98.76
H2O-	0.12	-0.10	0.10	0.12	0.18	0.10	0.07	-0.04
IFEO	0.00	0.00	0.00	9.79	0.00	8.89	0.00	0.00
INA_2O	0.00	0.00	0.00	5.65	0.00	6.10	0.00	0.00
SC	0.00	0.00	0.00	9.11	0.00	5.94	0.00	0.00
V	122	107	87	97	51	81	54	76
CR	17	11	30	30	<10	<10	10	<10
ICR	0	0	0	25	0	3	0	0
NI	9	10	6	13	5	5	7	6
CU	34	30	42	31	29	20	28	24
ZN	111	106	94	114	109	130	95	81
GA	25	22	23	24	24	24	22	24
AS	0.0	0.0	0.0	1.8	0.0	1.2	0.0	0.0
RB	49	66	46	72	59	73	62	59
IRB	0	0	0	70	0	69	0	0
SR	1461	1376	1434	1123	1169	1200	1436	1448
Y	43	43	38	46	46	42	40	39
ZR	443	497	401	540	522	532	460	451
NB	131	157	122	183	165	177	147	150
SB	0.0	0.0	0.0	0.1	0.0	0.1	0.0	0.0
CS	0.00	0.00	0.00	0.70	0.00	0.79	0.00	0.00
BA	746	769	599	819	809	806	735	765
IBA	0	0	0	763	0	842	0	0
LA	0.0	0.0	0.0	100.2	0.0	95.4	0.0	0.0
CE	0.0	0.0	0.0	205.7	0.0	191.1	0.0	0.0
ND	0	0	0	91	0	80	0	0
SM	0.00	0.00	0.00	13.72	0.00	12.60	0.00	0.00
EU	0.000	0.000	0.000	3.900	0.000	3.580	0.000	0.000
TB	0.00	0.00	0.00	1.65	0.00	1.46	0.00	0.00
YB	0.00	0.00	0.00	3.49	0.00	3.25	0.00	0.00
LU	0.000	0.000	0.000	0.540	0.000	0.500	0.000	0.000
HF	0.00	0.00	0.00	11.11	0.00	10.47	0.00	0.00
TA	0.00	0.00	0.00	10.36	0.00	10.04	0.00	0.00
PB	<4	<4	<4	<4	<4	<4	<4	<4
TH	6	8	6	11	9	14	9	7
ITH	0.0	0.0	0.0	12.3	0.0	13.5	0.0	0.0
U	0.0	0.0	0.0	3.1	0.0	3.8	0.0	0.0

TABLE E.1. ANALYSES OF LAVAS FROM MT. EREBUS

SMPL#	83415	83203	83411	83403	83442	83417	83204	83410
SIO2	49.53	49.76	49.84	50.17	49.00	50.17	50.13	50.77
TIO2	2.12	2.15	2.25	2.16	2.29	2.18	2.23	1.95
AL203	19.87	18.68	19.72	19.86	18.31	18.64	18.35	18.91
FEO*	7.41	8.81	7.71	7.39	8.81	8.04	9.13	7.78
MNO	0.17	0.24	0.19	0.19	0.22	0.22	0.24	0.22
MGO	3.00	2.95	2.71	2.59	3.02	2.51	2.49	2.20
CAO	6.93	6.41	6.78	6.83	6.16	5.73	5.13	5.55
NA2O	6.22	6.37	6.01	5.94	7.66	6.44	7.25	6.90
K2O	3.00	3.23	2.93	2.99	3.42	3.52	4.19	3.38
P2O5	0.85	0.86	0.96	0.98	1.08	1.10	1.03	0.93
LOI	-0.22	-0.12	0.41	-0.10	0.42	-0.01	-0.40	0.17
TOTAL	98.89	99.34	99.49	99.00	100.39	98.53	99.76	98.76
H2O-	0.01	0.55	0.04	-0.03	0.12	0.07	0.01	0.04
IFEO	7.45	9.05	0.00	7.44	8.85	7.98	9.23	7.93
INA_2O	6.24	6.40	0.00	5.98	6.28	6.42	6.79	6.64
SC	7.06	4.92	0.00	5.53	5.68	6.32	5.11	5.09
V	95	37	79	75	76	62	38	37
CR	36	<10	<10	12	<10	<10	21	<10
ICR	33	<2	0	<2	6	<2	<2	<2
NI	13	5	7	9	10	7	5	7
CU	31	18	24	25	36	19	39	21
ZN	82	108	90	85	99	96	131	108
GA	23	24	24	24	23	23	25	24
AS	1.7	1.4	0.0	1.5	1.9	1.1	<1.0	2.1
RB	70	63	64	63	75	77	96	75
IRB	69	64	0	62	71	73	97	72
SR	1345	1463	1375	1433	1166	1270	870	1188
Y	33	45	38	38	42	46	49	47
ZR	448	502	480	481	550	632	662	608
NB	160	176	160	160	173	179	221	192
SB	0.1	0.1	0.0	0.1	0.1	0.2	0.2	0.1
CS	0.69	0.59	0.00	0.70	0.66	0.74	0.77	0.83
BA	763	994	766	784	842	828	1012	930
IBA	730	939	0	766	833	819	948	909
LA	74.9	90.3	0.0	80.1	98.8	101.2	114.9	107.9
CE	148.8	187.2	0.0	165.1	197.5	207.7	230.0	218.1
ND	57	83	0	70	85	91	98	95
SM	9.70	13.26	0.00	11.33	12.78	13.91	14.48	13.89
EU	3.060	3.980	0.000	3.500	3.590	3.940	3.940	4.110
TB	1.16	1.60	0.00	1.29	1.52	1.65	1.72	1.70
YB	2.48	3.62	0.00	3.06	3.44	3.76	4.20	3.95
LU	0.390	0.550	0.000	0.460	0.540	0.570	0.620	0.590
HF	8.43	10.43	0.00	9.53	11.06	13.16	12.97	12.57
TA	9.18	9.93	0.00	9.12	10.61	10.74	12.47	11.30
PB	<4	<4	<4	<4	<4	<4	<4	<4
TH	9	7	7	10	9	12	15	11
ITH	12.0	10.3	0.0	11.8	11.8	13.4	14.9	13.9
U	3.3	3.2	0.0	3.4	3.4	4.4	4.9	4.7

TABLE E.1. ANALYSES OF LAVAS FROM MT. EREBUS

SMPL#	AW82030	83202	83421	AW82015	83452	82407	83446	83433
SIO2	50.96	52.19	52.69	54.22	55.00	55.43	55.63	55.66
TIO2	1.98	1.53	1.38	1.58	1.36	1.28	1.18	1.17
AL203	19.05	19.79	21.23	18.84	18.29	18.42	19.46	19.50
FEO*	7.52	6.62	5.47	6.76	6.59	6.12	5.06	4.99
MNO	0.23	0.21	0.15	0.23	0.27	0.26	0.20	0.20
MGO	2.21	1.93	1.47	1.81	1.64	1.50	1.30	1.16
CAO	5.20	4.33	5.20	4.22	3.34	3.23	3.16	3.24
NA20	6.98	7.71	7.21	6.96	7.77	7.91	7.60	7.69
K20	3.91	4.13	3.86	3.90	4.39	4.37	4.47	4.16
P205	0.94	0.75	0.63	0.71	0.56	0.52	0.46	0.49
LOI	-0.19	-0.13	-0.10	-0.12	-0.28	-0.20	0.03	0.18
TOTAL	98.78	99.05	99.18	99.10	98.92	98.85	98.55	98.42
H20-	0.07	-0.03	0.07	0.16	0.02	0.01	-0.04	0.05
IFEO	7.72	0.00	0.00	6.92	6.61	6.25	5.16	5.07
INA_2O	6.87	0.00	0.00	6.77	7.10	7.06	7.77	7.28
SC	4.14	0.00	0.00	4.25	4.90	4.56	3.06	3.02
V	34	24	22	24	35	30	19	17
CR	<10	17	<10	16	13	12	<10	<10
ICR	<2	0	0	<2	3	5	2	<2
NI	5	5	7	7	9	9	6	6
CU	17	16	19	11	13	11	10	11
ZN	106	100	78	124	153	145	108	108
GA	24	23	24	26	28	28	28	28
AS	1.2	0.0	0.0	<1.0	<1.0	<1.0	2.0	2.6
RB	87	97	84	86	101	97	107	103
IRB	84	0	0	85	98	94	105	97
SR	1109	1038	1268	1171	744	795	885	897
Y	49	42	34	53	68	65	55	53
ZR	673	669	561	766	942	905	927	911
NB	212	232	189	214	259	249	255	252
SB	0.2	0.0	0.0	0.2	0.2	0.2	0.3	0.2
CS	0.85	0.00	0.00	0.98	1.12	1.17	1.37	1.24
BA	847	933	861	1029	1138	1205	917	925
IBA	873	0	0	990	1050	1163	1010	972
LA	106.3	0.0	0.0	111.0	134.4	128.6	109.2	109.5
CE	218.0	0.0	0.0	222.9	273.7	260.8	218.8	215.5
ND	92	0	0	96	114	108	85	85
SM	14.09	0.00	0.00	14.43	17.58	16.77	13.31	13.06
EU	4.020	0.000	0.000	4.480	5.170	5.190	4.210	4.180
TB	1.68	0.00	0.00	1.78	2.20	2.06	1.74	1.63
YB	4.07	0.00	0.00	4.70	5.96	5.63	4.87	4.98
LU	0.620	0.000	0.000	0.700	0.870	0.860	0.770	0.750
HF	13.45	0.00	0.00	16.77	20.92	19.95	19.86	19.41
TA	12.20	0.00	0.00	12.55	14.99	14.54	14.92	14.43
PB	<4	<4	<4	<4	<4	4	5	6
TH	14	16	11	13	20	19	20	19
ITH	15.1	0.0	0.0	15.4	18.1	17.5	18.9	18.5
U	4.3	0.0	0.0	4.8	6.4	6.8	5.6	5.4

TABLE E.1. ANALYSES OF LAVAS FROM MT. EREBUS

SMPL#	83447	83448	81001	83400	80020	82431	82403	83412
SIO2	55.71	55.93	56.25	56.27	56.57	55.04	52.69	54.28
TIO2	1.15	1.10	1.00	0.99	0.98	1.19	2.18	1.20
AL203	19.53	19.74	18.99	19.25	19.31	20.06	19.04	18.01
FEO*	4.87	4.59	5.57	5.26	4.95	5.13	7.52	8.46
MNO	0.19	0.18	0.25	0.23	0.23	0.18	0.24	0.29
MGO	1.21	1.23	0.96	0.95	0.99	1.14	2.50	1.57
CAO	3.19	3.20	2.57	2.78	2.75	3.73	5.98	4.40
NA2O	7.64	7.77	8.15	7.72	8.17	7.44	5.90	6.52
K2O	4.43	4.33	4.75	4.62	4.55	4.00	2.15	3.38
P2O5	0.46	0.44	0.43	0.40	0.42	0.47	1.13	0.51
LOI	0.05	0.15	-0.28	0.12	-0.21	0.19	-0.05	0.01
TOTAL	98.42	98.66	98.63	98.60	98.72	98.57	99.26	98.62
H2O-	0.06	0.04	0.04	0.04	0.05	-0.01	-0.04	0.11
IFEO	0.00	4.76	5.51	5.27	5.01	5.22	7.49	8.59
INA_2O	0.00	7.09	7.93	7.87	7.53	6.84	5.80	6.40
SC	0.00	2.80	2.96	3.02	2.58	2.87	4.81	2.20
V	16	13	<10	11	12	18	48	10
CR	12	10	14	14	10	15	10	<10
ICR	0	2	<2	2	<2	<2	2	<2
NI	6	7	5	6	7	7	7	6
CU	<10	10	<10	<10	10	<10	13	13
ZN	103	99	145	112	130	85	97	134
GA	27	27	29	28	29	26	24	25
AS	0.0	<1.0	<1.0	<1.0	<1.0	5.0	<1.0	<1.0
RB	105	99	109	105	102	88	44	75
IRB	0	96	105	108	102	85	47	72
SR	907	990	717	851	878	1081	1643	970
Y	53	49	68	60	64	49	51	42
ZR	903	855	1008	935	946	948	458	628
NB	248	236	276	247	261	251	140	172
SB	0.0	0.3	0.3	0.3	0.3	0.2	0.0	0.3
CS	0.00	1.20	1.20	1.14	1.27	0.80	0.41	0.70
BA	942	1034	1225	1107	1203	840	1259	897
IBA	0	1064	1160	1144	1164	889	1205	887
LA	0.0	103.9	136.0	120.7	126.9	97.7	117.2	111.5
CE	0.0	204.2	272.5	242.7	252.7	194.4	234.6	217.7
ND	0	80	110	101	97	78	106	86
SM	0.00	12.02	16.80	14.98	15.25	12.13	15.84	11.94
EU	0.000	4.270	5.050	4.830	4.970	3.860	5.500	3.510
TB	0.00	1.57	2.14	1.91	1.99	1.56	1.80	1.35
YB	0.00	4.74	6.06	5.55	5.64	4.83	3.92	3.64
LU	0.000	0.710	0.920	0.850	0.840	0.730	0.580	0.560
HF	0.00	18.10	22.20	20.59	20.56	20.08	10.63	13.78
TA	0.00	13.73	15.92	14.86	15.05	14.22	8.97	10.44
PB	4	<4	5	<4	<4	<4	<4	<4
TH	19	18	22	17	18	20	7	11
ITH	0.0	17.5	19.7	19.2	18.6	20.0	9.8	12.9
U	0.0	5.2	6.4	4.6	5.9	6.8	2.9	3.3

TABLE E.1. ANALYSES OF LAVAS FROM MT. EREBUS

SMPL#	81002	83402	AW82023	80018	82404	83408	83407	83454
SIO2	55.31	55.58	55.81	54.25	54.55	57.24	58.91	60.59
TIO2	1.28	1.02	1.07	1.23	1.23	0.61	0.44	0.74
AL203	18.68	18.20	18.03	19.15	19.26	19.07	18.47	15.85
FEO*	6.60	7.92	7.71	6.37	6.40	5.69	5.89	6.79
MNO	0.23	0.28	0.30	0.22	0.22	0.24	0.26	0.22
MGO	1.54	1.20	1.35	1.55	1.40	0.65	0.37	0.56
CAO	3.88	3.88	3.75	3.62	3.68	2.44	2.19	1.94
NA20	6.77	6.90	7.06	7.63	7.60	8.06	7.66	6.38
K20	3.96	3.63	3.50	4.04	4.19	4.65	4.67	5.16
P205	0.43	0.38	0.41	0.45	0.45	0.18	0.13	0.13
LOI	0.40	-0.18	-0.22	0.30	0.20	-0.17	0.03	0.07
TOTAL	99.07	98.80	98.75	98.79	99.16	98.65	99.02	98.42
H20-	0.06	0.04	0.05	0.07	0.01	0.06	0.09	0.08
IFEO	6.59	7.76	7.83	0.00	6.48	5.70	5.88	6.87
INA_2O	6.81	6.86	7.08	0.00	6.60	7.35	7.10	6.37
SC	3.40	1.74	2.07	0.00	2.31	1.05	0.58	5.47
V	20	<10	10	19	17	<10	12	<10
CR	<10	<10	<10	12	<10	<10	<10	<10
ICR	<2	<2	<2	0	<2	<2	<2	<2
NI	8	<5	7	7	6	8	6	7
CU	11	12	10	11	12	12	10	<10
ZN	113	121	122	107	106	101	123	176
GA	24	25	25	25	27	26	25	31
AS	2.6	2.9	<1.0	0.0	<1.0	<1.0	<1.0	3.8
RB	82	84	80	112	114	104	109	132
IRB	81	79	81	0	109	98	100	126
SR	862	852	923	702	704	538	381	81
Y	45	40	43	44	43	41	40	71
ZR	660	681	634	811	812	812	848	969
NB	189	171	193	229	229	220	201	232
SB	0.2	0.3	0.2	0.0	0.3	0.2	0.3	0.3
CS	0.84	0.85	0.73	0.00	1.36	0.94	1.07	1.94
BA	1230	982	1136	846	862	1237	1327	811
IBA	1190	935	1109	0	809	1221	1321	794
LA	103.5	110.7	113.0	0.0	107.7	114.0	119.3	132.2
CE	203.9	215.2	228.4	0.0	204.2	213.8	220.9	268.4
ND	84	81	88	0	79	75	74	109
SM	12.02	11.25	12.22	0.00	10.93	10.27	10.13	17.03
EU	3.700	3.310	3.830	0.000	3.020	2.990	2.800	3.360
TB	1.37	1.32	1.44	0.00	1.31	1.26	1.20	2.18
YB	3.95	3.71	3.93	0.00	4.15	4.21	3.99	6.31
LU	0.600	0.580	0.610	0.000	0.630	0.650	0.640	0.930
HF	14.16	14.58	13.92	0.00	16.34	17.04	17.54	21.50
TA	10.94	10.88	11.43	0.00	13.20	13.20	12.53	12.51
PB	8	7	6	8	9	8	12	16
TH	14	15	14	20	23	18	21	25
ITH	14.1	14.8	14.3	0.0	20.2	17.0	18.4	21.4
U	4.5	4.8	4.8	0.0	6.5	5.2	4.8	6.9

TABLE E.1. ANALYSES OF LAVAS FROM MT. EREBUS

SMPL#	83451	82405
SIO2	62.92	63.51
TIO2	0.43	0.43
AL203	15.12	15.33
FEO*	6.11	6.15
MNO	0.21	0.21
MGO	0.17	0.14
CAO	1.43	1.44
NA20	7.31	6.56
K20	5.17	5.23
P205	0.05	0.05
LOI	0.39	0.18
TOTAL	99.30	99.23
H20-	0.16	0.05
IFEO	6.17	6.27
INA_2O	6.28	5.56
SC	2.78	2.79
V	<10	<10
CR	10	11
ICR	<2	2
NI	7	9
CU	<10	<10
ZN	195	269
GA	34	33
AS	6.8	1.9
RB	162	161
IRB	152	159
SR	13	13
Y	88	92
ZR	1089	1085
NB	259	258
SB	0.6	0.5
CS	3.63	3.69
BA	232	253
IBA	314	304
LA	159.9	164.9
CE	322.0	325.1
ND	136	145
SM	20.40	21.00
EU	2.840	2.910
TB	2.63	2.87
YB	7.82	7.88
LU	1.140	1.170
HF	25.00	25.20
TA	14.31	14.59
PB	19	31
TH	30	29
ITH	25.3	25.4
U	8.0	7.9

Explanation of Table E.1. Analyses of lavas of Mt. Erebus.

83435: Basanite, Cape Barne.
83437: Basanite, Lower Fang Ridge.
79300: Basanite, Upper Fang Ridge.
83405: Ne-hawaiite, Inaccessible Island.
83404: Ne-hawaiite, Inaccessible Island.
83432: Ne-hawaiite, Cape Barne.
83406: Ne-hawaiite, Inaccessible Island.
83426: Ne-hawaiite, Cape Barne.
83428: Ne-hawaiite, Cape Barne.
AW82044: Ne-hawaiite, Turks Head
83427: Ne-hawaiite, Cape Barne.
AW82032: Ne-hawaiite, Tryggve Point.
AW82029: Ne-hawaiite, Tryggve Point.
83439: Ne-hawaiite, Lower Fang Ridge.
83438: Ne-hawaiite, Lower Fang Ridge.
AW82038: Ne-hawaiite, Turks Head.
83418: Ne-hawaiite, Tent Island.
83441: Ne-hawaiite, Lower Fang Ridge.
83436: Ne-hawaiite, Lower Fang Ridge.
83409: Ne-hawaiite, Inaccessible Island.
AW82041: Ne-hawaiite, Turks Head.
83453: Ne-hawaiite, flow south of Abbott Peak.
83440: Ne-hawaiite, Lower Fang Ridge.
83401: Ne-hawaiite, Inaccessible Island.
83415: Ne-hawaiite, Tent Island.
83203: Ne-hawaiite, Upper Fang Ridge.
83411: Ne-hawaiite, Inaccessible Island.
83403: Ne-hawaiite, Inaccessible Island.
83442: Ne-mugearite, Lower Fang Ridge.
83417: Ne-mugearite, Tent Island.
83204: Ne-benmoreite, Upper Fang Ridge.
83410: Ne-benmoreite, Inaccessible Island.
AW82030: Ne-benmoreite, Tryggve Point.
83202: Ne-benmoreite, Upper Fang Ridge.
83421: Ne-benmoreite, Tent Island.
AW82015: Ne-benmoreite, Turks Head.
83452: Anorthoclase phonolite, flow, Bomb Peak.
82407: Anorthoclase phonolite, bomb, Bomb Peak.
83446: Anorthoclase phonolite, Cape Royds.
83433: Anorthoclase phonolite, Cape Barne.
83447: Anorthoclase phonolite, Cape Royds.
83448: Anorthoclase phonolite, Cape Royds.
81001: Anorthoclase phonolite, Hooper's Shoulder.
83400: Anorthoclase phonolite, Cape Evans.
80020: Anorthoclase phonolite, Three Sisters Cones.
82431: Anorthoclase phonolite, inclusion, Bomb Peak.
82403: Anorthoclase-clinopyroxene cumulate inclusion, Bomb Peak.

83412: Benmoreite, Inaccessible Island.
81002: Benmoreite, Abbott Peak.
83402: Benmoreite, Inaccessible Island.
AW82023: Benmoreite, Lewis Bay.
80018: Kaersutite phonolite, Bomb Peak.
82404: Kaersutite phonolite, Bomb Peak.
83408: Kaersutite phonolite, Inaccessible Island.
83407: Kaersutite phonolite, Inaccessible Island.
83454: Trachyte, Aurora Cliffs.
83451: Comenditic trachyte, Bomb Peak.
82405: Comenditic trachyte, Bomb Peak.

APPENDIX E continued.

Part 2. Analyses of Mt. Erebus lavas from Kyle (1976).

Major elements and some trace elements are from Kyle (1976) and are mostly XRF determinations. FeO* is total Fe reported as FeO. Trace and rare earth elements are INAA determinations made in this study. Analyses of FeO*, Na_2O, Cr, Rb, Ba and Th by INAA are prefixed by I. Undetected elements are represented by zeros. The limits of detection of certain elements are prefixed by less-than symbols. Sample nomenclature and locations are given at the end of the table.

Table E.2. Analyses of Mt. Erebus lavas from Kyle (1976).

Sample	25754	25754*	25758	25758*	25742	25748	25748*	25749
SiO_2	47.27	44.99	47.44	45.70	51.17	53.09	52.52	54.00
TiO_2	2.43	3.20	2.49	3.21	1.86	1.66	1.64	1.40
Al_2O_3	19.31	16.72	19.30	16.83	19.49	20.09	18.63	19.18
FeO*	8.41	10.94	8.54	11.08	7.21	6.39	7.16	7.11
MnO	0.22	0.26	0.20	0.26	0.20	0.19	0.24	0.22
MgO	2.50	3.35	2.65	3.26	1.87	1.66	2.02	1.58
CaO	7.78	6.92	7.75	6.85	5.52	4.81	3.78	3.81
Na_2O	5.61	5.78	5.68	5.75	6.70	6.80	7.29	7.00
K_2O	2.52	2.95	2.66	3.20	3.71	3.88	4.88	4.35
P_2O_5	1.19	1.40	1.21	1.45	1.12	0.84	1.02	0.54
H_2O+[1]	1.58	1.81	1.08	1.24	0.25	0.00	0.00	0.16
Total	98.82	98.32	99.00	98.83	99.10	99.41	99.18	99.35
IFEO*	9.18	10.95	8.41	10.92	7.25	6.77	7.06	7.14
INA_2O	5.68	5.59	5.60	5.69	7.10	0.00	7.61	7.84
SC	6.9	7.7	6.1	7.8	5.5	5.3	5.9	4.7
V	52	68	51	0	36	<3	14	24
CR	30	12	5	0	12	9	14	7
ICR	7	8	3	<2	2	2	2	<2
NI	<5	<5	<5	0	<5	<5	<5	<5
CU	41	52	44	0	28	11	15	10
ZN	100	123	102	0	92	99	121	108
RB	51	63	52	0	74	84	113	101
IRB	59	70	54	68	72	86	114	98
SR	1375	991	1378	0	1111	1194	568	610
SB	0.15	0.26	0.18	0.21	0.19	0.22	0.00	0.32
CS	0.54	0.59	0.60	0.65	0.76	0.89	1.20	1.08
BA	483	529	593	0	740	789	658	791
IBA	793	708	694	813	899	944	879	982
LA	95.9	106.5	88.8	109.7	115.1	0.0	131.0	111.0
CE	188.2	208.6	174.4	218.0	220.3	215.0	253.6	210.3
SM	14.1	15.7	12.9	16.2	14.9	0.0	16.4	12.8
EU	4.20	4.39	4.03	4.57	4.37	3.99	3.92	3.48
TB	1.34	1.54	1.52	1.72	1.38	1.65	1.79	1.32
YB	3.5	4.2	3.3	4.3	4.1	4.6	5.6	4.4
LU	0.44	0.56	0.46	0.56	0.64	0.00	0.78	0.65
HF	8.8	10.0	8.1	10.3	11.9	14.1	17.7	14.6
TA	10.0	10.9	8.5	11.0	11.6	13.1	15.9	13.4
ITH	11.8	13.3	10.7	13.8	15.8	16.9	21.5	17.4
U	3.9	3.9	3.6	4.8	6.3	0.0	7.2	4.9

[1]Loss on ignition

Table E.2. Analyses of Mt. Erebus lavas from Kyle (1976).

Sample	25745	25774	25782	25777	25778	25778*	25781	25726
SiO_2	57.49	47.49	48.83	49.37	49.64	48.94	55.32	55.32
TiO_2	0.63	2.71	2.50	2.26	2.02	2.53	1.29	1.07
Al_2O_3	19.40	18.63	18.52	18.35	19.58	18.23	19.13	19.69
$FeO*^3$	5.72	8.94	8.79	9.08	8.13	9.86	6.53	5.17
MnO	0.23	0.22	0.22	0.23	0.22	0.26	0.22	0.25
MgO	0.65	3.41	2.99	2.09	2.12	2.10	1.42	1.09
CaO	2.52	7.41	6.41	5.01	6.63	5.19	3.93	2.68
Na_2O	7.59	5.73	6.05	6.66	6.10	6.68	6.54	7.92
K_2O	4.66	2.92	3.14	4.18	3.04	3.87	3.95	4.71
P_2O_5	0.18	1.12	1.18	1.10	0.88	0.82	0.46	0.45
H_2O+^1	0.13	0.06	0.11	0.14	0.05	0.07	0.24	0.05
Total	99.20	98.64	98.74	98.47	98.41	98.55	99.03	98.40
IFEO*	5.66	9.02	8.66	9.15	8.06	9.73	6.56	0.00
INA_2O	8.22	5.70	6.17	6.70	6.26	6.81	7.10	0.00
SC	1.7	9.3	6.4	5.8	5.1	5.3	4.0	0.0
V	0	111	66	25	17	0	11	5
CR	11	31	<5	13	33	0	0	<5
ICR	<2	24	3	2	<2	<2	<2	<2
NI	<5	10	<5	<5	<5	0	<5	<5
CU	7	0	18	38	21	0	10	4
ZN	100	102	102	125	104	0	97	135
RB	107	61	70	93	56	0	81	111
IRB	98	63	70	96	55	81	77	0
SR	536	1262	1146	830	1560	0	834	735
SB	0.31	0.11	0.13	0.17	0.21	0.23	0.21	0.00
CS	0.89	0.66	0.74	0.82	0.48	0.70	0.74	0.00
BA	1073	549	595	722	754	0	993	871
IBA	1240	828	795	989	980	975	1228	0
LA	119.3	86.2	97.5	117.2	89.5	104.7	107.7	0.0
CE	211.4	167.2	186.7	223.8	176.0	203.5	197.3	0.0
SM	10.9	11.9	12.5	14.9	12.8	14.4	12.5	0.0
EU	2.96	3.66	3.71	4.07	4.24	4.13	3.76	0.00
TB	1.10	1.40	1.28	1.44	1.60	1.51	1.57	0.00
YB	4.4	3.0	3.2	4.4	3.8	4.2	4.5	0.0
LU	0.68	0.40	0.50	0.59	0.52	0.66	0.59	0.00
HF	15.9	9.1	9.6	11.9	9.1	11.4	12.9	0.0
TA	13.8	10.6	10.4	13.0	9.7	12.2	11.3	0.0
ITH	19.0	10.8	14.1	15.6	10.6	13.6	14.9	0.0
U	5.0	3.3	4.5	5.5	5.0	4.4	5.2	0.0

Table E.2. Analyses of Mt. Erebus lavas from Kyle (1976).

Sample	25726*	25727	25724	25724*	25725	25725*
SiO_2	54.94	56.42	56.65	55.54	56.68	55.81
TiO_2	1.10	0.91	0.92	1.06	1.00	1.10
Al_2O_3	19.27	20.18	20.09	19.09	19.84	18.84
FeO*	4.89	4.36	4.52	4.88	4.66	4.96
MnO	0.30	0.21	0.22	0.31	0.22	0.28
MgO	0.85	0.95	0.97	0.80	1.06	0.87
CaO	2.03	2.80	2.79	1.95	2.92	2.06
Na_2O	8.85	7.88	7.75	9.05	7.88	8.27
K_2O	5.42	4.40	4.45	5.43	4.45	5.38
P_2O_5	0.00	0.37	0.38	0.00	0.40	0.00
H_2O+	0.00	0.00	0.00	0.00	0.04	0.00
H_2O-	0.00	0.02	0.02	0.00	0.00	0.00
Total	97.65	98.50	98.76	98.11	99.15	97.57
V	0	4	<5	0	<5	0
CR	0	<5	<5	0	<5	0
NI	0	<5	<5	0	<5	0
CU	0	6	5	0	5	0
ZN	0	112	132	0	119	0
RB	0	95	107	0	99	0
SR	0	1020	721	0	932	0
BA	0	1133	876	0	1027	0

Explantion of Table E.2. Analyses of Mt. Erebus lavas from Kyle (1976).

25754: Ne-hawaiite, Turks Head
25754*: Groundmass of 25754.
25758: Ne-hawaiite, Tryggve Point.
25758*: Groundmass of 25758.
25742: Ne-benmoreite, Inaccessible Island.
25748: Ne-benmoreite, Tent Island.
25748*: Groundmass of 25748.
25749: Ne-benmoreite, Big Razorback Island.
25745: Phonolite, Inaccessible Island.
25774: Ne-hawaiite, Fang Ridge.
25782: Ne-hawaiite, flow south of Abbott Peak.
25777: Ne-benmoreite, Fang Ridge.
25778: Ne-hawaiite, Fang Ridge.
25778*: Groundmass of 25778.
25781: Mugearite, Abbott Peak.
25726: Anorthoclase phonolite bomb, summit, Mt. Erebus.
25726*: Groundmass of 25726.
25727: Anorthoclase phonolite flow, summit, Mt. Erebus.
25724: Anorthoclase phonolite bomb, summit, Mt. Erebus.
25724*: Groundmass of 25724.
25725: Anorthoclase phonolite flow, summit, Mt. Erebus.
25725*: Groundmass of 25725.

APPENDIX F: CIPW NORMATIVE MINERALOGY OF MT. EREBUS LAVAS

Table F.1. CIPW norms of Mt. Erebus lavas.

	83435	83437	79300	83405	83404	83406	83432	83426	83428	AW82044
NZ										
CO										
OR	10.19	12.36	12.76	11.38	12.03	12.03	12.31	12.68	12.49	18.59
AB	8.28	14.93	15.36	17.05	15.97	18.13	18.41	18.98	20.44	16.81
AN	16.07	18.66	17.80	17.53	17.33	17.10	16.80	17.31	19.21	13.58
LC										
NE	16.75	13.40	11.01	12.03	12.65	12.73	14.21	14.02	11.71	12.96
KP										
HL										
TH										
AC										
NS										
KS										
WO										
DI	23.61	16.12	16.79	18.33	18.25	16.71	15.20	14.74	13.46	15.71
DIWO	12.07	8.18	8.52	9.32	9.27	8.47	7.69	7.46	6.82	7.99
DIEN	8.89	4.31	4.52	5.00	4.95	4.42	3.91	3.82	3.49	4.29
DIFS	4.65	3.63	3.74	4.01	4.03	3.81	3.59	3.46	3.15	3.44
HY										
HYEN										
HYFS										
OL	12.20	10.89	9.68	11.40	11.51	11.18	9.36	9.13	9.53	10.09
OLFO	7.00	5.65	5.07	6.05	6.07	5.73	4.65	4.57	4.78	5.36
OLFA	5.21	5.24	4.61	5.35	5.44	5.45	4.71	4.56	4.75	4.73
CS										
MT	2.90	2.93	2.92	2.94	2.92	2.94	3.65	3.65	3.65	3.67
CM										
IL	7.19	7.19	7.05	6.66	6.65	6.40	6.11	5.92	5.92	6.06
HM										
SP										
PF										
AP	2.87	3.60	3.72	2.76	2.74	2.83	4.04	3.64	3.68	2.79
FL										
CC										
D.I.[1]	35.22	40.69	42.13	40.46	40.66	42.89	44.93	45.68	44.64	48.16
MGNO.[2]	54.00	47.62	47.51	49.90	49.73	48.35	45.49	45.73	45.74	48.80

*** ALL ZERO VALUES PRINTED AS BLANKS. ***

[1]Differentiation index.

[2]Mg number ($100Mg/(Mg+Fe^{2+})$)

Table F.1. CIPW norms of Mt. Erebus lavas.

	83427	AW82032	AW82029	83439	83438	AW82038	83418	83441	83436	83409
QZ										
CO										
OR	12.78	11.32	14.91	16.19	17.26	16.98	14.15	16.65	12.98	19.57
AB	19.13	17.25	22.58	24.71	22.46	22.10	24.92	23.28	25.32	23.75
AN	15.35	16.46	12.68	15.36	14.34	15.37	18.45	14.30	23.92	13.08
LC										
NE	16.32	12.33	17.33	12.32	14.25	15.27	10.36	14.51	10.39	13.17
KP										
HL										
TH										
AC										
NS										
KS										
WO										
DI	15.53	17.38	13.30	9.80	11.51	11.85	11.42	11.14	10.84	10.84
DIWO	7.88	8.88	6.74	4.97	5.85	6.00	5.79	5.68	5.53	5.50
DIEN	4.12	5.05	3.51	2.58	3.12	3.11	3.03	3.13	3.08	2.86
DIFS	3.54	3.44	3.05	2.25	2.54	2.74	2.60	2.33	2.23	2.49
HY										
HYEN										
HYFS										
OL	8.32	10.15	7.17	9.21	8.22	6.64	8.87	8.33	5.60	8.12
OLFO	4.27	5.80	3.66	4.69	4.33	3.37	4.56	4.58	3.12	4.14
OLFA	4.05	4.36	3.50	4.52	3.89	3.27	4.31	3.75	2.48	3.98
CS										
MT	3.62	3.63	3.68	3.69	3.68	3.68	3.67	3.66	3.68	3.67
CM										
IL	5.61	5.96	5.45	5.34	5.31	5.23	5.46	5.20	4.79	5.01
HM										
SP										
PF										
AP	3.43	2.57	2.97	3.46	3.04	2.94	2.77	3.00	2.54	2.85
FL										
CC										
D.I.[1]	48.23	43.90	54.82	53.22	53.97	54.36	49.43	54.43	48.68	56.50
MGNO.[2]	46.79	52.40	45.07	45.85	46.87	44.06	46.22	48.74	46.58	45.77

*** ALL ZERO VALUES PRINTED AS BLANKS. ***

Table F.1. CIPW norms of Mt. Erebus lavas.

	AW82041	83453	83440	83401	83415	83203	83411	83403	83442	83417
QZ										
CO										
OR	18.71	18.77	17.10	15.96	17.85	19.13	17.41	17.81	20.19	21.03
AB	25.45	26.19	25.50	28.32	25.41	24.99	28.73	29.41	19.79	28.75
AN	15.68	13.34	19.75	17.72	17.55	12.88	18.29	18.82	5.48	11.73
LC										
NE	13.48	13.90	14.31	13.00	14.93	15.74	12.18	11.46	24.30	14.28
KP										
NE										
TH										
AC										
NS										
KS										
WO										
DI	10.06	9.10	8.73	8.96	9.30	11.05	7.59	7.23	14.81	8.03
DIWO	5.08	4.78	4.43	4.58	4.78	5.59	3.88	3.70	7.51	4.07
DIEN	2.54	2.59	2.35	2.66	2.89	2.82	2.21	2.15	3.69	2.13
DIFS	2.44	2.03	1.95	1.72	1.63	2.64	1.50	1.38	3.42	1.83
HY										
HYEN										
HYFS										
OL	5.82	7.47	4.70	5.27	5.28	6.48	5.62	5.21	5.00	5.74
OLFO	2.83	4.00	2.46	3.08	3.25	3.19	3.21	3.05	2.54	2.95
OLFA	2.99	3.46	2.24	2.19	2.02	3.29	2.41	2.16	2.46	2.79
CS										
MT	3.70	3.66	3.65	3.66	3.65	3.63	3.65	3.65	3.62	3.67
CM										
IL	4.62	4.67	4.08	4.49	4.06	4.10	4.29	4.13	4.33	4.19
HM										
SP										
PF										
AP	2.54	2.66	2.25	2.68	2.03	2.04	2.28	2.33	2.56	2.64
FL										
CC										
D.I.[1]	57.64	58.86	56.90	57.29	58.18	59.86	58.33	58.68	64.27	64.07
MGNO.[2]	41.80	47.15	43.20	47.65	50.91	44.50	46.93	47.37	45.08	43.60

*** ALL ZERO VALUES PRINTED AS BLANKS. ***

Table F.1. CIPW norms of Mt. Erebus lavas.

	83204	83410	AW82030	83202	83421	AW82015	83412	81002	83402	AW82023
QZ										
CO										
OR	24.67	20.23	23.27	24.55	22.93	23.18	20.18	23.64	21.62	20.87
AB	21.48	29.79	27.29	28.51	30.44	37.99	41.26	41.11	42.86	44.50
AN	5.13	10.71	9.19	7.23	14.22	8.72	10.03	8.98	7.99	7.22
LC										
NE	21.45	15.87	17.44	20.10	16.71	11.47	7.88	9.11	8.67	8.50
KP										
NL										
TH										
AC										
NS										
KS										
WO										
DI	11.27	9.06	8.74	7.71	6.09	6.30	7.33	6.36	7.56	7.49
DIWO	5.65	4.58	4.43	3.92	3.14	3.19	3.62	3.20	3.71	3.69
DIEN	2.57	2.28	2.30	2.11	1.96	1.64	1.23	1.50	1.13	1.26
DIFS	3.04	2.20	2.01	1.68	0.99	1.47	2.49	1.66	2.72	2.53
HY										
HYEN										
HYFS										
OL	5.81	4.71	4.44	3.57	1.87	4.04	6.16	3.68	4.81	4.77
OLFO	2.52	2.29	2.27	1.90	1.20	2.03	1.91	1.66	1.32	1.49
OLFA	3.28	2.43	2.18	1.67	0.67	2.00	4.25	2.02	3.49	3.29
CS										
MT	3.51	3.67	3.65	3.65	3.64	3.64	3.67	3.66	3.65	3.65
CM										
IL	4.22	3.75	3.78	2.92	2.63	3.01	2.30	2.46	1.95	2.05
HM										
SP										
PF										
AP	2.42	2.23	2.25	1.80	1.51	1.69	1.22	1.02	0.92	0.97
FL										
CC										
D.I.[1]	67.60	65.90	67.99	73.16	70.08	72.64	69.32	73.86	73.15	73.87
MGNO.[2]	39.21	41.52	42.70	44.01	44.82	41.77	31.11	38.61	27.41	30.59

*** ALL ZERO VALUES PRINTED AS BLANKS. ***

Table F.1. CIPW norms of Mt. Erebus lavas.

	80018	82404	83408	83407	83452	82407	83446	83433	83447	83448
QZ										
CO										
OR	24.20	24.93	27.73	27.82	26.10	26.02	26.72	24.95	26.53	25.91
AB	36.30	35.71	41.24	47.10	36.29	37.77	39.25	41.62	39.79	40.49
AN	6.14	6.12	2.10	2.21	2.05	1.87	5.87	6.52	6.01	6.27
LC										
NE	15.75	15.76	14.94	9.88	16.16	16.04	14.00	13.23	13.94	14.14
KP										
NL										
TH										
AC										
NS										
KS										
WO										
DI	7.49	7.75	7.53	6.84	9.08	8.92	5.60	5.31	5.63	5.49
DIWO	3.78	3.90	3.70	3.29	4.58	4.51	2.89	2.74	2.92	2.88
DIEN	1.86	1.81	1.16	0.61	2.23	2.30	1.84	1.73	1.93	2.09
DIFS	1.85	2.04	2.67	2.94	2.27	2.10	0.87	0.84	0.78	0.52
HY										
HYEN										
HYFS										
OL	3.04	2.68	1.15	1.35	2.79	2.07	1.54	1.29	1.14	0.90
OLFO	1.45	1.19	0.33	0.21	1.31	1.03	1.01	0.84	0.79	0.71
OLFA	1.59	1.48	0.82	1.14	1.48	1.04	0.53	0.45	0.35	0.19
CS										
MT	3.67	3.65	3.66	3.65	3.65	3.65	3.67	3.68	3.68	3.67
CM										
IL	2.37	2.35	1.16	0.84	2.60	2.44	2.26	2.26	2.21	2.11
HM										
SP										
PF										
AP	1.08	1.07	0.43	0.31	1.33	1.25	1.11	1.17	1.11	1.05
FL										
CC										
D.I.[1]	76.24	76.40	83.92	84.80	78.55	79.83	79.97	79.80	80.26	80.54
MGNO.[2]	40.22	37.57	25.11	15.19	40.18	40.93	45.18	43.04	45.19	48.36

*** ALL ZERO VALUES PRINTED AS BLANKS. ***

Table F.1. CIPW norms of Mt. Erebus lavas.

	81001	83400	80020	82431	82403	83454	83451	82405
QZ							0.36	2.11
CO								
OR	28.31	27.65	27.11	23.94	12.74	30.91	30.83	31.14
AB	38.67	40.51	40.41	40.00	45.72	52.34	49.39	50.06
AN	1.21	4.28	2.59	9.64	19.20			
LC								
NE	16.72	13.89	15.49	12.93	2.41	0.67		
KP								
MU								
TH						1.06	7.29	5.17
AC							1.10	
NS								
KS								
WO								
DI	7.34	5.81	6.29	4.88	2.62	7.68	6.06	6.09
DIWO	3.69	2.94	3.52	2.51	1.34	3.71	2.86	2.88
DIEN	1.68	1.47	2.00	1.52	0.75	0.77	0.18	0.17
DIFS	1.98	1.40	1.38	0.85	0.53	3.20	3.01	3.04
HY							4.06	3.44
HYEN							0.23	0.18
HYFS							3.83	3.26
OL	1.18	1.33	0.60	1.54	6.90	2.49		
OLFO	0.51	0.65	0.34	0.95	3.86	0.45		
OLFA	0.66	0.68	0.26	0.59	3.04	2.04		
CS								
MT	3.66	3.67	3.60	3.68	3.64	3.15		1.06
CM								
IL	1.92	1.91	1.88	2.29	4.15	1.42	0.81	0.81
HM								
SP								
PF								
AP	1.02	0.96	0.99	1.14	2.68	0.31	0.11	0.11
FL								
CC								
D.I.[1]	83.70	82.06	83.41	76.87	60.87	83.91	80.57	83.32
MGNO.[2]	34.16	36.06	39.57	41.25	45.83	17.90	7.14	6.05

*** ALL ZERO VALUES PRINTED AS BLANKS. ***